Analysis and visualization of multi-omics data

Inaugural-Dissertation

zur Erlangung des Doktorgrades
der Mathematisch-Naturwissenschaftlichen Fakultät

der Heinrich-Heine-Universität Düsseldorf

vorgelegt von

Freya Maria Rosemarie Ziegler

aus Mönchengladbach

Düsseldorf, März 2025

aus dem Institut für Biological Data Science

der Heinrich-Heine-Universität Düsseldorf

Gedruckt mit der Genehmigung der
Mathematisch-Naturwissenschaftlichen Fakultät der

Heinrich-Heine-Universität Düsseldorf

Berichterstatter:

1. Prof. Dr. Björn Usadel

2. Prof. Dr. Oliver Ebenhöh

Tag der mündlichen Prüfung: 13.10.2025

Table of contents

List of figures

List of tables

1 Abstract

Crop production is influenced by biophysical, technological, and socioeconomic factors, with climate change and abiotic stressors significantly impacting crop physiology and yield. Understanding the molecular mechanisms underlying stress responses and physiological development is essential for improving plant performance. Omics technologies such as genomics, transcriptomics, proteomics, and metabolomics can offer comprehensive insights into plant biology and are essential for studying these processes.

This study aimed to generate, visualize, and integrate multi-omics datasets to investigate molecular mechanisms in strawberry (*Fragaria* × *ananassa*) during floral initiation and blackcurrant (*Ribes nigrum*) under drought stress. An R-based function was developed to integrate gene functional annotations into principal component and overrepresentation analyses (PCA-ORA), facilitating the identification of key genes across plant species.

In strawberry, transcriptomic analyses of leaf and terminal bud (TB) samples from two cultivars ('Clery' and 'Gariguette') grown in France and Germany focused on early floral initiation. Differential gene expression analysis revealed enrichment for genes involved in carbohydrate metabolism, phytohormone pathways, and protein classes related to cytoskeleton organization, cell cycle regulation, and chromatin structure. Key floral integrators, including TFL1, SOC1, and genes linked to phytohormone regulation (*XTH23*, *PP2*, *EIN3*), were identified.

For blackcurrant, a high-quality chromosome-scale genome assembly of *R. nigrum* ('Rosenthals Langtraubige') was produced using Oxford Nanopore Technologies (ONT) and PacBio HIFI sequencing, resulting in eight pseudo-chromosomes. Integration with transcriptomic and metabolomic data revealed drought stress responses, including differentially expressed transcription factors (*bZIP*, *bHLH*, *MYB*, *WRKY*) and kinases (*PERK*, *DUF26*). Metabolomic analysis indicated increased proline and decreased organic acids under stress, suggesting metabolic adaptation.

This integrated multi-omics approach provides new insights into the genes involved in early floral initiation in strawberry and the genetic and metabolic pathways underlying drought stress responses in blackcurrant. These findings offer valuable resources for future research and potential applications in improving crop resilience and breeding strategies.

2 Zusammenfassung

Die Pflanzenproduktion wird von biophysikalischen, technologischen und sozioökonomischen Faktoren beeinflusst, wobei Klimawandel und abiotische Stressfaktoren die Pflanzenphysiologie und den Ertrag erheblich beeinträchtigen. Ein Verständnis der molekularen Mechanismen hinter Stressreaktionen und physiologischen Prozessen ist entscheidend, um die Pflanzenleistung zu verbessern. Omics-Technologien wie Genomik, Transkriptomik, Proteomik und Metabolomik bieten umfassende Einblicke in diese Prozesse.

Ziel dieser Studie war es, Multi-Omics-Datensätze zu generieren, visualisieren und integrieren, um molekulare Mechanismen bei Erdbeeren (*Fragaria* × *ananassa*) während der Blüteninitiation und bei Schwarzen Johannisbeeren (*Ribes nigrum*) unter Trockenstress zu untersuchen. Eine R-basierte Funktion wurde entwickelt, um funktionale Genannotationen in Hauptkomponentenanalyse (PCA) und Overrepresentation Analysis (ORA) zu integrieren und so die Identifikation zentraler Gene zu erleichtern.

Bei Erdbeeren zeigten transkriptomische Analysen von Blatt- und Terminalknospen-Proben aus zwei Sorten ('Clery' und 'Gariguette') eine Anreicherung von Genen, die am Kohlenhydratstoffwechsel, an Phytohormon-Signalwegen sowie an der Zellzyklusregulation beteiligt sind. Wichtige Blütenintegratoren wie *TFL1*, *SOC1* sowie Gene zur Phytohormonregulation (*XTH23*, *PP2*, *EIN3*) wurden identifiziert.

Für die Schwarze Johannisbeere wurde ein chromosomenskaliertes Genom-Assembly von *R. nigrum* ('Rosenthals Langtraubige') mithilfe von Oxford Nanopore Technologies (ONT) und PacBio HiFi-Sequenzierung erstellt. Die Integration mit transkriptomischen und metabolomischen Daten zeigte Trockenstressreaktionen, darunter differentiell exprimierte Transkriptionsfaktoren (*bZIP*, *bHLH*, *MYB*, *WRKY*) und Kinasen (*PERK*, *DUF26*). Die Metabolomanalyse zeigte eine erhöhte Prolinkonzentration und eine Abnahme organischer Säuren unter Stress, was auf eine metabolische Anpassung hinweist.

Dieser integrierte Multi-Omics-Ansatz liefert neue Erkenntnisse über die genetischen und metabolischen Signalwege bei der Blüteninitiation in Erdbeeren und der Trockenstressantwort in Schwarzen Johannisbeeren. Diese Ergebnisse bieten wertvolle Ressourcen für zukünftige Forschungsarbeiten und Anwendungen zur Verbesserung der Pflanzenresilienz und Züchtungsstrategien.

3 Introduction

3.1 Analyzing plants through omics technologies and bioinformatic tools

Crop production is a dynamic and multifaceted system influenced by biophysical, technological, and socioeconomic factors. Climate change and abiotic stressors significantly impact crop physiology and yield through the increased frequency and intensity of extreme weather events. Therefore, understanding the core mechanisms and pathways dictating reactions such as stress response and physiological development is essential for utilization and comprehensive understanding of plants within a resource-efficient framework. For this purpose, omics technologies have emerged as invaluable tools (Raza *et al.*, 2022). The term ‘omics’ refers to several methods in the field of biological sciences and includes genomics, proteomics, transcriptomics and metabolomics, among others, being widely applied (Jamla *et al.*, 2012a; Khan *et al*., 2021) and are frequently employed in conjunction, enabling a comprehensive analysis of plants at multiple molecular levels.

3.1.1 Genomics as the foundation of biological existence

The access to primary DNA sequences and how genes are encoded within the genome is a fundamental resource in biology. Genomics encompasses a comprehensive investigation of the structural organization, functional interactions, and genetic characteristics of plant genomes through processes such as sequencing, marker profiling and genetic prediction (Gilliham *et al.*, 2017; Hamilton and Buell, 2012). Plant genome sequencing is particularly challenging due to repetitive sequences, heterozygosity, transposable elements and polyploidy (Hamilton and Buell, 2012; Bolger *et al.*, 2017; Rai *et al*., 2019). Over the last decades, significant progress has been made in sequencing technologies, marked by enhanced throughput, reduced sequencing expenses, and the advent of Next Generation Sequencing (NGS) methods. These encompass short-read sequencing, exemplified by Illumina. Third-generation sequencing technologies, including PacBio single-molecule real-time (SMRT) sequencing and Oxford Nanopore Technologies (ONT) sequencing, represent an

advanced sequencing approach that addresses the limitations of short-read NGS platforms. These methods enable the generation of long-read sequences, facilitating the resolution of complex genomic regions, structural variants, and repetitive sequences that are challenging to analyze using short-read technologies (Hamilton and Buell, 2012; Bolger *et al.*, 2017). For ONT sequencing extracted DNA is forwarded to ONT library preparation and then loaded onto an ONT flow cell for sequencing. Here a single DNA strand passed through the nanopore, the different nucleobases are detected by changes in electrical conductance, and this data is used to generate the sequencing information (Figure 1).

Advancements in sequencing technologies, coupled with novel computational

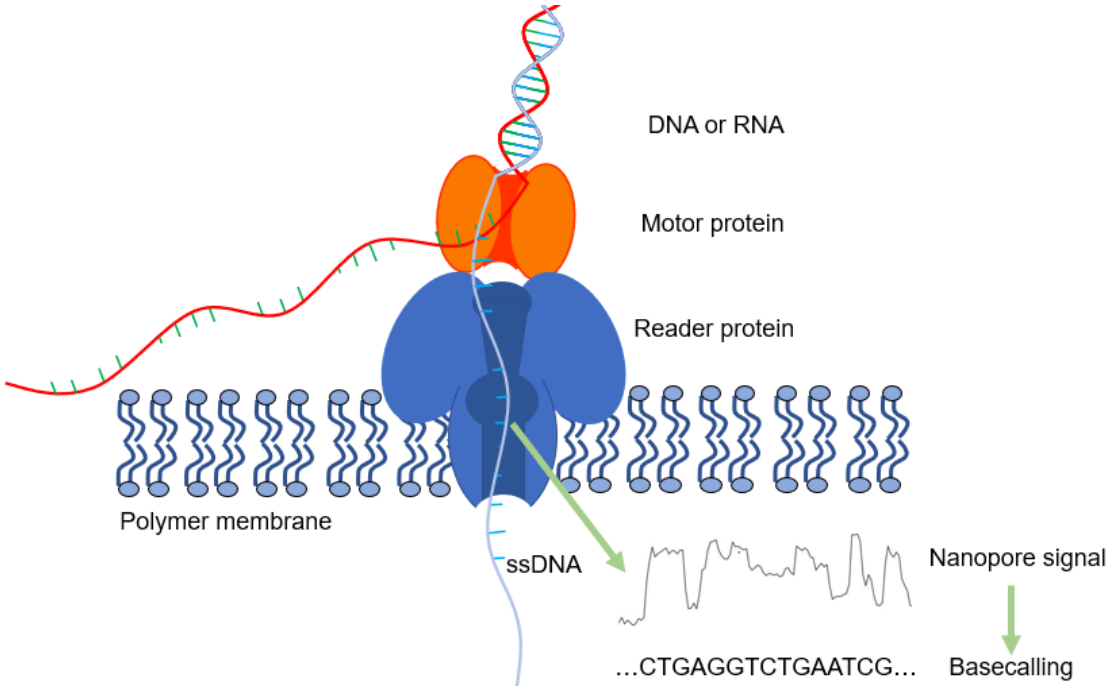

methodologies, enable the attainment of highly contiguous genome assemblies. Long read sequencing using PacBio SMART sequencing typically achieves >99.9% average read accuracy with 15-20 kb average read lengths. In contrast, ONT exhibits slightly lower average read accuracy (99.75%) but yields longer reads, ranging from 10-100 kb for long-reads and 100-300 kb for ultra-long reads (Olson *et al.*, 2021; Tan *et al.*, 2022; Marx, 2023). To compensate for the error-proneness, several toolkits and pipelines are available to build genome assemblies based on different algorithms especially for noisy ONT long-reads. In this context, assembly tools like Flye (Kolmogorov *et al.*, 2019) generate diverse

paths within an unidentified repeat graph, while Necat (Chen *et al.*, 2021) serves as an error correction and *de novo* assembly tool specifically designed for ONT reads, utilizing a rapid two-step progressive approach to correct nanopore sequencing data efficiently. Furthermore, the recently published Nextdenovo assembler corrects the reads first and then assembles them (Hu *et al.*, 2023). Additional methods to enhance assembly accuracy involve post-assembly polishing using tools like Pilon (Walker *et al.,* 2014), Racon (Vaser *et al*., 2017), NextPolish (Hu *et al*., 2019) and Medaka (https://github.com/nanoporetech/medaka). These tools utilize precise short-reads to rectify the contigs obtained from an assembly (Bolger *et al.,* 2018).

While the accuracy can be improved by pre- or post-correction, outcrossing species and clonally propagated crops are highly heterozygous, with diverse genetic elements like repetitive sequences, single nucleotide polymorphism (SNP), and structural variants across haplotypes. Long-read assembly methods can correct and distinguish divergent haplotypes, resulting in assemblies larger than the monoploid genome size, capturing the complexity of heterozygous genomes. But the resulting genomes contain a mixture of 'duplicated' regions where divergent haplotypes are assembled separately, and single copy regions with relatively few polymorphisms are sometimes collapsed into a single sequence. To avoid problems in downstream processing the duplicated regions need to be marked down (Kajitani *et al.*, 2014; Michael and VanBuren, 2020). Tools like Purge Haplotigs (Roach *et al.*, 2018), HaploMerger2 (Huang *et al.*, 2017), and purge dups (Guan *et al*., 2020) address this issue. Purge Haplotigs uses read depth and sequence similarity to find haplotigs, requiring specified depth cutoffs and lacking identification of heterozygous overlaps. HaploMerger2 identifies both haplotigs and overlaps but does not consider read depth. On the other hand, Purge dups resolve haplotig overlaps in primary assemblies using sequence similarity and read depth, automatically setting coverage thresholds. The choice of deduplication method should match the genome assembly's heterozygosity level and the combination of assembly and deduplication tool. The interplay between assembly and deduplication tools could shrink the genome size while potentially compromising completeness score

and coverage (Guiglielmoni *et al*., 2021; Zhang *et al*., 2022). Hence, it is crucial to assess various combinations to optimize results.

The final step in genome assembly is ordering and orientating the assembled sequences to form chromosomal pseudomolecules. This step is called scaffolding and is crucial for downstream analyses such as marker-assisted breeding, genotype-phenotype associations and chromosome evolution. The reconstruction of chromosomes can be achieved by using guided marker sequences from independently determined genetic maps, which were utilized for scaffolding of *Arabidopsis thaliana* and rice genomes (Kaul *et al.*, 2000; Goff *et al.*, 2002; Yu *et al.*, 2002). Recent technologies for fast and accurate scaffolding of plant genomes are BioNano optical maps and chromatin conformation capture technique (Hi-C) (Yuan *et al.*, 2020). Hi-C relies on chromatin proximity ligation, detecting long-distance DNA interactions to establish linkage between contigs (Bolger *et al.*, 2018; Pal *et al.*, 2019; Kong *et al.*, 2023; Luo *et al.*, 2021). Hi-C and similar derived techniques have become a standard procedure, particularly for complex polyploid genomes (Zhang *et al.*, 2018; Chen *et al.*, 2020; Kong *et al.*, 2023). ONT recently introduced Pore-C, a method combining chromatin conformation capture and nanopore sequencing of concatemers (Deshpande *et al*., 2022). Unlike other Hi-C approaches using short-read-based chromatin structure and generating pairwise data, Pore-C relies on long reads. This technique enables researchers to explore close-range interactions within high-order chromatin structures across the entire genome (Deshpande *et al*., 2022). Furthermore, integrating long-read sequencing data into genome assembly pipelines can substantially enhance the quality and contiguity of assembled genomes, enabling reconstruction at the chromosome level or achieving telomere-to-telomere completeness. It supports scaffolding contigs by providing long-range connectivity information, making it easier to order and orient the contigs into larger, more accurate scaffolds. This was already shown in Mari *et al.* (2024) where Pore-C data robustly validated the haplotype concordance of the haplotype *Solanum tuberosum* assembly.

Following the genome assembly, DNA sequence annotation involves the identification of functional elements across the genome. Gene prediction is

primarily approached through two main methods: extrinsic and intrinsic. Extrinsic methods identify genes based on similarities to known sequences, enhancing accuracy by incorporating diverse biological evidence, like RNA sequencing or protein homology (Cho and Walbot, 2001; Mathé *et al*., 2002). Intrinsic methods solely analyze inherent DNA patterns without external data, potentially limiting their scope but offering direct genomic analyses (Fickett, 1996; Borodovsky *et al.*, 1994; Mathé *et al*., 2002). These tools vary in their algorithms, reliance on external data, and accuracy levels. Often, a combination of intrinsic and extrinsic methods can provide more accurate gene predictions by leveraging both sequence features and external evidence. Gene prediction tools such as AUGUSTUS/ BRAKER2 (Hoff *et al.,* 2016) employ hidden Markov models (HMMs) and incorporate RNA-Seq data and protein homology. Additionally, GeneMark-EP+ combines unsupervised and supervised machine learning with RNA-Seq data, while Helixer has also been available for gene prediction, primarily relying on ab initio algorithms to predict genes based on intrinsic sequence features (Stiehler *et al*., 2020). This process is crucial because the functions of DNA sequences remain unknown at this stage. Upon the completion of structural annotation, biological functions can be assigned to each gene. To streamline this process, various tools have been developed that automatically annotate genes using ontologies. Examples of such tools include MapMan (Lohse *et al.*, 2014), Blast2Go (Conesa and Gotz, 2008), and the KEGG Automatic Annotation Server (Moriya *et al*., 2007). These tools aid in the efficient and automated functional annotation of genes by assigning relevant biological functions.

3.1.2 Transcriptome: The next level

The genome serves as the genetic foundation, whereas the transcriptome furnishes insights into genetic responses, e.g. induced by environmental stimuli or the genetic processes at specific developmental stages. In conjunction with the enhancement of DNA sequence data through transcript data, transcriptome sequencing has emerged as a highly prevalent technology in contemporary biology. It is widely employed to investigate both model and non-model organisms, facilitating the analyses of functional genes and regulatory

mechanisms in plants. Through the application of transcriptome sequencing, advancements in biological research, plant breeding, and selection techniques can be achieved, contributing to the improvement of crops and plant-based agricultural practices (Cao *et al.*, 2019; Guo *et al.*, 2021).

The field of gene expression profiling has witnessed a profound revolution in the last two decades. This transformation can be attributed to significant advancements in transcriptome sequencing and analyses technologies. As a result, a diverse range of molecular techniques for expression profiling and transcription quantification has emerged, demonstrating remarkable achievements in the field (Nejat *et al.*, 2018). The ONT platform offers a high throughput capacity and long read lengths at a cost-effective rate, making it an advantageous choice. Visualization of such data sets refers to the graphical representation and analyses of data related to gene expression at the transcript level. Visualizing transcriptomic data is crucial for understanding gene expression patterns, identifying differentially expressed genes, and gaining insights into the molecular mechanisms underlying various biological processes. Visualizing this data often begins with the creation of expression profiles, showing the abundance of RNA transcripts for each gene across different samples, conditions of time points through Whisker-Box Plots, heatmaps or volcano plots. But having large data sets with plenty of genes, the selection of single genes to plot through different samples or conditions is difficult. Therefore, functional annotation of the genes is essential. Specialized databases, including Gene Ontology (GO) and KEGG pathway annotations, along with functional annotations using the Mercator/MapMan framework, can be utilized for comprehensive functional characterization. Based on this annotation, enrichment plots, network diagrams or pathway analyses can be performed. Additionally, dimensional reduction techniques such as PCA, t-distributed stochastic neighbor embedding (t-SNE) or uniform manifold approximation and projection (UMAP) are used to reduce high-dimensional transcriptomic data while preserving important relationships (van der Maaten and Hinton, 2008; McInnes *et al.*, 2018; Huang *et al.*, 2022). Transcriptome analyses with RNA-Seq data serves as a valuable scientific approach to investigate specific pathways and mechanisms, such as those related to drought stress or developmental stages.

3.1.3 Metabolomics: A biological response

The metabolome refers to the collective profile of metabolites within an organism, an organ, a tissue or even an individual cell. It is sensitive to environmental conditions and varies along developmental phases and reflects the status of a specific time point and prevailing conditions, if measurements are not taken as time series (Alonso *et al*., 2015; Kumar *et al.*, 2017). The emerging discipline of analyzing the metabolome at a certain time and under specific physiological conditions is called metabolomics. Metabolites are compounds that act as intermediate or end products arising from a cascade of enzymatic reactions. These molecules play a crucial role in providing valuable insights into an organism's biochemical activity (Alonso *et al*., 2015). Metabolites are classified into primary and secondary metabolites. Primary metabolites including sugars, fatty acids, and amino acids play a fundamental role in growth, development and reproduction of organisms and contribute to essential physiological processes. In contrast, secondary metabolites do not play an essential role but are involved in specialized functions such as defense mechanisms, reproduction, defense and adaptation to stressors (Roessner *et al.*, 2001; Roessner *et al.*, 2002; Shulaev *et al.*, 2008). In general, metabolomic studies enhance plant breeding by identifying biochemical markers, elucidating plant stress responses, and improving nutritional quality.

One of the most popular method applied in metabolomics is gas chromatography-mass spectroscopy (GC-MS) (Patel *et al.* 2021; Shulaev *et al.*, 2008), further techniques are liquid chromatography-mass spectroscopy (LC-MS) or nuclear magnetic resonance (NMR). GC-MS is widely used to detect compounds like sugars, organic acids, amino acids, alcohols, amines, terpenes, and fatty acids. In contrast, LC-MS is used for non-volatile compounds with higher separation efficiency and throughput (Giri *et al.,* 2007). Various metabolites are identifiable across diverse platforms, yet employing a range of analytical tools is key to reveal the spectrum of compounds synthesized by plants (Ma and Qi, 2021).

Metabolomic analyses can further be classified by their technical approach depending on the target of the study. It is mainly divided into complementary

approaches, such as untargeted and targeted metabolomics. Untargeted metabolomics strives for a thorough profiling of diverse metabolites in a biological sample, encompassing both known and unknown compounds. In contrast, targeted metabolomics aims at quantifying and identifying a predetermined set of established metabolites (Bhalla *et al.*, 2005; Mihailova *et al.*, 2021). Identified metabolites are annotated using spectral mass databases like NIST (https://www.nist.gov/pml/atomic-spectra-database), PMN (https://www.plantcyc.org/), MetaboLights (https://www.ebi.ac.uk/metabolights/), METLIN (Smith *et al.,* 2005) or SIRIUS (Böcker *et al.*, 2009), along with information on biochemical reactions found in databases like KEGG (https://www.genome.jp/kegg/; Ogata *et al.*, 1999), MetaCyc (https://metacyc.org/; Karp and Caspi, 2011), WikiPathways (https://www.wikipathways.org; Martens *et al.,* 2021) and PlantCyc (https://plantcyc.org; Hawkins *et al.*, 2021, Ma and Qi, 2021).

3.2 Integration of multi-omics data

For complex networks of biological regulation, the full potential of omics is tapped when combining them for the comprehensive characterization of specific biological phenomena (Yang *et al.*, 2023; Kumar *et al*., 2023). Genomic and transcriptomic analyses can directly aid in plant breeding by identifying and manipulating genes and gene expression patterns. Proteomic approaches enable the identification of plant proteins, and provide insights into changes in protein expression in response to various factors, such as environmental stresses. In contrast, metabolomic analysis reveals the end products, such as human health-beneficial compounds. Furthermore, epigenomics focuses on epigenetic modifications, which affect gene expression without altering the DNA sequence. Integrating multiple omics techniques bridges gaps between findings. McLoughin *et al.* (2018) combined mRNA-Seq and protein abundance analyses to identify organelles, protein complexes, and individual proteins, uncovering autophagic substrates in maize autophagy mutants. A multi-omics approach with integrated network analysis was used to reveal system relationships between structural genes, transcriptional regulators and metabolites in developing grape berries exposed to water deficit (Savoi *et al*. (2017). Each omics approach individually

possesses considerable efficacy, but a combination of them exponentially increases the possibilities to draw conclusions on biological questions elucidating a holistic picture of processes that happen in a plant at molecular level. By integrating different approaches to a multi-layer study, a more profound understanding of molecular mechanisms and gene-phenotype relationships can be achieved in response to scientific inquiries (Raza *et al*., 2020; Mahmood *et al*., 2022). This process can be particularly difficult as it needs multiple steps of data evaluation such as prioritizing candidate genes, hypothesizing the mechanisms by finding data types such as gene-phenotype associations, expression/ co-expression information and protein-DNA interactions (Hassani-Pak and Rawlings, 2017; Weighill *et al.*, 2017).

The underlying information is often distributed across several databases from various sources that might lack interoperability, leading to difficulties in the integration of plant data due to their metabolic diversity and poorly annotated larger genomes, especially for non-model species (Jamil *et al.*, 2020). In general, integration of methods can be divided into three main groups such as detecting biomarkers, classifying samples, and inferring functional relationships between the molecular levels. Strategies for data interpretation such as element-based, pathway-based and mathematical-based approaches lead to more refined correlations (Jamil *et al.*, 2020). The element-based approach is divided into correlation algorithms such as the univariate analysis methods of Pearson (Benesty *et al.*, 2009) or Spearman, where significant results suggest strong relationships between datasets and clustering which allows grouping of datasets using e.g. k-means or random forests regression. Additionally, multivariate analysis allows using more complex data sets with greater flexibility employing techniques such as PCA, partial least squares (PLS) or orthogonal projection to latent structures discriminant analyses (OPLS-DA) (Silva *et al.*, 2017; Ye *et al.*, 2017; Wang *et al*., 2016; Acharjee *et al*., 2016; Ma *et al.*, 2014; Silva *et al.,* 2019). In terms of genomics and transcriptomics, overrepresentation and enrichment analyses are widely used. These are versatile tools to identify involved biological processes. However, they might be limited due to the lack of comprehensive annotations (Liu *et al.*, 2022). The pathway-based approaches can be divided into pathway-mapping with tools such as PathVisio (Kutmon *et al.,* 2015), KEGG

or MapMan and weighted interaction networks such as Co-expression or tools such as Cytoscape (Shannon *et al.*, 2003) (Bjornson *et al*., 2017; Zhu *et al.,* 2018; Lòpez-Hidalgo *et al*., 2018; He *et al.*, 2018; Jiang *et al.*, 2019). The mathematical approach encompasses both differential and genome-scale methods, which can be utilized to predict metabolic responses across various environments or stress conditions, optimize plant breeding strategies, and identify novel target genes for genetic modifications. Here, the differential approach, flux balance analyses or ordinary differential equation are used, while flux variability analyses and tools such as PlantSEED (Seaver *et al.*, 2018) and MetNetDB (Wurtele *et al.*, 2003) are used (Soubeyrand *et al.*, 2018; Wang *et al.*, 2018, Scheunemann *et al.*, 2018; Li *et al*., 2015; Bogart and Myers *et al*., 2016). Limiting factors for the differential approach are the lack of flexibility by the statistical analyses due to absence in the available map and by pathway boundaries. These are based on curators' decisions and by the number of molecular features included in the maps, which may not cover the measured features or belong to multiple features (Liu *et al.,* 2022). Concluding, the integrative omics technologies produce a massive amount of data and thus an effective methodological approach is needed to relate the data to the research objectives and find connections in between.

3.3 Application of omics technologies

Each omics layer offers distinct insights into plant physiology and metabolism. As previously mentioned, transcriptome sequencing facilitates progress in biological research, plant breeding, and selection strategies, thereby aiding in the optimization of crops and the improvement of plant-based agricultural practices. The integration of multi-omics data thus serves as a powerful bridge between cutting-edge molecular insights and tangible improvements in plant production strategies. Optimizing plant production extends beyond traditional methods, converging with a focus on utilizing secondary metabolites. These compounds, intricately linked to plant defense and adaptation, shape crop resilience and contribute to nutritional and medicinal value.

Plants such as berries play an economically important role as fruit crops worldwide, representing an invaluable source of vitamins, minerals, and human

health-promoting secondary compounds like flavonoids and polyphenols (López *et al.*, 2021). In the family of *Rosaceae* apple, cherry and strawberry are the most important crop fruit species. They show a high economical value and popularity with high diversity within natural and breeding populations with regard to important traits such as yield, fruit size, color and flavor (Carbone *et al.,* 2009) and are also the best studied species.

3.3.1 Transcriptomics in strawberry

The floral initiation is a pivotal event in the life cycle of angiosperm plants and has a substantial influence on crop yield. This transition from vegetative to reproductive phases occurs in the shoot apical meristem (SAM), which generates leaves, shoots and flowers (Benlloch *et al.*, 2007; Figure 2A). Flowering plays a critical role in a plant's reproductive success, significantly impacting pollination and fruit production (Weberling 1989; Wyatt, 1982).

Strawberry (*Fragaria ×ananassa*) is the most cultivated berry worldwide. In this species, fruit yield depends on timing and duration of floral initiation (Costes *et al.*, 2014). Most strawberry genotypes are seasonal flowering (SF), also referred to as 'short-day,' 'single cropping plants,' or 'June-bearing'. They show a single period of production in spring in year N. The floral initiation occurred the previous autumn in year N-1 and is triggered by decreasing temperatures and day length, which corresponds to the end of summer – beginning of autumn (Heide *et al.,* 2013; Figure 2). Floral initiation is followed by floral development with the organogenesis of flowers, which compose the inflorescence. Following dormancy and the fulfillment of chilling requirements, the flowers initiated in autumn emerge in spring.

In addition, strawberry can reproduce asexually via stolons, which are elongated stems bearing daughter plants (Tenreira *et al.*, 2017). The trade-off between sexual and asexual reproduction takes place in the axillary meristem (AXM), which can produce either an inflorescence-bearing branch or a stolon and determines two antagonist traits: fruit yield, a major trait for producers; and daughter-plant yield, a major trait for nurseries (Tenreira *et al.*, 2017; Gaston *et al.*, 2021).

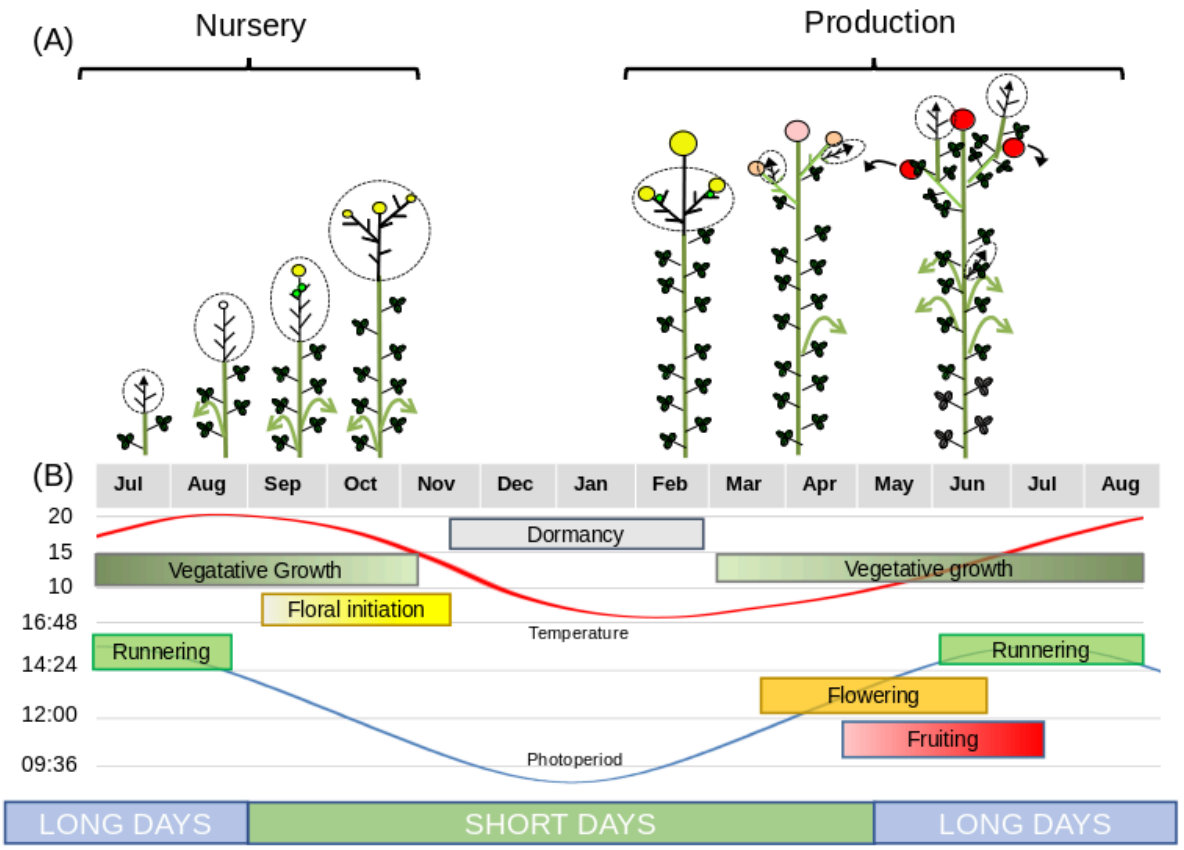

Figure 2: Schematic illustration of the different developmental processes in seasonal flowering (SF) cultivated octoploid strawberry. (A) Along nursery, temperatures and photoperiod decrease, allowing the floral initiation to occur. The shoot apical meristem (SAM) which was vegetative (arrow) became floral (yellow sphere). Because strawberry is a rosette, the terminal bud (TB) is not visible and represented here inside the dotted line on the bottom of the plant. (B) Runnering occurs on long days. Dormancy occurs during the end of autumn and winter when temperatures do not allow the vegetative development. Circle with a dotted line indicates the terminal bud, that includes the terminal meristem and foliar primordia. (taken from Ziegler et al., 2025)

The interplay of photoperiod, temperature, and their combined influence on floral initiation have been extensively documented (Stewart and Folta 2010; Heide *et al.* 2013). Experimental investigations were meticulously conducted under controlled environmental settings, ensuring that plants were maintained in non-inductive conditions until they were transferred to conditions that favor floral initiation (Durner *et al.*, 1984; Verheul *et al.*, 2006; Sønsteby and Heide, 2008). Notably, to keep non-initiated plants, they were maintained under long-day conditions, which exhibit a pronounced inhibitory effect on floral initiation (Vince-Prue and Guttridge, 1973). To specify temperatures, photoperiods and their interaction that promote floral initiation, Heide *et al*. (2013) collated the

results of a large number of studies. The overarching consensus from these observations suggests that optimal conditions for floral initiation involve temperatures ranging from 12 to 18°C and photoperiods of 10 to 12 hours, maintained over a period of 3 to 4 weeks. Variations in these parameters are mainly due to cultivar-specific responses (Verheul *et al*., 2006).

In strawberry, thanks to the considerable advances in the genetic and molecular control of flowering, flowering pathway genes modulating floral initiation and plant architecture and yield have only recently begun to be deciphered (Hytonen and Kurokura, 2020). The CENTRORADIALIS/TERMINAL FLOWER 1/SELF-PRUNING (CETS) family, represented by *FT/TFL1* genes, assumes a pivotal role in maintaining this equilibrium and plays a crucial role in regulating floral initiation and reproductive development (Wickland and Hanzawa, 2015; Kurokura *et al*., 2017; Gaston *et al*., 2021). In the context of woody strawberries (*F. vesca*) a natural mutation affecting the floral repressor *FveTFL1* (*tfl1*) results in perpetual flowering (PF) (Iwata *et al*., 2011; Koskela *et al*., 2012). The role of this floral repressor has been confirmed in the cultivated strawberry (Koskela *et al*., 2016). Furthermore, tfl1 was found to be involved in floral initiation of cultivated strawberry cv. ‘Benihoppe’ (Liang *et al.*, 2022). Three *FTs* have been identified in the FT/TFL1 family. FveFT1 has been shown to function as a long day floral activator in the *tfl1* genetic background (Koskela *et al*., 2012; Rantanen *et al*., 2014). FveFT2 serves as a non-photoperiodic florigen (Gaston *et al*., 2021) and operates in tandem with the photoperiodic antflorigen, *FveTFL1* (Gaston *et al*., 2021). Overexpression of *FveFT2* leads to very early flowering phenotype. *FveFT3* has not been identified as a florigen despite its possible role as a floral inducer in flowering in the octoploid cultivated strawberry (Koembuoy *et al*., 2020). The overexpression of *FveFT3* promotes increased plant branching when overexpressed in a genetic background with *tfl1* mutations, likely by influencing AXM fate.

The regulation of flowering is closely associated with stolon production in strawberries. Gibberellin biosynthesis and signaling play a critical role in determining plant architecture and fruit yield by directing whether the axial meristem forms a stolon or an inflorescence-bearing branch crown (Tenreira *et*

al., 2017; Caruana *et al.*, 2018). A natural mutation in *FveGA20ox4* results in a runnerless phenotype (Tenreira *et al.*, 2017), which can be reversed by mutating *FveRGA1* (*REPRESSOR OF GIBBERELLIC ACID1*), a gene encoding a DELLA protein (Caruana *et al.*, 2018). Despite these insights, the molecular mechanisms regulating the balance between sexual and asexual reproduction in the axial meristem remain poorly understood.

The molecular regulation of floral initiation in cultivated strawberry (*Fragaria* × *ananassa*) under natural conditions has not yet been extensively characterized. In this study, we investigated the early molecular events underlying floral initiation through transcriptomic analysis, considering both genetic and environmental influences. We analyzed two cultivars—Clery (CL) from Italy and Gariguette (GA) from France—at two different locations, one in France and the other in Germany. RNA-Seq data were collected from leaf and terminal bud tissues during the transition from the vegetative phase to the early stages of floral initiation in the shoot apical meristem (SAM) at weeks 29, 32, 33, and 35. As expected, both cultivars exhibited an enrichment of differentially expressed genes (DEGs) during early floral initiation. These DEGs encoded proteins not only involved in flowering regulation but also associated with chromatin organization, cytoskeletal dynamics, serine/threonine phosphatase signaling, cell division, cell wall modification, and RNA biosynthesis.

3.3.2 A multi-omics approach in blackcurrant

Beyond the Rosaceae family, berry crops from the Grossulariaceae family produce widely consumed fruits and exhibit significant diversity in natural breeding populations. This diversity extends to berry traits, resistance to abiotic and biotic stresses, and adaptation to various environmental conditions, making them valuable for crop improvement and breeding programs. Blackcurrant (*Ribes nigrum* L.) is a winter-hardy shrub (family: *Grossulariaceae*) grown in temperate regions that is primarily cultivated for its edible berries. These are associated with several health benefits reflecting the high levels of vitamin C, anthocyanins, antioxidants and flavonoids (Mitchell *et al.,* 2011). However, drought stress caused by climate change impairs plant growth and development, and seriously affects crop production and yield. Under drought stress conditions during

flowering, certain blackcurrant cultivars experience diminished flower biomass and increased flower abortion, resulting in decreased commercial yield during harvest (Yang *et al.*, 2021; Čereković *et al.*, 2013).

Drought stress influences multiple biochemical and physiological processes at the cellular and whole-plant levels (Bhargava and Sawant, 2012), including growth, membrane integrity, pigment content, osmotic adjustment, water relations, and photosynthetic activity (Yang *et al.*, 2021; Anjum *et al.*, 2011). It also promotes senescence, which is necessary for plant survival. Leaf senescence requires the combined activity of phytohormones and transcriptional factors such NAC, AP2/ERF and WRKY, which are modulated by ethylene (Munné-Bosch and Allegre, 2004; Jan *et al.,* 2019). One of the key phytohormones that mediates drought stress responses and tolerance is abscisic acid (ABA), which regulates stomatal closure and the expression of stress response genes (Cutler *et al.,* 2010). Roots transmit information about water deficit to the leaves, where ABA accumulates in the vasculature (Kuromori *et al.,* 2018; Takahashi *et al.,* 2020). Drought stress is also regulated by calcium signaling, reactive oxygen species (ROS) and phytohormone translocation (Choi *et al.,* 2017). Furthermore, plants synthesize and accumulate osmolytes such as soluble carbohydrates, proteins, free amino acids, glycine betaine and proline, to increase their osmotic potential at the cellular level (Kishor *et al.,* 2005; Ozturk *et al.,* 2020).

Multiple omics analyses of drought stress responses have focused on the model and several major crops such as rice (Lawas *et al.*, 2018), chickpea (Awasthi *et al.*, 2017) and maize (Farooqi *et al*., 2022) their relatives. Additionally, drought stress effects on non-model species such as *Solanum lycopersicoides* (Powell *et al*., 2022) or grape berries (Hewitt *et al.*, 2023) were reported. However, significantly less data is available for currants. Indeed, only two studies have considered drought stress in blackcurrants. Čereković et al. (2013) compared irrigated and non-irrigated specimens of cvs. ‘Narve Viking’ and ‘Ben Gairn’ after 12 days of treatment and 17 days of recovery, revealing that drought stress reduced the cumulative evapotranspiration of both cultivars during flowering due to stomatal closure and reduced leaf area. The same authors also

investigated the effect of drought on gene expression in the leaves of Ben Gairn plants (Čereković *et al.*, 2015), discovering more than 2000 differentially expressed genes during drought treatment based on a custom *Ribes* microarray. In this context, various transcription factors, including bZIP, WRKY, MYB, and zinc finger, were identified up- and downregulated. Additionally, genes associated with the cell wall and cell cycle belonging to the cytochrome P450 family, gibberellin-regulated family, and 2-oxoglutarate superfamily were detected up- and downregulated. Although this provided initial insights into the molecular basis of drought stress in blackcurrant, the specific functions of many genes remain unknown.

The blackcurrant transcriptome was analyzed in more detail by Russell *et al.* (2011), who identified transcriptome-based markers from blackcurrant leaf buds and mapped them to parental genotypes of a reference mapping population using 454 sequencing. Jarret *et al.* (2018) assessed blackcurrant fruit at different developmental stages for changes in gene expression and for variation in metabolite content and used RNA-Seq data to create a *de novo* transcriptome assembly. A transcriptome assembly based on blackcurrant fruit was then published by Thole *et al.* (2019) and the transcriptomic response of blackcurrant cultivar Aldoniai to the blackcurrant reverse virus infection was studied by Mažeikienė et al. (2022) and Juškytė et al. (2022). However, despite the shortcomings of transcriptome assemblies, only a chloroplast genome (Sun *et al.*, 2023) but no reference genome for the family Grossulariaceae or the genus *Ribes* (Chiche *et al.*, 2003) is currently available.

3.4 Aims of this thesis

The objective of this study was to generate, analyze, visualize, and integrate diverse omics datasets to gain comprehensive insights into complex biological systems of strawberry and blackcurrant. Omics technologies, such as genomics, transcriptomics, and metabolomics, generate large-scale data sets that provide a holistic view of biological processes. The objective was to utilize omics data, visualization methods for a comprehensive understanding of the molecular mechanisms occurring in *F. ×ananassa* cv. ‘Gariguette’ and cv. ‘Clery’ during the floral initiation for French and German populations. By establishing an exemplary

ONT Pore-C pipeline on *S. tuberosum*, we laid the foundation to achieve pseudo-chromosome level assembly for the *de novo* genome of *R. nigrum.* Followed by the integration of transcriptomic and metabolomic data, we gained valuable insights into the molecular processes involved in blackcurrant plants under drought-induced stress.

A standardized method to integrate gene functional annotation into dimensional reduction for evaluating the influence of protein groups on sample separation remains limited. To address this, we developed an R function that incorporates protein function data from plant organisms into PCA, facilitating the visualization of RNA-Seq sample differentiation. This integration relies on the analyses of differentially expressed genes and their Mercator annotation file using ORA. This approach facilitated a comprehensive overview of different treatments and allowed for the identification of significant gene clusters. Transcriptomic data visualization and evaluation was done for strawberry leaves and meristem samples. The aim was to examine the early molecular event of floral initiation by checking the stage of the SAM into the terminal buds. We tested two distinct cultivars, namely, 'Clery' (Italian variety, CL) and 'Gariguette' (French variety, GA), at two locations, one in France and one in Germany. The previously established PCA/ORA plot will be utilized to initially grasp the distribution of individual treatments, like location, genotype, and tissue. The results were then used to identify genes associated with floral initiation or early organogenesis to gain insights on the molecular mechanisms of floral initiation in strawberry.

The final section of this thesis focuses on the integration of genomic, transcriptomic, and metabolomic data for *R. nigrum* under drought-stress. To accomplish this, we generated a partially haplotype-resolved chromosome-scale genome assembly of blackcurrant (*R. nigrum* L. cv. ‘Rosenthals Langtraubige’) relying on a hybrid ONT long-read and PacBio HIFI sequencing. The chromosome scale genome with eight pseudo-chromosomes was then used to investigate drought stress effects in ‘Rosenthals Langtraubige’ leaves and roots at transcriptomic and metabolomic levels. Our results could help to optimize production, breeding and cultivation of blackcurrant and other *Ribes* species such as redcurrant or gooseberry.

4 Material and Methods

4.1 Visualization of omics results

Effective visualization of omics data is essential for interpreting complex, high-dimensional biological datasets and identifying meaningful patterns. Principal component analysis (PCA) is a widely used dimensionality reduction technique that facilitates the identification of major sources of variation and the clustering of samples. In this study, a combined visualization approach was developed, integrating PCA with overrepresentation analysis (ORA) to annotate functional gene categories that contribute to sample separation in RNA-Seq data.

The function enables the visualization of RNA-Seq data from differentially expressed gene (DEG) analyses by combining PCA and ORA based on MapMan annotations for plant datasets. Users must first generate a MapMan annotation for the reference transcriptome or proteome and analyze the RNA-Seq data using software such as *edgeR* (Robinson *et al.*, 2010). The resulting data is used to produce graphical outputs, log files, and tables summarizing the PCA and ORA results.

4.1.1 Implementation

The PCA-ORA plot is an open-source function on Github (https://github.com/fZiegle/PCA-ORA_plot) implemented in R v4.2.3 (R Core Team, 2023). The function incorporates other R packages, including *dplyr* v1.1.2 (Wickham *et al.*, 2023), *stringr* v1.5.0 (Wickham, 2022) and *RColorBrewer* v1.1-3 (Neuwirth, 2022) PCA and ORA calculation and visualization. The plotting is done in the base R graphic system.

As case studies, RNA-Seq data of strawberry (chapter 4.2.1.2) and blackcurrant (chapter 4.2.3.8) were used.

4.2 Evaluation of multi omics data

Single-omics technologies, including genomics, transcriptomics, and metabolomics, provide comprehensive insights into plant biology and are crucial for investigating processes such as developmental transitions and stress responses. Integrating these approaches enables a more holistic understanding

of complex biological mechanisms. In this study, transcriptomic analysis was conducted to examine gene expression dynamics in cultivated strawberry (*Fragaria x ananassa*) during floral initiation in leaf and terminal bud tissues. Additionally, an integrated multi-omics approach combining genomic, transcriptomic, and metabolomic analyses was applied to blackcurrant (*Ribes nigrum*) to elucidate drought stress responses in leaf and root tissues.

4.2.1 Transcriptomic response of floral initiation stage in *F. ×ananassa*

4.2.1.1 Plant material and floral initiation timing

The timing of floral initiation was determined by non-invasive architectural analysis of the *Fragaria* × *ananassa* cultivars Gariguette (GA) and Clery (CL), discriminating between the vegetative and floral stages of the shoot apical meristem (SAM) in the terminal bud. Plant architecture assessments were conducted over time throughout the summer and autumn at two locations: Bordeaux in France and Geisenheim in Germany. The first samples were collected in mid-July (T0, w29), coinciding with the presence of daughter plants featuring only small root primordia on stolons. Subsequent sampling took place in August (w32), 3 weeks after the transplantation of rooted plants to the field or nursery, and at 10-day intervals until early October (w40), making eight sampling dates in total.

Plant architecture was assessed as previously described (Krüger *et al.*, 2022). Briefly, we described the daughter plants (including the number of developed leaves and the stage of the terminal bud) using a stereomicroscope with 40–60× magnification. A single terminal bud from the main crown of each plant was dissected for analysis (Supplemental Material Figure 1A). We dissected 9–12 plants representing each cultivar and environment at each sampling date. The vegetative or floral status of the terminal buds was assessed as previously

described (Krüger *et al*., 2022) as adapted from earlier methods (Jahn and Dana 1970; Taylor et al., 1997). The data was kindly provided by Béatrice Denoyes, Amèlia Gaston (INRA*e,* France) and by Erika Krüger, Bastienne Brauksiepe and Klaus Eimert (University of Geisenheim, Germany) on context of the GoodBerry project.

4.2.1.2 Processing of RNASeq data

Adaptors were removed from the Illumina RNA-Seq dataset using Trimmomatic v0.38 “SE -phred33 ILLUMINACLIP:TruSeq3-SE:2:30:10 LEADING:3 SLIDINGWINDOW:4:15 MINLEN:40” (Bolger *et al.*, 2014) followed by alignment to the Fragaria_ananassa_v1.0.a2 cv. Camarosa reference genome (GDR database https://www.rosaceae.org; Liu *et al.* 2021) using the pseudo-aligner Salmon v1.10.1 with default settings for read count quantification (Patro *et al*., 2017). DEGs were identified using *edgeR* v3.40.1 (Robinson *et al.*, 2010). Contrasts were calculated between the different sampling points (T0, T10A, T10B and T50) and cultivars separately for both tissues. The transcripts per million (TPM) were evaluated by PCA, and ORA was applied to the PC1 and PC2 axes. This provided insights into the leading MapMan (Schwacke *et al*., 2019) protein classes contributing to the separation along PC1 and PC2 in positive and negative directions. The outcomes were visually represented as bar charts illustrating the enrichment factor along these axes. The top five genes in both directions along PC1 and PC2 were also depicted on the PCA plot. Venn diagrams were generated to identify shared DEGs in different comparisons using VennDiagram v1.7.3 (Chen and Boutros, 2011) in R. A threshold of FDR < 0.05 was used to filter significant DEGs. Heat map clustering was applied to discern gene relationships within each tissue.

4.2.1.3 Gene correspondence and functional analysis

To link our work to the published literature (Li *et al.*, 2019; Liang *et al.*, 2022), we matched gene names between the current Camarosa *F.* × *ananassa* annotation (v2) and the diploid genome of *F. vesca* or the Camarosa v1 annotation used by Liang *et al.* (2022). The genes were checked bidirectionally against the diploid transcriptome of *F. vesca* and *F.* × *ananassa* cv. Camarosa using Blast+ v2.15.0 (Camacho *et al.*, 2009). We focused on the DEGs in our study and applied ORA to the overlapping genes to identify MapMan protein classes that potentially influence floral initiation. Statistical analysis was carried out using R Studio base version 2023.06.0 (RStudio Team, 2023).

4.2.2 Generating Pore-C data for *S. tuberosum* cv. 'Altus' as example

4.2.2.1 Potato Plant Material and sample collection

A potato plant (*Solanum tuberosum* cv. 'Altus') was grown from a tuber under long-day conditions at 22 °C in the greenhouse of Heinrich-Heine University of Düsseldorf. After four weeks (30.03.2023), young leaves were harvested and immediately flash-frozen in liquid nitrogen for subsequent Pore-C analysis.

Additional young leaf samples were similarly collected and flash-frozen on 04.07, 04.08, 18.08, and 23.08.2023 for Pore-C analysis.

4.2.2.2 Pore-C library construction

RE-Pore-C libraries were prepared according to the ONT Plant Pore-C protocol using the restriction enzyme DpnII. The enzyme was heat-denatured after overnight incubation and crosslinked DNA clusters were ligated in proximity. The protein was then degraded and decrosslinked, releasing the chimeric Pore-C dsDNA polymers. DNA degradation and contamination were monitored by 1% agarose gel electrophoresis. DNA purity was checked using a NanoDrop spectrophotometer (Thermo Fisher Scientific, Waltham, MA, USA) and the DNA concentration was determined using the Qubit DNA Assay Kit and a Qubit fluorometer (Thermo Fisher Scientific). Remaining DNA fragments were used to prepare Oxford Nanopore Technologies (Qubit DNA Assay Kit and a Qubit fluorometer (Thermo Fisher Scientific)) libraries for sequencing. Samples with a low A260/230 ratio (indicating the presence of polysaccharides) were cleaned up by phenol–chloroform (1:1) extraction and ethanol precipitation. Genomic DNA fragments were damage-repaired, end-repaired, and A-tailed using NEBNext FFPE DNA Repair Mix and the NEBNext Ultra II End Repair/A-Tailing Module. Libraries were constructed using the ONT Ligation Sequencing Kit (SQK-LSK114) and were sequenced using two R10.4.1 PromethION flow cells. The runtime was set to 100 h and the accurate speed mode (260 bps) was selected. Flowcells were flushed and reloaded after 24, 48 and 72 hours. Basecalling was performed using guppy v6.4.8 (ONT, model “super”) resulting in ~52 Gb of ONT Pore-C data.

4.2.2.3 Quality assessment Pore-C data

The quality of the generated Pore-C data was assessed by using a similar pipeline to wf-pore-c (EPI2ME Labs, 2024) that was developed by ONT. Initially, basecalled reads were processed using pore-c-py v2.0.6 (https://github.com/epi2me-labs/pore-c-py) digest with default settings and restriction enzyme DpnII. Resulting reads were aligned to the haplotype resolved genome assembly of *S. tuberosum* generated in Mari *et al.* (2024) employing Minimap2 v2.24 (Li, 2018; Li, 2021) with default settings for ONT data (“-ay -x map-ont”). After alignment, annotation of monomer sequences was done using pore-c-py v2.0.6 “annotate” with parameters “--monomers --stdout true --summary”. Then spurious alignments were filtered, and ligation junctions were detected using pairtools v1.0.3 (Open2C *et al.*, 2023) command "parse2”. Restriction fragments were then assigned to pairs using pairtools command “restrict” and a matrix was prepared utilizing pairtools commands “flip” and “sort”. Optical duplicates and PCR duplicates were removed with pairtools command “dedup”. Pairtools commands were used with default settings. Resulting files were forwarded to juicer tools v1.22.01 (Durand *et al.*, 2016) to create a contact map, which was plotted using Juicebox v1.11.08 (Dudchenko *et al.*, 2018), showing the intensity of the physical interaction between genome regions. For further quality validation, the contact map in .hic format was converted to .mcool format using HiCExplorer v3.7.3 (Ramirez *et al.*, 2018) hic2cool with default settings. Resulting files were processed using HiCExplorer hicPlotDistVsCounts with default settings to show Pore-C corrected counts vs. genomic distance. Furthermore, HiCExplorer hicPlotSVL was used to create boxplots showing the relation between short- and long-range interactions.

4.2.3 Drought stress response of *R. nigrum* leaves and roots

4.2.3.1 Plant material

For DNA sequencing, young blackcurrant (*R. nigrum* cv Rosenthals Langtraubige) leaves were collected from a single adult plant and flash frozen in liquid nitrogen. For the drought stress experiments, plants in 3-L pots were irrigated with 150 mL of water per day (control) or water was withheld for 4 days (stress treatment). Root and leaf samples (three replicates per plant) were taken the morning after the last treatment day. The samples were collected by Lucas Munnes under the supervision of Freya M.R. Ziegler. Blackcurrant cv Tihope plants were grown under field conditions in Poland. Samples were taken at different developmental stages: flower initiation, dormancy induction, and dormancy release. Bud samples were collected at nine different time points, whereas leaf samples were taken at three time points during flower initiation. The samples were used for RNA deep sequencing on the Illumina HiSeq 2500 platform. Blackcurrant RNA-Seq datasets of cv Ben Gairn were generated from 20 bud samples on the same sequencing platform. The Illumina RNA-Seq datasets were provided by Anita Sønsteby, Łukasz Seliga, Sylwia Keller-Przybyłkowicz as part of the GoodBerry EU project.

Stem cuttings of *Ribes nigrum* cv. 'Rosenthals Langtraubige' were cultivated in 500 mL pots for five weeks under controlled greenhouse conditions. For the drought stress experiment, plants were initially irrigated until the soil reached full water-holding capacity. Subsequently, plants in the control group were watered to maintain 70% of pot weight based on water loss, while those in the stress treatment group received no water for a period of nine days. Leaf samples were collected the morning following the final day of treatment. RNA was extracted as described below and samples were used for RNA deep sequencing on the Illumina HiSeq 2500 platform.

4.2.3.2 DNA library construction and sequencing

DNA was extracted from 1 g of frozen leaf material using the NucleoBond HMW DNA Kit (Machery Nagel, Thermo Fisher Scientific, Waltham, MA, USA). Short fragments were separated using the Circulomics short read eliminator (SRE XL) Kit (Pacific Biosciences, Melno Park, CA, USA) with a threshold of > 40 kbp. DNA degradation and contamination were monitored by 1% agarose gel electrophoresis. DNA purity was checked using a NanoDrop spectrophotometer (Thermo Fisher Scientific) and the DNA concentration was determined using the Qubit DNA Assay Kit and a Qubit fluorometer (Thermo Fisher Scientific). Filtered long fragments were used to prepare ONT libraries for sequencing (Qubit DNA Assay Kit and a Qubit fluorometer). We used the standard ONT protocol for the SQK-LSK112 Kit. Genomic DNA fragments were repaired and 3′-adenylated using the NEBNext FFPE DNA Repair Mix and the NEBNext Ultra II End Repair/A-Tailing Module (New England Biolabs/NEB, Ipswich, MA, USA). Sequencing adapters provided by ONT were then ligated using the NEBNext Quick Ligation Module (NEB). After purification with AMPure XP beads (Beckmann Coulter, Brea, CA, USA), libraries were loaded onto primed 10.4.1 Spot-On Flow Cells and sequenced using a PromethION device (ONT) with 72-h runs. Cells were flushed and reloaded after 18 h. Basecalling was achieved using guppy v6.1.1 (ONT). PacBio sequencing of the ONT long-read sequences was carried out by Genohub (Brigham Young University, Provo, UT, USA). Filtered short-read sequences were sequenced by Genewiz (Leipzig, Germany).

4.2.3.3 Pore-C library preparation and nanopore sequencing

RE-Pore-C libraries were prepared according to the ONT Plant Pore-C protocol using the restriction enzyme DpnII. The enzyme was heat-denatured after overnight incubation and crosslinked DNA clusters were ligated in proximity. The protein was then degraded to remove crosslinks, releasing the chimeric Pore-C dsDNA polymers. DNA concentration and purity were determined as described above. Samples with a low $A_{260/230}$ ratio (indicating the presence of polysaccharides) were cleaned up by 1:1 phenol/chloroform extraction and ethanol precipitation. Genomic DNA fragments were damage repaired, end repaired, and A-tailed using NEBNext FFPE DNA Repair Mix and the NEBNext Ultra II End Repair/A-Tailing Module. Libraries were constructed using the ONT Ligation Sequencing Kit (SQK-LSK114) and were sequenced using two R10.4.1 PromethION flow cells. The runtime was set to 100 h in accurate speed mode (260 bps).

4.2.3.4 Genome assembly

After basecalling, any remaining adapters were removed from the genomic DNA using Porechop v0.2.4 (Wick *et al*., 2017) and the longest reads (> 50 kbp) were selected using Filtlong v2.9.1 (https://github.com/rrwick/Filtlong) and setting '--min_length 50,000'. The filtered ONT reads were assembled with the PacBio single-molecule real-time (SMRT) reads using hifiasm v0.19.6-r595 (Cheng *et al.*, 2022; Cheng *et al*., 2024) in hybrid mode where the nanopore data was supplied with setting '–ul' and an estimated genome size of 0.8 Gbp. For

k-mer analysis, we used Jellyfish v2.2.10 (https://github.com/gmarcais/Jellyfish) and GenomeScope (http://qb.cshl.edu/genomescope/) with default parameters (*k* = 23). PurgeHaplotigs v1.1.2 (Roach *et al.*, 2018) was used to remove duplicate sequences. The Pore-C sequences were virtually digested using pore-c-py 'digest' (https://github.com/epi2me-labs/pore-c-py) and aligned with the previously generated genome using minimap2 v2.25 (Li et al., 2018). Aligned files were annotated using pore-c-py 'annotate' in paired-end mode (with settings '--monomers --chromunity --chromunity_merge_distance -1 --paired_end --filter_pairs --paired_end_minimum_distance 100 --paired_end_maximum_distance 200') and duplicates were removed using picard v2.21.8 with setting 'MarkDuplicates' (https://github.com/broadinstitute/picard) and default parameters. The aligned Pore-C data were then used by yahs scaffolder v1.1 (Zhou *et al.*, 2022) to scaffold the contig assembly, followed by manual curation using Juicebox Assembly Tools v1.11.08 (Dudchenko *et al.*, 2018). Quality was assessed using Quast v4.6.3 (Gurevich *et al.,* 2013) and BUSCO v5 (Simão *et al.*, 2015) to provide information on assembly completeness and genome quality.

Finally, the two resulting haplotypes constructed by hifiasm were scaffolded to the haploid genome representation using RagTag v2.1.0 (Alonge *et al*., 2022) using correct and scaffold with default parameters to obtain complete chromosome scale haplotypes. Synteny and structural rearrangements were visualized using Syri v1.7.0 (Goel *et al*., 2019) with default parameters.

Single nucleotide polymorphisms (SNP) were called using Freebayes v1.3.6 (Garrison & Marth, 2012) with DNA short reads and default parameters for diploid organisms. SNPs were then annotated using SNPEff v5.2c (Cingolani *et al.*, 2012). Furthermore, SNPs were functionally annotated using MapMan protein classes, and an enrichment analysis based on these classes was conducted using R Studio (version 2023.06.0, RStudio Team, 2023).

4.2.3.5 Genome analysis

Methylated site probabilities from mapped PacBio reads were generated using pb-CpG-tools v2.3.2 (https://github.com/PacificBiosciences/pb-CpG-tools) with a threshold of 75% for methylated motifs and were plotted with gene density, GC content and TE abundance, heterozygous SNP rate, stop gained and stop lost SNP Codons in 1-Mb windows using the R circlize package v0.4.15 (Gu *et al*., 2014). Furthermore, we used the EDTA (Ou *et al*., 2019) pipeline and LTR_retriever 'LAI' v2.9.8 (Ou and Jiang, 2018), CRAQ v1.0.9α (Li *et al*., 2023) and Meryl v1.4 followed by Merqury v1.3 (Rhie *et al.*, 2020) for quality validation using the Pacbio reads.

We used blastn in BLAST v2.15.0+ (Camacho *et al.*, 2008) to compute the synteny of 73 SNPs common to the SCRI 9328 and MP7 linkage map (Russell *et al*., 2011) and our genome assembly. Quality parameters were visualized using R Studio base v2023.06.0 (RStudio Team, 2023).

The scaffolded genome assembly was annotated using Helixer v0.3.1 (Holst *et al.*, 2020) with the model 'land_plant_v0.3_a_0080.h5' and StringTie v2.2.1 (Shumate *et al.*, 2022) with RNA-Seq Illumina short-reads and cDNA nanopore RNA-Seq reads. Splice junctions were detected with Portcullis v1.2.0 (https://github.com/EI-CoreBioinformatics/portcullis) and analyzed with the Helixer and StringTie annotation results in Mikado v2.3.0 (Mapleson *et al.*, 2018).

The transcriptome and proteome were extracted from the annotated genome using Gffread v0.12.4 (Pertea and Pertea, 2020). The resulting protein sequences were used in Mercator and MapMan4 v5.0 (Schwacke *et al.,* 2019) for functional gene annotation. Transcriptome quality was assessed using BUSCO v5.

4.2.3.6 cDNA library construction and sequencing

Total RNA was extracted from leaves and roots of adult plants of treated and control plants using the RNeasy Plant Mini Kit (Qiagen, Hilden, Germany) according to the manufacturer's recommendations, with minor changes. Briefly, 50 mg of frozen tissue from each plant was lysed (1.5 M NaCl, 2% CTAB, 30 mM EDTA pH 8, 100 mM Tris-Cl, 2% β-mercaptoethanol in RNase-free water) for 10 min at 70 °C. Further extraction and on-column digestion with DNase I was carried out according to Qiagen recommendations. RNA quality was monitored as described above for DNA. For cDNA sequencing, 200 ng of RNA per sample was used in a strand-switching step followed by cDNA amplification by PCR using primers containing 5′ tags according to the ONT protocol for cDNA PCR sequencing (SQK-PCS111). We then added rapid sequencing adapters and loaded 25–55 ng onto primed 9.4.1 Spot-On Flow Cells for sequencing using a PromethION device.

4.2.3.7 Analysis of gene expression of selected drought-responsive genes by qRT-PCR

Based on the results of the RNA-Seq analysis, genes responsive to the drought stress treatment were selected for validation of their expression in leaves and roots of adult plants and leaves in young plants (Supplemental Material Table S10). Actin and eIF4A (Juškyté *et al*., 2022; Hedley *et al*., 2010) were selected for normalization. For cDNA synthesis, 1 µg of RNA was reverse transcribed into cDNA using iScript cDNA Synthesis kit (Bio-Rad) in a 20 µL reaction following the manufacturer's instructions. Quantitative real-time PCR of selected genes was conducted with a CFX Opus 384 Real-Time PCR System (Bio-Rad). The amplification was carried out in a reaction mixture containing 5 µL iQ SYBR Green Supermix (Bio-Rad1 µL of primers (mix of forward and reverse primer,500 nM), and 4 µL cDNA (diluted 20-fold) in triplicate for each sample and gene. The PCR program started with polymerase activation at 95 °C for 3 min, followed by 39 cycles of cDNA denaturation at 95 °C for 10 s, annealing and amplification at 60 °C for 30 s, and a melt curve analysis at 65–95 °C with an increment of 0.5 °C and 5 s per step at the end. The qRT-PCR was performed by Sarah Spettmann and Franziska Genzel.

The relative gene expression and fold change (FC) were determined using the threshold cycle value (C_t) and efficiency based $2^{-\Delta\Delta C}{}_T$ method described by

Ganger *et al.* (2017), with a modification where $\log_2$ transformation was applied instead of $\log_{10}$. The reaction efficiencies were calculated using Real-time PCR Miner (Zhao & Fernald, 2005) averaged for each gene for tissue and treatment. Actin and eIF4A were employed as internal reference genes for normalization. The $\log_2$ fold changes ($\log_2$FC) were visualized in a heatmap, depicting the upregulation and downregulation of the analyzed genes. Data processing and visualization were performed in R v4.2.2, utilizing the RColorBrewer v1.1-3, dplyr v1.1.4, and EnrichedHeatmap v1.28.1 packages.

4.2.3.8 Evaluation of the drought stress experiment

The cDNA long reads were mapped onto the transcriptome assembly using Minimap2 assembler v2.25 (settings '-ax splice -ts') (Li *et al.*, 2018). The read count was quantified using Salmon v1.10.1 (Patro *et al.*, 2017). Paired-end Illumina short reads for leaf samples of young plants were pseudo-mapped and quantified using Salmon v1.10.1**.** DEGs were identified using edgeR v3.40.1 (Robinson et al., 2010) and we calculated the p values and adjusted p values (FDR). The transcripts per million (TPM) data were evaluated by PCA. Furthermore, overrepresentation analysis based on MapMan annotation was used to find drought stress-related pathways in leaves and roots, and candidate genes were then selected.

4.2.3.9 Metabolite analysis

Metabolites in leaf and root samples of adult plants and leaf samples of young plants were analyzed by GC-MS and were kindly performed by Dr Vallarino and Prof Osorio (Osorio *et al.*, 2012, Vallarino *et al*., 2018). Mass spectra were

compared with the Golm Metabolome database for identification (Kopka *et al*., 2005). Metabolomic data were log_2-transformed and the average values were calculated for control and treated tissues. The data were normalized against the average values of the control samples. To assess the significance of differences, we calculated the log_2 fold change (log_2FC), p values (t-test), and adjusted p values (FDR, Benjamini-Hochberg). The statistical tests were used to detect significant differences between the control and stressed samples for each metabolite. The data were visualized using enhanced volcano plots.

4.2.3.10 Data integration

A database was built using MariaDB v10.6.5 to establish a connection between the transcriptome and metabolome. Protein sequences representing land plant genes with known functions were extracted from the UniProt SWISSPROT database (May 2022) and linked to MapMan protein classes. These annotated genes were supplemented with associated enzymatic reactions from the RHEA database (https://www.rhea-db.org/). The substrates and products of each reaction were linked to their CHEBI (https://www.ebi.ac.uk/chebi/) and PubChem (https://pubchem.ncbi.nlm.nih.gov/) IDs. We then used the hierarchical organization of MapMan bins, which categorize major biological processes as top-level bins and their sub-processes as child bins, to establish connections between the enzymatic reactions and their associated metabolites. This was achieved by identifying closely related DEGs that associated with these processes and their corresponding bins. By linking the DEGs and their MapMan protein functions to the corresponding metabolites, we established a comprehensive understanding of the relationship between gene expression, biological processes and metabolites. Genes associated with metabolites were filtered by FDR < 0.05 and pathway-related genes were selected. Statistical analysis was conducted using R Studio base v2023.06.0 (RStudio Team, 2023).

5 Results

5.1 Visualization of omics data for plants

Omics data typically generates large and complex datasets that require thorough analysis and effective visualization. Within plant research complex transcriptomics data featuring many different time points and or conditions needs to be analyzed frequently. To analyze and visualize differentially expressed genes derived from RNA-Seq data in plant species, a function was developed.

5.1.1 Visualization of RNA-Seq data for plants

In transcriptomics, particularly when evaluating DEGs based on RNA-Seq data, it was crucial to obtain a comprehensive overview of the dataset and the experiment. Principal component analysis (PCA) provided an initial insight into the main sources of variation across different conditions or variables. By incorporating overrepresentation analysis (ORA), functional annotations were added to contextualize gene expression patterns and highlight biologically relevant processes.

Plotting RNA-Seq data using this developed R function required two steps of data preprocessing. First, RNA-Seq data had to be quantified, and differential gene expression analysis has to be performed using tools such as edgeR (Robinson *et al.*, 2009) or DESeq2 (Love *et al.*, 2014). The resulting TPM values and contrasts between experimental groups served as the basis for subsequent PCA calculations. Second, the reference transcriptome or proteome was processed using MapMan (Schwacke *et al.*, 2019) to obtain functional annotations corresponding to the analyzed genes. These processed data files served as input for the R function.

For PCA, normalization was applied by default but can be set manually. In the subsequent ORA, the number of genes included was determined by PCA scores or loadings. Sample-specific attributes such as colors, symbols, and border colors were automatically assigned but could also be customized by providing a user-defined table.

The foundation of this plot was the PCA in the center, which plotted the differences between the input variables of a dataset (Figure 3A). Based on the

selected format of the input table and the chosen normalization method for the PCA, the tool used loadings or scores to calculate an overrepresentation analysis for defined PCA axes (e.g., PC1 and PC2) (Figure 3A, D). The log_{10}-transformed enrichment factor was then plotted as a bar plot along the selected PCA axes (Figure 3A, D). The color scheme used red and blue to indicate direction along the axes (red = positive direction, blue = negative direction), with color gradations based on the p-value (Figure 3B). The legend was plotted on the bottom left (Figure 3C). The five genes with the highest loadings or scores in the positive and negative directions were plotted above and to the right of the PCA, using the same color scheme as the bar plots (Figure 3E, G).

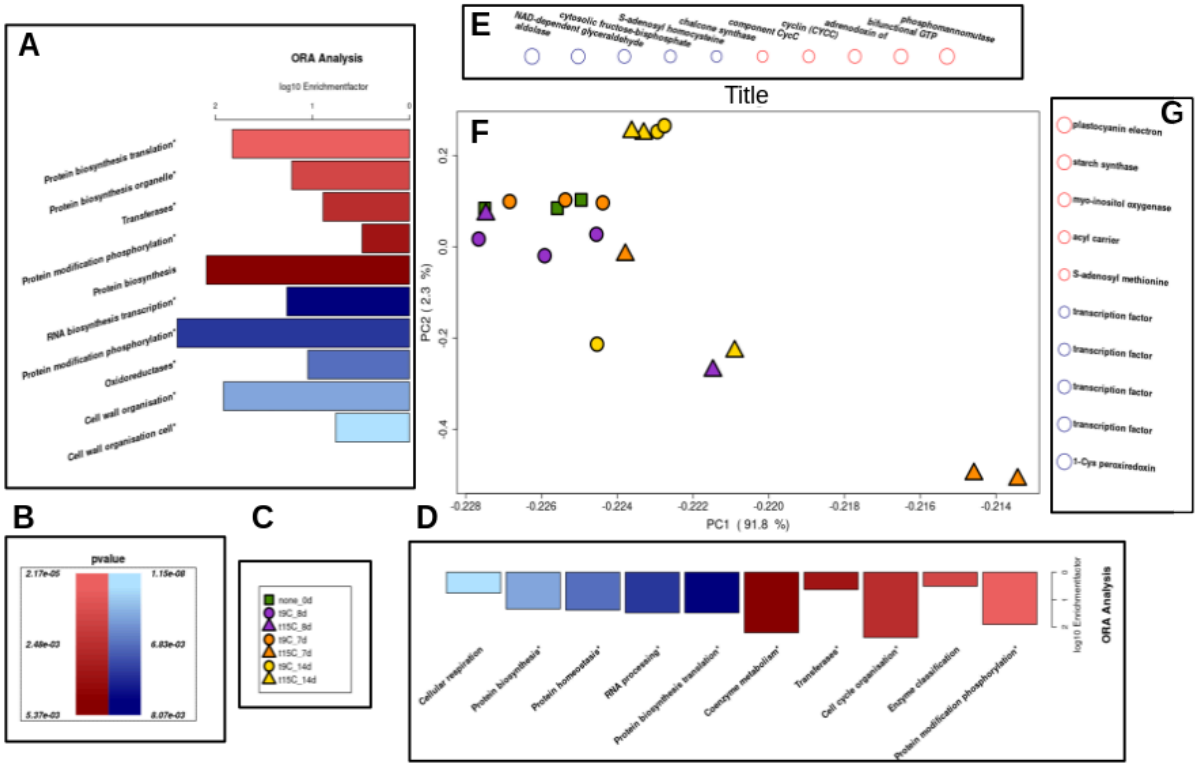

Figure 3: Example of combined principal component analysis (PCA) and overrepresentation analysis (ORA) results based on transcripts per million (TPM) values of differentially expressed genes (DEGs). A) ORA represented as a barplot of log_{10} enrichment factor (ERF) for MapMan protein classes based on PCA loadings in positive (red) and negative (blue) direction of PC2. B) Legend of adjusted p-values for ORA in positive (red) and negative (blue) direction of PC1 and PC2. C) Legend of PCA. D) ORA represented as a barplot of log_{10} enrichment factor (ERF) for MapMan protein classes based on PCA loadings in positive (red) and negative (blue) direction of PC1. E) Genes highly implicated in the positive (red) and negative (blue) separation of PCA are depicted on PC1. F) PCA plot of RNA-Seq data. G) Genes highly implicated in the positive (red) and negative (blue) separation of PCA are depicted on PC2.

In addition to the main plot, several individual plots were generated and saved in a PDF file (Figure 4). This file included an elbow plot to assess the importance of

the principal component (PC) axes in the experiment (Figure 4A), a PCA plot based on scores and loadings (Figure 4B, C), and PCA plots displaying all combinations of the first three PC axes (Figure 4D-F).

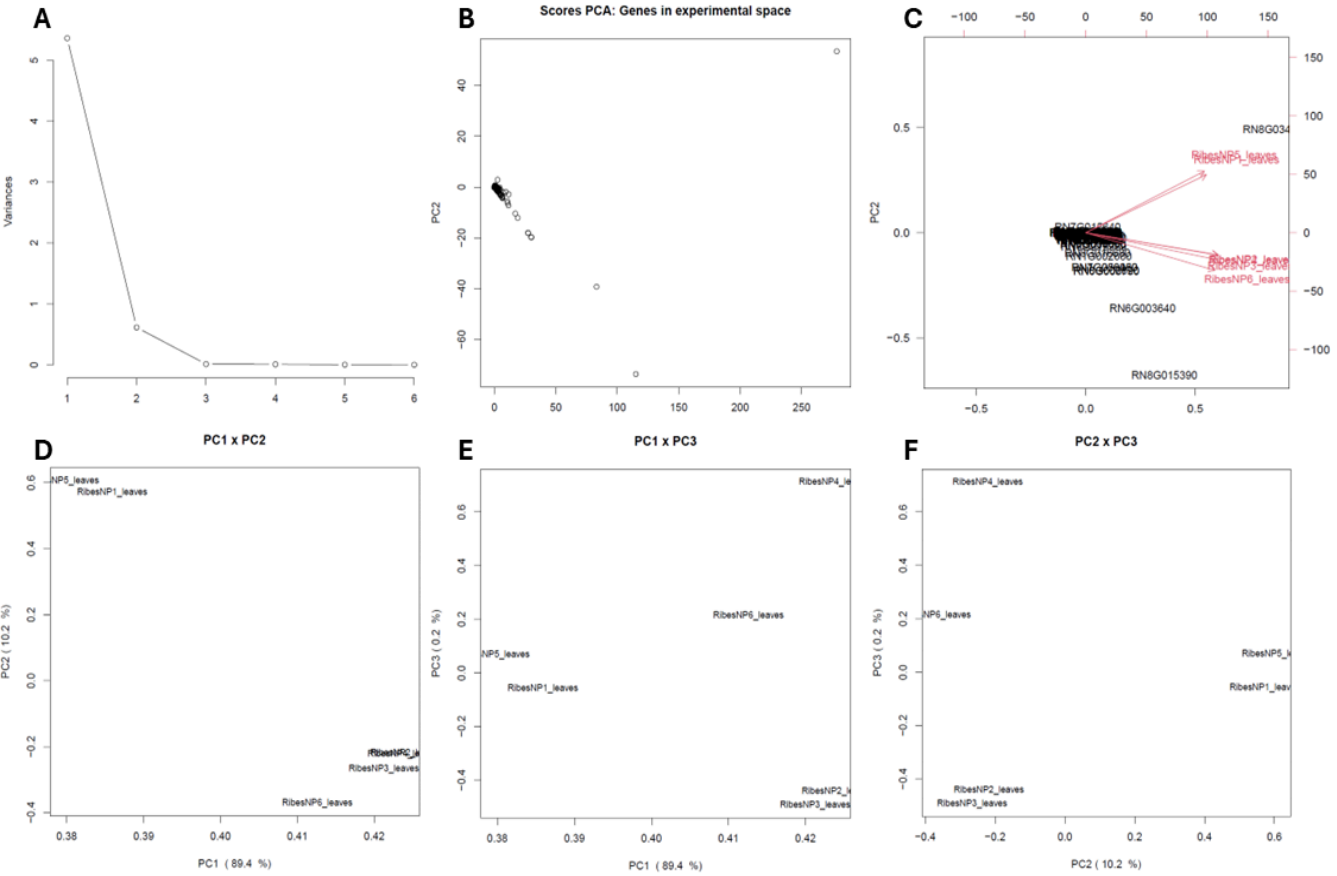

The principal component analysis and overrepresentation analysis plot (PCA-ORA plot) and the resulting tables were employed to provide initial insights, offering a general overview of data distribution, separation, or clustering of data points, and to identify key MapMan protein classes (Schwacke *et al.*, 2019) associated with the transcriptomic responses. To demonstrate a typical application of this plotting function, RNA-Seq data from strawberry, generated using Illumina short reads (Chapter 5.2.3), and blackcurrant data, obtained from Oxford Nanopore long reads (Chapter 5.3.4), were utilized. Here, various biological experiments were plotted to visualize gene expression profiles, investigating early floral initiation events on molecular level in strawberry and preliminary insights into the drought stress response in adult and juvenile plants of *R. nigrum*.

5.2 Phenotypic and transcriptomic variation of floral initiation in *Fragaria x ananassa*

The molecular regulation of floral initiation in the cultivated strawberry *Fragaria* × *ananassa* under natural conditions remains poorly understood. This study investigated early molecular events during floral initiation through transcriptomic analysis, considering both genotype and environment. RNA-Seq data were analyzed from leaf and terminal bud tissues of two cultivars—'Clery' (CL) from Italy and 'Gariguette' (GA) from France—grown in France and Germany. Sampling occurred during the transition from the vegetative phase to early floral initiation in the shoot apical meristem (SAM) (weeks 29, 32, 33, and 35).

5.2.1 Phenotypic variation of floral initiation according to the environment and the cultivar

We investigated floral initiation over time by dissecting the terminal bud in cultivars CL and GA and observing the SAM from the middle of July until the end of October over 3 years (2016–2018) in two different environments in France and Germany. The SAM in the terminal bud was always vegetative on the first sampling date in July regardless of the genotype or location (Figure 5). The SAM transitioned to a floral identity when its apical dome rose above the level of the developing stipules (Krüger *et al.,* 2022).

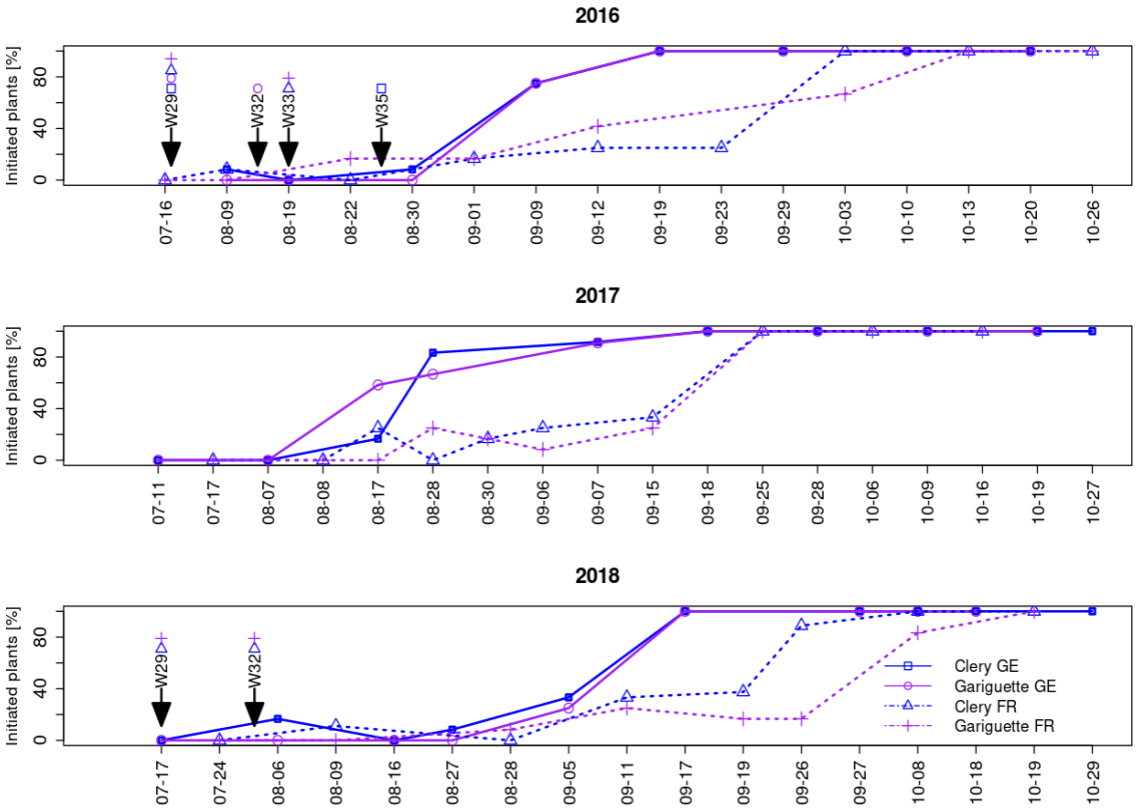

Figure 5: Evolution of the percentage of floral initiated plants of strawberry per cultivar ('Clery', 'Gariguette') and location (GE: Germany, FR: France). Plants were categorized as floral initiated when the stage of the SAM was at least 2 (TB dome raises above the developing stipules). Dates for sampling for RNA-Seq analysis of leaf and terminal bud are highlighted by arrows and their week of sampling week 29 (T0), 32 (T10A), 33 (T10B) and 35 (T50).

Because different plants were tested in each sample, the percentage of initiated plants (those with a floral terminal bud) fluctuated between consecutive sampling dates. The beginning of floral initiation was similar in France and Germany, with a low percentage (<10%) of initiated plants during the first weeks, rising steadily and then jumping from 20–40% to 90–100% in a single week (Figure 6). In Germany, this week was in the middle or at the end of August (depending on the year) whereas in France it was in the middle or at the end of September (Figure 6).

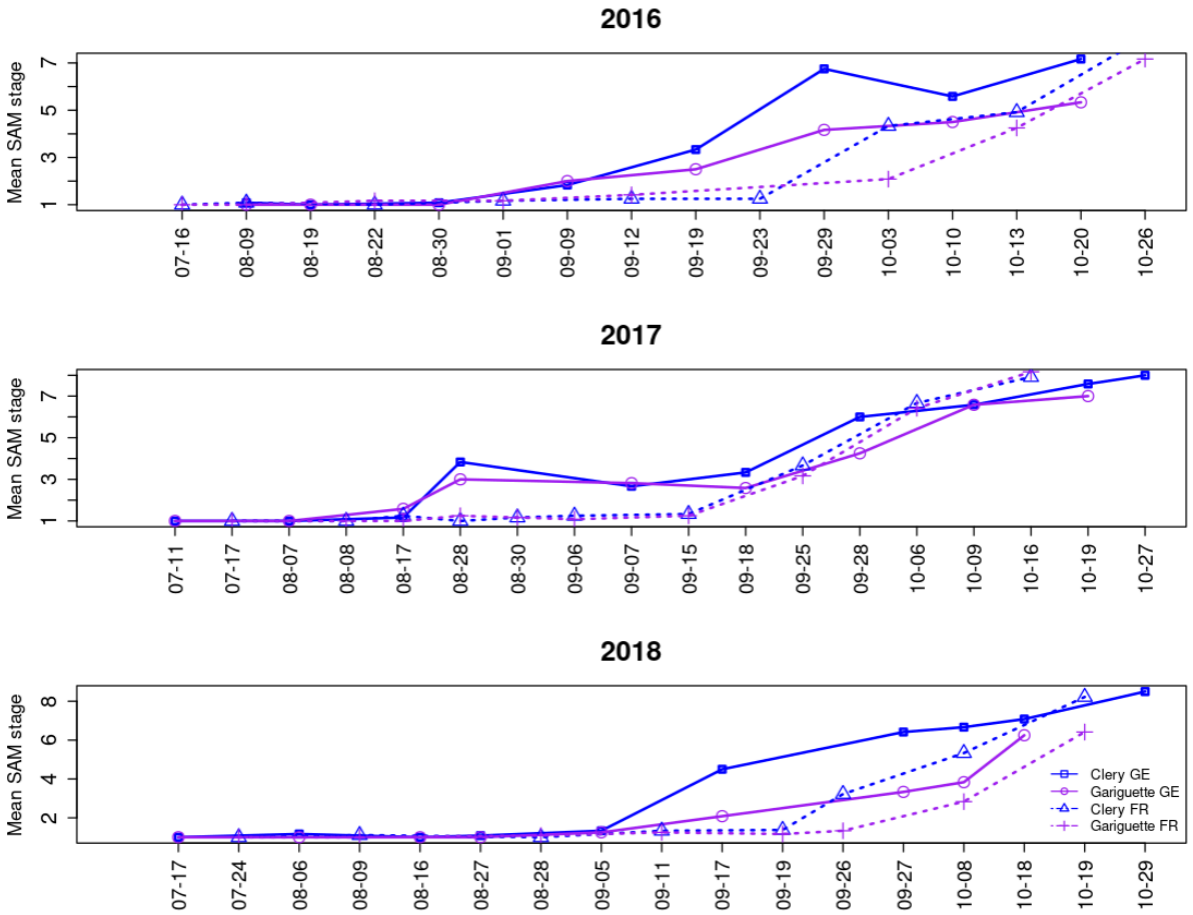

Figure 6: Evolution of the floral developmental stage of the shoot apical meristem (SAM) of strawberry per cultivar ('Clery', 'Gariguette') and location (GE: Germany, FR: France). The scale of the SAM is reported in Supplemental Figure S1A.

Floral initiation was followed by organogenesis in the SAM, resulting in the formation of an entire inflorescence with differentiated flower organs (still in the terminal bud, Figure 1). SAM development into an inflorescence followed the same tendency every year at both locations, although it occurred earlier for genotype CL than GA, and earlier in Germany than in France, as anticipated given the earlier floral initiation in Germany (Figure 6).

5.2.2 Choosing relevant dates of sampling for studying the first stage of floral initiation

Samplings for RNA-Seq were performed at three timepoints, when all plants were vegetative (T0, 0% of initiated plants), T10 when about 10% of plants were initiated and T50 when about half of plants were initiated (50%). Because of genotype and environmental effects, these timepoints can differ by year, the

location and the genotype (Table 1; Figure 5). For T0, RNA leaf and TB samples were obtained from daughter plants just sampled from their mother plants in the “calendar week 29/30” (CL_GE16_T0, GA_GE16_T0, CL_FR16_T0, GA_FR16_T0, CL_FR18_T0, GA_FR18_T0).

Table 1: Floral initiation [%] for sample extraction dates of strawberry leaf (L) and terminal bud (terminal bud, TB) tissue for locations in France (FR) and Germany (GE) and the cultivars Clery (CL) and Gariguette (GA).

ID	Location	Year	Cultivar	Date observation	Tissue	Week	Timepoint	Floral initiation [%]
Starting Point (T0)								
CL_GE16_T0	GE	2016	CL	2016-07-19	L, TB	29	T0	0
GA_GE16_T0	GE	2016	GA	2016-07-19	L, TB	29	T0	0
CL_FR16_T0	FR	2016	CL	2016-07-16	L	29	T0	0
GA_FR16_T0	FR	2016	GA	2016-07-16	L	29	T0	0
CL_FR18_T0	FR	2018	CL	2018-07-24	L	30	T0	0
GA_FR18_T0	FR	2018	GA	2018-07-24	L	30	T0	0
Floral initiated plants								
Early floral initiation (around 10% of initiated plants) (T10)								
CL_GE16_T10	GE	2016	CL	2016-08-30	L, TB	35	T10	8.3
GA_GE16_T10	GE	2016	GA	2016-08-09	L, TB	32	T10	8.3
CL_FR16_T10	FR	2016	CL	2016-08-22	L	33	T10	0
GA_FR16_T10	FR	2016	GA	2016-08-22	L	33	T10	16.6
CL_FR18_T10	FR	2018	CL	2018-08-09	L	32	T10	11.1
GA_FR18_T10	FR	2018	GA	2018-08-09	L	32	T10	0
Floral initiation continued (around 50% of initiated plants) (T50)								
CL_GE16_T50	GE	2016	CL	2016-09-09	L	36	T50	75
GA_GE16_T50	GE	2016	GA	2016-09-09	L	36	T50	75
CL_FR16_T50	FR	2016	CL	2016-09-12	L	37	T50	25
GA_FR16_T50	FR	2016	GA	2016-09-12	L	37	T50	41.1

For the second timepoint (T10), the percentage varied from 0% to 17%. 0% initiated was observed in two samples: (1) CL_FR16 but the percentage was 8.3% 10 days before, and (2) GA_FR18, with a percentage of 11% the week after (Figure 2; Table 1). The samples were: CL_GE16_T10, GA_GE16_T10, CL_FR16_T10, GA_FR16_T10, CL_FR18_T10, GA_FR18_T10. Four samples were recovered at the third timepoint T50: CL_GE16_T50, GA_GE16_T50, CL_FR16_T50, GA_FR16_T50.

5.2.3 Transcriptome variation in strawberry leaf and terminal bud in floral initiation

To find differences and similarities between cultivars during early floral initiation, the RNA-Seq samples for leaf and terminal bud were compared using a combination of PCA and ORA. All three replicates of each sample were grouped, confirming their homogeneity. For the leaf samples (Figure 4), the gene expression patterns for cultivars CL and GA grown in France were initially similar (CL_FR16_T0 and GA_FR16_T0) but began to segregate along the PC1 axis by stage T10 (CL_FR16_T10 and GA_FR16_T10). This was attributed to genes associated with photosynthesis, uptake of transition metal ions, phytohormone activity, lipid metabolism, and RNA biosynthesis. Notably, for both cultivars at both locations at stage T10 (w32, w33 and w35), a more pronounced separation was observed along the PC2 axis. The separation patterns of both cultivars aligned closely across these time points (Figure 7).

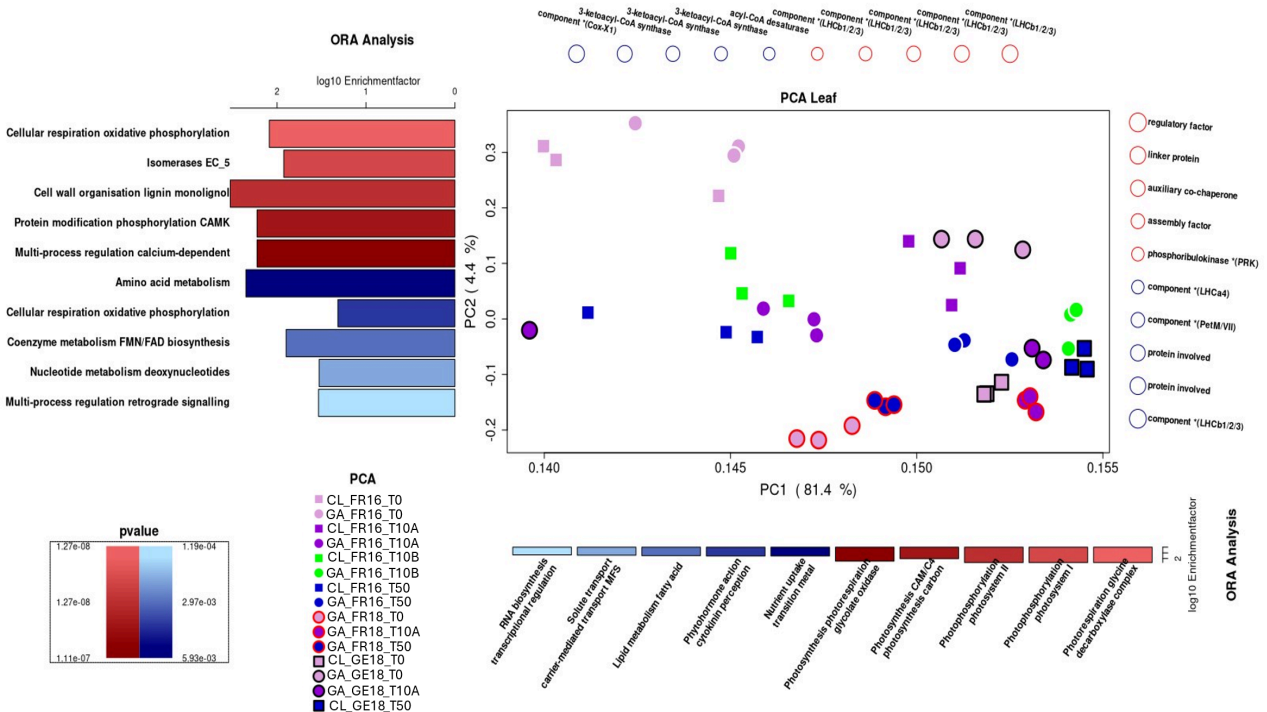

In Germany, cultivars CL and GA were separated along the PC2 axis from the first time point T0 (CL_GE18_T0 and GA_GE18_T0), particularly for protein classes involved in cellular respiration, cell wall organization, protein modification, and multi-process regulation (Figure 7). But by stage T10, the cultivars were dispersed clusters, which disguised the separation between them (CL_GE18_T10 and GA_GE18_T10A).

For TB tissue (Supplemental Material Figure S3), the FI of GA_FR18 during the developmental progression is delineated along the PC1 axis. Notably, protein homeostasis, biosynthesis, and the multi-process regulation of phosphoinositide exerted a substantial influence on the separation observed between week 29 (w29), w32 and w35. Moreover, the segregation evident for T10 (w32) exhibited an impact in the PC2 axis, with protein classes such as cell wall organization of lignin, RNA processing, and secondary metabolism of phenolics playing a pivotal role. Comparably, for GA_GE16_T0 and T10, as well as CL_GE16_T0 and T50, analogous outcomes were discerned in terms of separation. While the cultivars CL and GA exhibited distinct separation along the PC1 axis in T0, both cultivars demonstrated similar results in T10 and T50.

5.2.4 Common DEGs between T0 and T10 in first stage of floral initiation

We chose to focus on the little-known process of early FI in natural conditions by analysing differential expression between the two first timepoints T0 (w29) and T10 (w32, w33, or w35 according to the country and the year). We compared in pairs the transcript profiles of the T0 and T10 samples, within each cultivar, CL or GA and within organ, L or TB. As an example, pair comparison was named CL_GE16_T0xT10 when transcripts of the sample CL_GE16_T0 were compared with the ones of the sample CL_GE16_T10. A L or TB was added to the end of the name according to comparisons concerned by LF or TB. In total analysis that included all pair comparisons, a total of 71,369 DEGs were identified (FDR corrected p-value ≤ 0.05 used in all).

Focusing on leaves, the two pair comparisons for CL from GE and FR - CL_GE16_T0xT10L and CL_FR16_T0xT10L - revealed 7,119 DEGs

(Supplemental Material S2A). For the cultivar GA, similar pair comparisons - GA_GE16_T0xT10L, GA_FR16_T0xT10L and GA_FR18_T0xT10L, revealed 787 DEGs in common (Supplemental Figure S2B). In total, the two cultivars shared 417 DEGs in L.

The TB tissue of cultivar CL for comparison - CL_GE16_T0xT10TB - showed 3,385 DEGs. The contrasts of cultivar GA – GA_GE16_T0xT10TB and GA_FR18_T0xT10TB - revealed 1549 DEGs. Pair contrasts using both cultivars resulted in 1,208 shared DEGs in TB (Supplemental Material S2C).

To identify additional protein classes involved in FI, we conducted an enrichment analysis for MapMan protein classification on common genes. In the leaf tissue of CL, particularly in plant reproduction flowering modulation, enzyme activity, secondary metabolism related to terpenoids, and carbohydrate metabolism related to starch protein classes were enriched (Figure 7). Conversely, leaf tissue of GA exhibited notable enrichment in response to multi-stress, cytoskeleton organisation related to microtubular network, chromatin organisation and structure, phytohormone action, carbohydrate metabolism and RNA biosynthesis (Figure 8) Moreover, the common DEGs between CL and GA demonstrated a peak solute transport channel, cell wall organisation related to pectin rhamnogalacturonan, cell division and photosynthesis (Figure 7).

In TB tissue of CL, classes of proteins like those in leaf tissue were found, such as carbohydrate metabolism and amino acid metabolism of aspartate and cell wall organisation of hydroxyproline-rich glycoprotein. Additionally, DEGs showed high enrichment in RNA biosynthesis of bZIP TF superfamily circadian clock system, and photosynthesis (Figure 8). In TB tissue of GA, we have found high enrichment for protein classes of secondary metabolism related to terpenoids and external stimuli response. We also found cell wall organisation related to pectin rhamnogalacturonan, redox homeostasis and photosynthesis (Figure 8). Overlapping DEGs between both cultivars of TB tissue belonged to highly enriched protein classes of chromatin organization of chromatin structure, cytoskeleton organization of microtubular network, serine/threonine phosphatase

superfamily, cell division, cell wall organization cellulose, RNA biosynthesis of bZIP TF and plant reproduction flowering (Figure 8).

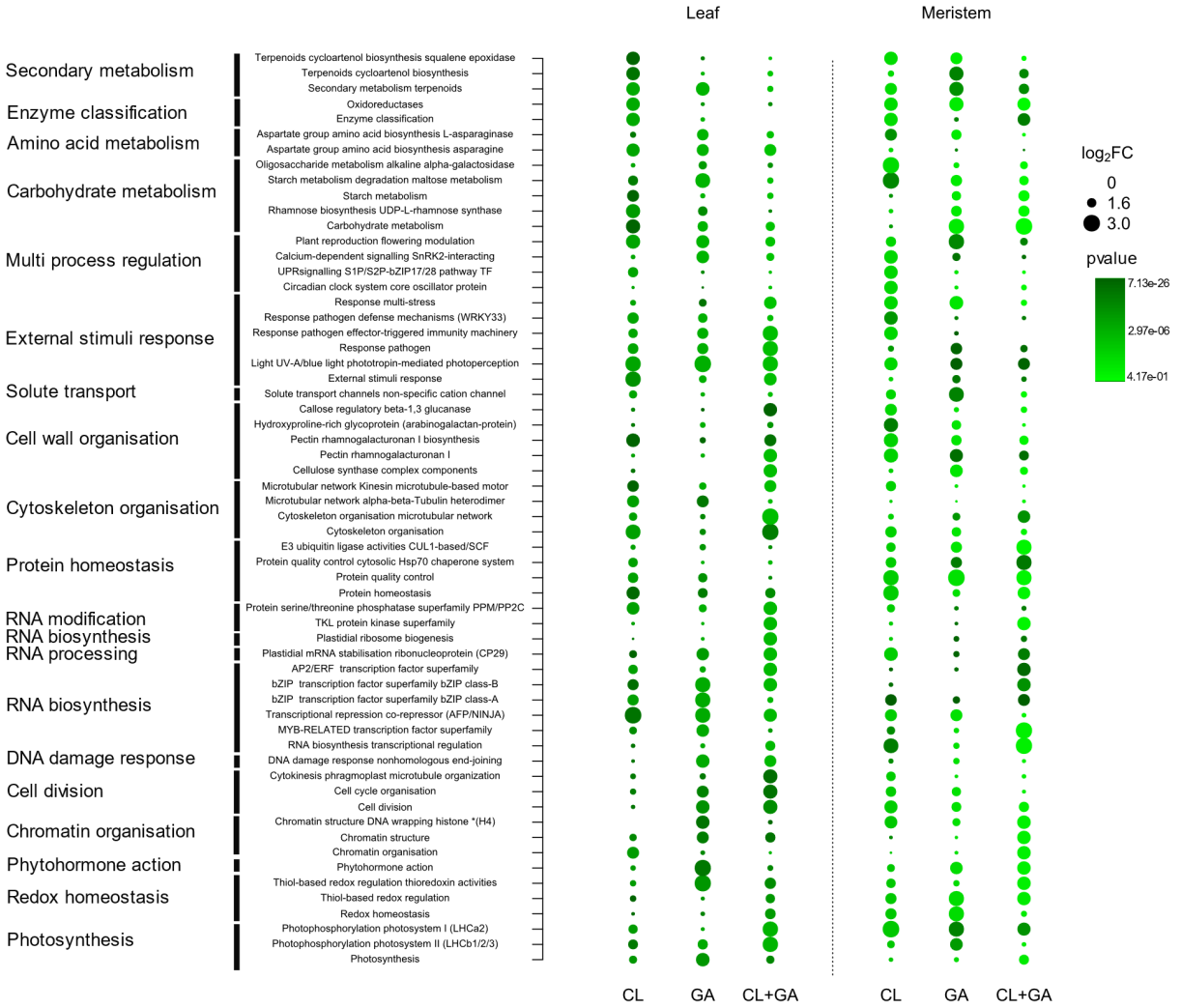

The geographical location exerted a significant impact on the differences observed during the FI stage of both tissues. Furthermore, multi-process signalling and phosphoinositide, cytoskeleton organization as well as cellular respiration were the protein classes that differed most between the two sites, Germany and France.

5.2.5 Overview of DEGs in the first stage of floral initiation highlight known genes involved in the flowering pathway

Within these common DEGs for different genotypes and tissues, several genes related to plant reproduction of flowering and TF were identified based on a literature search. Analyses highlighted DEGs specific to the location (GE or FR), to the tissue (leaf or TB) or to the combination of location and tissue (Figure 9).

Notably, in the case of transcription factors, eight DEGs of the bHLH-type transcription factor/ transcriptional co-activator FBH were predominantly downregulated in leaf tissue for both genotypes for the GE location in the beginning (T0xT10), whereas these transcription factors showed a trend of upregulation in leaf tissue for both genotypes in the FR location for the early stages of FI (T0xT10).

During FI (T0xT10) seven genes encoding for CONSTANS-like (COL) proteins were differentially expressed (Figure 9). The variation of the expression of these *COL* genes in the leaves and from T0 to T10 was dependant on the location with a significant decrease in both cultivars in Germany (CL_GE16_T0xT10L and GA_GE16_T0xT10L) while an increase was observed in France (GA_FR16_T0xT10 and CL&GA_FR18_T0xT10). The downregulation of *COL* genes was observed in all samples in the TB tissues. However, in the comparison involving CL_FR16_T0xT10L, there was significant upregulation observed in five *COLs* genes in leaf tissue. In contrast to TB tissue, differential expression analysis of *COLs* revealed a strong, shared downregulation of five genes across both cultivars. Additionally, the French cultivar GA exhibited significant downregulation in two specific genes (Figure 9).

DEGs encoding the regulatory protein GIGANTEA (GI) exhibited significant downregulation in L and TB for T0xT10 for the plants grown at the FR location, while they were upregulated in leaf samples for the whole period of FI of the DE. In the early stage of FI FD-like transcription factors, TFL1 showed little to no expression in L tissue. In contrast a significant upregulation was found in TB tissue (Figure 9).

In addition, several MADS/AGL-type genes showed differential expression. Specifically, the gene FxaC_19g36190 displayed significant upregulation across almost all comparisons in both tissues, except in TB tissue of cultivar GA. Among the DEGs associated with SVP/AGL24, the gene FxaC_17g50871 exhibited upregulation in leaf tissue across both French cultivars (T0xT10) but displayed downregulation in TB tissue specifically within the GE location comparisons (Figure 9).

DEGs of the TFs MYB3R1 were upregulated for all contrasts and especially in TB tissue. For the gibberellin pathway we have found several TFs such as DELLA and GRAS-type TF. Some of these showed a significant downregulation for leaf tissue of CL grown in GE and for TB of both cultivars, while most genes in the CL_FR16 leaf tissue were upregulated for T0xT10. Four DEGs of GRAS-type transcription factor showed downregulation in all leaf samples and one CL_GE16_ T0xT10 for TB, while other DEGs were upregulated in all TB samples. However, GA samples in general showed lower significance than CL across countries and years. We identified two DEGs that belong to the small regulatory polypeptide DEVIL/ROT-FOUR-LIKE (DVL/RTFL) family. They show a similar expression pattern as GI genes for both genes. The second gene (FxaC_4g34880) exhibited significant downregulation only in leaf and TB of GA grown in FR in 2018 (Figure 9).

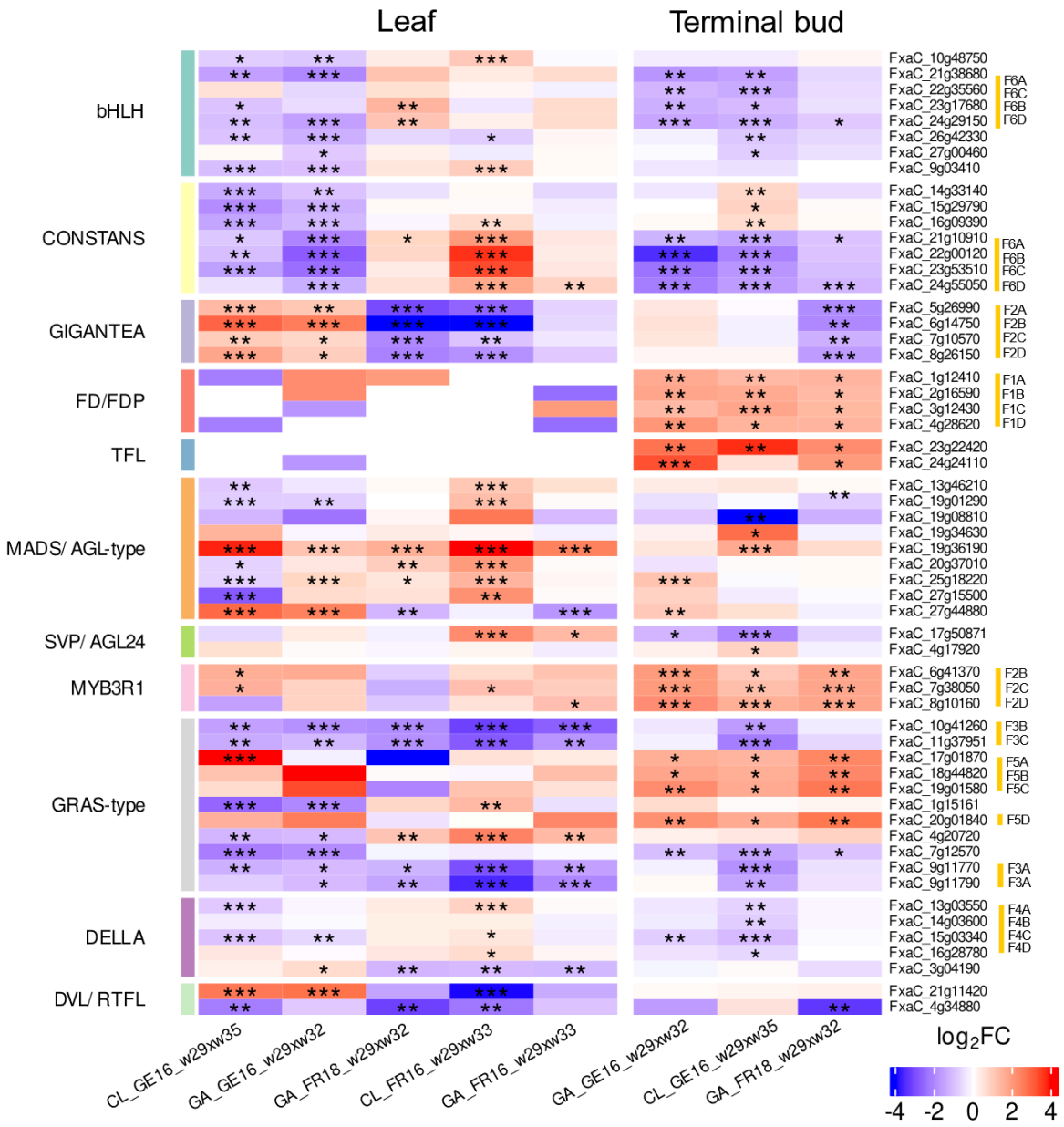

Considering the octoploid status of cultivated strawberry (2n = 8*x* = 56) up to eight homoeoalleles for each gene located at orthologous location on the four subgenomes (A, B, C, D) of *F. x ananassa* may be expressed. However, expression of a gene can be due to only some of the four subgenomes. We illustrate hereafter different situations with different genes (Figure 9). Expressions of homoeoalleles belonging to the four subgenomes were observed for the bHLH

transcription factor on the homoeologous group 6. They were all significantly downregulated for both genotypes and the GE location in TB tissue (Figure 10). Similarly, *FanRGA*, a DELLA transcription factor, was expressed in the four subgenomes of the homoeologous group 4. They were all significantly downregulated in CL in GE, while only alleles of a single genome (FxaC_15g03340) were significantly downregulated in GA (Figure 10).

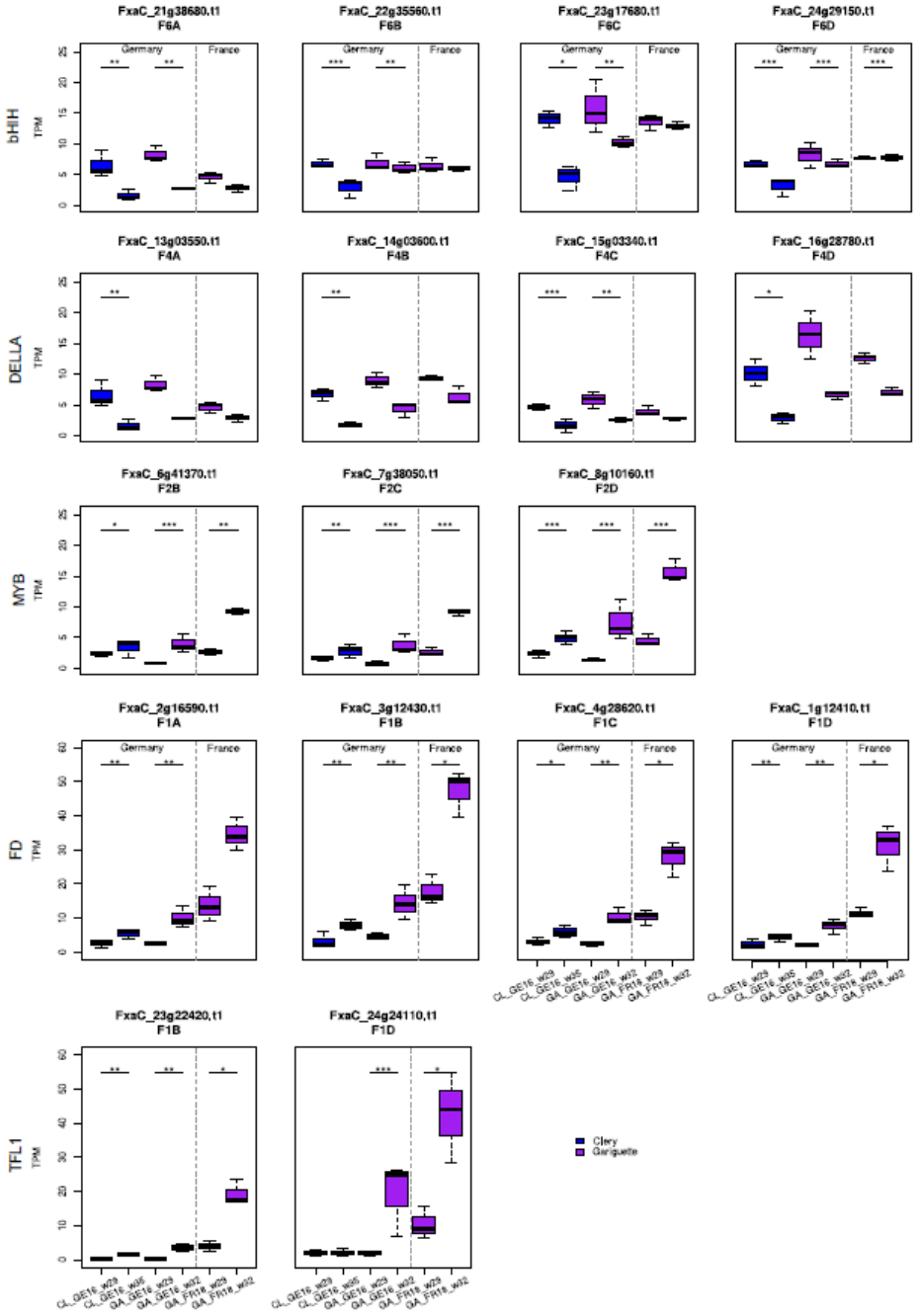

Concerning flowering genes, *FanFD* was expressed in the four subgenomes while *FanTFL1* was only expressed in two subgenomes. These genes exhibited significant upregulation for most TB samples but no significant regulation in leaf tissue (Figure 9 and 10; FDR<0.05).

5.2.6 Comparative analysis of selected genes in floral initiation based on reference data in cultivated strawberry

We compared our DEGs to those reported in a previous study of floral initiation in the cultivated strawberry cv. Benihoppe (Liang *et al*., 2022). This revealed 19 common DEGs in leaf or terminal bud tissues, from which we selected six expressed in the terminal bud and associated with hormone pathways or carbohydrate metabolism for analysis at the subgenomic level (Figure 11).

One gene encoding a type 2C protein phosphatase (PP2) involved in the abscisic acid (ABA) pathway was significantly downregulated in three subgenomes across both locations and cultivars, except subgenome 7C (*FxaC_28g02380*) in Germany and subgenome 7D (*FxaC_26g04770*) in the terminal bud (Figure 11). Furthermore, the *EIN3* gene encoding a brassinosteroid ethylene-like transcription factor was downregulated in three subgenomes but strongly expressed in subgenome 7A (*FxaC_25g07481*) in the terminal bud in both Germany and France (Figure 11; FDR < 0.001). The *XTH23* gene involved in ethylene signaling was only significantly downregulated in subgenome 4A for both locations and both cultivars (FDR < 0.001). The expression of *FxaC_15g33220* on subgenome 4B was significantly downregulated for cultivar CL in Germany (Figure 11; FDR < 0.05). In the context of carbohydrate metabolism, a *TPS* gene in homoeology group 4 was expressed at different levels depending on the subgenome, with significant downregulation in subgenomes 4C and 4D only in Germany, but significant downregulation in subgenomes 4A and 4B for both cultivars at both locations (Figure 11).

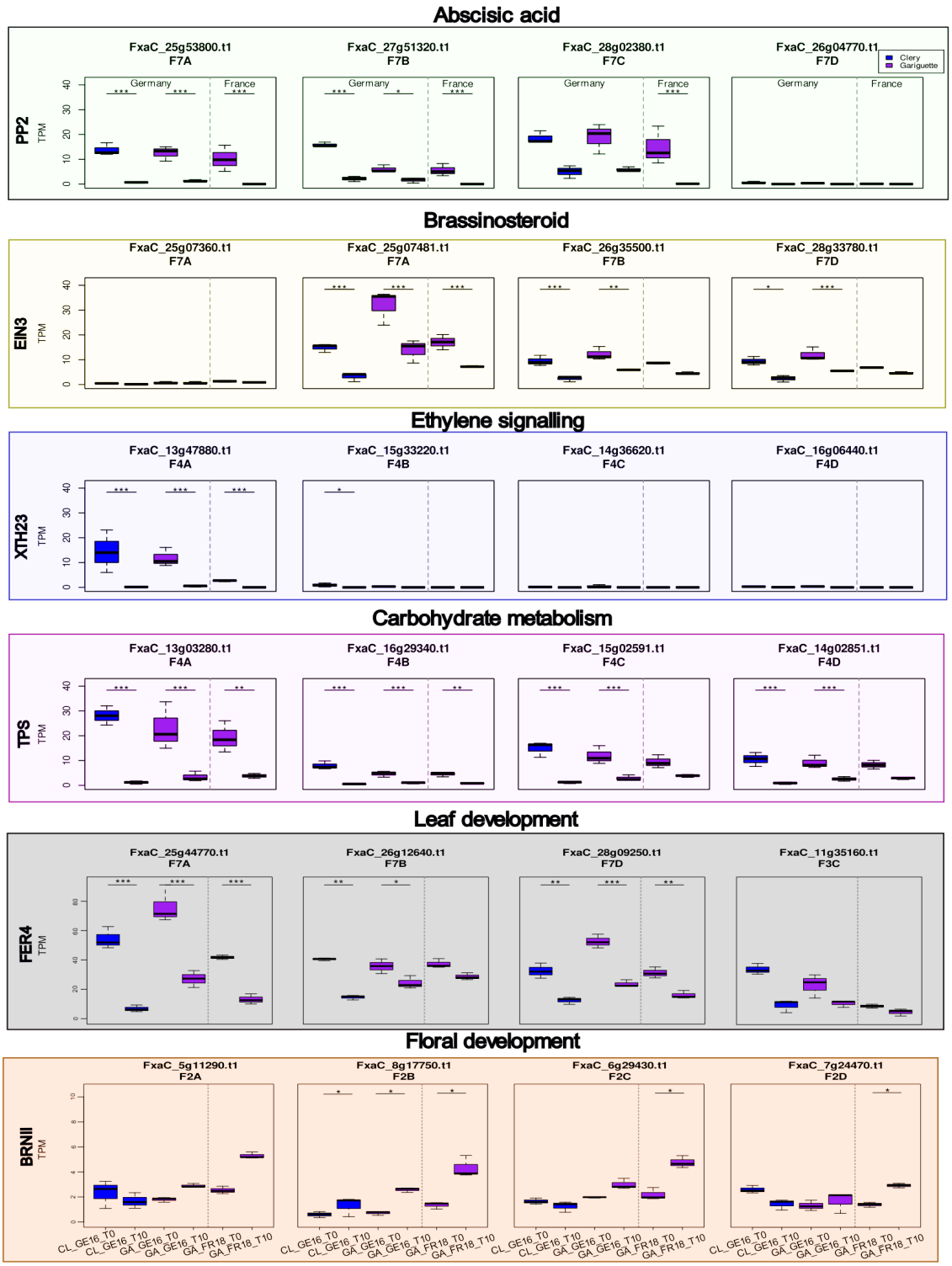

Figure 11: Whisker-boxplots illustrating TPM values for the candidate genes of PP2, EIN3, XTH23, TPS, FER4 and BRNII involved in the pathways of abscisic acid, brassinosteroid, ethylene signaling and carbohydrate metabolism and their homologous sequences across various dates during the floral initiation stage in *Fragaria* × *ananassa* TB tissue, comparing the genotypes Clery and Gariguette at German (GE) and French (FR) locations. The genotype Clery (CL) is highlighted in blue and for Gariguette (GA) in purple. Significance levels are stated as FDR<0.001 ***, FDR<0.01 ** and FDR<0.05 *.

We analyzed two DEGs associated with leaf and/or floral development. The *FanFER4* gene, involved in leaf development, was significantly downregulated in both cultivars at both locations (FDR < 0.01) in subgenomes 7A and 7D, but the expression in subgenome 7B was only significant in Germany (FDR < 0.001). Three homeologous alleles of *FER4* were identified on chromosome 7 (FDR < 0.05), and the fourth was located on chromosome 3 (Figure 11). The *BRN1* gene encoding an RNA-binding protein involved in the regulation of flowering time was significantly upregulated in subgenomes 2C and 2D for cultivar GA in France and in subgenome 2B at both locations (Figure 11; FDR < 0.05).

Key gene expression profiles and differences between the cultivars "'Clery" (CL) and "Gariguette" (GA) across two environments (Germany and France) were identified. Genes such as *PP2*, *EIN3*, *XTH23*, *TPS*, *FER4*, and *BRNII*, along with transcription factors including *FBH*, *CO*, and *GI*, were implicated in early floral initiation. Additionally, pathways related to carbohydrate metabolism reprogramming, phytohormone signaling, and photoperiod-dependent regulation were associated with the early stages of floral initiation in strawberry.

5.3 Quality assessment of Pore-C data on the tetraploid haplotype genome assembly of *S. tuberosum* cv. Altus

The ONT Pore-C is a sequencing-based method used to investigate the three-dimensional organization of the genome. Similar to Hi-C or Omni-C, it provides a detailed view of chromatin interactions, including those between regulatory elements such as enhancers and promoters.

To determine the suitability of Pore-C reads of the potato (*S. tuberosum)* cv. Altus data was digested and aligned against a tetraploid haplotype reference genome. Overall, 138,371,859 contacts with a cis:trans ratio of 2.18 were found (Table 2). The cis:trans ratio represents the proportion of chromatin interactions occurring within the same chromosome (cis) relative to those occurring between different chromosomes (trans). This ratio serves as a key quality metric, reflecting the accuracy of chromatin conformation capture and providing insights into genome organization and long-range regulatory interactions.

Table 2: Pore-C metrics of all samples after alignment to the reference genome of *S. tuberosum* and deduplication.

Pore-C metrics	
Total reads	138,371,859
Total unmapped reads	63,798,807
Total mapped reads	24,589,048
Uniquely mapped reads	18,399,035
Duplicated reads	6,190,013
Cis contacts	12,608,812
Trans contacts	5,790,223
cis:trans ratio	2.18

In total 7 samples were taken some in spring (March& April) and some in summer (August). Samples 1-3, taken in March and April, exhibited a notably higher cis:trans ratio (>5) compared to samples 4-7, collected in August, which displayed a cis:trans ratio ranging between 0.75 and 0.89 (Supplemental Material Table 1).

To further evaluate the quality of the data, corrected Pore-C counts for genomic distances for a resolution of 10kb were plotted, showed a distribution for all Pore-C samples of *S. tuberosum* and reflecting the proportion of long-range and short-range contacts (Figure 12). The data from Sample2 and Sample3 collected in spring exhibit a strong correlation, and Sample1 also displayed a slight correlation with these samples. However, the remaining samples collected in August (4-7) showed correlations among themselves but not with samples 1-3 (Figure 12).

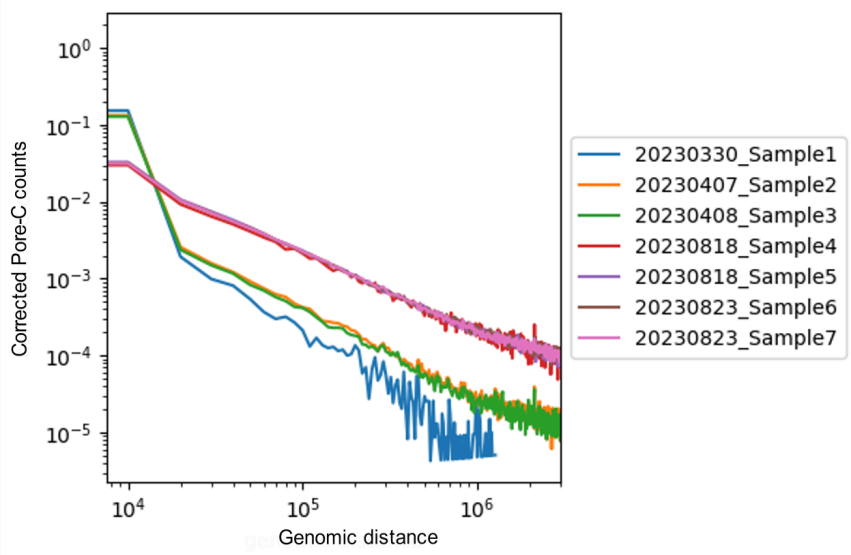

Figure SEQ Figure * ARABIC 12: Comparison of corrected Pore-C counts of seven biological replicates for leaf tissue of *S. tuberosum* cv. Altus by genomic distance at a 10 kb resolution.

Additionally, the comparison between short range and long-range contacts showed slight differences between the Pore-C samples (Figure 13). While samples 1-3 and samples 4-7 showed no significant difference among themselves (p-value>0.1), there is a significant difference (p-value<0.001) between the samples 1-3 and samples 4-7 (Figure 13).

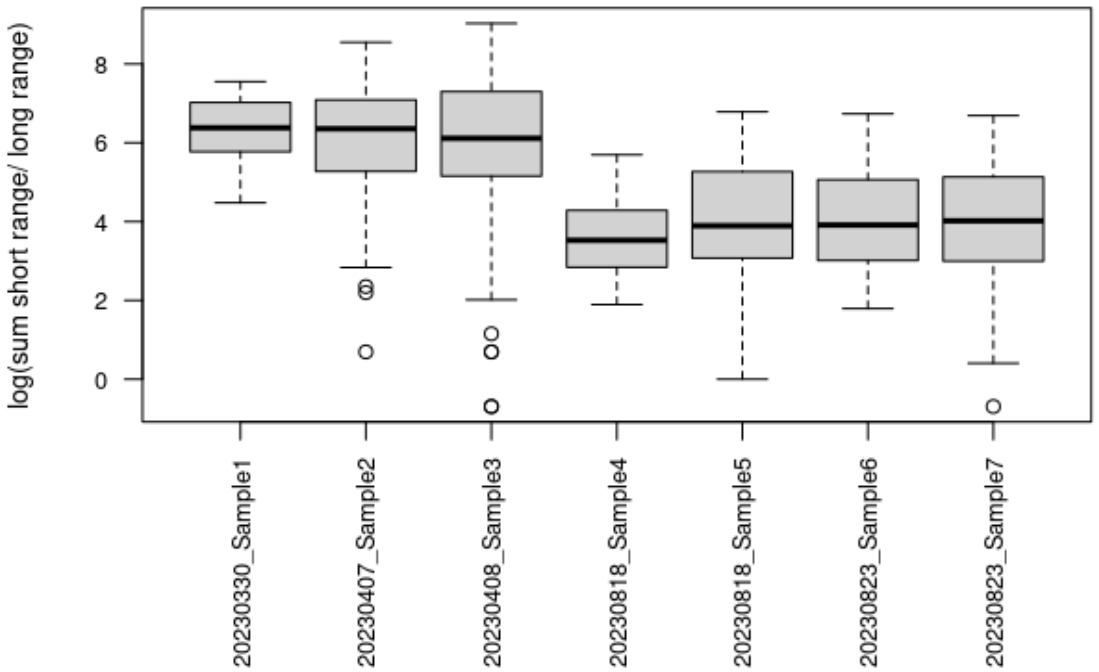

Figure 13: Whisker-boxplots representing the relation between short- and long-range interactions for biological replicates for leaf tissue of *S. tuberosum* cv. Altus. The data points show the ratio per chromosome for the first 63 chromosomes of the reference assembly.

Pore-C contact matrix of raw data showed intra/inter-chromosome interaction to the haplotype-resolved reference genome assembly of *S. tuberosum* (Mari et al., 2023) (Figure 14). A distinct linear diagonal pattern was evident, depicting intrachromosomal interactions across the genome, while a checkerboard-like structure illustrated potential interchromosomal interactions (Figure 14).

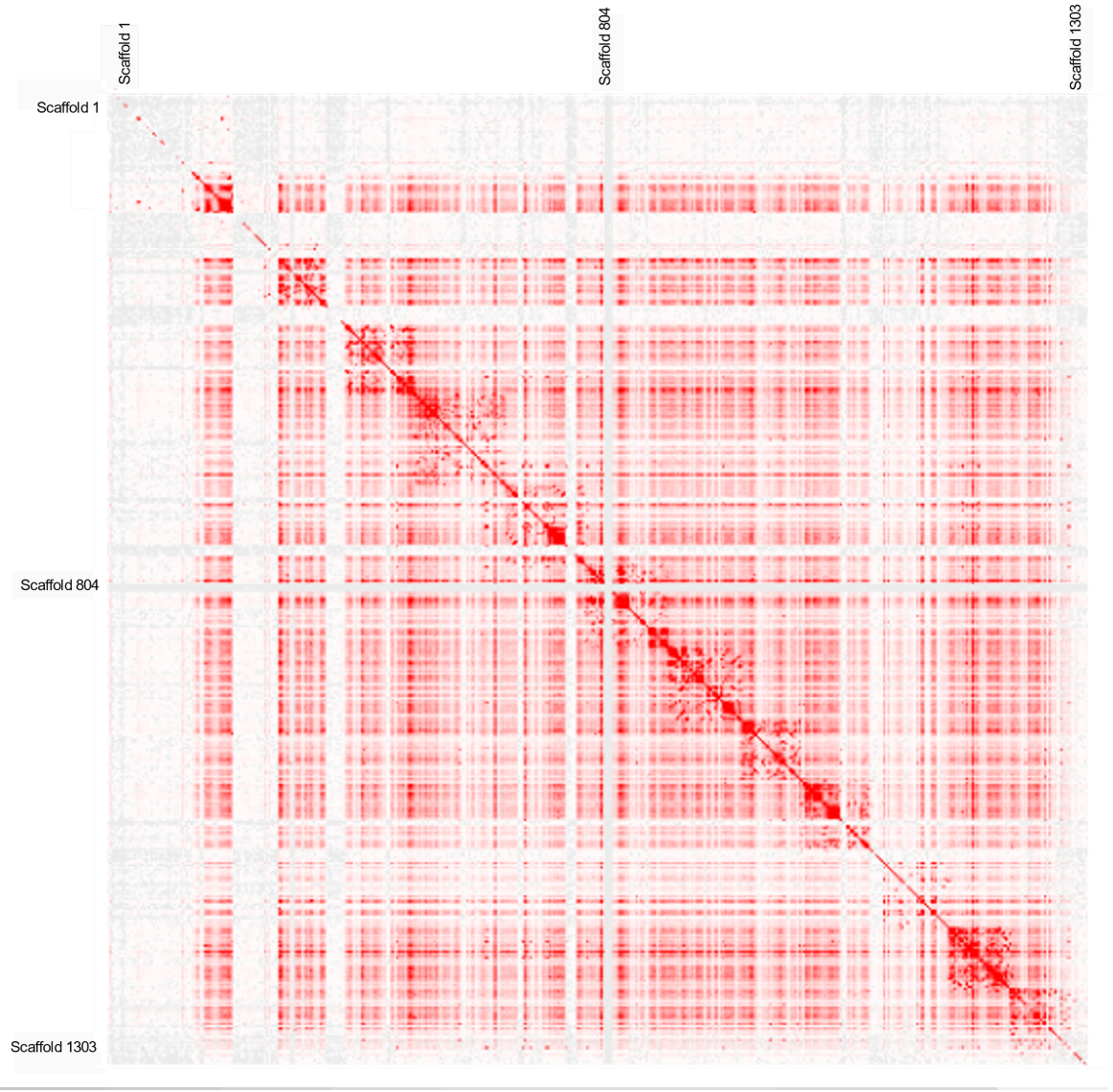

Seasonal differences in S. tuberosum chromatin organization were observed using Pore-C data. Spring samples (1-3) showed a higher cis:trans ratio and distinct long-range contact patterns compared to summer samples (4-7), which exhibited lower cis:trans ratios and different interaction profiles. These findings indicate significant seasonal variation in chromatin conformation.

5.4 Constructing the *R. nigrum* genome for assessing drought stress-induced transcriptomic and metabolomic responses

The German *Ribes nigrum* cultivar Rosenthals Langtraubige was selected for genomic analysis due to its vigorous, spreading bushy growth, and medium-sized, early-maturing berries with a high vitamin C content. To gain molecular insights into the drought stress response, we generated a genome assembly as a foundation for constructing the transcriptome. This allowed us to analyze RNA-Seq data from leaf and root tissues of adult plants. Additionally, metabolite profiling was integrated to provide a comprehensive view of the drought response. To validate our findings, a further drought stress experiment was conducted using young plants and leaf tissue.

5.4.1 *Ribes nigrum* genome sequencing and assembly

The German blackcurrant cultivar *Rosenthals Langtraubige* was selected for genomic analysis due to its robust, widely branching bushy growth form and medium-sized, early ripening berries with high vitamin C content. We utilized a combination of PacBio HiFi sequencing, ONT sequencing, and the Pore-C method for nanopore chromosome conformation capture to generate a high-quality genome assembly. Specifically, we employed hifiasm (UL), using PacBio HiFi reads for initial string graph assembly and ONT nanopore data as “ultralong” reads, which hifiasm integrated into the string graph to produce the final assembly (Cheng *et al*., 2024). Furthermore Pore-C contact data was generated as for potato. (Incorporating the Pore-C data enabled us to construct a genome-scale assembly totaling 871,555,738 base pairs (bp) (Figure 15), with 99.03% of the sequence (867,416,594 bp) anchored to eight pseudo-chromosomes (Figure 14, 15).

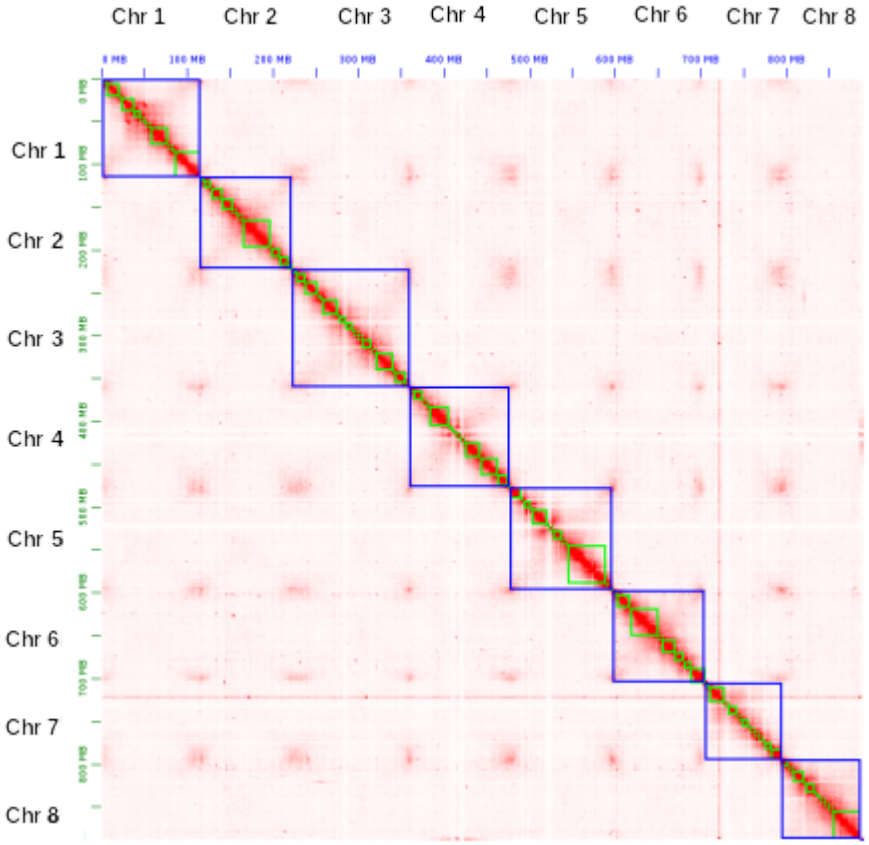

We next investigated dene density and epigenetic patterns of CpG methylation. Our analysis revealed a gene distribution pattern characteristic of many plant genomes, with genes enriched at chromosome ends and fewer near centromeric regions, which were instead populated by transposable elements (TEs), high levels of CpG methylation, and increased GC content (Figure 16).

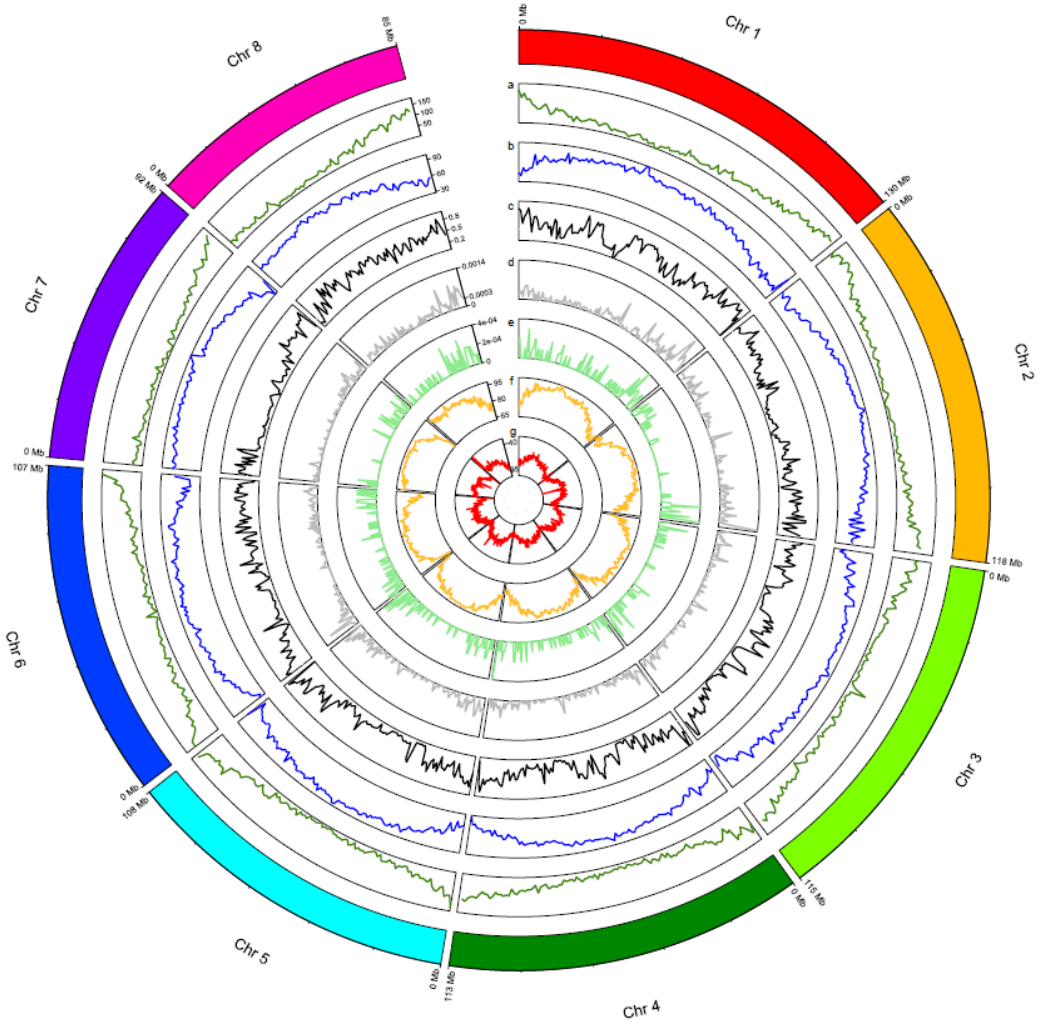

K-mer analysis estimated the genome size at approximately 800 Mb with a predicted heterozygosity of 0.75%, indicating a relatively heterozygous genome for *Rosenthals Langtraubige* blackcurrant (Figure 17).

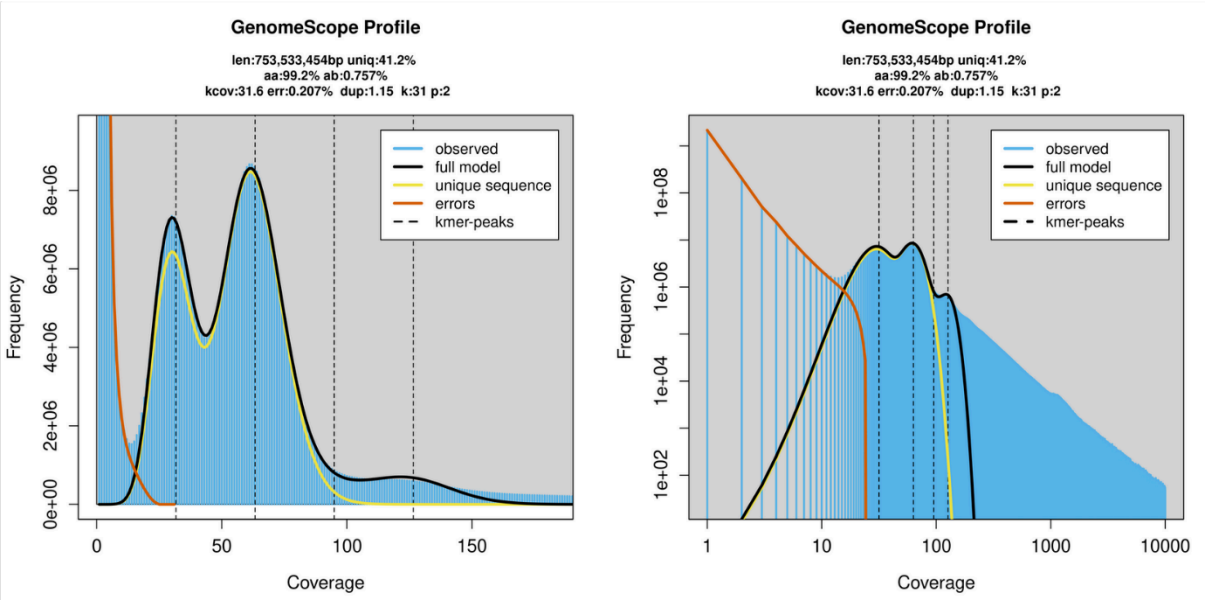

Genome quality assessment using the k-mer analysis tool Merqury (Rhie *et al*., 2020) indicated a high consensus-based quality value (QV) of 57.50 and a k-mer completeness rate of 98.59%, demonstrating a highly accurate and comprehensive genome assembly. Telomeric sequences were detected at the beginning of chromosomes 2 and 4, as well as the ends of chromosomes 3, 5, 6, and 7, with chromosome 8 achieving a complete telomere-to-telomere assembly (Figure 17). The assembly exhibited minimal gaps, with a low gap content of 0.16 Ns per 100 kbp, and a long terminal repeat (LTR) assembly index (LAI) of 14.77, comparable to established reference genome standards such as *Arabidopsis thaliana* (Arabidopsis) (Table 3) (Ou *et al*., 2018).

Supporting these high-quality metrics, the CRAQ quality analysis (Li *et al*., 2023) reported a low clip-based regional error rate (CRE = 0.39) and a minimal clip-based structural error rate (CSE = 0.02). The regional and structural assembly quality indicators (R-AQI = 96.13 and S-AQI = 97.87) exceeded the threshold of 90, reflecting reference-grade assembly quality according to Li *et al*. (2023). Further validation using BUSCO (Benchmarking Universal Single-Copy Orthologs) analysis (Simão *et al*., 2015) yielded a gene completeness score of 98.3% and a duplication rate of 3.9%, affirming the near-complete coverage of single-copy orthologs within the genome assembly. Collectively, these results underscore the exceptional accuracy and completeness of our de novo genome assembly.

Table 3: Assembly statistics for the R. nigrum genome at the pseudo-chromosomal level. (QV = quality value based on *k*-mers; LAI = LTR assembly index; R-AQI = regional assembly quality index; S-AQI = structural assembly quality index).

Genome features	*R. nigrum* genome assembly
No. of chromosomes	8
Total length [bp]	867,416,594
GC content [%]	36.97
N per 100 kbp	0.16
k-mer completeness	98.60
QV	57.50
CRE(R-AQI) [%]	0.39 (96.13)
CRE(S-AQI) [%]	0.02 (97.87)
LAI	14.77

We compared the *R. nigrum* genome assembly to existing genetic data by aligning 73 SNPs with the linkage map derived from the blackcurrant SCRI 9328 population (Russell *et al.*, 2011) (Figure 18, Supplemental Material Table S4). SNP markers associated with the same linkage group were consistently located on the corresponding chromosome within our assembly, and the markers exhibited a largely collinear alignment. Notably, while SNPs from linkage group LG7 were collinear with our assembly, they were positioned exclusively at the start of pseudo-chromosome 7 (Figure 18).

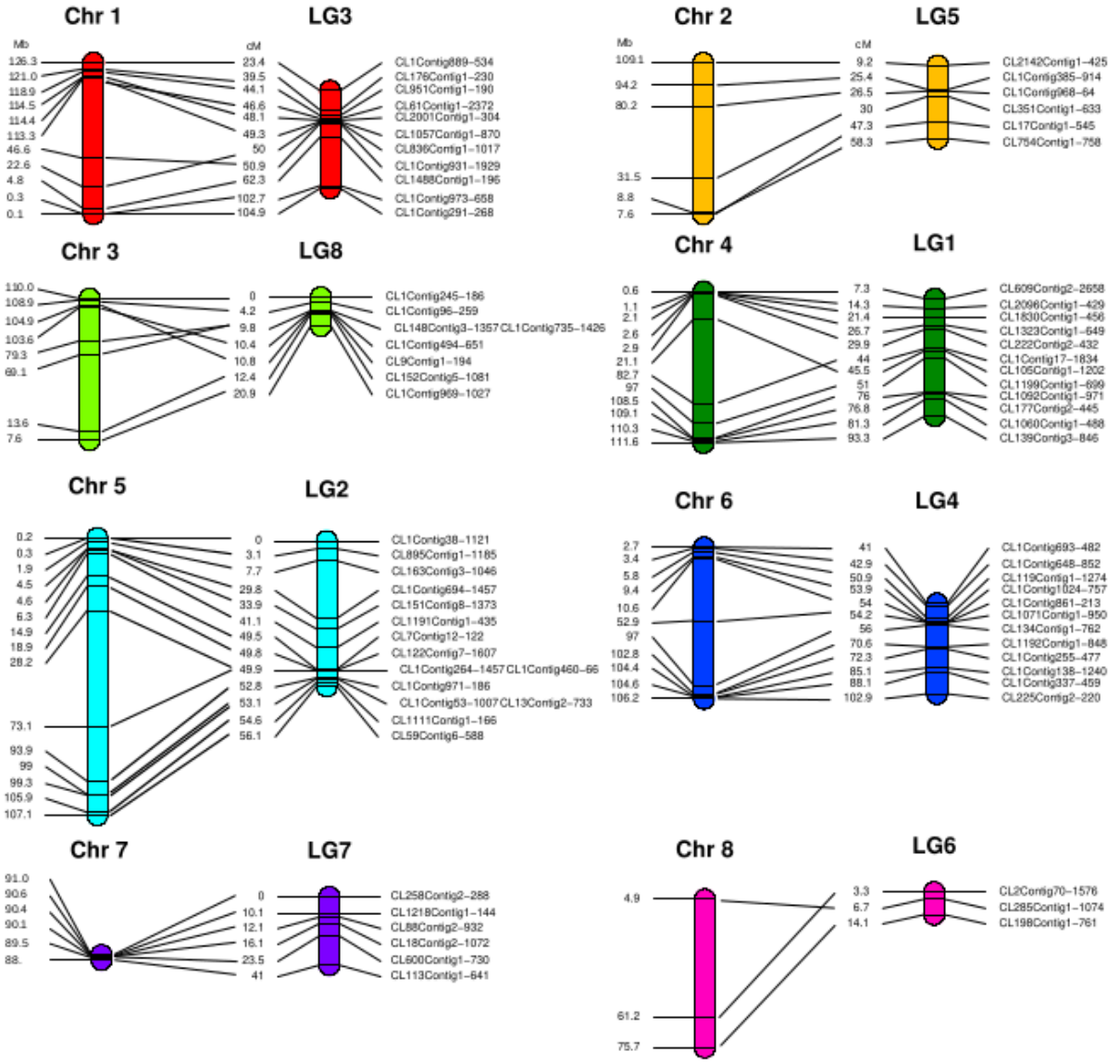

Transposable elements (TE) in the blackcurrant genome were identified using the EDTA pipeline (Ou et al., 2019), revealing that TEs comprise 73.33% of the genome (Table 2). Approximately half of these TEs are LTRs, with Gypsy elements constituting 30.35% and Copia elements 9.03% of the total TE content (Table 4). Terminal inverted repeat (TIR) elements were identified and include Mutator, CACTA, PIF-Harbinger, Tc1/Mariner, hAT, and polintron families. Non-LTR elements, specifically long interspersed nuclear elements (LINEs), represented only 0.27% of all TEs, while non-TIR helitron elements accounted for 2.96% (Table 4).

Table 4: Repetitive DNA content of the scaffolded blackcurrant genome at the anchored pseudo-chromosome level. LTR = long terminal repeat, TIR = terminal inverted repeat.

Class	Superfamily	Count	Masked	Masked

			sequences [bp]	sequences [%]
LTR	Copia	93,001	78,309,531	9.03
	Gypsy	201,313	261,507,560	30.15
	unknown	194,422	94,960,513	10.95
TIR	CACTA	64,085	25,369,267	2.92
	Mutator	158,420	65,986,508	7.61
	PIF-Harbinger	34,197	11,702,040	1.35
	Tc1_Marnier	18,514	4,910,143	0.57
	hAT	55,797	19,738,629	2.28
	polintron	8	3,314	0.00
Non-LTR	LINE	4,848	2,379,098	0.27
Non-TIR	helitron	73,220	25,686,508	2.96
Repeat-region		147,113	45,549,242	5.25
Total		1,044,938	636,102,353	73.33

The hybrid HiFi assembly approach enabled the generation of haplotype-resolved assemblies, yielding haplotype 1 at 900 Mbp and haplotype 2 at 885 Mbp, with corresponding N50 values of 61 Mbp and 51 Mbp, respectively (Figure 16). Individual k-mer analysis of each haplotype showed k-mer completeness values of 84.74% and 84.84%, with QV of 56.96 for haplotype 1 and 58.12 for haplotype 2. These results further confirmed the high heterozygosity of the genome, aligning with the 0.75% heterozygosity estimated by Genoscope analysis (Figure 15). Based on this heterozygosity, we conducted SNP calling between the two haplotypes using both long-read and short-read data for SNPs, while identifying structural variants using long-read data alone. This analysis yielded 2,176,479 SNPs and 64,644 heterozygous structural variants. Notably, lower heterozygosity was observed in the internal regions of chromosome 7 (Figure 16c).

Further analysis identified 1,256 variants that introduced premature stop codons and 373 variants that converted stop codons into non-stop codons (Figure 16d-e; Ziegler *et al*., 2024 Supplemental Material Table S5). Functional annotation of SNPs revealed a significant enrichment of variants leading to premature stop

codons in genes associated with secondary metabolism (FDR < 0.05; Ziegler *et al*., 2024 Supplemental Material Table S5), while genes involved in photosynthesis and phytohormone signalling were depleted of such variants (FDR < 0.001; Ziegler *et al*., 2024 Supplemental Material Table S5).

To enhance data accessibility, RagTag was used to scaffold the two haplotypes to the complete genome assembly, producing a streamlined chromosome-scale representation of each haplotype (Supplemental Figure S4).

5.4.2 *R. nigrum* genome annotation

Genome annotation, performed with an integrative pipeline combining *ab initio* and evidence-based methods, predicted a total of 42,380 gene sequences. Of these, 86.20% were functionally annotated using Mercator (Schwacke *et al*., 2019). The quality of the annotated gene models was verified through BUSCO analysis, which indicated a proteome completeness score of 97.6%.

5.4.3 Drought stress-induced DEGs

To investigate the drought stress response in adult blackcurrant plants leaves and roots, water was withheld for a period of four days. The drought-treated plants exhibited characteristic stress symptoms, including leaf curling and dryness (Figure 19A-C). In contrast, control plants that received continuous irrigation over the same period showed no visible changes in appearance (Figure 19D-F).

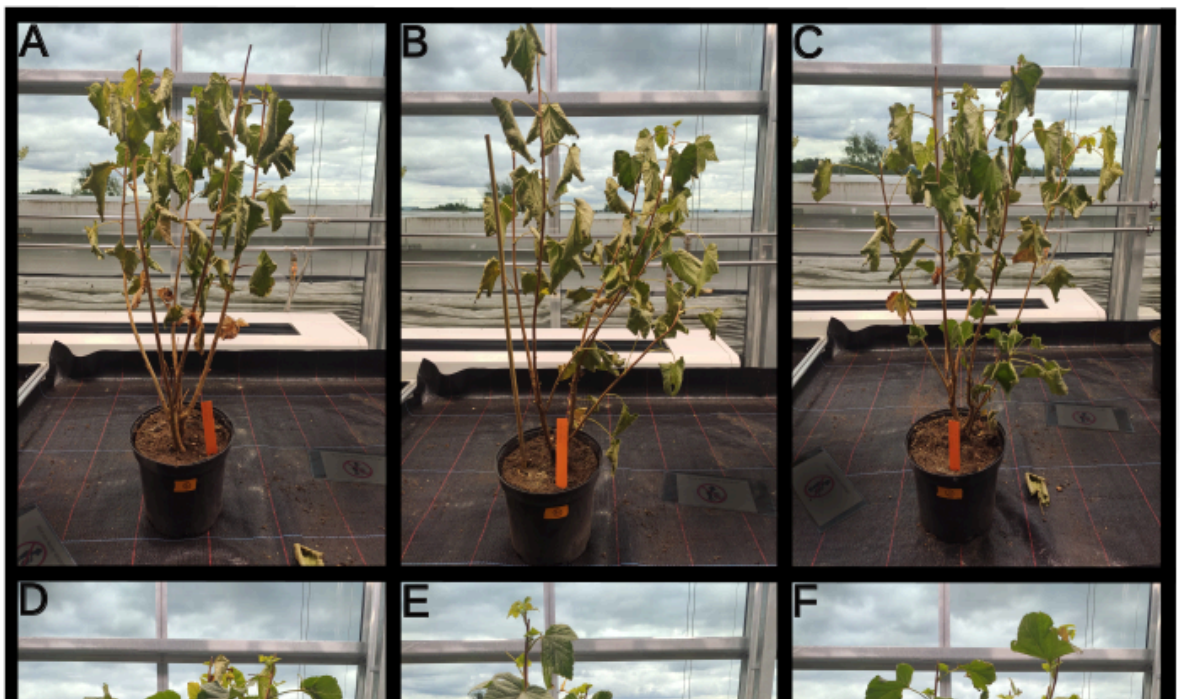

To identify differentially expressed transcripts in the leaves and roots of adult blackcurrant plants under drought stress, we utilized nanopore-based RNA-Seq. In leaf samples, we detected 540 differentially expressed genes (DEGs) with an FDR < 0.1, comprising 48 upregulated and 492 downregulated genes. Root samples showed a much larger number of DEGs, totalling 8,353 even with a more stringent FDR threshold of < 0.05; among these, 3,697 genes were upregulated, and 4,656 were downregulated.

To validate these findings, a second drought stress experiment was conducted on younger plants, where water was again withheld for 10 days (Figure 20).

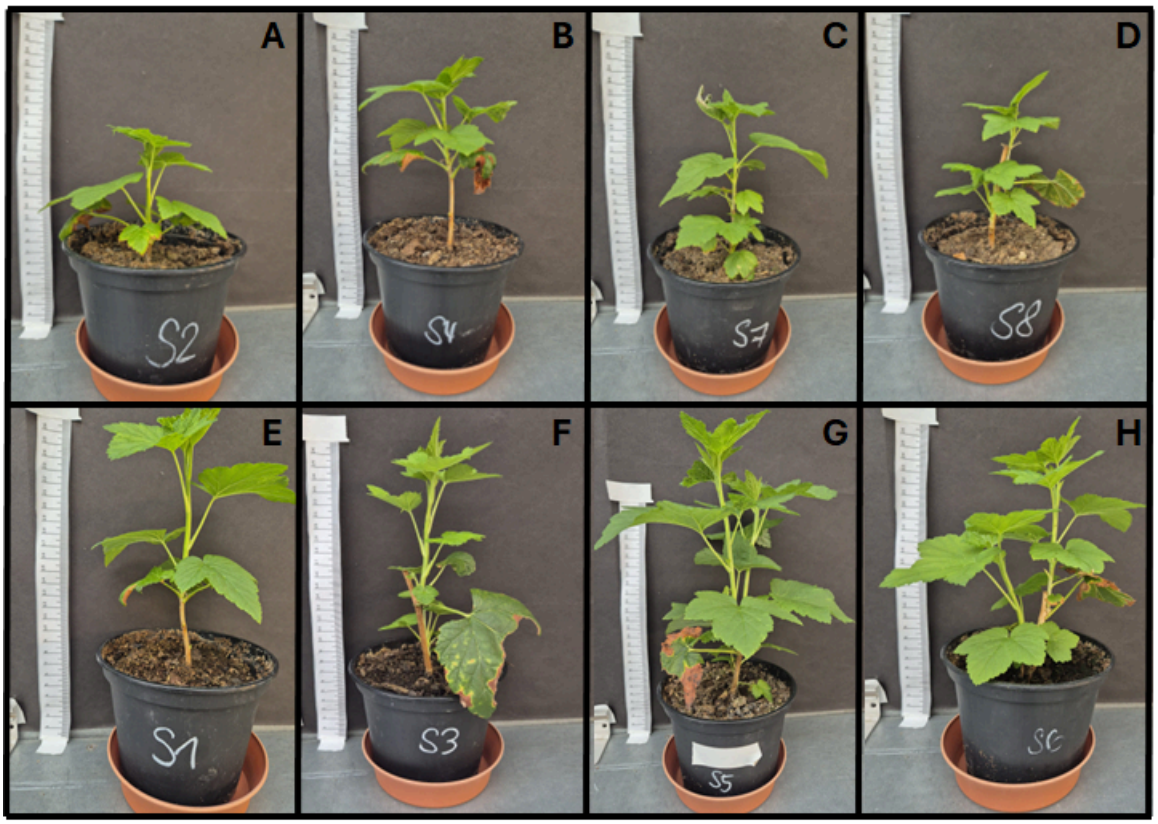

Figure 20: Drought stress treatment of young *R. nigrum* cv Rosenthals Langtraubige plants. A-D) Stressed plants after 10 days without water. E-H) Control plants with continuous irrigation according to their weight.

The response of drought-treated young plants exhibited distinct differences compared to adult plants. Minimal to no leaf curling or desiccation was observed, with only a single plant (Figure 20C) displaying slight curling and dryness on one leaf following drought exposure. Additional physiological metrics, including leaf count, plant height, growth rate, and total weight, were assessed (Figure 21). All parameters demonstrated significant differences ($p < 0.05$) between the control

and drought-treated groups (Figure 21). Drought-treated plants showed reduced leaf number and height, and overall growth was adversely impacted by drought stress (Figure 21).

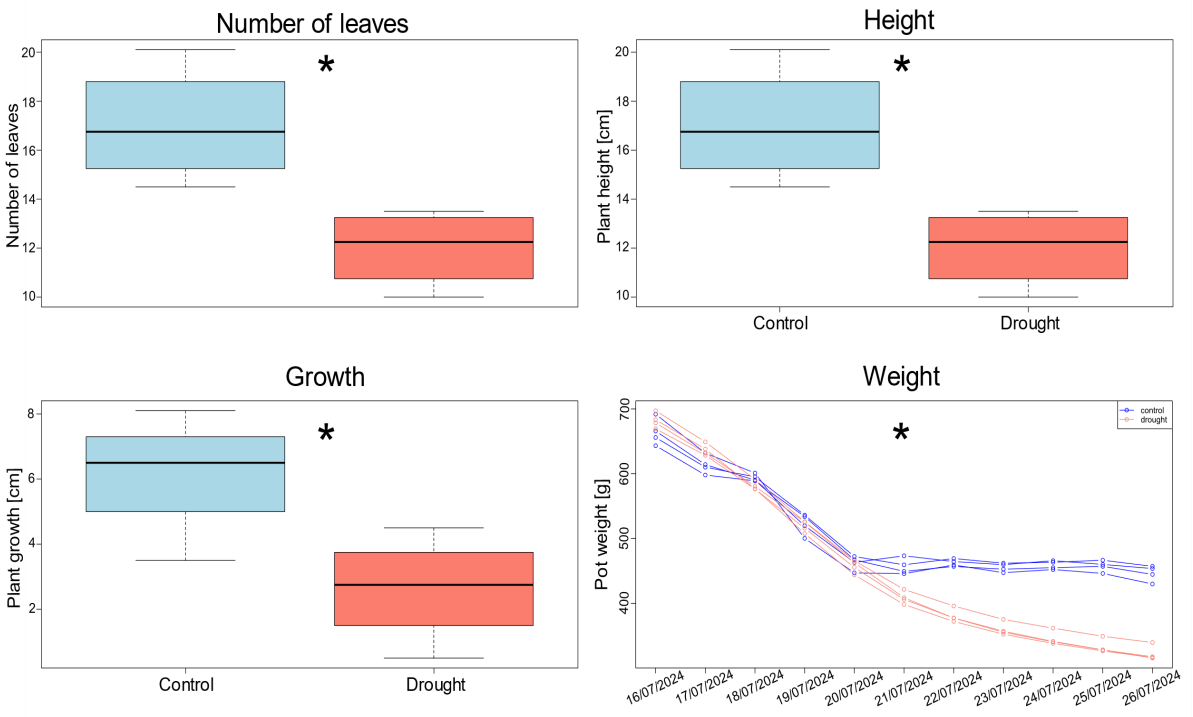

Figure SEQ Figure * ARABIC 21: Physiological parameter of young blackcurrant plants under drought stress treatment. Number of leaves, height and growth are shown as boxplots for control (blue) and drought (red) treated plants. Weight of the plants in soil are shown as line diagram for the different dates throughout the experiment with the same colour coding. Significance level of p-values marked *p value < 0.05, **p value < 0.01 and ***p value < 0.001.

In the leaf samples of young plants, we identified 7,891 DEGs at an FDR < 0.05, with 3,642 genes upregulated and 4,249 downregulated. Cross-examining the 540 DEGs from the first experiment, we found that 80 genes (FDR < 0.1) demonstrated consistent regulatory patterns across both studies. In this analysis, three DEGs demonstrated upregulation across both studies, while 77 DEGs exhibited consistent downregulation in leaf tissue of both young and adult plants (Figure 22).

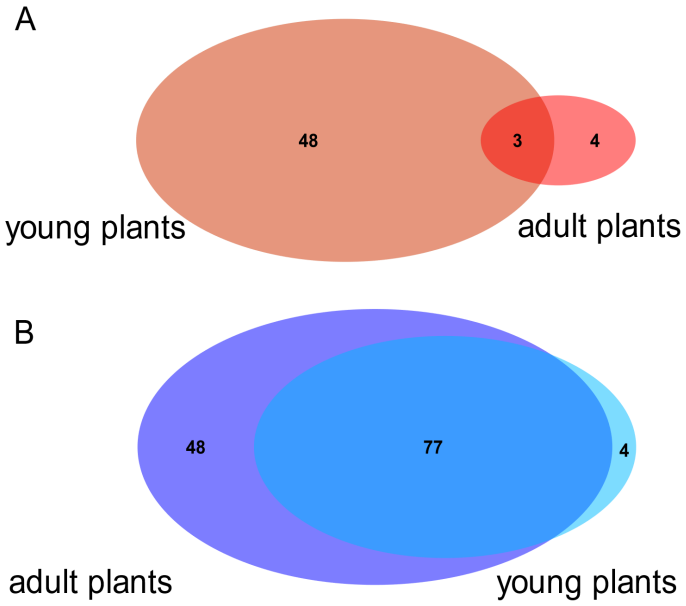

Figure 22: Overlapping differentially expressed genes (FDR < 0.1) between young and adult blackcurrant plants under drought stress treatment in leaf tissue. A) Overlap between upregulated DEGs and B) downregulated DEGs in leaf tissue.

5.4.4 Drought stress induced MapMan protein classes

To get a first overview of protein classes involved in drought stress between controlled and treated plants in leaf and root tissue a PCA-ORA plot (3.1.1) was used. Showing differences and similarities between leaf tissue of adult and young plants.

In adult plants, control and drought stress samples displayed clear separation along the PC1 and PC2 axes, except for a single control sample that clustered similarly to a drought-stressed sample. Along the PC1 axis, solute transport, phytohormone signaling involving signaling peptides, response to external stimuli, and micronutrient homeostasis through metallochaperone activity had the greatest impact on sample differentiation (Figure 23). Separation along the PC2 axis was primarily driven by factors related to chromatin organization, DNA structural modifications, response to external stimuli, RNA modification, protein homeostasis via the ubiquitin-proteasome system, and RNA biosynthesis (Figure 23).

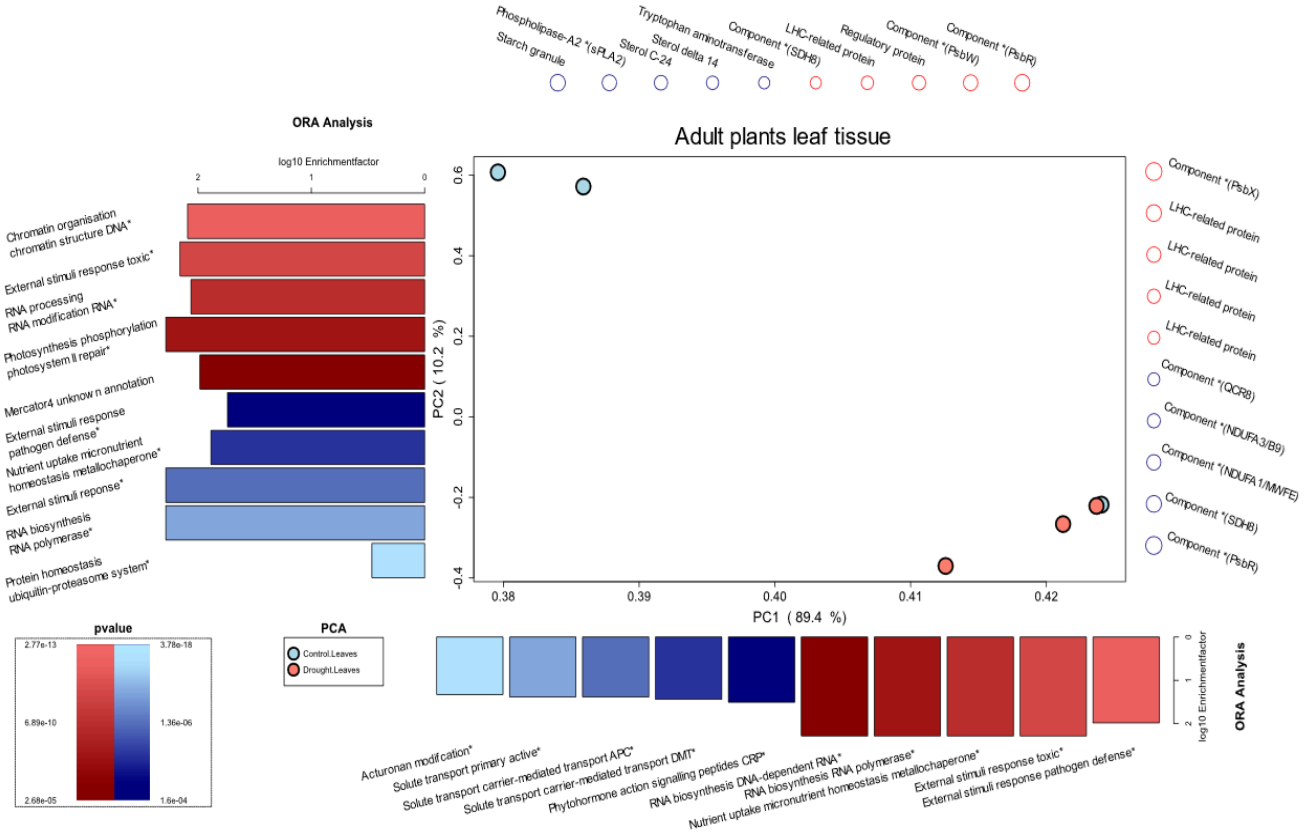

In young plants under drought stress, sample separation was observed along the PC1 axis within groups and along the PC2 axis between groups. Key drivers along the PC1 axis included solute transport channels, RNA biosynthesis and processing, response to external stimuli, micronutrient homeostasis via metallochaperones, and photosynthetic pathways such as CAM/C4 (Figure 24). Separation along the PC2 axis was influenced by lipid metabolism, coenzyme metabolism, cell wall organization, RNA biosynthesis, protein synthesis, and micronutrient uptake (Figure 24).

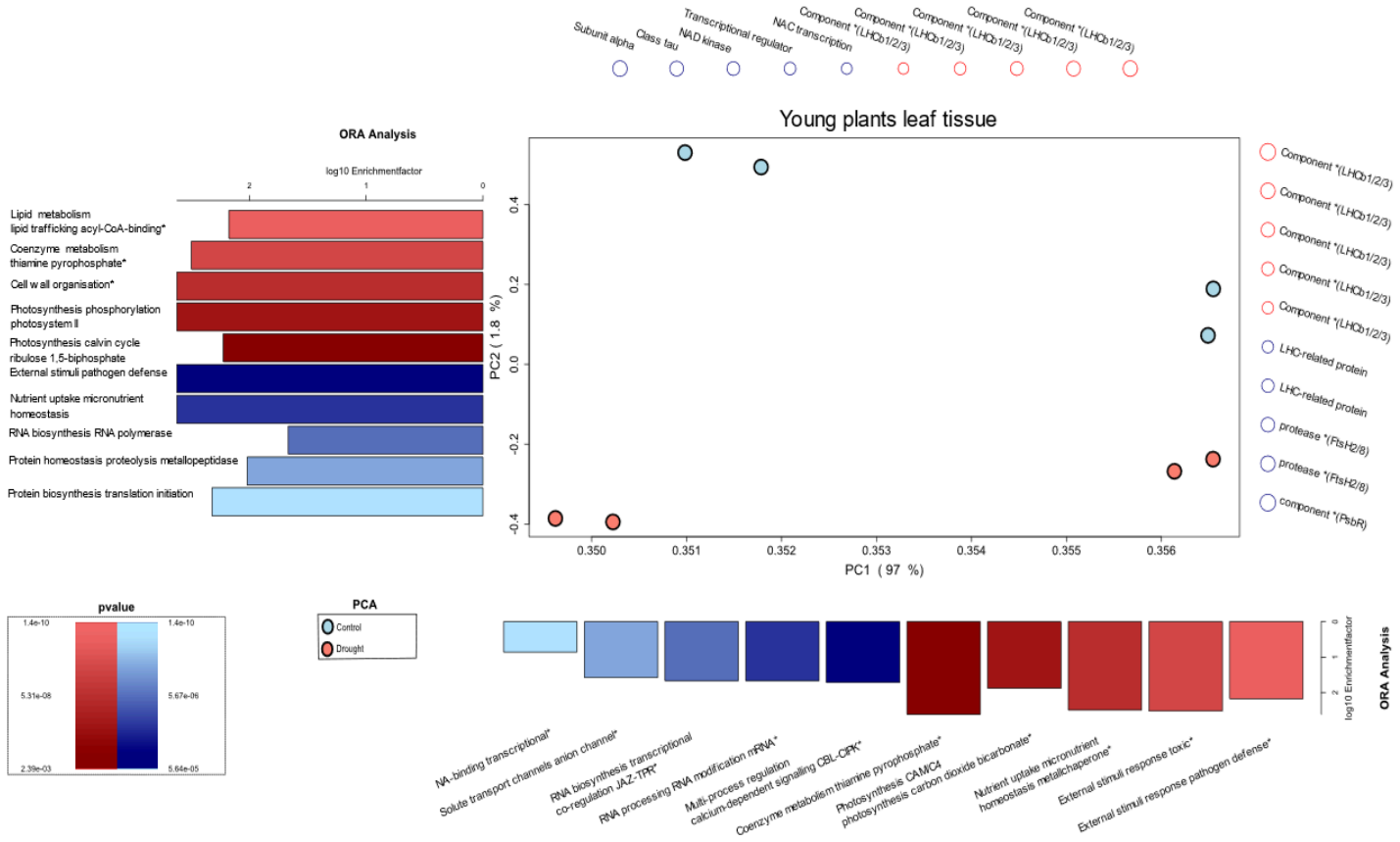

Although the separation patterns differed between adult and young plants, several MapMan protein classes were prominently involved in both age groups. These included responses to external stimuli, micronutrient homeostasis mediated by metallochaperones, and processes related to RNA biosynthesis and processing.

5.4.5 Impact of drought stress on protein kinases

In the adult plants, we identified 243 genes encoding leucine-rich repeat (LRR) protein kinases, mainly representing families I–XV (Supplemental Material Table S7). For the young plants, 206 of these LRR encoding transcripts were found, showing similar expression results for most transcripts. Most LRR protein kinases were downregulated in leaves (Supplemental Material Table S7). Most LRR protein kinases were downregulated in leaves. However, three LRR-XV genes were slightly upregulated in leaves and 16 LRR-XII genes where transcripts were strongly downregulated ($log_2FC < -2$) in leaves (Supplemental Material Table S7). Here, we could find 10 of these transcripts downregulated in young plants. In the roots, most LRR protein kinases were downregulated (FDR < 0.05).

Another member of the LRR family, the receptor-like cytoplasmic kinases (RLCK) multiple transcripts were of RLCK-IXb, V, VI, VIIa, VIIb, VIII, X, XI, XII, XV found differentially expressed. Six RLCK-V transcripts were significantly downregulated in roots of adult plants (FDR<0.01). Three transcripts of RLCK-VI (RN5G010110.1, RN1G011660.1, RN1G053710.1) were significantly downregulated in roots and have shown a strong downregulation in leaves in adult plants ($Log_2FC<-2$). This expression pattern was also observed in leaf tissue in young plants (Supplemental Material Table S7). The downregulation was also identified for RN1G032180.1 (RLCK-X) and RN3G051940.2 (RLCK-XII) for both tissues in adult plants and was significant for roots. The RLCK-IXb gene RN4G001630.1 was significantly upregulated in roots (FDR<0.05) and leaf tissue in young plants (FDR<0.05) (Supplemental Material Table S7).

Several DEGs encoded components of the MAPK cascade. Three MAPK kinases (NPK/ANP) were upregulated in leaves but significantly downregulated in roots (FDR < 0.05) (Supplemental Material Table S7). In contrast, the transcript encoding MAP2K (RN3G007350.1) was slightly upregulated and MAP3K-MEKK (RN5G010030.1) was strongly downregulated ($log_2FC < –2$) in leaves and RN3G007350.1 was slightly upregulated in roots (Supplemental Material Table S7). In young plants these transcripts were slightly regulated but not significantly so. Ca^{2+}-dependent protein kinase (CDPK) transcripts were mostly upregulated in leaves and roots, with RN1G025100.1 significantly upregulated in roots (FDR < 0.01). In contrast, two CDPK transcripts (RN1G043640.1 and RN5G008650.1) were significantly downregulated in roots and RN1G043640.1 was downregulated in leaves. One DOMAIN OF UNKNOWN FUNCTION 26 (DUF26) transcript was significantly (FDR < 0.05) upregulated in roots and two others were significantly downregulated (Supplemental Material Table S7). In young plants the transcript RN8G019550.2 (DUF26) was significantly upregulated (FDR < 0.01), which showed the same expression in leaf and root tissue of adult plants.

Five transcripts encoding proline-rich extensin-like receptor kinases (PERKs) were downregulated in leaves, including RN4G048640.1, RN7G025360.1 and RN7G034400.1, which were also significantly downregulated in roots (FDR < 0.01). In contrast, RN3G015760.1 was significantly upregulated in roots (FDR < 0.01) (Supplemental Material Table S7). Transcripts in young plants in leaf tissue

showed the same expression pattern as roots in adult plants and RN3G015760.1 was also significantly upregulated (FDR < 0.01).

5.4.6 Transcription factors and metabolism

Transcripts encoding *AP2/ERF*, *bZIP*, *CBF/DREB1*, *DREB2*, *C2H2*, *HD-ZIP*, *R2R3-MYB*, *WRKY*, *HD-ZIP*, *bHLH* and *NAC* transcription factors were differentially expressed in both tissues of adult plants. Transcripts associated with carotenoid and ABA metabolism, including those encoding PYL/RCAR and abscisic aldehyde oxidase, were generally downregulated, and the PYL/RCAR transcripts RN3G031060.1, RN4G014070.1 and RN4G030230.1 were significantly (FDR < 0.01) downregulated in the roots (Supplemental Material Table S7). In young plants in leaf tissue RN3G031060.1 showed the same significant downregulation (FDR < 0.001) as in roots in adult plants. Several transcripts encoding SnRK1 and SnRK2 SNF1-related protein kinases were modulated in both tissues in adult plants and also in leaf tissue in young plants, with significant differential expression in the roots. Several transcripts associated with cell wall regulation were identified in the leaves. Genes encoding *p-coumaroyl shikimate/quinate 3-hydroxylase* were modulated in leaves and roots (Supplemental Material Table S). RN6G009060.1, encoding hydroxyproline-O-galactosyltransferase (GALT29), was significantly downregulated in roots and slightly downregulated in leaves. Transcripts encoding caffeoyl-CoA 3-O-methyltransferase were significantly downregulated in roots but were expressed at minimal levels in leaves (Supplemental Material Table S8).

5.4.7 Relative expression of drought stress induced through qRT-PCR

To validate the results of drought-stress induced genes, a total of 13 DEGs, comprising 6 upregulated and 7 downregulated genes in leaf tissue of adult plants, were selected for qRT-PCR. The raw qPCR data was kindly provided by Sarah Spettman and Franziska Genzel. The analysis was conducted using Actin and eIF4A as endogenous controls. The results indicated that the selected genes exhibited comparable gene expression fold changes between quantitative qRT-PCR and computational analyses in both leaf and root tissues of mature plants (Figure 25 B). Additionally, qRT-PCR was conducted for the same genes,

excluding 4HbD and WRKY, which could not be reliably quantified in the leaf tissue of young plants. Of these 11 genes, the expression of 8 genes were consistent with those observed in the leaf tissue of drought-stressed adult plants, further validating the selected candidate genes involved in the *R. nigrum* response to drought stress (Figure 25 A-B).

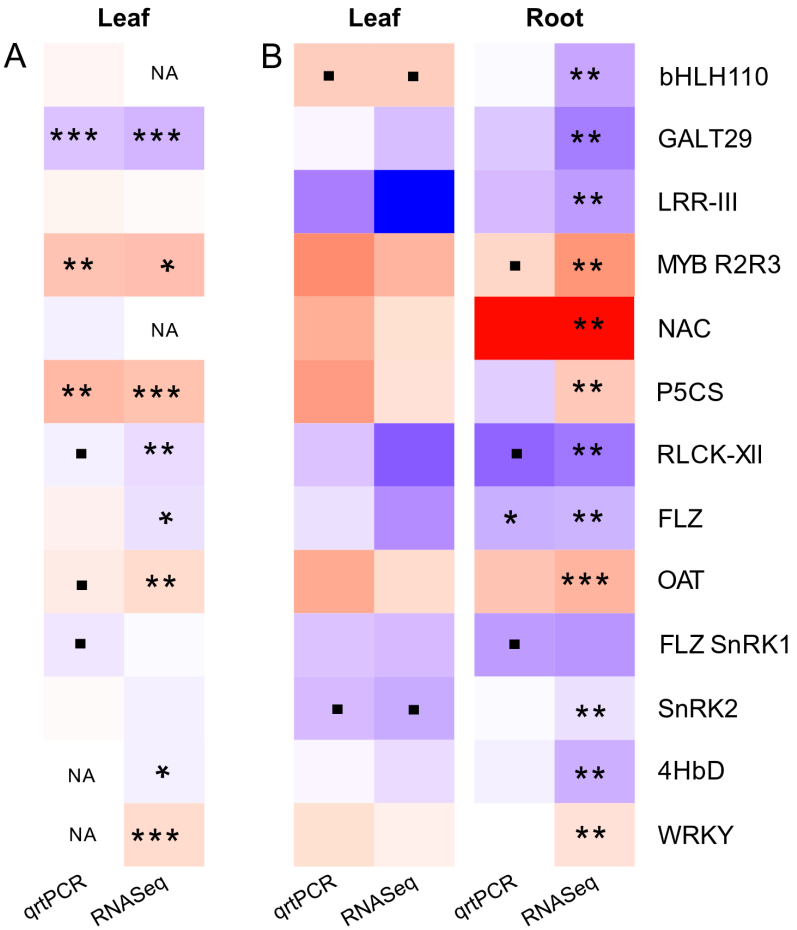

5.4.8 Metabolite changes due to drought stress

Next, we compared the abundance of 60 primary metabolites that were measured by Jose Valleriano and Sonio Osorio (Uni Malaga) in response to drought stress in leaves and roots of mature plants. Several were barely affected, but 14 leaf metabolites became significantly more abundant under stress ($log_2FC > 1$, FDR < 0.05). Most of these metabolites were amino acids and their derivatives such as threonine, valine, proline, isoleucine, methionine, glutamine, glutamic acid, tryptophan, phenylalanine, alanine and 4-aminobutanoic acid (GABA) (Table 5, Supplemental Material Table S7, S8). Sugars such as

mannose, sugar derivatives such as galactinol, and the organic acid quinic acid also accumulated in response to drought, whereas citric acid was the only metabolite that was significantly depleted.

Table 5: Metabolites in blackcurrant leaf and root tissue for adult and young plants that change in abundance in response to drought stress. Upregulation (red) and downregulation (blue) are shown according to the log_2FC of the genes. Significance levels of adjusted p-values (FDR) are shown in bold. Metabolites that were not measured are designated as "NA".

	Leaf				**Root**			
	Adult plants		Young plants		Adult plants		Young plants	
Metabolite	**Log_2FC**	**FDR**	**Log_2FC**	**FDR**	**Log_2FC**	**FDR**	**Log_2FC**	**FDR**
Amino acids								
Alanine	1.09	0.025*	-0.74	0.174	0.18	0.61	1.57	0.04*

Valine	2.23	0.004**	0.66	0.03*	0.83	0.13	1.73	0.04*
Isoleucine	2.57	0.005**	0.75	0.043	1.47	0.07	1.84	0.04*
Proline	2.67	0.015*	0.64	0.03*	0.59	0.23	1.20	0.04*
Serine	0.92	0.056	-0.86	0.199	-0.10	0.23	0.83	0.17
Threonine	2.05	0.003**	0.43	0.049	0.15	0.68	NA	NA
GABA	1.28	0.017*	0.78	0.041*	-0.28	0.61	0.87	0.16
Methionine	2.31	0.015*	-0.01	0.454	-0.78	0.13	0.98	0.16
Glutamic acid	2.12	0.024*	-0.66	0.03*	0.43	0.23	NA	NA
Phenylalanine	2.72	0.009**	1.23	0.021*	0.45	0.13	1.11	0.10
Glutamine	2.86	0.006**	-0.11	0.070	0.05	0.83	1.33	0.16
Tryptophan	3.45	0.004**	-0.06	0.380	NA	NA	NA	NA
Organic acids								
Quinic acid	0.82	0.017*	-0.16	0.199	NA	NA	NA	NA
Citric acid	-1.39	0.047*	-0.10	0.203	-0.90	0.13	0.04	0.24
Sugars & derivatives								
Galactinol	0.62	0.011*	-0.56	0.037*	NA	NA	NA	NA

Few metabolic changes were observed in the roots. However, mannose and isoleucine accumulated in response to drought stress ($log_2FC > 1.3$) whereas β-alanine was depleted ($log_2FC < –1.3$). We also observed a slight increase in the levels of valine, isoleucine and methionine ($log_2FC > 0.5$), and a slight decrease in the levels of citric acid ($log_2FC < –0.5$) (Supplemental Material Figure S8). Although these metabolites showed minor changes according to their log_2FC values, the adjusted p value suggested that the changes were not significant. In the leaf tissue of young plants, similar patterns were observed for valine, isoleucine, proline, threonine, GABA, and phenylalanine compared to the leaf tissue of adult plants. Additionally, valine, proline, GABA, and phenylalanine exhibited significant upregulation (FDR > 0.05), while alanine, serine, and glutamic acid showed a slight downregulation (Supplemental Material Table S9).

5.4.9 Connecting DEGs with metabolites in response to drought stress

The integration of data from the analysis of DEGs and metabolites revealed associations involving the tricarboxylic acid (TCA) cycle, GABA biosynthesis, cysteine and methionine metabolism, proline metabolism, alanine and aspartate metabolism, as well as branched-chain amino acid metabolism. We also found associations between groups of altered metabolites in leaves (FDR < 0.05), and between groups of DEGs in both tissues (Figure 26). In the context of the TCA cycle and the depletion of citric acid, all related transcripts in leaves in adult plants were strongly upregulated (Supplemental Material Table S9) except for ATP citrate ligase (*ACLY)* (RN7G026170.1), which was downregulated in leaves and roots. In young plants this transcript showed a similar significant downregulation (FDR < 0.01). GABA-associated genes were mainly upregulated in both tissues in adult and young plants. Notably, one gene encoding a bifunctional γ-hydroxybutyrate dehydrogenase (RN1G038820.1) was significantly downregulated in roots, while another (RN3G012700.1) showed no significant differential expression in roots. *Glutamate decarboxylase* genes were significantly upregulated (RN8G004390.1) or downregulated (RN6G037990.1) in roots but were not expressed at significant levels in leaves. The *succinate-semialdehyde dehydrogenase* gene RN8G041850.1 was significantly upregulated in roots but showed no expression in young plants in leaf tissue (Supplemental Material Table S9). Genes involved with alanine, aspartate and glutamate metabolism were generally downregulated in both adult and young plants (except *ASAT*, demonstrated upregulation). Furthermore, genes encoding *CPS* and *NADH-GOGAT* were observed to be upregulated in leaves, while a threonine aldolase gene demonstrated a significant downregulation in the roots (Supplemental Material Table S9). All transcripts associated with valine, leucine and isoleucine metabolism showed significantly upregulated in adult plants. One *threonine dehydratase* gene (RN6G010130.1) exhibited a marked decrease in roots (Supplemental Material Table S9). In young plants most of these transcripts

were downregulated except RN4G055970.1 and RN2G016250.1, which were upregulated (Supplemental Material Table S9).

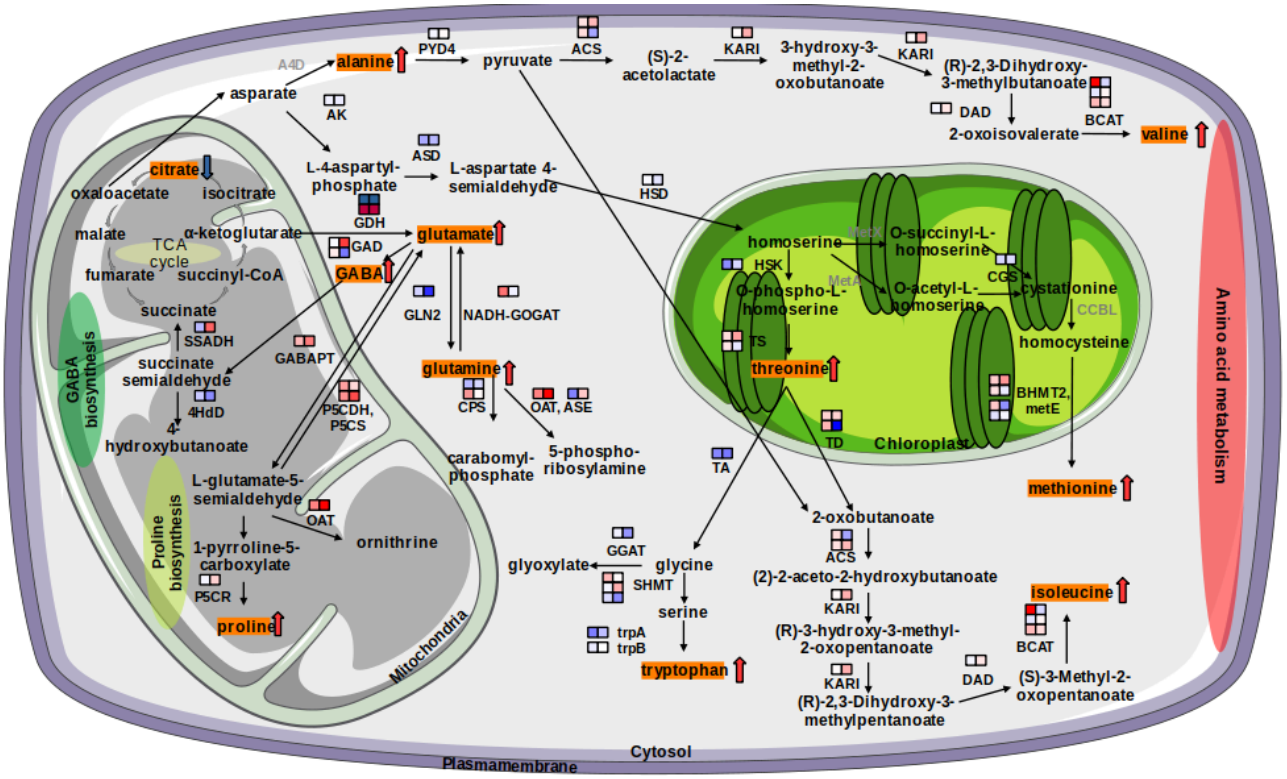

Transcripts in adult plants involved in proline metabolism were mostly upregulated in leaves, although several glutamate dehydrogenase transcripts were downregulated, and the same genes were significantly (FDR < 0.05) downregulated in roots (Table 6, Figure 27). These results were also found in leaf tissue in young plants, except for some glutamate dehydrogenase, which have shown no expression. For transcripts of P5CDH (RN8G016110.1), OAT (RN2G017990.2), P5CR (RN2G007260.1) and P5CS (RN4G032560.1) expression in young plants was similarly regulated as in leaf tissue of young plants, while OAT, P5CR, P5CS were significantly differentially expressed (FDR < 0.05). Transcripts encoding ornithine-γ-aminotransferase and two $^{1}\Delta$-pyrroline-carboxylate synthases were significantly upregulated in roots of adult plants (FDR < 0.01).

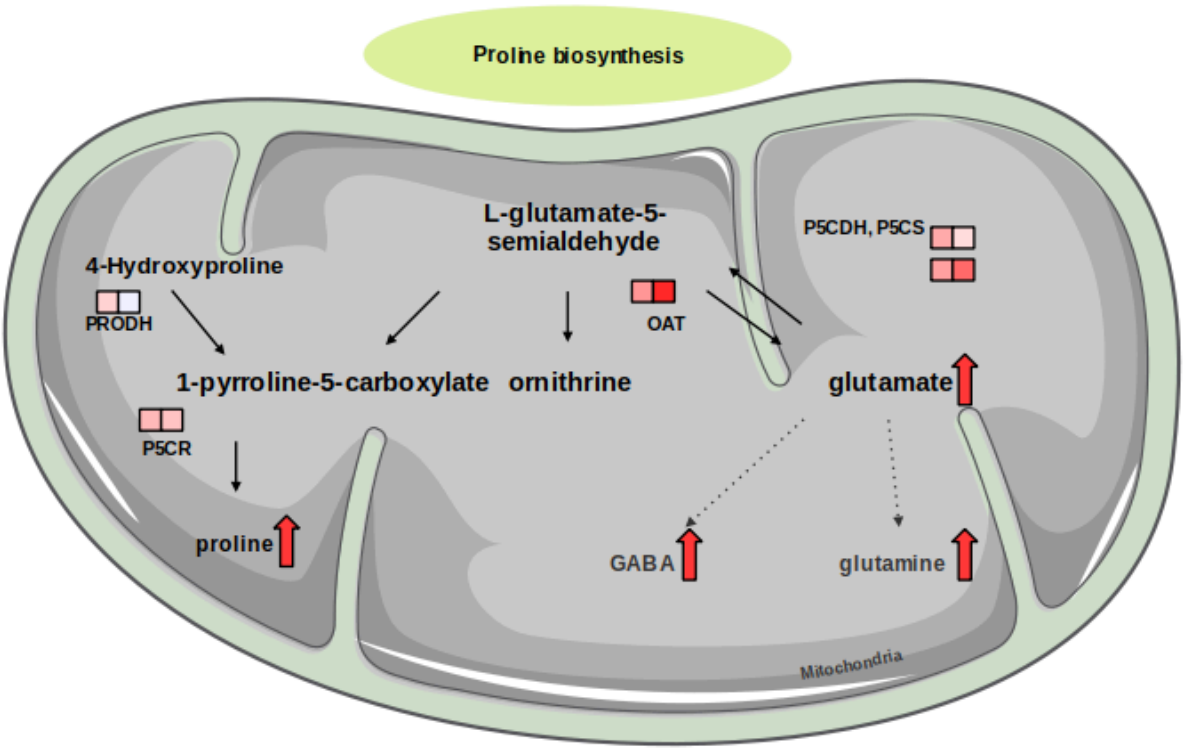

Figure 27: Proline biosynthesis metabolites with significantly altered levels under drought stress in the leaves of *R. nigrum*. Differentially expressed genes (Table 4) encoding enzymes (annotated using MapMan) are aligned with specific metabolic reactions. Upregulated genes are denoted by red squares and downregulated genes by blue squares, with squares on the left and right indicating leaves and roots, respectively. Multiple rows of squares denote multiple genes with the same enzymatic functions. Metabolites that accumulate under drought stress (Table 5 and Supplemental Tables S1 and S2) are highlighted with a red arrow. Abbreviations: OAT = ornithine-γ-aminotransferase; P5CDH = $^{1}\Delta$-pyrroline-carboxylate dehydrogenase; P5CR = pyrroline-carboxylate dehydrogenase; P5CS = $^{1}\Delta$-pyrroline-carboxylate synthase; PRODH = proline dehydrogenase.

Table 6: Differentially expressed transcripts involved in proline metabolism and their MapMan annotations. Upregulation (red) and downregulation (blue) reflect the log_2FC values, with significance (FDR adjusted p values) shown in bold.

Gene ID	MapMan annotation	Enzyme Name	Leaf [log_2FC]	Leaf [FDR]	Root [log_2FC]	Root [FDR]
RN8G016110.1	¹Δ-pyrroline-carboxylate dehydrogenase	P5CDH	0.72	0.13	0.31	0.23
RN1G008890.1	Glutamate dehydrogenase *(GDH)	GDH	-3.66	0.12	-1.17	0.08
RN1G008920.1	Glutamate dehydrogenase *(GDH)	GDH	-5.77	0.11	-1.52	0.05
RN1G008960.1	Glutamate dehydrogenase *(GDH)	GDH	-2.73	0.23	-1.69	***0.03****
RN1G008980.1	Glutamate dehydrogenase *(GDH)	GDH	-1.82	0.35	-1.89	***0.03****
RN3G012920.1	Glutamate dehydrogenase *(GDH)	GDH	0.43	0.27	0.22	0.38
RN3G035860.1	Glutamate dehydrogenase *(GDH)	GDH	0.35	0.57	-1.68	***0.008****
RN4G025340.1	Glutamate dehydrogenase *(GDH)	GDH	0.51	0.82	1.12	0.08
RN2G017990.1	Ornithine aminotransferase	OAT	0.92	0.43	1.94	***0.0004*****
RN1G015520.1	Proline dehydrogenase	PRODH	0.38	0.56	-0.26	0.57
RN1G019530.1	Pyrroline-5-carboxylate reductase	P5CR	-0.19	0.58	0.33	0.15
RN2G007260.1	Pyrroline-5-carboxylate reductase	P5CR	-0.10	0.78	0.25	0.22
RN3G051060.1	¹Δ-pyrroline-carboxylate synthase	P5CS	0.83	0.61	1.38	***0.007****
RN4G032560.1	¹Δ-pyrroline-carboxylate synthase	P5CS	0.81	0.68	1.35	***0.005****

A partially haplotype-resolved, chromosome-scale genome assembly of blackcurrant (*R. nigrum* L. cv Rosenthals Langtraubige) was generated using a hybrid approach combining ONT and PacBio HiFi long-read sequencing. The genome, comprising eight pseudo-chromosomes, was used to investigate drought stress responses in leaves and roots at the transcriptomic and metabolomic levels. Differential gene expression analysis revealed transcription factors (*bZIP*, *bHLH*, *MYB*, *WRKY*) and tyrosine kinase-like kinases (*PERK*, *DUF26*) involved in the drought response. Gene expression correlated with primary metabolite abundance, identifying 14 metabolites with significant

differences under drought stress. Proline levels increased under stress, while organic acids decreased, indicating a metabolic adaptation.

6 Discussion

This study aimed to generate, analyse, visualize, and integrate multi-omics datasets to gain comprehensive insights into the complex biological systems of strawberry (*Fragaria* × *ananassa*), blackcurrant (*Ribes nigrum*), and potato (*Solanum tuberosum*). High-throughput omics technologies, including genomics, transcriptomics, and metabolomics—were utilized to produce large-scale datasets, enabling a holistic understanding of biological processes.

This study developed and applied a PCA-ORA plot, a novel method combining dimensionality reduction with over-representation analysis based on MapMan protein classes. This visualization approach not only highlights enriched functional categories driving dataset variation but also provides a powerful tool for multi-omics integration and hypothesis generation.

The applicability of these methods was demonstrated in diverse biological contexts. For *F.*×*ananassa*, transcriptomic data were analysed to explore molecular mechanisms underlying early floral initiation in the cultivars ‘Gariguette’ and ‘Clery,’ representing French and German populations, respectively.

A Pore-C pipeline for chromosomal scaffolding was first developed using *S. tuberosum* as a model system, establishing a workflow for achieving pseudo-chromosome-level assemblies. This was subsequently adapted for the main focus of this study, namely the generation of a *de novo* genome assembly for *R. nigrum*, where multiple omics techniques—including genome, transcriptome, and metabolome—were integrated and evaluated. These analyses leveraged the Oxford Nanopore Technology (ONT) Pore-C pipeline and visualization plots.

6.1 Exploring and visualizing RNA-Seq data: Gaining first impressions and analysing DEGs

Visualizing RNA-Seq data, particularly differentially expressed genes (DEGs) along with their functional annotations, is a critical step in identifying genes of interest in a given experiment. RNA-Seq experiments typically produce large datasets that require filtering and prioritization to pinpoint relevant genes. The visualization approach developed in this study integrates dimensionality reduction

using Principal Component Analysis (PCA) with annotation based on overrepresentation analysis (ORA) of underlying MapMan protein classes (Schwacke *et al*., 2019; Bolger *et al*., 2021). This methodology provides an initial comprehensive overview of the unfiltered DEG dataset for the plant species under investigation.

In the final plot a PCA gives a first impression how the data might be clustered and is quite common for DEG analysis. Here, raw DEG data can be plotted without previous filtering or gene selection steps with highlighted experimental groups. The PCA was selected due to its widespread use, simplicity, speed, and computational efficiency. While alternative methods, such as t-distributed Stochastic Neighbour Embedding (t-SNE) (Maaten and Hinton, 2008) and Uniform Manifold Approximation and Projection (UMAP) (McInnes *et al*., 2018), address certain limitations of PCA—such as capturing non-linear relationships and fine-grained local structures—PCA remains highly accurate and performs well in downstream analyses. Furthermore, its computational stability was a key consideration in its selection for this study (Sun 2019; Hsu and Culhane, 2023).

To enhance the analysis, gene annotation was integrated to support functional interpretations of the dataset, ensuring compatibility with both model and non-model species. MapMan was chosen for its suitability in providing intuitive, ontology-based annotations that align with the requirements of the plot. Its automated, web-based process efficiently assigns biological functions to proteins or nucleotide sequences, making it ideal for linking genes to metabolic and regulatory pathways (Schwacke *et al*., 2019; Bolger *et al*., 2021).

Other widely used tools for gene annotation include the Gene Ontology (GO) knowledgebase, Panther, and EggNOG. GO provides a comprehensive and structured vocabulary for describing gene functions across three main domains: molecular function, biological process, and cellular component (Ashburner *et al*., 2000; The UniProt Consortium, 2019). While highly versatile, GO annotations often require additional computational processing to group genes into higher-order categories or pathways for visualization. Panther, on the other hand, incorporates data from 144 genomes, including 40 plant genomes, offering a broad comparative platform with functional annotations and phylogenetic insights

(Thomas *et al*., 2021). However, its focus on comparative genomics can make it less specialized for the metabolic and regulatory categorization required for this plot. EggNOG, with its extensive database covering 1,322 eukaryotic organisms, excels in orthology prediction and functional annotation across diverse taxa (Hernández-Plaza *et al*., 2022). While valuable for evolutionary studies, it lacks the direct focus on plant-specific pathways and processes that MapMan provides. In contrast, MapMan's intuitive binning system and plant-centric focus make it particularly well-suited for the visualization and interpretation needs of this plot, ensuring a clear representation of functional gene categories, especially for plant metabolic and regulatory pathways. Its ability to handle data from non-model plants effectively sets it apart, as it simplifies functional annotation even for species with limited genomic resources (Schwacke *et al*., 2019).

To further analyse the functional relevance of the annotated genes, this annotation was incorporated through an ORA. The ORA in this study considers up to 1,000 DEGs that exhibit high statistical significance along PC axes. This analysis identifies MapMan protein classes that contribute to the separation along each PC axis, additionally highlighting 10 annotated DEGs per axis that are particularly influential in driving this separation. By integrating ORA, the study pinpoints functional categories that are enriched and critical for understanding the biological processes underlying the observed variations.

To date, the combination of dimensionality reduction and ORA based on MapMan protein classes has not been published as an automated function. Existing visualization methods often rely on separate approaches, each with limitations. For example, annotated scatterplots, such as KEGG enrichment scatterplots integrating KEGG pathway information, are effective for visualizing dimensionality reduction coordinates enriched with functional annotations (Kanehisa *et al*., 2008). In cotton or *Oryza sativa*, these plots have been utilized to identify novel pathways involved in DEG analyses (Lu *et al*., 2024; Cai *et al*., 2021). However, their application necessitates substantial preprocessing. Additionally, cluster-specific enrichment analysis serves as another visualization approach; however, it requires extensive preprocessing and is limited to displaying only a subset of the data.

Heatmaps offer an alternative that provides an overview of gene expression data but are limited by the number of DEGs that can be displayed while maintaining interpretability. Interactive network visualizations, such as those generated using Cytoscape (Gustavsen *et al*., 2019), integrate multiple plots and provide insights into gene annotations but are best suited for exploratory analyses and may lack the focus needed for hypothesis-driven research (Gustavsen *et al*., 2019).

In contrast, combining dimensionality reduction methods such as PCA with ORA offers significant advantages. This approach integrates the high-level overview provided by dimensionality reduction with the detailed functional insights from ORA, enabling the identification of key functional categories driving the separation along principal component axes. Unlike isolated plots, this combination avoids the need for repetitive preprocessing or excessive data filtering while ensuring that both global patterns and detailed annotations are captured. By highlighting enriched functional categories across thousands of DEGs, this integrated approach provides a comprehensive yet scalable visualization framework, offering a clearer understanding of the biological processes underlying dataset variation.

In this study, the PCA-ORA visualization framework was successfully applied to *F.* × *ananassa*, providing the first comprehensive overview of early floral initiation events, and to the analysis of drought stress responses in *R. nigrum* leaf and root tissues of both juvenile and mature plants. Our R-based plotting function effectively integrates transcript abundance data (TPM) with MapMan annotation files, facilitating streamlined visualization of functional gene expression patterns. By automating critical steps such as dimensionality reduction and annotation overlay, the function eliminates the need for manual adjustments, including colour or symbol assignments. This automation enhances consistency and reproducibility across diverse datasets while preserving user flexibility for downstream analyses.

6.2 Floral initiation of strawberry

Floral initiation is a precisely regulated developmental process influenced by both endogenous and exogenous cues (Koorneef *et al*., 1998; Wellmer and Riechmann, 2010). In cultivated strawberry, an economically significant crop,

flowering time directly impacts fruit yield. Recent studies demonstrate that floral initiation (Krüger *et al*., 2022) and flowering time (Prohaska *et al*., 2024) are determined by both genetic factors and environmental conditions. Specifically, floral initiation is triggered by reductions in temperature and day length, highlighting the interaction between these two environmental variables (Heide *et al*., 2013). Consequently, the timing of floral initiation can vary annually at the same geographical location. To account for this variability, sampling dates were determined based on the percentage of plants exhibiting floral initiation rather than fixed calendar dates. Monitoring the progression of floral initiation at 0%, 10%, and 50% across the population revealed a significantly accelerated process in Germany compared to France. This difference is likely attributed to the steeper decline in temperature and photoperiod in Germany relative to France (Krüger *et al*., 2022).

Research on the model plant *Arabidopsis thaliana* and various crop species has uncovered multiple regulatory pathways controlling floral initiation, including autonomous pathways and those responsive to photoperiod, temperature, vernalization, gibberellins, age, and carbohydrate availability (Mouradov *et al*., 2002; Boss *et al*., 2004). In the present study, we investigated two strawberry cultivars (Gariguette and Clery) grown in two distinct locations (France and Germany) over three years, identifying key components of these pathways involved in regulating floral initiation in strawberry, as further detailed below.

6.2.1 Photoperiodic pathway and floral integrators

The photoperiodic pathway of floral initiation comprises a complex regulatory network that responds to day length. In *Arabidopsis thaliana*, the principal genes involved in this process are well characterized. GIGANTEA (*GI*) regulates circadian rhythms and facilitates flowering under long-day conditions by stabilizing the CONSTANS (*CO*) protein (Michaels *et al*., 2003; Brandoli *et al*., 2020). *CO* plays a pivotal role in sensing day length, accumulating specifically during long days to directly activate the expression of the florigen gene *FLOWERING LOCUS T* (*FT*) (Kardailsky *et al*., 1999; Kobayashi *et al*., 1999; Abe *et al*., 2005; Wigge *et al*., 2005; Corbesier *et al*., 2007). In the shoot apical meristem (SAM), *FT* competes with the floral repressor *TERMINAL FLOWER 1* (*TFL1*) for binding to *FD*, a bZIP transcription factor that promotes floral transition

(Zhu et al., 2020). *SUPPRESSOR OF OVEREXPRESSION OF CONSTANS 1* (*SOC1*) functions as an integrator of the photoperiod, gibberellin, and temperature pathways, ultimately promoting flowering at the SAM (Li *et al*., 2008; Jung *et al*., 2012).

In strawberry, we identified orthologs of these key genes—*FanCO*, *FanSOC1*, *FanFD*, *FanTFL1*, and *FanGI*—that were differentially expressed during early floral initiation. The roles of *FanCO*, *FanSOC1*, and *FanTFL1* in the seasonal regulation of floral initiation have been previously demonstrated (Iwata *et al*., 2012; Koskela *et al*., 2012; Mouhu *et al*., 2013; Koskela *et al*., 2016; Korukura *et al*., 2017; Munoz-Avila *et al*., 2022). Additionally, we, along with others (Liang *et al*., 2022), observed differential expression of *FanBRN1* during floral initiation. The *Arabidopsis* ortholog *AtBRN1* is known to function as a repressor of *SOC1* activity (Kim *et al*., 2013). These findings suggest that the regulatory mechanisms underlying floral initiation in strawberry share significant conservation with those in *Arabidopsis*, while also exhibiting species-specific dynamics.

6.2.2 Phytohormones signaling

We identified multiple DEGs associated with the gibberellic acid, brassinosteroid, abscisic acid (ABA), and jasmonic acid pathways. The gibberellic acid (GA) pathway is known to promote the transition from vegetative growth to flowering (Yu *et al*., 2004; Mutasa-Göttgens and Hedden, 2009; Achard and Genschik, 2009). In this study, *FanRGA* was differentially expressed in the terminal buds of both strawberry cultivars. In diploid strawberry, the ortholog *FveRGA* encodes a DELLA protein that suppresses stolon development (Li *et al*., 2018; Caruana *et al*., 2018). DELLA proteins function as negative regulators of GA signaling, acting directly downstream of the gibberellic acid receptor (Eckardt, 2007).

Brassinosteroids are known to promote flowering in *Arabidopsis* (Li and He, 2020). We identified differential expression of *FanXTH2*, a key component of the brassinosteroid pathway that encodes xyloglucan endotransglucosylase/hydrolase. This gene showed variation between cultivars and locations, consistent with previous findings in strawberry terminal bud tissue (Liang *et al*., 2022) and loquat bud tissue (Xia *et al*., 2020).

Furthermore, we observed the downregulation of *FanPP2* during floral initiation in both cultivars and locations, corroborating prior results (Liang *et al*., 2022). The *Arabidopsis* ortholog of *FanPP2* encodes a negative regulator of ABA signaling, suggesting its role in influencing the timing of floral initiation through the repression of ABA-responsive genes. Additionally, *FanEIN3*, encoding an ethylene-responsive transcription factor, was also downregulated during floral initiation, consistent with previous reports (Liang *et al*., 2022). The *Arabidopsis* ortholog delays flowering by activating *ERF1* and members of the *APETALA2* (*AP2*)/ERF protein family (Guo and Ecker, 2004).

These findings provide evidence that multiple hormone-related pathways are intricately involved in regulating floral initiation in strawberry, with conserved roles observed across species.

6.2.3 Transcription factors

Multiple transcription factor families, including bHLH, MADS-box, and MYB, were differentially expressed during floral initiation, consistent with their established roles in the transition from vegetative growth to reproductive development (Bemer and Angenent, 2009; Woodger *et al*., 2003; Liang *et al*., 2022). Notably, we identified two differentially expressed members of the *DVL/RTFL* family, which are known to participate in organogenesis (Guo *et al*., 2015). While one member was upregulated across both cultivars and locations, the other exhibited location-specific expression, being downregulated in German samples but upregulated in French samples of the cultivar *Clery* (CL). In *Arabidopsis*, *DVL/RTFL* proteins are involved in controlling leaf shape and plant architecture. For instance, the overexpression of *DEVIL1* (*DVL1*) and *ROTUNDIFOLIA4* (*ROT4/DVL16*) in *Arabidopsis* results in pleiotropic phenotypes characterized by reduced stature, rounder rosette leaves, and clustered inflorescences (Wen *et al*., 2004; Valdivia *et al*., 2012).

Plant peptides also play critical roles in developmental processes, including the regulation of terminal bud organization, root growth, and leaf morphology (Matsubayashi, 2014; Matsubayashi and Sakagami, 2006; Guo *et al*., 2015). In our study, we observed tissue-specific expression patterns of GRAS-type proteins, which are putative transcriptional regulators. This finding aligns with

previous reports highlighting their roles in diverse developmental processes. Specifically, GRAS-type genes were predominantly expressed in roots, with a subset also detected in shoots and leaves (Heckmann *et al*., 2006; Liang *et al*., 2022).

These results underscore the complex interplay between transcriptional regulation and tissue-specific signaling during floral initiation, emphasizing the coordinated involvement of transcription factors, plant peptides, and signaling pathways in driving the transition to reproductive development.

6.2.4 Carbohydrate and energy metabolism

DEGs associated with carbohydrate metabolism, particularly starch metabolism, and certain secondary metabolic pathways, such as the terpenoid pathway, were identified in both strawberry cultivars (Figure 9). Trehalose-6-phosphate (T6P), a sugar derivative, has been proposed to play a regulatory role in flowering within both the terminal bud and the shoot apical meristem (SAM). The *TPS1* gene, which encodes trehalose-6-phosphate synthase, is a critical component of the genetic network controlling flowering time (Wahl *et al*., 2013; Rojas *et al*., 2023). In our study, *FanTPS1* was downregulated in terminal buds in both cultivars and locations, consistent with previous observations (Liang *et al*., 2022).

The carbohydrate pathway not only governs floral initiation but also plays a broader role in plant development by providing the energy and molecular building blocks required for flower development (Zhang *et al*., 2013; Qiao *et al*., 2021). The interplay between carbohydrate metabolism, phytohormonal signaling, and environmental cues ensures that the transition from vegetative growth to flowering occurs at an optimal time to maximize reproductive success (Corbesier *et al*., 1998; Sawicki *et al*., 2015). In the terminal bud of cultivar Clery (CL), we observed a significant overrepresentation of DEGs associated with starch metabolism, which acts as a vital energy reserve. Mobilized starch, converted to sucrose in leaves and stems, serves as an early signal for floral induction (Bernier *et al*., 1993).

Key differences between the cultivars were also identified, including higher production of asparagine and rhamnogalacturonan I (RG-I) in Gariguette (GA).

Asparagine plays a crucial role in providing nitrogen for signaling proteins that integrate internal and external signals to coordinate floral induction (Khurana et al., 1988).

The *FERONIA 4* (*FER4*) gene encodes a protein involved in carbohydrate metabolism, particularly glycolysis, through its interaction with the cytosolic enzyme glyceraldehyde-3-phosphate dehydrogenase (GAPDH). FER deficiency reduces GAPDH activity, leading to the accumulation of starch (Yang *et al*., 2015). In our study, *FER4* was downregulated in both cultivars, consistent with findings in the cultivated strawberry cultivar *Benihoppe*, where its downregulation was linked to leaf development (Liang et al., 2022). Protein classes related to starch metabolism were also enriched in our analysis, further underscoring the role of *FER4* in regulating carbohydrate metabolism during floral initiation.

These results highlight the intricate connections between carbohydrate metabolism, floral induction, and overall plant development, emphasizing how energy reserves, nitrogen signaling, and starch mobilization integrate to drive the transition to reproductive growth.

6.2.5 Cytoskeleton, cell division and cell wall dynamics

In the terminal buds of cultivar GA, we identified DEGs associated with cytoskeletal organization, particularly the microtubule network, which is essential for cell division and expansion and plays a critical role in tissue patterning during floral initiation (Chandler, 2012; Denay *et al*., 2017). Notably, DEGs related to cell division were overrepresented in the terminal buds of cultivar CL, suggesting a more pronounced role for cellular proliferation in this cultivar during floral initiation.

In contrast, DEGs associated with tRNA biosynthesis, bZIP TFs, and RG-I biosynthesis were overrepresented in the terminal buds of cultivar GA. RG-I is known to be critical for cell wall integrity (Yapo, 2011), although its specific role in floral induction remains unclear. The differential representation of these gene classes may indicate cultivar-specific regulatory mechanisms during floral initiation.

Disparities in the enrichment of protein classes between the two cultivars could also reflect the influence of the field experiment setup and environmental variability, which may have masked inherent genetic differences between the cultivars. These findings highlight the interplay between cytoskeletal organization, cell wall biosynthesis, and transcriptional regulation in floral initiation, while also emphasizing the impact of environmental factors on gene expression dynamics.

6.2.6 Subgenome expression regulation

In the octoploid cultivated strawberry (*F.* × *ananassa*), the plasticity of traits such as flowering (Prohaska *et al*., 2024) is thought to contribute to the polyploid advantage in heterogeneous environments (Wei *et al*., 2019). This advantage arises because each gene may be represented by up to eight homoeoalleles located on four homoeologous subgenomes (Rousseau-Gueutin *et al*., 2019). However, polyploidization is often followed by a process of diploidization, which reduces gene redundancy through mechanisms such as gene silencing, sequence elimination, and chromosomal rearrangement (Chen, 2007; Doyle *et al*., 2008).

In strawberry, gene redundancy analysis has shown that only 46% of genes retain alleles across all four subgenomes, while 7%, 23%, and 14% retain alleles on one, two, and three homoeologous chromosomes, respectively (Jin *et al*., 2023). In our analysis, the majority of *F.* × *ananassa* genes identified, including those encoding *FBH*, *CO*, *GI*, *GRAS-type*, *DELLA*, *FD/FDP*, *PP2*, *XTH23*, *TPS*, and *BRN1* proteins, retained sequences in all four subgenomes. Conversely, *MYB3R1*, *EIN3*, and *FER4* sequences were found in only three subgenomes but exhibited similar expression patterns across the datasets.

This suggests that the expression of these genes is likely subject to fine-tuned regulation, potentially influenced by mutations in promoter regions and/or the 5′ untranslated regions (UTRs). Such regulatory modifications could allow for precise control of gene expression despite partial gene loss, reflecting the complex evolutionary dynamics following polyploidization in octoploid strawberry.

On transcriptomic level, this study sheds light on the molecular basis of early floral initiation in *F.* × *ananassa* under natural conditions. Key gene expression profiles were identified and differences between cultivars CL and GA across two

environments (Germany and France). The roles of genes such as *XTH23, TPS and FER4* were highlighted, and those encoding transcription factors such as FBH, CO and GI, in the regulation of this developmental transition, which also involves the reprogramming of carbohydrate metabolism, phytohormone signaling, and photoperiod-dependent regulation. These findings offer valuable insights into the optimization of strawberry cultivation and breeding strategies, but more research is needed to determine the precise functions of the key genes involved in floral initiation and the influence of their differential expression.

6.3 Generating Pore-C data with Potato

In this study, the ONT Pore-C sequencing technique was applied to *Solanum tuberosum* cv. ‘Altus’ as a model system. The resulting data supported the use of low-depth sequencing from an offspring population to enable chromosomal clustering and haplotype phasing on the assembly graph, as demonstrated by Mari *et al*. (2024). However, the primary objective was to evaluate the Pore-C method for generating chromosomal contact information to facilitate the genome assembly of *R. nigrum* (chapter 4.5.1).

Pore-C, like other chromatin conformation capture techniques such as Hi-C, capture Hi-C, and Capture-C, is a powerful tool for analyzing the three-dimensional folding of chromatin. These techniques reveal interactions between chromosomal regions that are spatially proximal to the nucleus, elucidating functional relationships between elements such as promoters and enhancers. Moreover, they have proven invaluable for addressing complex challenges, including 3D chromatin structural analysis and the scaffolding of large genome assemblies (Belton *et al*., 2012; DeMaere and Darling, 2021; Yardımcı *et al*., 2019).

In this study, seven samples were analyzed across five timepoints. Samples collected less than one month apart exhibited similar chromatin interaction patterns. However, corrected Pore-C contact counts showed marked differences between samples collected earlier in the year (March and April) and those collected in August. Typically, samples derived from the same biological replicate are expected to display similar patterns (Ramirez *et al*., 2018; Wolff *et al*., 2020). These differences may be explained by biological replicate and age-related

changes in chromatin structure, as developmental stages and tissue aging are associated with dynamic alterations in epigenetic marks such as DNA methylation and histone modifications. These epigenetic changes influence chromatin folding and 3D architecture (Ramirez *et al.*, 2018; Kumar and Mohapatra, 2021), potentially leading to variability in Pore-C sequencing results.

A key metric impacted by these differences was the cis:trans ratio. Samples collected in March and April displayed a high cis:trans ratio (>5), indicative of good data quality, as intrachromosomal (cis) interactions are far more frequent than interchromosomal (trans) interactions (Hansen *et al*., 2019; Dozmorov *et al*., 2021). By contrast, August samples exhibited a much lower cis:trans ratio (<1). Apart from age, no differences were observed in data generation using the selected restriction enzyme or in the subsequent data evaluation. This suggests that age plays a significant role in influencing chromosomal interactions. These results highlight the critical importance of considering seasonal and developmental factors when interpreting chromatin conformation data.

Furthermore, significant differences were observed in the balance of short- and long-range contacts between samples collected in March/April and those from August. Short-range contacts, which typically represent local chromatin looping and interactions between regulatory elements such as enhancers and promoters or structural domains, were more prominent in the earlier samples. This observation aligns with studies indicating that enhancer–promoter interactions are crucial for gene regulation and can vary under different conditions (Zhang *et al*., 2024).

A strong short-range signal reflects high resolution of fine-scale chromatin structure, as chromatin looping enables transcription-factor-bound distal enhancers to contact their target promoters and regulate transcription (Rosa and Shaw, 2013). Conversely, long-range contacts, critical for scaffolding genome assemblies and understanding higher-order chromatin organization, were less pronounced in the August samples. Long-range chromatin interactions play significant roles in gene regulation and genome maintenance, and their alteration can impact higher-order chromatin organization (Pei *et al*., 2021). These differences may reflect age-related chromatin remodeling, which can alter

chromosomal compartments and topological domains, affecting the balance of short- and long-range contacts.

Variability in chromatin structure due to plant age and developmental stage can result in inconsistent Hi-C or Pore-C data, manifesting as fluctuations in cis:trans ratios and contact patterns. To mitigate these issues, DNA extraction and library preparation should be performed immediately after harvesting, as outlined in established protocols. Additionally, ensuring sufficient tissue material is critical, as limited tissue availability can be a constraint for certain plant species. Biological stressors, such as environmental factors, must also be managed carefully, as they can influence chromatin structure and, consequently, data quality. For instance, a study on *Solanum lycopersicum* demonstrated that heat stress induces rapid changes in chromatin architecture, leading to the transient formation of promoter-enhancer contacts, which likely drive the expression of heat-stress responsive genes (Huang *et al*., 2023). This finding underscores the importance of controlling environmental conditions during sample collection to maintain consistent chromatin structures. Furthermore, research on *Zea mays* has highlighted the necessity of optimizing tissue collection and DNA extraction protocols to obtain high-quality chromatin conformation data. Ensuring the immediate processing of harvested tissues and the availability of sufficient material are critical steps to prevent degradation and maintain the integrity of chromatin interactions (Hsieh *et al*., 2024).

In this study, the data generated with Pore-C proved valuable for validating the genome assembly approach in *S. tuberosum*. to achieve consistent and reliable Hi-C or Pore-C data in plant studies, it is essential to consider factors such as plant age, developmental stage, environmental conditions, and tissue handling protocols, as these can significantly influence chromatin structure and, consequently, the quality of the data obtained. Furthermore, it has been successfully applied in other plant species. For instance, in *Brassica rapa*, Pore-C showed comparable performance to Omni-C in terms of scaffold N50 and L50, with a slightly better N90 (Istace *et al*., 2021). In *Arabidopsis*, Pore-C was used to capture genome-wide multi-way chromatin interaction landscapes at the single-molecule level, revealing epigenetic modifications of interacting DNA fragments (Li *et al*., 2022). In the study of Jo *et al.* (2024) ONT long reads

combined with Pore-C produced the first high-quality chromosome-level genome assembly of *Sageretia thea*. And in Sierro *et al*. (2024) Pore-C was used to generate chromosome-level assemblies of three *Nicotiana* species.

Based on our findings and insights from the literature, we conclude that the Pore-C method offers a promising approach for the genome assembly of *R. nigrum*.

6.4 Molecular response to drought stress effects of blackcurrant

Blackcurrant (*R. nigrum*) is an important fruit crop because the edible berries confer a number of health benefits. In this study we were able to establish the blackcurrant genome assembly on pseudo-chromosomal level, and identified multiple genes associated with drought stress as well as related changes in metabolites.

6.4.1 Genome assembly of *R. nigrum*

The total size of our blackcurrant genome assembly was ~871 Mbp, which is close to the estimated genome size of ~1 Gbp for the genus *Ribes* Chiche *et al.* (2003) and in line with the genoscope estimation of 750 Mbp (Supplemental Material Figure S2). Using a hybrid approach facilitating ONT long read and precise HIFI PacBio data directly in hifiasm as well as using contact data generated with the PoreC ONT approach, coupling long reads directly to sequence multi-way chromatin contacts without amplification (Ulahannan *et al.*, 2019) we were able to accomplish a pseudo-chromosomal scaffolding resulting in 8 chromosomes. This is building on the complementarity of simplex ONT and very precise HiFi reads (van Rengs *et al*., 2022; Cheng *et al.*, 2023).

Our data are in line with Ribes cultivars reported in literature to be diploid with a basic chromosome number of 8 (Zielinski, 1953; Chiche *et al.,* 2003). As we investigated a relatively high heterozygosity, we were able to get very contiguous individual haplotype assemblies for haplotype one and two. These haplotype assemblies had a comparable size with 900 Mbp for haplotype one and 885 Mbp for haplotype 2.

Genome assembly quality was checked using the LTR assembly index (LAI), which estimates genome completeness including more repetitive genome regions by calculating the percentage of intact LTR retrotransposon (LTR-RT) sequences (Manchanda *et al*., 2020; Feron and Waterhouse; 2022). The blackcurrant genome assembly produced an LTR assembly index (LAI) score of 14.77, aligning closely with the LAI score of the ultra-long-read ONT based Arabidopsis genome (LAI=14.9) (Michael *et al*., 2018; Ou *et al.*, 2018). Long-read sequencing methods, like ONT and PacBio, typically yield Leaf Area Index (LAI) scores exceeding 10. An LAI ranging from 10 to 20, as per Ou *et al*. (2018), designates a genome of reference quality. This is supported by the assessment of genome errors through CRAQ, which revealed a Reference Assembly Quality Index (R-AQI) of 96.21% and a Scaffold Assembly Quality Index (S-AQI) of 98.64% for the generated blackcurrant genome. According to Li *et al.* (2023), genomes with an AQI exceeding 90% are classified as reference quality.

Notably, the AQI results for the blackcurrant genome were comparable to those of the haplotype PacBio Complete Long Reads (CLR) *Oryza sativa* MH63 (R-AQI=96.25; S-AQI=94.96) (Li *et al.*, 2023; https://www.ncbi.nlm.nih.gov/datasets/genome/GCA_001623365.2) and the haplotype PacBio CLR *O. sativa* R498 (R-AQI=96.96; S-AQI=98.22) (Li *et al.*, 2023; -Du *et al*., 2017) genomes on chromosomal level. Our results surpassed the existing assemblies of ONT *Solanum pennellii* (R-AQI<=95.57; S-AQI=91.47) and ONT-based *Arabidopsis* KM74 (R-AQI=85.95; S-AQI=93.34), as well as the PacBio CLR-based *Arabidopsis* KM74 genome assemblies (Michael *et al*., 2018) on the contig level (R-AQI=95.57; S-AQI=96.29) (Li *et al*., 2023; Table 1). The observed distinctions can likely be attributed to variations in sequencing methodologies but also to transposons identification. Notably, PacBio HIFI exhibits error rates that are generally lower than those of simplex ONT reads, culminating in assemblies of heightened accuracy. Consequently, the Reference Assembly Quality Index (AQI) values for our assembly align closely with the PacBio reference genome for *O. sativa* and *Arabidopsis*.

Furthermore, our assembly reached a consensus assembly quality value (QV) of 57.49 assessed by Merqury. As per Rhie et al. (2020), our QV corresponds to

99.999% accuracy. Our assembly is higher than the PacBio MH63 gap-free reference genome of *O. sativa* (Song *et al.*, 2021), which achieved a QV of 55.05, and the chromosome-level assembly based on PacBio and Hi-C data of the berry *Fragaria pentaphylla* (Sun et al., 2022), which attained a QV of 54.76. Our high QV underscores the high quality of our genome assembly for *R. nigrum*, making it comparable to these reference genomes. Furthermore, our genome assembly has reached a k-mer completeness of 98.59, which is higher than known values of PacBio and Hi-C based *de novo* assemblies such as for *F. pentaphylla* and *Arctostaphylos glauca* with a k-mer completeness of 84.71 and 74.39 (Sun et al., 2022; Huang et al., 2022). The k-mer completeness of the PacBio data-based haplotype resolved assembly of *Coriaria nepalensis* is 98.87 comparable to our haplotype resolved assembly. For further genome validation and to make the genome useful for QTL studies, marker sequences published by Russell et al. (2011) located on the linkage map of the population SCRI 9328 and MP7 were mapped to our genome. Genetic markers identified on a specific chromosome of the linkage map were also identified on a corresponding chromosome within our genome assembly. This implies concordance between the genetic linkage relationships and the tangible physical locations of genetic elements within the genome. This signifies that our assembly is likely accurate and will allow us to analyze legacy data against our genome assembly.

Our sequence assembly exhibited high quality as indicated by the BUSCO completeness assessment, with a BUSCO score of 98.3%. This gene completeness surpasses that of chromosomal-level genomes within the *Saxifragaceae* family, which is additionally part of the Saxifragaceae alliance, alongside the Grossulariaceae (Soltis *et al*., 2011). For Saxifragaceae, three genomes have been published at the chromosomal level. Notably, the genome of *Paeonia ostii*, the largest among them at 12 Gb across five chromosomes, achieved a BUSCO completeness score of 94.4%, while the smallest genome of *Tiarella polyphylla* with 412 Mb reached a BUSCO completeness of 97.31% (Yuan *et al.,* 2022; Liu *et al*., 2023). The genome of *Cercidiphyllum japonicum*, spanning 719 Mb and 19 chromosomes, attained a BUSCO completeness score of 94.1%. The genomic assembly of *T. polyphyll*a relies on a combination of Illumina short reads, ONT long reads, and Hi-C data, whereas the assembly of

the *C. japonicum* genome utilizes PacBio long reads, Illumina short reads, and Hi-C data. Our analysis indicates a significantly elevated BUSCO completeness in our genome assembly, possibly attributed to the synergistic effect of integrating PacBio and ONT long reads along with ONT PoreC data. The high BUSCO completeness underlines the high quality of our assembly and is the first published genome in the Grossulariaceae family. These gene completeness values surpasses the 97–98% range reported for other berry crops. Examples include a blueberry wild relative (*Vaccinium darrowii*), with a BUSCO score of 97.5% and 95.7% functionally annotated genes (Yu *et al.,* 2021), and raspberry *(Rubus ideaus*) with a BUSCO score of 91.3% functionally annotated genes (Davik *et al.,* 2022). These genomes were assembled using PacBio, Hi-C, and Illumina short-read sequencing methods, resulting in slightly lower BUSCO scores compared to our assembly. Our assembly, anchored on 8 pseudo-chromosomes, successfully mapped 99% of the genome, while the comparable *C. japonicum* genome only anchored 90.18% on 19 pseudo-chromosomes. (Zhu *et al*., 2020). Our annotation of the blackcurrant genome assembly on pseudo-chromosomal level resulted in 42,380 genes with a BUSCO completeness score for the transcriptome of 96.8% for cv. ‘Rosenthals Langtraubige’. In comparison, Thole *et al.* (2019) assembled 145,906 transcripts with an N50 value of 1,480 bp and a read mapping rate of 90.4% for cv. ‘Ben Hope’. Another 40,225 genes were predicted in a microarray analysis (Čereković *et al.*, 2015). Unfortunately, this data was not publicly available for a comparison. Concerning the RNA-Seq dataset, we anticipated a typical mapping rate exceeding 80% against the transcriptome. However, our observed mapping rate is lower, standing at 74%. This discrepancy may be attributed to the utilization of ONT for RNA-Sequencing, wherein longer sequences are generated but are associated with a higher error rate compared to short-read technologies such as PacBio or Illumina.

6.4.2 Differentially expressed genes during drought stress in leaf and root tissue

In this study, we identified various DEGs associated with drought stress. Notably, the stressed plants exhibited distinct phenotypic alterations, characterized by desiccated and curled leaves lacking turgidity. Nonetheless, our genome

assembly for *R. nigrum* successfully revealed the presence of genes already acknowledged for their involvement in plant drought stress.

6.4.3 Protein kinases

The final genome assembly and its annotated transcriptome were utilized to identify differentially expressed genes in leaf and root tissue samples that were collected during our drought stress experiment. Plants exhibit diverse responses to abiotic and biotic stimuli, employing specialized mechanisms tailored to the intensity and duration of the stress. During drought stress, plants enact strategies such as closing stomata to minimize water loss, fostering deeper root growth for enhanced water acquisition, and shedding leaves to reduce transpiration rates. Furthermore, abiotic and biotic stimuli through activation of adaptive mechanisms and receptors act as sensors for these stimuli to transduce information through the plant such as receptor-like kinases (RLK) (Gish and Clark 2011; Soltabayeva *et al.*, 2022). Amongst other genes, we have found leucine-rich repeat receptor-like kinases (LRR-RLK) genes mostly highly downregulated in roots and leaves under drought conditions. Ksouri *et al*. (2016) previously observed a similar trend in Prunus persica rootstocks, noting a prominent downregulation of LRR-RLK genes, particularly in leaves.

Besides that, one gene annotated as a member of the subfamily of LRR-XV was upregulated in leaves and significantly downregulated in roots. Within this subfamily, in *Arabidopsis*, the gene RPK1 showed an enhanced ABA sensitivity and drought tolerance with increased superoxide dismutase (SOD) level and decreased ROS accumulation (Osakabe *et al*., 2005; Osakabe *et al*., 2010; Osakabe *et al.,* 2013). In our study, the genes Cu/Zn-SOD and Fe-SOD were differentially expressed in leaves and roots. This finding agrees with Saed-Moucheshi *et al.* (2021), who studied triticale grain samples to assess the correlation between SOD (superoxide dismutase) expression and drought resistance in different triticale genotypes. The authors revealed elevated Cu/Zn-SOD expression in the roots of a drought-resistant triticale genotype, whereas Fe-SOD remained unaffected (Saed-Moucheshi *et al*., 2021). The genes RN2G000320.1 and RN8G015790.1 annotated as hydrogen peroxide receptor kinase (GHR1) were downregulated in root tissue. This gene was previously

described in *Arabidopsis* as a critical early component in ABA signaling that is a plant hormone that inhibits growth under stress conditions (Hua et al., 2012). Furthermore, one gene annotated as hydrogen peroxide receptor kinase (HPCA) was downregulated in roots and leaves. The LRR-RLK HPCA1 was previously identified in *Arabidopsis* and belongs to a previously uncharacterized subfamily featuring two extra pairs of cysteine residues in the extracellular domain. It is activated by H_2O_2 and activates Ca^{2+} channels in guard cells, which are required for stomatal closure (Wu et al., 2020).

In our study, one gene annotated as a brassinosteroid co-receptor protein kinase gene (BAK/SERK) was downregulated in both tissues. This gene category serves as a converging point for several receptor-like kinase (RLK) signaling pathways and functions as a shared co-receptor (He *et al*., 2018). Additionally, we observed an upregulation of a gene specific to PSKR in root tissue, where PSKR1 collaboratively regulates plant growth in conjunction with BAK1, SERK1, and SERK2 (Wang *et al*., 2015). The gene responsible for the transcription of PXY is also regulated by BAK1, SERK1, and SERK2 and exhibited downregulation in both tissues in our study, suggesting a suppression of root development and xylem differentiation (Ou *et al*., 2016; Shinohara *et al*, 2016).

In addition to LRR-RLK, our study has identified multiple receptor-like cytoplasmic kinases (RLCK) that exhibited up- and downregulation in both leaf and root tissues. These cytoplasmic kinases are associated with various RLK complexes responsible for transmitting intracellular signals and have crucial functions in plant growth, development, as well as responses to biotic and abiotic stresses, as indicated by previous research (Lin *et al*., 2013; Liang and Zhou, 2018). The RLCK family consists of several members, with particular attention to RLCK VII, which is closely linked to plant growth and development, suggesting its significant role in the transduction of RLK signaling (He *et al.* in 2018). Several RLCK VII receptors in *Arabidopsis* are known to be involved in BR-signaling and root hair growth as well as root development and stomatal defense (Mara-Garcia *et al*., 2004). Furthermore, RLCK VIII has been related to oxidative stress signaling (Anthony *et al*., 2016; Forzani *et al*., 2011; Liang and Zhou, 2018). In our research, we observed up- and downregulation of various members of the

RLCK classes VII, VIII, and XII in both tissues, indicating an impact on growth and development. Furthermore, we detected members of the RLCK classes V, VI, X, XI, and XII, which have not been extensively characterized previously but appear to be involved in responses to drought stress in both tissues as well. Especially, in roots where high significant downregulation was found.

As previously stated, certain RLCKs form associations with various RLKs to transmit intracellular signals via protein phosphorylation, leading to the activation of the mitogen-activated protein kinase (MAPK) cascade as a critical outcome (He *et al*., 2018). In our study, MAPK genes were mostly downregulated in roots. In *Arabidopsis* under drought stress activated AtMPK3 and AtMPK6 were found via the activity of MAPKKK NPK1-RELATED PROTEIN KINASE1 (ANP1) strongly inducing NUCLEOTIDE DIPHOSPHATE KINASE2 (AtNDPK2) (Huang *et al*., 2012). In our study, the leaves of our blackcurrant plants showed no significant change in gene expression of MAPK (NPK/ANP), while drought-stressed roots have shown a strong downregulation. Contrarily, we observed no differentially expressed genes linked to AtNDPK2 in our investigation, suggesting that our cultivar might not be responsive to drought stress through this signaling pathway (Laloi *et al*., 2004). The Ca^{2+}-dependent protein kinases (CDPKs) represent another signal transduction way. We have found several genes transcribing for CDPK/CPK. These kinases play key roles in abiotic stress tolerance by modulating ABA signaling, reducing the accumulation of ROS, and are directly involved in physiological processes like growth, development, and stress responses (Bi *et al*., 2021). In our study, the genes encoding CDPK/CPK were mainly upregulated in leaves and significantly in roots. Previous studies have shown their role as potential targets in improving drought stress tolerance in *Arabidopsis*, maize, rice, sorghum, and potato (Mittal *et al*., 2017; Yip Delormel and Boudsocq, 2019; Bie *et al*., 2021). Our results match those in the literature and suggest a positive answer to the ABA signal chain for both tissues.

Proline-rich extensin-like receptor kinases (PERKs), a RLK subfamily, were differentially expressed. Our investigation identified six active genes in both leaf and root tissues. Interestingly, one gene showed upregulation in one root tissue

while being downregulated in the leaf tissue. The function of the PERK4 gene in *Arabidopsis* has been predicted to be a key regulator of Ca^{2+} signaling contributing to production of ABA in roots (Bai *et al*., 2009). Furthermore, several ZmPERK genes with cis-elements in their promoter regions were found for maize stress response (Shahid *et al*., 2022). Another member of the RLK family is the cysteine-rich repeat RLK (CRK), which is characterized by the presence of typically two DOMAIN OF UNKNOWN FUNCTION 26 (DUF26). These domains can recognize different ligands such as protein-protein interactions on the cell surface and allow it to acquire new functions. It is assumed to be involved in the perception of environmental signals and plant development (Wrzaczek *et al.,* 2010; Vaattovaara *et al*., 2019; Arellano-Villagómez *et al*., 2021). In our study we have found three genes downregulated in roots. Only a few proteins have been functionally characterized in literature so far and the mechanism on how CRKs enhance drought tolerance in plants remains unknown. A point mutation in the kinase domain of CRK10 was previously described in *Arabidopsis* to impede water transport due to collapsed vessels and to lead to an increased ABA content, while the overexpression of CRK4 and CRK5 enhances ABA sensitivity of stomatal movement and drought tolerance in tobacco (Piovesana et al., 2023; Lu et al., 2016). Furthermore, upregulated CRK33 was identified in *Arabidopsis* to decrease transpiration and to be involved in influencing stomatal density. CRK7 is involved in the response to extracellular ROS production and CRK36 interacts with the RLCK gene ARCK1 and negatively regulates ABA and osmotic stress signal transduction (Idänheimo *et al*., 2014; Tanaka *et al*., 2012).

6.4.4 Hormone related genes

In the ABA signaling cascade pyrabactin resistance (PYR), pyrabactin like (PYL) and the regulatory component of ABA receptors (RCAR) are major components responsible for the regulation of ABA signaling pathway (Kundu and Gantait, 2017). These components are negative regulators of the ABA pathway if no ABA is available. Our results showed most PYL/ RCAR receptor components in leaf and root are downregulated. These ABA receptors are involved in the complex of SnRK1, SnRK2 and PP2C. Here, ABA can bind to PYR/PYL/ RCAR receptors and SnRK1, SnRK2 and SnRK3 protein kinases are synthesized. In our study, several SnRK3 (data not shown) and SnRK2 were upregulated and a gene of

regulatory protein FCS-like zinc finger (FLZ) of SnRK1 complex was down regulated, leading to the assumption that this ABA pathway was activated against drought stress. The involvement of these genes and pathway was already shown in several plants against abiotic stresses and drought stress for plants such as *Arabidopsis* (Baena-González *et al*. 2007*)*, barley (Zhang *et al*., 2001), pea (Radchuk *et al*., 2006) and fava bean (Yang *et al*., 2013). Here these genes were involved in the development, growth inhibition and control of stomatal movement (Radchuk *et al*., 2006; Hasan *et al*., 2021a; Hasan *et al*., 2022).

6.4.5 Transcription factors

Drought stress induced signaling mechanisms result in regulation at the transcriptional level, leading to accumulation of stress responsive TFs. In our study, several TFs were differentially expressed in both tissues. The TFs for ERF-I, II, IV, IX, VI, VIII, X and DREB1/2 were upregulated in both tissues during drought stress. These subfamilies have been reported to be involved as regulators in drought stress response (Wang *et al*., 2016; Chen *et al*., 2022). CBF/DREB1 and DREB2 were previously described in signal transduction and drought tolerance in rice, soybean and *Arabidopsis* (Dubouzet *et al*., 2003; Chen *et al*., 2022). We obtained similar results, finding most CBF/DREB1 and DREB2 genes upregulated under drought.

Čereković *et al.* (2015) showed the involvement of three basic leucine zipper (bZIP) TFs in *R. nigrum* leaves under drought stress: AT3G58120 (upregulated), AT5G24800 and AT4G35900 (downregulated). In our study, multiple bZIP TFs were upregulated in both tissues, which might be due to the use of another cultivar and/or the use of another annotated genome as a reference as in Čereković *et al.* (2015). The TF IRE1/bZIP60 and corresponding regulatory mediators were found strongly downregulated in roots. IRE1/bZIP60 functions as the signaling arm of the unfolded protein response (UPR). Furthermore, TFs such as R2R3-MYB, bHLH, WRKY, NAC, zinc finger (C2H2) and HD-ZIP are known to be involved in drought stress response in plants (Huang *et al*., 2009a; Liu *et al*., 2014; Joshi *et al*., 2016; Qiu *et al*., 2019; Li *et al*., 2021; Khoso *et al*., 2022). The TFs R2R3-MYB and bHLH are previously described to be involved in the anthocyanin pathway, in plant stress response in tthe ABA-dependent regulatory

systems and in *R. nigrum* under drought stress (Qiu *et al*., 2019; Valliyodan and Nguyen, 2006; Abe *et al*., 2003; Čereković et al., 2015). Čereković et al. (2015) has found MYB TFs downregulated after drought stress induction, which is consistent with the results in our study of the TFs, where R2R3-MYB were downregulated in root tissue in *R. nigrum* during drought stress. Furthermore, WRKY, NAC, C2H2 and HD-ZIP TFs were both up- and downregulated in leaf and root tissues during drought stress in our study. The TF WRKY33 was previously described in *R. nigrum* leaves under drought stress (Čereković *et al*., 2013) and acts as a positive regulator in drought stress response in *Caragana korshinskii* (Li *et al*., 2021). Here, CkWRKY33 plants had higher survival rates and higher soluble sugar, proline and peroxidase content. Furthermore, WRKY70 and WRKY45 are known to be involved in ABA related pathways during drought stress in *Arabidopsis* (Li *et al*., 2013, Chen *et al*., 2017; Qiu and Yu, 2009; Li *et al*., 2021). Additionally, several NAC TFs were differentially expressed in leaves and highly significant in the roots of *R. nigrum*. These results align with previous findings. It is well-documented that this TF category plays a key role in responding to abiotic stress, such as drought, by either activating stress-responsive genes or enhancing drought resistance in transgenic plants, as reported by Takasaki *et al.* (2010) and Tran *et al.* (2004). Čereković *et al.* (2013) detected downregulation of several C2H2 genes in leaves and roots of *Caragana*, while some C2H2 genes were up- and some were downregulated in both tissues in our study. C2H2 genes are well studied in different plant species and regulate ROS scavenging by regulating expression of genes in rice encoding for antioxidants and are also linked to osmoregulation by synthesis of osmoprotectants such as proline or soluble sugars (Huang *et al*., 2009a; Huang *et al*., 2009b; Wang *et al*., 2018). Additionally, they are involved in ABA signaling by modulating expression of genes associated with stomatal closure and root development by regulating growth and development in response to drought (Wang et al., 2018). In addition to the ABA signaling pathway, these TFs enhance abiotic stress resistance by the MAPK signaling pathway (He *et al*., 2020; Lin *et al*., 2021; Ku *et al*., 2018). For instance, genes of HD-ZIP I/II were up- and down regulated in both tissues in our study. These TFs are well known to be involved in the regulation of growth and development, drought stress response, ABA

signaling and stomatal regulation (Himmelbach *et al*. 2002; Olsson *et al*. 2004; Agalou *et al*., 2008; Perotti *et al*., 2021).

6.4.6 The primary response to drought: from differentially expressed genes to metabolites

In this drought study several genes related to the ABA phytohormone, GABA biosynthesis, proline biosynthesis and amino acid metabolism were differentially expressed. In this context, several metabolites with changing contents could be identified. Most striking findings were observed comparing control and drought-stressed leaf tissue, while the differences in root tissue could be neglected, contrary to other studies for various plants such as peanut and various *Triticeae* species that detected significant differences in leaves and roots (Jiang and Hartung, 2008; Hu *et al*., 2016; Ullah *et al*., 2017). This might be specific to species or to the short drought stress period for blackcurrant. In our study, the main differences were in amino acid levels between control and stressed plants. Changes in amino acids are crucial for enhancing plant resilience to stress. Amino acids serve as osmolytes, fuel the production of energy-related compounds, function as antioxidants against reactive oxygen species (ROS), and may also participate in regulating and signaling processes (Pratelli and Pilot, 2014; Hildebrandt *et al*., 2015). Accumulation of proline and GABA are the first reactions to abiotic stress and especially drought stress. Proline acts as an osmolyte or chemical chaperone and shows the highest accumulation among metabolites under dehydration stress (Rizhsky *et al*., 2004; Szabados and Savoure, 2010; Huang and Jander 2017; Takahashi *et al*., 2020; Wang *et al*. 2022). GABA increases osmolytes and leaf turgor, while reducing oxidative damage via antioxidant regulation. It is also essential for guard cell production and increases water efficiency and drought tolerance (Hasan *et al*., 2021b). In our study, there was observed upregulation of proline and GABA, aligning with established findings in the scientific literature. Additionally, genes intricately associated with these pathways, serving as enzymes catalyzing the fundamental reactions within these biosynthetic processes, exhibited notably distinct expression patterns (Table 2; Figure 3). Like proline and GABA, glutamine is an osmoprotectant and accumulates under drought stress (Hildebrandt *et al*., 2015). It is shortly metabolized from and to aspartate and glutamate, which act as

distance signal transducer for Ca^{2+}, ROS and electric signaling and as a precursor for proline, asparagine, arginine, and GABA (Sun *et al*. 2015; Qiu *et al*., 2020; Mousavi *et al*., 2013; Nguyen *et al*., 2018; Toyota et al., 2018). These amino acids and the corresponding transformation enzymes play key roles in the plants' nitrogen metabolism. In our study these metabolites were upregulated in drought-stressed leaf tissue, which is consistent with literature, and we were able to identify the regulating genes transcribing for enzymes of the underlying reactions in *R. nigrum* (Table 2; Figure 3).

The organic acid citric acid can be utilized for amino acid or GABA biosynthesis through the production of glutamate (Cercós *et al*., 2006; Degu *et al*., 2011). Furthermore, citric acid is a critical intermediate compound within the tricarboxylic acid (TCA) cycle. Drought stress can disrupt the TCA cycle due to reduced oxygen availability and impaired respiration, leading to alterations in citric acid levels (Araújo *et al*., 2014). In our study, citric acid fold change was decreased in leaves, which confirm results of previous studies (Ashrafi *et al*., 2018). Quinic acid and its derivatives have various roles in plant metabolism, physiology and are known to be involved in drought stress response in plants, where it can serve as precursor for biosynthesis of various phenolic compounds or have anti-drought properties to maintain cellular osmotic balance in plants (Qu *et al*., 2019; Wan *et al*., 2021). However, the precise mechanisms and functions of quinic acid under drought stress may vary depending on plant species and environmental conditions.

Besides the ABA independent metabolites proline and GABA, the amino acids threonine, methionine, isoleucine and valine were upregulated in our study due to drought stress treatment. Threonine and methionine act as precursors for isoleucine and valine, which are known to accumulate as a response to osmotic stress in *Arabidopsis* and other plant species (Sanchez *et al*., 2008; Székely et al., 2008; Joshi *et al*., 2010; Huang *et al*., 2017). These amino acids play key roles in regulating cell osmosis and reducing active oxygen damage (Singh *et al*., 2015; Bohnert and Jensen, 1996). The gene DROUGHT-INDUCED BRANCHED-CHAIN AMINO ACID AMINOTRANSFERASE (OsDIAT) was found to be the key regulator for BCAA accumulation in rice (Shim *et al*., 2023). In our

study the gene RN4G058050.1 (BCAT) upregulated, which in combination with the accumulation of isoleucine and valine is consistent with the results of our study (Table 2; Figure 4).

Aromatic acids like phenylalanine and tryptophan are precursors for several secondary metabolites such as indole acetate, lignin via the shikimate pathway and serve as input in the flavonoid pathway, all of which play important roles in drought stress response and tolerance (Maeda and Dudareva 2012; Suguiyama *et al*., 2014). Furthermore, they play key roles in plant protein synthesis and serve as precursors for several secondary metabolites, which are essential for plant growth (Tzin and Galili, 2010; Kumar *et al*., 2021). L-Tryptophan is a primary precursor for auxin production in plants, which regulates vacuolar osmotic pressure and mediate translocation of different metabolites improving osmotic balance and growth under water deficit conditions (Awan *et al*., 1999; Wang *et al*., 2008). Accumulation of this amino acid has been reported under drought stress conditions (Bowne *et al*., 2012), which is consistent with our results.

The accumulation of sugars in plants during drought stress represents an important adaptive strategy that supports plant survival and recovery when facing water scarcity (Kaur *et al*., 2021). In our study, galactinol content was increased in leaves after drought stress treatment. Accumulation of galactinol in response to abiotic stresses such as drought was previously described for many plant species (Taji *et al*. 2002, Nishizawa *et al*. 2006, Nishizawa-Yokoi *et al*. 2008; You *et al*., 2019). Besides that, particularly soluble sugars like sucrose, glucose, and fructose are known to play a significant role under drought stress in various plant tissues. However, our study did not show an upregulation of these sugars. An explanation can be the shorter stress period compared to other studies, which might have been insufficient to heavily affect processes such as photosynthesis as a main energy source or breakdown of storage sugars such as starch into soluble sugars.

To combine multi-omics data, a *de novo* genome assembly at the pseudo-chromosomal level for blackcurrant (*R. nigrum*) was generated, which was prepared using a combination of ONT long reads, Illumina short reads and

Hi-C ONT PoreC sequencing data. The approach resulted in a high-quality sequence assembly as revealed by the BUSCO scores. This is the first genome assembly for the genus *Ribes* and indeed the family Grossulariaceae as a whole. Furthermore, the transcriptome analysis revealed plenty of differentially expressed genes involved in drought stress mechanisms. Based on this data connections between intermediary metabolites in biosynthesis pathways were identified, such as the citrate cycle and alanine, aspartate, glutamate metabolism. These pathways are directly linked to valine, isoleucine, leucine metabolism, as well as proline and GABA biosynthesis. The integrated findings enhance our comprehension of stress-related genes and their associated metabolites within *R. nigrum* metabolism under drought stress conditions. But qRT-PCR and targeted metabolomics would be needed to establish precise relationships spanning the genome, transcriptome and metabolome levels. However, the annotated blackcurrant genome generated in this study lays the foundation for further research to understand the molecular basis of drought stress response in this important fruit crop. Our results can also be combined with existing genetic resources such as quantitative trait loci to facilitate marker-assisted selection and genetic engineering for the development of improved blackcurrant varieties.

7 Conclusion

These studies provide integrated approaches to understanding complex biological systems in plants, offering detailed functional insights and broad applicability for future research. The visualization framework combining PCA and ORA based on MapMan protein classes simplifies the interpretation of large RNA-Seq datasets, enabling efficient identification of gene expression patterns across both model and non-model species. By linking transcriptomic data to functional biological processes, it allows a better interpretation of complex data demonstrated in studies of floral initiation in *F.* × *ananassa* and drought stress responses in *R. nigrum*.

Furthermore, the *F.* × *ananassa* and *R. nigrum* studies have provided new insights into floral initiation and drought stress responses. The identification of key genes and metabolic pathways offers valuable insights for crop optimization and breeding strategies.

The generation of a high-quality *R. nigrum* genome provides a foundational resource for future genetic and functional studies, particularly in relation to drought stress, paving the way for improved blackcurrant varieties through marker-assisted selection and genetic engineering.

Overall, these studies contribute to plant biology by providing robust datasets, comprehensive functional annotations, and integrated approaches to explore gene expression and metabolic processes, advancing agricultural practices and crop resilience.

8 Abbreviations

4HbD	Bifunctional γ-hydroxybutyrate dehydrogenase
A4D	Aspartate 4-decarboxylase
ABA	Abscisic acid
ACLY	ATP citrate ligase
ACO	Aconitase
ACS	Acetolactate synthase
AK	Aspartate kinase
AP2/ERF	APETALA2/ETHYLENE RESPONSIVE FACTOR
ASAT	Aspartate transaminase
ASD	Aspartate-semialdehyde dehydrogenase
ASE	Amidophosphoribosyltransferase
AXM	Axillary meristem
BAK/SERK	Brassinosteroid co-receptor protein kinase gene
BCAT	Branched-chain-amino-acid transaminase
bHLH	Helix-loop-helix
BHMT2	Homocysteine S-methyltransferase
bp	Base pairs
BRN1	Bruno ortholog Bruno-like 1
BUSCO	Benchmarking Universal Single-Copy Orthologs
bZIP	Basic leucine zipper
C2H2	Zinc finger
CCBL	Kynurenine-oxoglutarate transaminase
CDPK	Ca^{2+}-dependent protein kinase
CETS	CENTRORADIALIS/TERMINAL FLOWER 1/SELF-PRUNING
CGS	Cystathione-γ-synthase
CL	Clery
CLR	Complete Long Reads
COL	CONSTANS-like
CPS	Large subunit of carbamoyl phosphate synthetase
CPS	Large subunit of carbamoyl phosphate synthetase heterodimer
CRK	Cysteine-rich repeat RLK
C_t	Threshold cycle value
CTAB	Cetyltrimethylammoniumbromid
DAD	Dihydroxy-acid dehydratase
DEG	Differentially expressed gene
DREB2	Dehydration-responsive element-binding protein 2
DUF26	DOMAIN OF UNKNOWN FUNCTION 26
DVL/RTFL	DEVIL/ROT-FOUR-LIKE
DVL1	DEVIL1
EDTA	Ethylendiamintetraessigsäure
EIN3	Ethylene Insensitive 3
Fan	Fragaria ananassa
FBH	FLOWERING BHLH
FD/FDP	FLOWERING LOCUS D/ FD PARALOGUE
FDR	False discovery rate

FER4	FERONIA 4
FI	Floral initiation
FLZ	Regulatory protein FCS-like zinc finger
FR	France
FT	FLOWERING LOCUS T
Fve	Fragaria vesca
GA	Gariguette
GABA	4-aminobutanoic acid
GABAPT	GABA pyruvate transaminase
GAD	Glutamate decarboxylas
GAPDH	Glyceraldehyde-3-phosphate dehydrogenase
GAT	GABA transporter
GC-MS	Gas chromatography-mass spectroscopy
GDH	Glutamate dehydrogenase
GE	Germany
GGAT	Glycine transaminase
GHR1	Hydrogen peroxide receptor kinase
GI	GIGANTEA
GLN1	Cytosolic glutamine synthetase
GLN2	Plastidial glutamine synthetase
GO	Gene Ontology
HD-ZIP	Homeodomain leucine zipper
Hi-C	Chromatin conformation capture technique
HMM	Hidden Markov models
HPCA	Hydrogen peroxide receptor kinase
HSD	Homoserine dehydrogenase
HSK	Homoserine kinase
IDH3	Isocitrate dehydrogenase heterodimer subunit 1
KARI	Ketol-acid reductoisomerase
L	Leaf
LAI	Assembly index
LC-MS	Liquid chromatography-mass spectroscopy
LINE	Long interspersed nuclear element
log_2FC	Log_2 fold changes
LRR	Leucine-rich repeat
LRR-RLK	Leucine-rich repeat receptor-like kinases
LTR	Long terminal repeat
LTR-RT	Intact LTR retrotransposon
MADS/AGL-type	MCM1; AGAMOUS, DEFICIENS, SRF / AGAMOUS-Like
MAPK	Mitogen-activated protein kinase
metA	Homoserine O-succinyltransferase
metE	5-methyltetrahydropteroyltriglutamate homocysteine methyltransferase
metX	Homoserine O-acetyltransferase
MYB	v-Myb myeloblastosis viral oncogene homolog
NAC	NO APICAL MERISTEM (NAM), ARABIDOPSIS TRANSCRIPTION ACTIVATOR FACTOR 1/2 (ATAF1/2), and CUP-SHAPED COTYLEDON (CUC2)
NaCl	Natriumchlorid
NADH-GOGAT	NADH-dependent glutamate synthase
NGS	Next Generation Sequencing

OAT	Ornithine-γ-aminotransferase
ONT	Oxford Nanopore Technologies
OPLS-DA	Orthogonal projection to latent structures discriminant analyses
ORA	Overrepresentation analysis
OsDIAT	DROUGHT-INDUCED BRANCHED-CHAIN AMINO ACID AMINOTRANSFERASE
P5CDH	$^{1}\Delta$-pyrroline-carboxylate dehydrogenase
P5CR	Pyrroline-carboxylate-dehydrogenase
P5CS	$^{1}\Delta$-pyrroline-carboxylate synthase
PC	Principal component
PCA	Principal component analysis
PCR	Polymerase chain reaction
PERK	Proline-rich extensin-like receptor kinases
PLS	Partial least squares
PP2	Phloem protein 2
PRODH	Proline dehydrogenase
PSKR	Phytosulfokine receptor
PYD4	Alanine aminotransferase
PYL	Pyrabactin like
PYR	Pyrabactin resistance
qRT-PCR	Real time quantitative PCR
QV	Quality value
R-AQI	Reference Assembly Quality Index
RCAR	Regulatory component of ABA receptors
RGA1	REPRESSOR OF GIBBERELLIC ACID1
RG-I	Rhamnogalacturonan I
RLCK	Receptor-like cytoplasmic kinases
RLK	Receptor-like kinases
RNA-Seq	RNA Sequencing
ROS	Reactive oxygen species
ROT4/DVL16	ROTUNDIFOLIA4
SAM	Shoot apical meristem
S-AQI	Scaffold Assembly Quality Index
SF	Seasonal flowering
SHMT	Serine hydroxymethyltransferase
SMRT	PacBio single-molecule real-time
SNP	Single nucleotide polymorphism
SnRK	SNF-related protein kinases
SOC1	SUPPRESSOR OF OVEREXPRESSION OF CONSTANS 1
SOD	Superoxide dismutase
SSADH	Succinate-semialdehyde dehydrogenase (NAD+)
SVP/AGL24	SHORT VEGETATIVE PHASE/ AGAMOUS-LIKE 24
T6P	Trehalose-6-phosphate
TA	Threonine aldolase
TB	Terminal bud
TCA	Tricarboxylic acid
TD	Threonine dehydratase
TE	Transposable element
TF	Transcription factor

TFL1	TERMINAL FLOWER 1
TIR	Terminal inverted repeat
TPM	Transcripts per million
TPS1	TREHALOSE-6-PHOSPHATE SYNTHASE1
trpA	Subunit α of tryptophan synthase complex
trpB	Subunit β of tryptophan synthase complex
TS	Threonine synthase
t-SNE	t-distributed stochastic neighbor embedding
UMAP	Uniform manifold approximation and projection
UPR	Unfolded protein response
UTRs	5′ untranslated regions
XTH23	Xyloglucan endotransglucosylase (XET)/hydrolase 23

9 Literature

Acharjee A, Kloosterman B, Visser RGF, Maliepaard C (2016). Integration of multi-omics data for prediction of phenotypic traits using random forest. BMC Bioinformatics 17(5): 363–373.

Abe H, Urao T, Ito T, Seki M, Shinozaki K, Yamaguchi-Shinozaki K (2003). Arabidopsis AtMYC2 (bHLH) and AtMYB2 (MYB) function as transcriptional activators in abscisic acid signaling. Plant Cell 15:63–78.

Agalou A, Purwantomo S, Overnaes E, Johannesson H, Thu X, Estiati A, de Kam RJ, Engström P et al. (2008). A genome-wide survey of HD-Zip genes in rice and analysis of drought-responsive family members. Plant Molecular Biology 66:87–103.

Akula R & Ravishankar GA (2011). Influence of abiotic stress signals on secondary metabolites in plants. Plant Signaling and Behavior 6(11):1720-1731.

Alonge M, Lebeigle L, Kirsche M, Jenike K, Ou S, Aganezov J, Wang X, Lippman ZB, Schatz MC, Soyk S (2022). Automated assembly scaffolding using RagTag elevates a new tomato system for high-throughput genome editing. Genome Biology 23: 258.

Alonso A, Marsal S, Julia A (2015). Analytical Methods in Untargeted Metabolomics: State of the Art in 2015. Frontiers in Bioengineering and Biotechnology 3.

Alqudah AM, Sallam A, Baenziger PS, Börner A (2020). GWAS: Fast-forwarding gene identification and characterization in temperate cereals: lessons from Barley- A review. Journal of Advanced Research 22: 119-135.

Arabidopsis Genome Initiative (2000). Analysis of the genome sequence of the flowering plant Arabidopsis thaliana. Nature 408, 796– 815.

Araújo WL, Martins AO, Fernie AR, Tohge T (2014). 2-oxoglutarate: linking TCA cycle function with amino acid, glucosinolate, flavonoid, alkaloid, and gibberellin biosynthesis. Frontiers in Plant Science 5(552).

Ashburner M, Ball CA, Blake JA, Botstein D, Butler H, Cherry JM, Davis AP, Dolinski K, Dwight SS, Eppig JT, Harris MA, Hill DP, Issel-Tarver L, Kasarski A, Lewis S, Matese JC, Richardson JE, Ringwald M, Rubin GM, Sherlock G (2000). Gene Ontology: tool for the unification of biology. Nature Genetics 25, 25–29.

Baena-González E, Rolland F, Thevelein JM, Sheen J (2007). A central integrator of transcription networks in plant stress and energy signalling. Nature 448(7156): 938-942.

Bai L, Guozeng Z, Yun Z, Zhaopei Z, Wei W, Yanyan D, Zhongyi W, Chun-Peng S (2009). Plasma membrane-associated proline-rich extensin-like receptor kinase 4, a novel regulator of Ca2+ signaling, is required for abscisic acid responses in Arabidopsis thaliana. Plant Journal 60(2): 314-327.

Bairoch A, Apweiler R (1997). The SWISS-PROT protein sequence data bank and its supplement TrEMBL. Nucleic Acid Research 25(1): 31-6.

Bansal P, Morgat A, Axelsen KB, Muthukrishnan V, Coudert E, Aimo L, Hyka-Nouspikel N, Gasteiger E, Kerhornou A, Neto TB, Pozzato M, Blatter MC, Ignatchenko A, Redaschi N, Bridge A (2021). Rhea, the reaction knowledgebase in 2022. Nucleic Acids Research 50(D1): D693-D700.

Belton J-M, McCord RP, Gibcus JH, Naumova N, Zhan Y, Dekker J (2012) Hi–C: a comprehensive technique to capture the conformation of genomes. Methods 58:268–276.

Benesty J, Chen J, Huang Y, Cohen I (2009). Pearson correlation coefficient. in Noise Reduction in Speech Processing., (Springer, Berlin Heidelberg: Springer) 1–4.

Benlloch R, Berbel A, Serrano-Mislata A, Madueño F (2007). Floral initiation and inflorescence architecture: a comparative view. Annals of Botany 100(3): 659-676.

Bernier G, Havelange A, Houssa C, Petitjean A, Lejeune P (1993). Physiological signals that induce flowering. Plant Cell 5(10). 1147-1155.

Bersanelli M, Mosca E, Remondini D, Giampieri E, Sala C, Castellani G, Milanes L (2016). Methods for the integration of multi-omics data: mathematical aspects. BMC Bioinformatics 17: 15.

Bhalla R, Narasimhan K, Swarup S (2005). Metabolomics and its role in understanding cellular responses in plants. Plant Cell Reports 24:562-571.

Bjornson M, Balcke GU, Xiao Y, de Souza A, Wang JZ, Zhabinskaya D, Tagkopoulos I, Tissuer A, Dehesh K (2017). Integrated omics analyses of retrograde signaling mutant delineate interrelated stress-response strata. Plant Journal 91(1): 70-84.

Böcker S, Letzel MC, Lipták Z, Pervukhin A (2009). SIRIUS:decomposing isotope patterns for metabolite identification. Bioinformatics 25:218–224.

Bogart E, Myers CR (2016). Multiscale metabolic modeling of C4 plants: connecting nonlinear genome-scale models to leaf-scale metabolism in developing maize leaves. PloS One 11(3): e0151722.

Bolger AM, Lohse M, Usadel B (2014). Trimmomatic: a flexible trimmer for Illumina sequence data. Bioinformatics 30(15): 2114-2120.

Bolger AM, Poorter H, Dumschott K, Bolger ME, Arend D, Osorio S, Gundlach H, Mayer KFX, Lange M, Scholz U, Usadel B (2019). Computational aspects underlying genome to phenome analysis in plants. The Plant Journal 97, 182-198.

Bolger M, Schwacke R, Gundlach H, Schmutzer T, Chen J, Arend D, Oppermann M, Weise S, Lange M, Fiorani F, Spannagl M, Scholz U, Mayer K, Usadel B (2017). From plant genomes to phenotypes. Journal of Biotechnology 261: 46-52.

Bolger M, Schwacke R, Usadel B (2021). MapMan visualization of RNA-Seq data using Mercator4 functional annotations. Springer Protocols: 195-212.

Borodovsky M, Rudd KE and Koonin EV (1994). Intrinsic and extrinsic approaches for detecting genes in a bacterial genome. Nucleic Acids Research v22(22).

Bowne JB, Erwin TA, Jutter J, Schnurbusch T, Langridge P, Bacic A, Roessner U (2012). Drought responses of leaf tissues from wheat cultivars of differing drought tolerance at the metabolite level. Molecula Plant 5(2): 418-429.

Brandoli C,Petri C, Egea-Cortines M, Weiss J (2020). Gigantea: Uncovering new functions in flower development. Genes 11(10): 1142.

Bray NL, Pimentel H, Melsted P, Pachter L (2016). Near-optimal probabilistic RNA-seq quantification. Nature biotechnology 34: 525-527.

Brůna T, Lomsadze A, Borodovsky M (2020). GeneMark-EP+: eukaryotic gene prediction with self-training in the space of genes and proteins. NAR Genomics and Bioinformatics 2(2):lqaa026

Cai Z, Huang Z, Wang Z, Tao Y, Wu F, Yu X, Luo J (2021). Identification of the related genes on the asymmetric root growth of Oryza sativa induced by ethylene through transcriptome sequencing, GO and KEGG analysis. Acta Physiologiae Plantarum 43(99).

Camacho C, Coulouris G, Avagyan V, Ma N, Papadopoulos J, Bealer K, Madden TL (2009). BLAST+: architecture and applications. BMC Bioinformatics 10:421.

Cao Z, Kapoor K, Banniza S (2019). Using a transcriptome sequencing approach to explore candidate resistance genes against stemphylium blight in the wild lentil species Lens ervoides. BMC PLant Biology 19(399).

Carbone F, Mourgues F, Perrotta G, Rosati C (2008). Advances in functional research of berry antioxidants and organoleptic traits in berry crops. BioFactors 34.

Caruana JC, Sittman JW, Wang W, Liu Z (2018). Suppressor of Runnerless Encodes a DELLA protein that controls runner formation for asexual reproduction in strawberry. Molecular Plant 11: 230-233.

Čereković N, Jarret D, Pagter M, Cullen DW, Morris JM, Hedley PE, Brennan R, Petersen KK (2015). The effects of drought stress on leaf gene expression during flowering in blackcurrant (Ribes nigrum L.). European Journal Horticultural Sciences 80(1): 39-46.

Čereković N, Pagter M, Kristensen HL, Pedersen HL, Brennan R, Petersen KK (2013). Effects of drought stress during flowering of two pot-grown blackcurrant (Ribes nigrum L.) cultivars. Scientia Horticultirae 162: 365-373.

Chandler JW (2012). Floral meristem initiation and emergence in plants. Cellular and Molecular Life Sciences 69: 3807-3818.

Chen H & Boutros PC (2011). VennDiagram: a package for generation of highly customizable Venn and Euler diagrams in R. BMC Bioinformatics 12(35).

Chen HT, Zeng Y, Yang YZ, Huang LL, Tang BL, Zhang H, Hao F , Liu W, Li Y, Liu Y , Zhang X, Zhang R, Zhang Y, Li Y, Wang K, He H, Wang Z, Fan G, Yang H, Bao A, Shang Z , Chen J, Wang W, Qiu Q (2020). Allele-aware chromosome-level genome assembly and efficient transgene-free genome editing for the autotetraploid cultivated alfalfa. Nature Communications, 11: 2494.

Chen K, Tang W, Zhou Y, Chen J, Xu Z, Ma R, Dong Y, Ma Y, Chen M (2022). AP2/ERF transcription factor GmDREB1 confers drought tolerance in transgenic soybean by interacting with GmERFs. Plant Physiology and Biochemistry 170(1): 287-295.

Chen Y, Nie F, Xie SQ, Zheng YF, Dai Q, Bray T, Wang YX, Xing JF, Huang ZJ, Wang DP, He LJ, Luo F, Wang JX, Liu YZ, Xiao CL (2021). Efficient assembly of nanopore reads via highly accurate and intact error correction. Nature Communications 12 (60).

Chen ZJ (2007) Genetic and epigenetic mechanisms for gene expression and phenotypic variation in plant polyploids. Annual Review of Plant Biology 58:377-406.

Cheng H, Asri M, Lucas J, Koren S, Li H (2023). Scalable telomere-to-telomere assembly for diploid and polyploid with double graph. arXiv:2306.03399v1.

Cheng H, Asri M, Lucas j, Koren S, Li H (2024). Scalable telomere-to-telomere assembly for diploid and polyploid genomes with double graph. Nature Methods 21: 967-970.

Cheng H, Jarvis ED, Fedrigo O, Koepfli KP, Urban L; Gemmell NJ, Li H (2022). Haplotype-resolved assembly of diploid genomes without parental data. Nature Biotechnology 40: 1332-1335.

Cheng H, Qin L, Lee S, Fu X, Richards DE, Cao D, Luo D, Harberd NP, Peng J (2004). Gibberellin regulates Arabidopsis floral development cis suppression of DELLA protein function. 131(5): 1055-1064.

Chiche J, Brown SC, Leclerc JC, Siljak-Yakovlev S (2003). Genome size, heterochromatin organisation, and ribosomal gene mapping in four species of Ribes. Canadian Journal of Botany 81(11): 191-296.

Cho Y and Walbot V (2001) Computational methods for gene annotation: the Arabidopsis genome. Current Opinion Biotechnology 12: 126–130.

Choi WG, Miller G, Wallace I, Harper J, Mittler R, Gilroy S (2017). Orchestrating rapid long-distance signaling in plants with Ca2+, ROS and electric signals. Plant Journal 90 (4):698-707.

Cingolani P, Platts A, Wang le L, Coon M, Nguyen T, Wang L, Land SJ, Lu X, Ruden DM (2012). A program for annotating and predicting the effects of single nucleotide polymorphisms, SnpEff: SNPs in the genome of Drosophila melanogaster strain w1118; iso-2; iso-3 . Fly (Austin) 2:80-92.

Conesa A and Gotz S (2008). Blast2GO: a comprehensive suite for functional analysis in plant genomics. International Journal Plant Genomics 619832.

Corbesier L, Lejeune P, Bernier G (1998). The role of carbohydrates in the induction of flowering in Arabidopsis thaliana: comparison between the wild type and a starchless mutant. Planta 206: 131-137.

Cortez RE & Mejia EG (2019). Blackcurrants (Ribes nigrum): A review on chemistry, processing, and health benefits. Concise Reviews & Hypotheses in Food Science.

Costes E, Crespel L, Denoyes B, Morel P, Demene MN, Lauri PE, Wenden B (2014). Bud structure, position and fate generate various branching patterns along shoots of closely related Rosaceae species: a review. Frontiers in Plant Science Volume 5.

Darrow GM (1996). The Strawberry. CAB Direct. 19681601719, English, Book, History, breeding and physiology., (xvi + 447 pp.), Holt, Rinehart & Winston, New York, The strawberry. History, breeding and physiology.

Davik J, Røen D, Lysøe E, Buti M, Rossman S, Alsheikh M, Aiden EL, Dudchenko O, Sargent DJ (2022). A chromosome -level genome sequence assembly of the red raspberry (Rubus idaeus L.). PLOS ONE 17(3).

Davis SJ (2009). Integrating hormones into floral-transition pathway of Arabidopsis thaliana. Plant, Cell & Environment 32(9): 1201-1210.

Degu A, Hatew B, Nunes-Nesi A, Shilzerman L, Zur N, Katz E, Fernie AR, Blumwald E, Sadka A (2011). Inhibition of aconitase in citrus fruit callus results in a metabolic shift towards amino acid biosynthesis. Planta 234: 501-513.

DeMaere MZ, Darling AE (2021). qc3C: Reference-free quality control for Hi-C sequencing data. PLOS Computational Biology 17(10): e1008839.

Denay G, Chahtane H, Tichtinsky G, Parcy F (2017). A flower is born: an update on Arabidopsis floral meristem formation. Current Opinion in Plant Biology 35: 15-22.

Deshpande AS, Ulahannan N, Pendleton M, Dai X, Ly L, Behr JM, Schwenk S, Liao W, Augello MA, Tyer C, Rhugani P, Kudman S, Tian H, Otis HG, Adney E, Wilkes S, Mosquera JM, Barbieri CE, Melnick A, Stoddart D, Turner DJ, Juul S, Harrington E, Imieliǹski (2022). Identifying synergistic high-order 3D chromatin conformations from genome-scale nanopore concatemer sequencing. Nature biotechnology 40: 1488-1499.

Dickerson GW (2004). Home garden strawberry production in New Mexico. http://aces.nmsu.edu/pubs/_h/h324.pdf accessed 01 August 2023.

Dilokpimol A, Poulsen CP, Vereb G, Kaneko S, Schulz A, Geshi N (2014). Galactosyltransferases from Arabidopsis thaliana in the biosynthesis of type II arabinogalactan: molecular interaction enhances enzyme activity. BMC Plant Biology 14: 90.

Doyle JJ, Flagel LE, Paterson AH, Rapp RA, Soltis DE, Soltis PS, Wendel JF (2008). Evolutionary Genetics of Genome Merger and Doubling in Plants. Annual Review in Genetics 42:443-461.

Dozmorov MG, Tyc K, Sheffield NC, Boyd DC, Olex AL, Reed J, Harrell JC (2021). Chromatin conformation capture (Hi-C) sequencing of patient-derived xenografts: analysis guidelines. Gigascience 10(4):giab022.

Du H, Yu Y, Ma Y, Gao Q, Cao Y, Chen Z, Ma B, Qi M, Li Y, Zhao X, Wang J, Liu K, Qin P, Yang X, Zhu L, Li S, Liang C (2017). Sequencing and de novo assembly of a near complete indica rice genome. Nature Communication 8(15324).

Dubouzet JG, Sakuma Y, Ito Y, Kasuga M, Dubouzet EG, Miura S, Seki M, Shinozaki K, Yamaguchi-Shinozaki K (2003). OsDREB genes in rice, Oryza sativa L., encode transcription activators that function in drought-, high-salt- and cold-responsive gene expression. Plant J. 33, 751–763.

Dudchenko O, Shamim MS, Batra SS, Durand NC, Musial NT, Mostofa R, Pham M, St Hilaire PG, YAo W, Stamenova E, Hoeger M, Nyquist SK, Korchina V, Pletch K, Flanagan JP, Tomaszewicz A, McAloose D, Estrada CP, Novak BJ, Omer AD, Aiden EL (2018). The Juicebox Assembly Tools module facilitates de novo assembly of mammalian genomes with chromosome-length scaffolds for under $1000. bioRxiv 254797.

Dumschott K, Schmidt MHW, Chawla HS, Snowdon R, Usadel B (2020). Oxford Nanopore sequencing: new opportunities for plant genomics. Journal of Experimental Botany 71 (18): 5313-5322.

Durand NC, Shamim MS, Machol I, Rao SSP, Huntley MH, Lander ES, Aiden EL (2016). Juicer provides a one-click system for analyzing loop-resolution Hi-C experiments. Cell System 3(1): 95-98.

Durner EF, Barden JA, Himelrick DG, Poling EB (1984). Photoperiod and temperature effects on flower and runner development in day-neutral, junebearing, everbearing strawberries. Journal of the American Society for Horticultural Science 109(3): 396-400.

Durner EF, Barden JA, Himelrick DG, Poling EB (1984). Photoperiod and temperature effects on flower and runner development in day-neutral, junebearing, everbearing strawberries. Journal of the American Society for Horticultural Science 109(3): 396-400.

Eckhardt NA (2007). GA signaling: direct targets of DELLA proteins. The Plant Cell 19(10): 2970.

Edger PP, Poorten TJ, VanBuren R, Hardigan MA, Colle M, McKain MR, Smith RD, Teresi SJ, Nelson ADL (2019). Origin and evolution of the octoploid strawberry genome. Nature genetics 51: 541-547.

Fabregat A, Sidiropoloulos K, Viteri G, Forner O, Marin-Garcia P, Arnau V, D'Eustachio, Stein L, Hemjakob H (2017). reactome pathway analysis: a high-performance in-memory approach. BMC Bioinformatics 18(1).

Farooqi MQU, Nawaz G, Wani SH, CHoudhary JR, Rana M, Sah RP, Afzal M, Zahra Z, Ganie SA, Razzaq A, Reyes VR, Mahmoud EA, Elansary HO, El-Abedin TKZ, Siddique KHM (2022). Recent developments in multi-omics and breeding strategies for abiotic stress tolerance in maize (Zea mays L.). Frontiers in PLant Science 13:965878.

Feron R, Waterhouse RM (2022). Assessing species coverage and assembly quality of rapidly accumulating sequenced genomes. GigaScience 11.

Fickett JW (1996) The gene identification problem: an overview for developer. Computational Chemistry 20: 103–118.

Forzani C, Carreri A, de la Fuente van Bentem S, Lecourieux D, Lecourieux F, Hirt H (2011). The Arabidopsis protein kinase Pto-interacting 1–4 is a common target of the oxidative signal-inducible 1 and mitogen-activated protein kinases. FEBS Journal 278: 1126–36.

Fu Y (2010). The actin cytoskeleton and signaling network during pollen tube tip growth. Journal of Integrative Plant Biology 52(2): 131-137.

Ganger MT, Dietz GD, Erwing SJ (2017). A common base method for analysis of qPCR data and the application of simple blocking in qPCR experiments. BMC Bioinformatics 534.

Garrison E, Marth G (2012). Haplotype-based variant detection from short-read sequencing. arXiv preprint arXiv:1207.3907.

Gaston A, Perotte J, Lerceteau-Köhler E, Rousseau-Guetin M, Petit A, Hernould M, Rothan C, Denoyes B (2013). PFRU, a single dominant locus regulates the balance between sexual and asexual plant reproduction in cultivated strawberry. Journal of Experimental Botany 64(7): 1837-1848.

Gaston A, Potier A, Alonso, Sabbadini S, Delmas F, Tenreira T, Cochetel N, Labadie M, Prévost P, Folta KM, Mezetti B, Hernould M, Rothan C, Denoyes B (2021). The FveFT2 florigen/FveTFL1 antiflorigen balance is critical for the control of seasonal flowering in strawberry while FveFt3 modulates axillary meristem fate and yield. New Phytologist 232(1): 372-387.

Gibon Y, Usadel B, Blaesing OE, Kamlage B, Hoehne M, Trethewey R, Sitt M (2006). Integration of metabolite with transcript and enzyme activity profiling during diurnal cycles in Arabidopsis rosettes. Genome Biology 7: R76.

Gilliham M, Able JA., Roy SJ (2017). Translating knowledge about abiotic stress tolerance to breeding programmes. Plant Journal. 90, 898–917.

Giri S, Krausz KW, Idle JR, Gonzalez FJ (2007). The metabolomics of (±)-arecoline 1-oxide in the mouse and its formation by human flavin-containing monooxygenases. Biochemical Pharmacology 73(4):561-573.

Gish LA, Clark SE (2011). The RLK/Pelle family of kinases. Plant Journal 66(1): 117-127.

Goel M, Sun H, Jiao WB, Schneeberger K (2019). SyRI: finding genomic rearrangements and local sequence differences from whole-genome assemblies. Genome Biology 20: 277.

Goff SA, Ricke D, Lan TH et al. (2002) A draft sequence of the rice genome (Oryza sativa L. ssp. japonica). Science 296, 92– 100.

Goodstein DM, Shu S, Howson R, Neupane R, Hayes RD, Fazo J, Mitros T, Dirks W, Hellsten U, Putman N, Rokhsar DS (2012). Phytozome: a comparative platform for green plant genomics. Nucleic Acids Research 40(D1): D1178-D1186.

Gossens J, Mertens J, Gossens A (2017). Role and functioning of bHLH transcription factors in jasmonate signalling. Journal of Experimental Botany 68(6): 1333-1347.

Guan D, McCarthy SA, Wood J, Howe K, Wang Y, Durbin R (2020). Identifying and removing haplotypic duplication in primary genome assemblies. Bioinformatics 36(9):2896-2898.

Guiglielmoni N, Houtain A, Derzelle A, Van Doninck K, Flot JF (2021). Overcoming uncollapsed halpotypes in long-read assemblies of non-model organisms. BMC Bioinformatics 22(303).

Guo HW and Ecker JR (2004). The ethylene signaling pathway: New insights. Current Opinion Plant Biology 7:40–49.

Guo J, Huang Z, Sun J, Cui X, Liu Y (2021). Research progress and future development trends in medicinal plant transcriptomics. Frontiers in Plant Science 12.

Guo P, Yoshimura A, Ishikawa N, Yamaguchi T, Guo Y, Tsukaya H (2015). Journal of Plant Research 128(3): 497-510.

Gupta P, Elser J, Hooks E, D'Eustachio P, Jaiswal P, Naithani S (2023). Plant Reactome knowledgebase: empowering plant pathway exploration and OMICS data analysis. Nucleic Acid Research 52(D1): D1538-D1547.

Gurevich A, Saveliev V, Vyahhi, N Tesler (2013). QUAST: quality assessment tool for genome assemblies. Bioinformatics 29(8): 1072-1075.

Gustavsen JA, Pai S, Isserlin R, Demchak B, Pico AR (2019). RCy3: Network biology using Cytoscape from within R. F1000Research 8:1774.

Hamilton JP, Buell CR (2012). Advances in plant genome sequencing. The plant journal 70 (1): 177-190.

Hancock JF, Luby JJ, Dale A. Callow PW, Serçe S, El-Shiek A (2002). Utilizing wild Fragaria virginiana in strawberry cultivar development: Inheritance of photoperiod sensitivity, fruit size, gender, female fertility and disease resistance. Euphytica 126: 177-184.

Hansen P, Gargano M, Hecht J, Ibn-Salem J, Karlebach G, Roehr JT, Robinson PN (2019). Computational Processing and Quality Control of Hi-C, Capture Hi-C and Capture-C Data. Genes 10(7):548.

Hasan MM, Alabdallah NM, Alharbi BM, Waseem M, Yao G, Liu XD, El-Gawad HGA, El-Yazied AA, Ibrahim MFM, Jahan MS, Fang XW (2021b). GABA: a key player in drought stress resistance in plants. International Journal of Molecular Science 22(18): 10136.

Hasan MM, Liu XD, Waseem M, Guang-Qian Y, Alabdallah NM, Jahan MS, Feng XW (2022). ABA activated AnRK2 kinases: an emerging role in plant growth and physiology. Plant Signaling and Behaviour v-17(1).

Hassani-Pak K and Rawlings C (2017). Knowledge discovery in biological databases for revealing candidate genes linked to complex phenotypes. Journal Integration Bioinformatics 14(1).

Hastings J, Owen G, Dekker A, Ennis M, Kale N, Muthukrishnan, Turner S, Swainston N, Mendes P, Steinbeck C (2016). ChEBI in 2016: Improved services and expanding collection of metabolites. Nucleic Acids Research 44(D1):D1214-9.

Hawkins C, Ginzburg D, Zhao KM, Dwyer W, Xue B, Xu A, Rice S, Cole B, Paley S, Karp P, Rhee SY (2021). Plant metabolic network 15: a resource of genome-wide metabolism databases for 126 plants and algae. Journal of Integrative Plant Biology 63: 1888–1905.

He X, Wang C, Wang H, Li L, Wang C (2020). The function of MAPK cascades in response to various stresses in horticultural plants. Frontiers in Plant Science 11(952).

He Y, Han J, Liu R, Ding Y, Wang J, Sun L, Xang X, Zeng Y, Wen W, Xu J, Zhang H, Yan X, CHen Z, Gu Z, CHen H, Tang H, Deng X, Cheng Y (2018). Integrated transcriptomic and metabolomic analyses of a wax deficient citrus mutant exhibiting jasmonic acid-mediated defense against fungal pathogens. Horticulture Research 5(1): 43.

He Y, Zhou J, Shan L, Meng X (2018). Plant cell surface receptor-mediated signaling- a common theme amid diversity. Journal of Cell Science 131(2).

He M, Chi X, Ren J (2020). Applications of Oxford Nanopore Sequencing in Schizosaccharomyces pombe. Methods in Molecular Biology (MIMB, vol. 2196)

Heckmann AB, Lombardo F, Miwa H, Perry JA, Bunnewell S, Parniske M, Wang TL, Downie JA (2006). Lotus japanicus nodulation requires two GRAS domain regulators, one which is functionally conserved in a non-legume. Plant Physiology 142(4): 1739-1750.

Hedley PE, Russel JR, Jorgensen L, Gordon S, Morris JA, Hackett CA, Cardle L, Brennan R (2010). Candidate genes associated with bud dormancy release in blackcurrant (Ribes nigrum L.). BMC Plant Biology 10:202.

Heide OM, Stavang JA, Sønsteby A (2013). Physiology and genetics of flowering in cultivated and wild strawberries-a review. The Journal of Horticultural Science and Biotechnology 88(1): 1-18.

Hernández-Plaza A, Szklarczyk D, Botas J, Cantalapiedra CP, Giner-Lamia J, Mende DR, Kirsch R, Rattei T, Letunic I, Jensen LJ, Bork P, Von Mering C, Huerta-Cepas J (2022). eggNOG 6.0: Enabling comparative genomics across 12,535 organisms. Nucleic Acids Research gkac1022.

Hewitt S, Hernández-Montes E, Dhingra A, Keller M (2023). Impact of heat stress, water stress, and their combined effects on the metabolism and transcriptome of grape berries. Scientific Reports 13: 9907.

Hildebrandt TM, Nesi AN, Araújo WL, Braun HP (2015). Amino acid catabolism in plants. Molecular Plant 8: 1563-1579.

Himmelbach A, Hoffmann T, Leube M, Höhener B, Grill E (2002). Homeodomain protein ATHB6 is a target of the protein phosphatase ABI1 and regulates hormone responses in Arabidopsis. EMBO Journal 21:3029–3038.

Hoff KJ, Lange S, Lomsadze A, Borodovsky M, Stanke M (2016). BRAKER1: unsupervised RNA-Seq based genome annotation with GeneMark-ET and AUGUSTUS. Bioinformatics 32: 767-769.

Holst F, Bolger A, Günther C, Maß J, Triesch, Kindel F, Kiel N, Saadat N, Ebenhöh O, Usadel B, Schwacke R, Bolger M, Weber APM, Denton AK (2023). Helixer-de novo prediction of primary eukaryotic gene models combining deeep learning and a hidden markov model. bioRxiv, 2023.02.06.527280v2.

Hsieh JWA, Lin PY, Wang CT, Lee YL, Chang P, Lu RJH, Chen PY, Wang CJR (2024). Establishing an optimized ATAC-seq protocol for the maize. Frontiers in Plant Science 15.

Hsu LL and Culhane AC (2023). Correspondence analysis for dimension reduction, batch integration, and visualization of single-cell RNA-seq data. Nature Scientific Reports 13:1197.

Hu J, Fan J, Sun Z, Liu S (2019). NextPolish: a fast and efficient genome polishing tool for long-read assembly. Bioinformatics 36(7): 2253-2255.

Hu J, Wang Z, Sun Z, Hu B, Ayoola AO, Liang F, Li J, Sandoval JR, Cooper DN, Ye K, Ruan J, Xiao CL, Wang DP, Wu DD, Wang S (2023). An efficient error correction and accurate assembly tool for noisy long reads. BioRxiv Preprint.

Hu Z (2014). Using VisANT to analyze networks. Current Protocols in Bioinformatics 45: 8.81-8.8.39.

Huang J, Sun S, Xu D, Yang X, Bao Y, Wang Z, Tang H, Zhang H (2009b). Increased tolerance of rice to cold, drought and oxidative stresses mediated by the overexpression of a gene that encodes the zinc finger protein ZFP245. Biochemical and Biophysical Research Communications 389: 556–561

Huang S, Chaudhary K, Garmire LX (2017). More is better: recent progress in multi-omics data integration methods. Frontiers in Genetics 8(84).

Huang S, Kang M, Xu A (2017). HaploMerger2: rebuilding both haploid sub-assemblies from high-heterozygosity diploid genome assembly. Bioinformatics 33: 2577-2579.

Huang T and Jander G (2017). Abscisic acid-regulated protein degradation causes osmotic stress-induced accumulation of branched-chain amino acids in Arabidopsis thaliana. Planta 246: 737-747.

Huang XY, Chao DY, Gao JP, Zhu MZ, Shi M, Lin HX (2009a). A previously unknown zinc finger protein, DST, regulates drought and salt tolerance in rice via stomatal aperture control. Genes and Development 23: 1805–1817

Huang Y, An J, Sircar S, Bergis C, Lopes CD, He X, Costa BD, Tan FQ, Bazin J, Antunez-Sanchez J, Mammarella MF, Devani RS, Brik-Chaouche R, Bendahmane A, Frugier F, Xia C, Rothan C, Probst AV, Mohamed Z, Bergounioux C, Delarue M, Zhang Y, Zheng S, Crespi M, Fragkostefanakis S, Mahfouz MM, Ariel F, Gutierrez-Marcos J, Raynaud C, Latrasse D, Benhamed M (2023). HSFA1a modulates plant heat stress responses and alters the 3D chromatin organization of enhancer-promoter interactions. Nature communications 14: 469.

Huang Y, Escalona M, Morrison G, Marimuthu MPA, Nguyen O, Toffelheimer E, Shaffer HB, Litt A (2022). Reference genome assembly of the big berry Manzanita (Arctostaphylos glauca). Journal of Heredity 113(2): 188-196.

Hung FY, Lai YC, Wang J, Feng YR, Shih YH, Chen JH, Sun HC, Yang S, Li C, Wu K (2021). The Arabidopsis histone demethylase JMJ28 regulates CONSTANS by interacting with FBH transcription factors. The Plant Cell 33(4): 1196-1211.

Hytonen T and Kurokura (2020). Control of flowering and runnering in Strawberry. The Horticulture Journal 89(2):96-107.

Isatce B, Belser C, Falentin C, Labadie K, Boideau F, Deniot G, Maillet L, Cruaud C, Bertrand L, Chèvre AM, Wincker P, Rousseau-Gueutin M, Aury JM (2021). Sequencing and Chromosome-Scale Assembly of Plant Genomes, Brassica rapa as a Use Case. Biology 10(8): 732.

Ito S, Song YH, Joseph-Day AR, Miller RJ, Breton G, Olmsted RG, Imaizumi T (2012). FLOWERING BHLH transcriptional activators control expression of the photoperiodic flowering regulator CONSTANS in Arabidopsis. PNAS 109(9): 3582-3587.

Iwata H, Gaston A, Remay A, Thouroude T, Jeauffre J, Kawamura K, Oyant LHS, Araki T, Denoyes B, Foucher F (2011). The TFL1 homologue KSN is a regulator of continuous flowering in rose and strawberry. The Plant Journal 69(1):116-125.

Jahn OL, Dana MN (1970). Crown and inflorescence development in the strawberry, Fragaria ananassa. American Journal of Botany 57(6): 605-612.

Jamil IN, Remali J, Azizan KA, Muhammed NAN, Arita M, Goh HH, Aizat WM (2020). Systematic multi-omics integration (MOI) approach in plant systems biology. Secondary Plant Systems and Synthetic Biology 11.

Jamla M, Khare T, Joshi S, Patil S, Penna S, Kumar V (2021a). Omics approaches for understanding heavy metal responses and tolerance in plants. Current Plant Biology. 27: 100213.

Jan S, Abbas N, Ashraf M, Ahmad P (2018). Roles of potential plant hormones and transcription factors in controlling leaf senescence and drought tolerance. Protoplasma 256: 313-329.

Jarret D, Morris J, Cullen DW, Gordon SL, Verrall SR, Milne L, Hedley PE, Allwood JW, Brennan RM, Hancock RD (2018). A Transcriptome and Metabolite Atlas of Blackcurrant Fruit Development Highlights Hormonal Regulation and Reveals the Role of Key Transcription Factors. Frontiers in Plant Science 9:1235.

Jiang F and Hartung W (2008). Long-distance signaling of abscisic acid (ABA): the factors regulating the intensity of ABA signal. Journal of Experimental Botany 59(1): 37-43.

Jiang J, Xing F, Wang C, Zeng X, Zou Q (2019). Investigation and development of maize fused network analysis with multi-omics. Plant Physiology and Biochemistry 141: 380–387.

Jin X, Du H, ZhuC, Wan H, Liu F, Ruan J, Mower JP, Zhu A (2023). Haplotype-resolved genomes of wild octoploid progenitors illuminate genomic diversifications from wild relatives to cultivated strawberry. Nature Plants 9: 1252-1266.

Jo J, Park JS, Won H, Jeong JS, Jung TW, Lee KJ, Lee SA (2024). The first Chromosomal-level genome assembly of Sageretia thea using Nanopore long reads and Pore-C technology. Scientific Data 11: 959.

Joshi R, Wani SH, Singh B, Bohra A, Dar ZA, Lone AA, Pareek A, Singla-Pareek SL (2016). Transcription factors and plants response to drought stress: current understanding and future directions. Frontiers in Plant Science 7: 1029.

Joshi V, Joung JG, Fei Z, Jander G (2010). Interdependence of threonine, methionine and isoleucine metabolism in plants: accumulation and transcriptional regulation under abiotic stress. Amino acids 39: 933-947.

Jung S, Lee T, Cheng CH, Buble K, Zheng P, Yu J, Humann J, Ficklin SP, Gasic K, Scott K, Frank M, Ru S, Hough H, Evans K, Peace C, Olmstead M, DeVEtter LW, McFearson J, Coe M, Wegrzyn JL, Staton ME, Abbott AG, Main D (2018). 15 years of GDR: New data and functionality in genome database for Rosaceae. Nucleic Acid Research 47: D1137-D1145.

Juškytė AD, Mažeikienė I, Stanys V (2022). Analysis of R Genes Related to Blackcurrant Reversion Virus Resistance in the Comparative Transcriptome of Ribes nigrum cv. Aldoniai. Plants (Basel) 11(22): 3137.

Kajitani R, Toshimoto K, Noguchi H, Toyoda A, Ogura Y, Okuno M, Yabana M, Harada M, Ngayasu E, Maruyama H, Kohara Y, Fujiyama Asao, Hayashi T, Itoh T (2014). Efficient de novo assembly of highly heterozygous genomes from whole-genome shotgun short reads. Genome Research 24(8):1384–95.

Kanehisa M, Furumichi M, Sato Y, Kawashima M, shiguro-Watanabe M (2023). KEGG for taxonomy-based analysis of pathways and genomes. Nucleic Acids Research 51: D587-D592.

Kapoor B, Kumar A, Kumar P (2021). Transcriptome repository of North-Western Himalayan endangered medicinal herbs: a paramount approach illuminating molecular perspective of phytoactive molecules and secondary metabolism. Molecular Genetics and Genomics 296: 1177-1202.

Karp PD & Caspi R (2011). A survey of metabolic databases emphasizing the MetaCyc family. Archives of Toxicology 85: 1015-1033.

Kaul S, Koo HL, Jenkins J, Rizzo M, Rooney T, Tallon LJ, Feldblyum T, Nierman W, Benito MI, Lin X, Stiekema WJ (2000). Analysis of the genome sequence of the flowering plant Arabidopsis thaliana. Nature 408: 796-815.

Kaur H, Manna M, Thakur T, Gautam V, Salvi P (2021). Imperative role of sugar signaling and transport during drought stress responses in plants- Physiologia Plantarum 171(4): 833-848.

Kawamoto N, Sasabe M, Endo M, Machida Y, Araky Y (2015). Calcium-dependent protein kinases responsible for the phosphorylation of a bZIP transcription factor FD crucial for the florign complex formation. Nature Scientific reports 5: 8341.

Khan MIR, Chopra P, Chhillar H, Ahanger MA, Hussain SJ, Maheshwari C (2021). Regulatory hubs and strategies for improving heavy metal tolerance in plants: chemical messengers, omics and genetic engineering. Plant Physiology Biochemistry. 164, 260–278.

Khoso MA, Hussain A, Ritonga FN, Ali Q, Channa MM, Alshegaihi RM, Meng Q, Ali M, Zaman W, Brohi RD, Liu F, Manghwar H (2022). WRKY transcription factors (TFs): Molecular switches to regulate drought, temperature, and salinity stresses in plants. Frontiers in Plant Science 13: 3389.

Khurana JP, Tamot BK, Maheshwari SC (1988). Floral induction in a photoperiodically insensitive duckweed, Lemna paucicostata LP6: Role of glutamate, aspartate, and other amino acids and amides. Plant Physiology 86(3): 904-907.

Kim HS, Abbasi N, Choi SB (2013). Bruno-like proteins modulate flowering time via 3′ UTR-dependent decay of SOC1 mRNA. New Phytologist 198(3): 747-756.

Kim S, Chen J, Cheng T, Gidulyte A, He J, He S, Li Q, Shoemaker BA, Thiessen PA, Yu B, Zaslavsky L, Zhang J, Bolton EE (2023). PubChem 2023 update. Nucleic Acids Res. 2023;51(D1): D1373–D1380.

Koembuoy K, Hasegawa S, Otagaki S, Takahashi H, Nagano S, Isobe S, Shiratake K, Matsumoto S (2020). RNA-Seq analysis pf meristem cells indentifies the FaFT3 gene as a common floral inducer in japaneses cultivated strawberry. The Horticulture Journal 89(2): 138-146.

Kolmogorov M, Yuan J, Lin Y, Pevzner PA (2019). Assembly of long, error-prone reads using repeat graphs. Nature Biotechnology 37: 540-546.

Kong W, Wang Y, Zhang S, Yu J, Zhang X (2023). Recent advances in assembly of complex plant genomes. Genomics, Proteomics & Bioinformatics 21(3): 427-439.

Kopka J, Schauer N, krueger S, Birkemeyer C, Usadel B, Bergmüller E, Dörmann P, Weckwerth W, Gibon Y, Stitt M, Willmitzer L, Fernie AR, Steinhauser D (2005). GMD@CSB.DB: the golm metabolome database. Bioinformatics 21(8): 1635-1638.

Korneef M, Alonso-Blanco Cm Peeters JM, Soppe W (1998). Genetic control of flowering time in Arabidopsis. Annual Review of Plant Biology 49: 345-370.

Koskela EA, Mouha K, Albani MC, Kuokura T, Rantanen M, Sargent DJ, Battey NH, Coupland G, Elomaa P, Hytönen T (2012). Mutation in TERMINAL FLOWER 1 reverses the photoperiodic requirement for flowering in the wild strawberry Fragaria vesca. Plant Physiology 159(3): 1043-1054.

Koskela EA, Sonsteby A, Flachowsky H, Heide Om, Hanke MV, Elomaa P, Hytönen T (2016). TERMINAL FLOWER 1 is a breeding target for a novel everbearing trait and tailored flowering responses in cultivated strawberry (Fragaria x ananassa Duch.). Plant Biotechnology Journal 14(9): 1852-1861.

Krüger E, Woznicki TL, Heide OM, Kusnierek K, Rivero R, Masny A, Sowik I, Brauksiepe B, Eimert K, Mott D, Savini G, Demene M, Guy K, Petit A, Denoyes B, Sonsteby A (2022). Flowering Phenology of Six Seasonal-Flowering Strawberry Cultivars in a Coordinated European Study. Horticulturae 8(10): 933.

Ksouri N, Jiménez S, Wells CE, Contrera-Moreira B, Gogorcena Y (2016). Transcriptional responses in root and leaf of Prunus persica under drought stress using RNA sequencing. Frontiers in Plant Science 7(1715).

Ku YS, Sintaha M, Cheung MY, Lam HM (2018). Plant hormone signaling crosstalks between biotic and abiotic stress responses. International Journal of Molecular Sciences 19(10): 3206.

Kukurba KR & Montgomery SB (2015). RNA sequencing and analysis. Cold Spring Harbor Protocols.

Kumar M, Patel MK, Kumar N, Bajpai AB, Siddique KHM (2021). Metabolomics and molecular approaches reveal drought stress tolerance in plants. International Journal of Molecular Sciences 22(17): 9108.

Kumar R, Bohra A, Pandey AK, Pandey MK, Kumar A (2017). Metabolomics for plant improvement: status and prospects. Secondary Plant Biotechnology 8.

Kumar S and Mohapatra T (2021). Dynamics of DNA methylation and ist functions in plant growth and development. Frontiers in Plant Science 12: 596236.

Kumar V, Kumar P, Bhargava B, Sharma R, Irfan M, Chandora R (2023). Transcriptomic and metabolomic reprogramming to explore the high-altitude adaptation of medicinal plants: A review. Journal of Plant Growth Regulation.

Kundu S and Gantait S (2017). Abscisic Acid Signal Crosstalk during Abiotic Stress Response. Plant Gene. 11:61–69.

Kurokura T, Samad S, Koskela E, Mouhu K, Hytönen T (2017). Fragaria vesca CONSTANS controls photoperiodic flowering and vegetative development. Journal of Experimental Botany 68(17): 4839-4850.

Kuromori T, Seo M, Shinozaki K (2018). ABA transport and plant water stress responses. Trends in Plant Sciences 23 (6): 513-522.

Kutmon M, van Iersel MP, Bohler A, Kelder T, Nunes N, Pico AR, Evelo CT (2015). PathVisio 3: An Extendable Pathway Analysis Toolbox. PLoS Computational Biology 11(2): e1004085.

Langridge J (1957). Effect of day-length and gibberellic acid on the flowering of Arabidopsis thaliana. Nature 180: 36-37.

Lawas LMF, Zuther E, Jagadish SVK, Hincha DK (2018). Molecular mechanisms of combined heat and drought stress resilience in cereals. Current Opinion in Plant Biology 45(B): 212-217.

Li H (2018). Minimap2: pairwise alignment for nucleotide sequences. Bioinformatics 34(18): 3094-3100.

Li K, Xu P, Wang J, Yi X, Jiao Y (2023). Identification of errors in draft genome assemblies at single-nucleotide resolution for quality assessment and improvement. Nature Communications 14(6556).

Li Z, Liang F, Zhang, Fu N, Pei X, Long Y (2021). Enhanced tolerance to drought stress resulting from Caragana korshinskii CkWRKY33 in transgenic Arabidopsis thaliana. BMC Genomic Data 22:11.

Li Z, Long Y, Yu Y, Zhang F, Zhang H, Liu Z, Jia J, Mo W, Tian SZ, Zheng M, Zhai J (2022). Pore-C simultaneously captures genome-wide multi-way chromatin interaction and associated DNA methylation status in Arabidopsis. Plant Biotechnology Journal 20(6): 1009-1011.

Li, H (2021). New strategies to improve minimap2 alignment accuracy. Bioinformatics, 37:4572-4574.

Liang J, Zheng J, Wu Z, Wang H (2022). Time-course transcriptomic profiling of floral induction in cultivated strawberry. International Journal of Molecular Sciences 23: 6126.

Liang J, Zheng J, Wu Z, Wang H (2022). Time-course transcriptomic profiling of floral induction in cultivated strawberry. International Journal of Molecular Sciences 23: 6126.

Lin L, Wu J, Jiang M, Wang Y (2021). Plant mitogen-activated protein kinase cascades in environmental stresses. International Journal of Molecular Sciences 22(4): 1543.

Lin W, Ma X, Shan L, He P (2013). Big roles of small kinases: the complex functions of receptor-like cytoplasmic kinases in plant immunity and development. Journal of Integrative Plant Biology 55(12): 1188-1197.

Liu L, Chen M, Folk RA,Wang M, Zhao T, Shang F, Soltis DE, Li P (2023). Phylogenomic and syntenic data demonstrate complex evolutionary processes in early radiation of the rosids. Molecular Ecology Resources 23(7): 1673-1688.

Liu T, Li M, Liu Z, Ai X, Li Y (2021). Reannotation of the cultivated strawberry genome and establishment of a strawberry genome database. Horticulture Research 8:41.

Liu T, Salguero P, Petek M, Martinez-Mira C, Balzano-Nogueira L, Ramšak Ž, McIntyre L, Gruden K, Tarazona S, Conesa A (2022). PaintOmics 4: new tools for the integrative analysis of multi-omics datasets supported by multiple pathway databases. Nucleic Acids Research 50:W551-W559.

Liu W, Tai H, Li S, Gao W, Zhao M, Xie C, Li WX (2014). bHLH122 is important for drought and osmotic stress resistance in Arabidopsis and in the repression of ABA catabolism. New Phytologist 201: 1192-1204.

Lohse M, Nagel A, Herter T, May P, Schroda M, Zrenner R, Tohge T, Fernie AR, Sitt M, Usadel B (2014). Mercator: a fast and simple web server for genome scale functional annotation of plant sequence data. Plant, Cell & Environment 37: 1250– 1258.

Long-Roach R, Meredith M, Monlong J, Jain M, Olsen h, McNulty B, Porubsky D, Montague T, Lucas J, Condon C, Eizenga J, Juul S, McKenzie S, Simmonds SE, Park J, Asri M, Koren S, Eichler E, Axel R, Martin Bm, Carnevali P, Miga K, Paten B (2023). Phased nanopore assembly with Shasta and modular graph phasing with GFAse. BioRxiv 529152.

López J, Vera C, Bustos R, Florez-Mendez J (2021). Native berries of chile: a comprehensive review on nutritional aspects, functional properties, and potential health benefits. Journal of Food Measurement and Characterization 15: 1139-1160.

López-Hidalgo C, Guerrero-Sánchez VM, Gómez-Gálvez I, Sánchez-Lucas R, Castillejo-Sánchez MA, Maldonado-Alconada AM, Valledor L, Jorrín-Novo J (2018). A multi-omics analysis pipeline for the metabolic pathway reconstruction in the orphan species Quercus ilex. Frontiers in Plant Science 9, 935.

Love MI, Huber W, Anders S (2014). Moderated estimation of fold change and dispersion for RNA-seq with DESeq2. Genome Biology 15:550.

Lu H, Xiao Y, Liu Y, Zhang J, Zhao Y (2024). Integrative Transcriptomics and Proteomics Analysis of a Cotton Mutant yl1 with a Chlorophyll-Reduced Leaf. Plants 13(13): 1789.

Luo J, Wei Y, Lyu M, Wu Z, Liu X, Luo H, Yan C (2021). A comprehensive review of scaffolding methods in genome assembly. Briefings in Bioinformatics 22(5): bbab033.

Ma A and Qi X (2021). Mining plant metabolomes: Methods, applications, and perspectives. Plant Communications 2, 100238.

Ma C, Zhang HH, Wang X (2014). Machine learning for big data analytics in plants. Trends Plant Sciences 19(12): 798–808.

Mahmood U, Li X, Fan Y, Chang W, Niu Y, Li J, Qu C, Lu K (2022). Multi-omics revolution to promote plant breeding efficiency. Frontiers in Plant Science 13.

Majhi BB, Sobol G, Gachie S, Sreeramulu S, Sessa G (2021). BRASSINOSTEROID-SIGNALLING KINASES 7 and 8 associate with the FLS2 immune receptor and are required for flg22-induced PTI responses. Molecular Plant Pathology 22:786–799.

Majoros WH, Pertea M and Salzberg SL (2004). TigrScan and GlimmerHMM: two open-source ab initio eukaryotic gene-finders Bioinformatics 2878-2879.

Mapleson DL, Venturini L, Kaithakottil G, Swarbreck D (2018). Efficient and accurate detection of splice junctions from RNAseq with Portcullis. GigaScience 7(12): giy131.

Mari RS, Schrinner S, Finkers R, Ziegler FMR, Arens P, Schmidt MHW, Usadel B, Klau GW, Marschall T (2024). Haplotype-resolved assembly of tetraploid potato genome using long reads and low-depth offspring data. Genome Biology 25: 26

Martens M, Ammar A, Riutta A, Waagmeester A, Slenter DN, Hanspers K, Miller RA, Digles D, Lopes EN, Ehrhart F, Dupuis LJ, Winkcers LA, Coort SL, Willighagen EL, Evelo CT, Pico AR, Kurmon M (2021). WikiPathways: connecting communities. Nucleic Acids Research 49: D613–D621.

Mathé C, Sagot MF, Schiex T, Rouzé P (2002). Current methods of gene prediction, their strengths and weaknesses. Nucleic Acids Research 30(19): 4103-4117.

Matsubayashi Y (2014). Posttranslationally modified small-peptides signals in plants. Annual Reviews in Plant Biology 65: 385-413.

Matsubayashi Y, Sakagami Y (2006). Peptide hormones in plants. Annual Reviews in Plant Biology 57: 649-674.

Maxam AM, Gilbert W (1977). A new method for sequencing DNA. PNAS 74 (2): 560-564.

Mažeikienė I, Juškytė AD, Stanys V (2022). De Novo Transcriptome Analysis of R. nigrum cv. Aldoniai in Response to Blackcurrant Reversion Virus Infection. International Journal of Molecular Sciences 23(17).

McCombie WR, McPherson JD, Mardis ER (2019). Next-Generation sequencing technologies. Cold Spring Harbour Laboratory Press 9.

McInnes L, Healy J, Melville J (2018). Umap: Uniform manifold approximation and projection for dimension reduction. bioXiv. 1802:03426

McLoughlin F, Augustine RC, Marshall RS, Li F, Kirkpatrick LD, Otegui MS, Vierstra RD (2018). Maize multi-omics reveal roles for autophagic recycling in proteome remodelling and lipid turnover. Nature plants 4: 1056-1070.

Meng C, Zeleznik O, Thallinger G, Kuster B, Gholami A, Culhane A (2016). Dimension reduction techniques for the integrative analysis of multi-omics data. Brief. Bioinformatics 17: 628–641.

Marx V (2023). Method of the Year 2022: long-read sequencing. Nature Methods 20 (1), 2023.

Mezetti B, Hernould M, Rothan C, Denoyes B (2021). The FveFT2 florigen/FveTFL1 antiflorigen balance is critical for the control of seasonal flowering in strawberry while FveFt3 modulates axillary meristem fate and yield. New Phytologist 232(1): 372-387.

Michael TP & VanBuren R (2020). Building near-complete plant genomes. Current Opinion in Plant Biology 54: 26-33.

Michael TP, Jupe F, Bemm F, Motley ST, Sandoval JP, Lanz C, Loudet O, Weigel D, Ecker JR (2018). High contiguity Arabidopsis thaliana genome assembly with a single nanopore flow cell. Nature Communications 9:541.

Michaels SD, Ditta G, Gustafson_Brown C, Pelaz S, Yanofsky M, Amasino RM (2003). AGL24 acts as promoter of flowering in Arabidopsis and is positively regulated by vernalization. The Plant Journal 33(5): 867-874.

Mihailova A, Kelly SD, Chevallier OP, Elliott CT, Maestroni BM, Cannavan A (2021). High-resolution mass spectrometry-based metabolomics for the discrimination between organic and conventional crops: A review. Trends in Food Science & Technology 110:142-154.

Mitchell C, Brennan RM, Cross JV, Johnson SN (2011). Arthropod pests of currant and gooseberry crops in the UK: their biology, management and future prospects. Journal Agriculture Forest Entomology 13: 221-237.

Moon J, Suh SS, Lee H, Choi KR, Hong CB, Paek NC, Kim SG, Lee I (2003). The SOC1 MADS-box gene integrates vernalization and gibberellin signals for flowering in Arabidopsis. The Plant Journal 35(5): 613-623.

Moriya Y, Itoh M, Okuda S, Yoshizawa AC, Kanehisa M (2007). KAAS: an automatic genome annotation and pathway reconstruction server. Nucleic Acid Research 35: W182-W185.

Mouradov A, Cremer F, Coupland G (2002). Control of flowering time: Interacting pathways as a basis for diversity. Plant Cell 14: 111-130.

Mousavi SAR, Chauvin A, Pascaud F, Kellenberger S, Farmer EE (2013). GLUTAMATE RECEPTOR-LIKE genes mediate leaf-to-leaf wound signalling. Nature 500: 422–426.

Munné-Bosch S and Allegre L (2004). Die and let live: leaf senescence contributes to plant survival under drought stress. Functional Plant Biology 31(3): 203-216.

Mutasa-Göttgens E & Hedden P (2009). Gibberellin as a factor in floral regulatory networks. Journal Experimental Botany 60(7): 1979-1989.

Myers L, Sirois MJ (2004). Spearman correlation coefficients, differences between. International Encyclopedia Statistical Science 12, 1–3.

Neat N, Ramalingam A, Mantri N (2018). Advances in transcriptomics of plants. Advances in Biochemical Engineering/Biotechnology 164.

Neuwirth E (2022). _RColorBrewer: ColorBrewer Palettes_. R package version 1.1-3, <https://CRAN.R-project.org/package=RColorBrewer>.

Nguyen CT, Kurenda A, Stolz S, Chételat A, Farmer EE (2018). Identification of cell populations necessary for leaf-to-leaf electrical signaling in a wounded plant. PNAS 115: 10178–10183.

Ogata H, Goto S, Sato K, Fujibuchi W, Bono H, Kanehisa M (1999). KEGG: Kyoto Encyclopedia of Genes and Genomes. Nucleic Acids Research 27:29–34.

O'Leary NA, Wright MW, Brister JR, Ciufo S, Haddad D, McVeigh R, Rajput B, Robbertse B, Smith-White B, Ako-Adjei D, Astashyn A, Badretdin A, Bao Y, Blinkova O, Brover V, Chetvernin V, Choi J, Cox E, Ermolaeva O, Farrell CM, Goldfarb T, Gupta T, Haft D, Hatcher E, Hlavina W, Joardar VS, Kodali VK, Li W, Maglott D, Masterson P, McGarvey KM, Murphy MR, O'Neill K, Pujar S, Rangwala SH, Rausch D, Riddick LD, Schoch C, Shkeda A, Storz SS, Sun H, Thibaud-Nissen F, Tolstoy I, Tully RE, Vatsan AR, Wallin C, Webb D, Wu W, Landrum MJ, Kimchi A, Tatusova T, DiCuccio M, Kitts P, Murphy TD, Pruitt KD (2016). Reference sequence (RefSeq) database at NCBI: current status, taxonomic expansion, and functional annotation. Nucleic Acids Research 44(D1):D733-45 .

Olson ND, Wagner J, McDaniel J, Stephens SH, Westreich ST, Prasanna AG, Johanson E, Boja E, Maier EJ, Serang O, Jáspez D, Lorenzo-Salazar JM et al. (2020). precisionFDA truth challengeV2: calling variants from short- and long-reads in difficult-to-map regions. bioRxiv 380741v4.

Olsson AS, Engström P, Söderman E (2004). The homeobox genes ATHB12 and ATHB7 encode potential regulators of growth in response to water deficit in Arabidopsis. Plant Molecular Biology 55:663–677.

Open2C, Abdennur N, Fudenberg G, Flyamer IM, Galitsyna AA, Goloborodko A, Imakaev M, Venev SV (2023). Pairtools: from sequencing data to chromosome contacts. bioRxiv 528389

Oritz-Marchena MI, Albi T, Lucas-Reina E, Said FE, Romero-Campero FJ, Cano B, Ruiz MT, Romero JM, Valverde F (2014). Photoperiodic control of carbon distribution during the floral transition in Arabidopsis. The Plant Cell 26(2): 565-584.

Osorio S, Alba R, Nikoloski Z, Kochevenko A, Fernie AR, Giovannoni JJ (2012). Integrative comparative analyses of transcript and metabolite profiles from pepper and tomato ripening and development stages uncovers species-specific patterns of network regulatory behaviour. Plant Physiology 159(4): 1713-1729.

Ou S and Jiang N (2018). Assessing genome assembly quality using the LTR Assembly Index (LAI). Nucleic Acids Research gky730.

Ou S, Su W, Liao Y, Chougule K, Agda JRA, Hellinga AJ, Santiago C, Lugo B, Elliott TA, Ware D, Peterson T, Jiang N, Hirsch CN, Hufford MB (2019). Benchmarking transposable element annotation methods fro creation of streamlined, comprehensive pipeline. Genome Biology 20(275).

Ozturk M, Unal BT, García-Carparrós P, Khursheed A, Gul A, Hasanuzzaman M (2020). Osmoregulation and its actions during the drought stress in plants. Physiologia Plantarum 172 (2): 1321-1335.

Pal K, Forcato M, Ferrari F (2019). Hi-C analysis: from data generation to integration. Biophysical Reviews 11: 67-78.

Parker RM, Barnes NM (1999). mRNA: detection by in situ and northern hybridization. Methods Molecular Biology 106:247–283

Patel MK, Padney S, Kumar M, Haque MI, Pal S, Yadav NS (2021). Plants metabolome study: Emerging tools and techniques. Plants 10(11): 2409.

Patro R, Duggal G, Love MI, Irizarry RA, Kingsford C (2017). Salmon: fast and bias-aware quantification of transcript expression using dual-phase inference. Nature Methods 14(4): 417-419.

Paunović SM, Mašković P, Milinković M (2022). Chemical Compounds and Biological Activity in Black Currant (Ribes Nigrum L.) Berries Depending on Soil Temperature and Moisture. Erwerbs-Obstbau. 64(4), 621–629.

Pavlopoulos G, Kontou P, Pavlopoulou A, Bouyioukos C, Markou E, Bagos P (2018). Bipartite graphs in systems biology and medicine: a survey of methods and applications. GigaScience 7, giy014.

Pei L, Li G, Lindsey K, Zhang X, Wang M (2021). Plant 3D genomics: the exploration and application of chromatin organization. New Phytologist 230(5): 1772-1786.

Perilleux C, Bouche F, Randoux M, Orman-Ligeza B (2019). Turning meristems into fortresses. Trends in Plant Science 24: 431–442.

Perotti MF, Arce AL, Chan RL (2021). The underground life of homeodomain-leucine zipper transcription factors. J Exp Bot 72:4005–4021.

Pertea G and Pertea M (2020). GFF Utilities: GrrRead and GffCompare. F1000 Research: 23297.2.

Pertea M, Pertea GM, Antonescu CM, Chang TC, Mendell JT, Salzberg SL (2015). StringTie enables improved reconstruction of a transcriptome from RNA-Seq reads. Nature Biotechnology 33: 290-295.

Powell AF, Feder A, Li J, Schmidt MHW, Courtney L, Alseekh S, Jobson Em, Vogel A, Xu Y, Lyon D, Dumschott,McHale M, Sulpice R, Bao K, Lal R, Duhan A, Hallab A, Denton AK, Bolger ME, Fernie AR, Hind AR, Mueller LA, Marin GB, Fei Z, Martin C, Giovannoni JJ, Strickler SR, Usadel B (2022). A Solanum lycopersicoides reference genome facilitates insights into tomato specialized metabolism and immunity. The Plant Journal 110(6): 1791-1810.

Pratelli R and Pilot Guillaume (2014). Regulation of amino acid metabolic enzymes and transporters in plants. Journal of Experimental Botany 65(19): 5535-5556.

Prohaska A, Petit A, Lesemann S, Rey-Serra P, Mazzoni L, Masny A, Sánchez-Sevilla JF, Potier A, Gaston A, Klamkowski K, Rothan C, Mezzetti B, Amaya I, Olbricht K, Denoyes B (2024). Strawberry phenotypic plasticity in flowering time is driven by the interaction between genetic loci and temperature. Journal Experimental Botany.75(18):5923-5939.

Qiu XM, Sun YY, Ye XY, Li ZG (2020). Signaling role of glutamate in plants. Frontiers in Plant Science 10: 1743.

Qu X, Wang H, CHen M, Liao J, Yuan J (2019). Drought stress-induced physiological and metabolic changes in leaves of two oil tea cultivars. Journal of the American Society for Horticultural Science 144(6): 439-447.

Quiao Z, Hu H, Shi S, Yuan X, Yan B, Chen L (2021). An update on the function, biosynthesis and regulation of floral volatile terpenoids. Horticulturae 7(11): 451.

R Core Team (2023). _R: A Language and Environment for Statistical Computing_. R Foundation for Statistical Computing, Vienna, Austria. <https://www.R-project.org/>.

Rai A, Yamazaki M, Saito K (2019). A new era in plant functional genomics. Current opinion in Systems Biology 15: 58-67.

Ramirez F, Bhardwaj V, Villaveces J, Arrigoni L, Gruening BA, Lam KC, Habermann B, Akhtar A, Manke T (2018). High-resolution TADs reveal DNA sequences underlying genome organization in flies. Nature Communications 9(189).

Rantanen M, Kurokura T, Mouhu K, Pinho P, Tetri E, Halonen L, Palonen P, Elomaa P, Hytönen T (2014). Light quality regulates flowering in FvFT1/FvTFL1 dependent manner in the woodland strawberry Fragaria vesca. Frontiers in Plant Science 5.

Raza A, Razzaq A, Mehmood SS, Hussain MA, Wie S, He H, Zaman QU, Xuekun Z, Yong C, Hasanuzzaman M (2020). Omics: The way forward to enhance abiotic stress tolerance in Brassica napus L. GM Crops and Food 12(1): 251-281.

Raza A, Tabassum J, Zahid Z, Charagh S, Bashir S, Barmukh R, Khan RSA, Barbosa F, Zhang C, Chen H, Zhuang W, Varshney RK (2022). Advances in “Omics” Approaches for Improving Toxic Metals/Metalloids Tolerance in Plants. Frontiers in Plant Science. Vol. 12.

Redhal AA, Siddiqui SA, Zare R, Spadaccini D, Guazzotti S, Feng X, Wu YS, Ozeer FZ; Aluko RE (2022). Blackcurrants: A nutrient-rich source for the development of functional foods for improved athletic performance. Food Reviews International

Rhie A, Walenz BP, Koren S, Phillippy AM (2020). Merqury: reference-free quality, completeness, and phasing assessment for genome assemblies. Genome Biology 21(245).

Rizhsky L, Liang H, Shuman J, Shulaev V, Davletova S, Mittler R (2004). When defense pathways collide. The response of Arabidopsis to a combination of drought and heat stress. Plant Physiology 134(4): 1683–1696.

Roach MJ, Schmidt SA, Bornemann AR (2018). Purge Haplotigs: allelic contig reassignment for third-gen diploid genome assemblies. BMC Bioinformatics 19 (460).

Robinson MD, McCarthy DJ, Smyth GK (2010). edgeR: a Bioconductor package for differential expression analysis of digital gene expression data. Bioinformatics 26(1): 139-140.

Roessner U, Luedemann A, Brust D, Fiehn O, Linke T, Willmitzer L, Fernier AR (2001). Metabolic profiling allows comprehensive phenotyping of genetically or environmentally modified plant systems. The Plant Cell 13(1): 11-29.

Roessner U, Willmitzer L, Fernier A (2002). Metabolic profiling and biochemical phenotyping of plant systems. Plant Cell Report 21: 189-196.

Rojas BE, Tonetti T, Figueroa CM (2023). Trehalose 6-phosphate metabolism in C4 species. Current Opinion in Plant Biology 72.

Rosa S and Shaw P (2013). Insights into Chromatin Structure and Dynamics in Plants. Biology 2(4):1378-1410.

Rousseau-Gueutin M, Gaston A, Aïnouche A, Aïnouche ML, Olbricht K, Staudt G, Richard L, Denoyes-Rothan B (2009). Tracking the evolutionary history of polyploidy in Fragaria L. (strawberry): new insights from phylogenetic analyses of low-copy nuclear genes. Molecular Phylogenetics Evolution 51(3):515-30.

RStudio Team (2020). RStudio: Integrated Development for R. RStudio, PBC, Boston, MA URL http://www.rstudio.com/.

Russell JR, Bayer M, Booth C, Cardle, Hackett CA, Hedley PE, Jorgensen L, Morris JA, Brennan RM (2011). Identification, utilization and mapping of novel transcriptome-based markers from blackcurrant (Ribes nigrum). BMC Plant Biology 11:147

Russell JR, Hackett C, Hedley P, Liu H, Milne L, Bayer M, Marshall D, Jorgensen L, Gordon S, Brennan R (2013). The use of genotyping by sequencing in blackcurrant (Ribes nigrum): developing high-resolution linkage maps in species without reference genome sequences. Molecular Breeding 33:835-849.

Sanchez DH, Siahpoosh MR, Roessner U, Udvardi M, Kopka J (2008). Plant metabolomics reveals conserved and divergent metabolic responses to salinity. Physiology of Plants 132(2):209–219.

Sanger F, Nicklen S, Coulsen AR (1977). DNA sequencing with chain-terminating inhibitors. PNAS 74 (12): 5463-5467.

Savini G, Neri D, Zucconi F, Sugiyama N (2005). Strawberry Growth and Flowering, International Journal of Fruit Science 5(1): 29-50.

Savoi S, Wong DCJ, Degu A, Herrera JC, Bucchetti B, Peterlunger E, Fait A, Mattivi F, Castellarin SD (2017). Multi-Omics and Integrated Network Analyses Reveal New Insights into the Systems Relationships between Metabolites, Structural Genes, and Transcriptional Regulators in Developing Grape Berries (Vitis vinifera L.) Exposed to Water Deficit. Frontiers in Plant Science 8.

Sawicki M, Jacquens L, Baillieul F, Clément C, Vaillant-Gaveau N Jacquard C (2015). Distinct regulation in inflorescence carbohydrate metabolism according to grapevine cultivars during floral development. Physiologia Plantarum 154(3): 447-467.

Schena M, Shalon D, Davis RW, Brown PO (1995). Quantitative monitoring of gene expression patterns with a complementary DNA microarray. Science 270:467–470.

Scheunemann M, Brady SM, Nikoloski Z (2018). Integration of large-scale data for extraction of integrated Arabidopsis root cell-type specific models. Scientific Reports 8(1): 7919.

Schwacke R, Ponce-Soto GY, Krause K, Bolger AM, Arsova B, Hallab A, Gruden K, Stitt M, Bolger ME, Usadel B (2019). MapMan4: a refined protein classification and annotation framework applicable to multi-omics data analysis. Molecular Plant 12(6): 879-892.

Scossa F, Alseekh S, Fernie AR (2021). Integrating multi-omics data for crop improvement. Journal of Plant Physiology 257.

Seaver SMD, Lerma-Ortiz C, Conrad N, Mikaili A, Sreedasyam A, Hanson AD, Henry CS (2018). PlantSEED enables automated annotation and reconstruction of plant primary metabolism with improved compartmentalization and comparative consistency. Plant Journal 95(6): 1102-1113.

Shahid S, Sher MA, Ahmad F, Rehman S, Farid B, Raza H, Ali Z, Maqbool A, Alfarraj S, Ansari MJ (2022). Prediction of RNA editing sites and genome-wide characterization of PERK gene family in maize (Zea mays L.) in response to drought stress. Journal of King Saud University - Science. 34(8).

Shannon P, Markiel A, Ozier O, Baliga NS, Wang JT, Ramage D, Amin N, Schwikowski B, Ideker T (2003). Cytoscape: a software environment for integrated models of biomolecular interaction networks. Genome Research 13(11): 2498-2504.

Shim JS, Jeong HI, Bang SW, Jung SE, Kim G, KimYS, RedikIlas MCFR, Oh SJ, Seo JS, Kim JK (2018). DROUGHT-INDUCED BRANCHED-CHAIN AMINO ACID AMINOTRANSFERASE enhances drought tolerancein rice. Plant Physiology 191(2): 1435-1447.

Shulaev V, Cortes D, Miller G, Mittler R (2008). Metabolomics for plant stress response. Physiologia Plantarum 132(2): 199-208.

Shumate A, Wong B, Pertea G, Pertea M (2022). Improved transcriptome assembly using a hybrid of long and short reads with StringTie. PLOS Computational Biology 18(6).

Sierro N, Auberson M, Dulize R, Ivanov NV (2024). Chromosome-level genome assemblies of Nicotiana tabacum, Nicotiana sylvestris, and Nicotiana tomentosiformis. Scientific data 11:35.

Silva AT, Ligterink W, Hilhorst HWM. (2017). Metabolite profiling and associated gene expression reveal two metabolic shifts during the seed-to-seedling transition in Arabidopsis thaliana. Plant Molecular Biology 95 (4): 481–496.

Silva JCF, Teixeira RM, Silva FF, Brommonschenkel SH, Fontes EP (2019). Machine learning approaches and their current application in plant molecular biology: A systematic review. Plant Sciences 284:37–47.

Simão FA, Waterhouse RM, Ioannidis P, Kriventseva EV, Zdonov EM (2015). BUSCO: assessing genome assembly and annotation completeness with single-copy orthologs. Bioinformatics 31(19): 3210-3212.

Simpson D (2018). The economic importance of strawberry crops. The genomes of Rosaceous berries and their wild relatives. Springer, pp 1-7.

Singh KS, Van der Hooft JJJ, Van Wees SCM, Medema MH (2022). Integrative omics approach of biosynthetic pathway discovery in plants. Natural Product Reports. 39.

Smith CA, O'Maille G, Want EJ, Qin C, Trauger SA, Brandon TR, Custodio DE, Abagyan R Siuzdak G (2005). Metlin—a metabolite mass spectral database. Therapeutic Drug Monitoring 27:747–751.

Soltis DE, Smith SA, Cellinese N, Wurdack KJ, Tank DC, Brockington SF, Refulio-Rodriguez NF, Walker JB, Moore MJ, Carslward BS, Bell CD, Latvis M, Crwaley S, Black C et al. (2011). Angiosperm phylogeny: 17 genes, 640 taxa. American Journal of Botany 98(4): 704-730.

Song JM, Xie WZ, Wang S, Guo YX, Koo DH, Kudrna D, Gong C, Huang Y, Feng JW, Zhang W, Zhou Y, Zuccolo A, Long E, Lee S, Talag J, Zhou R, Zhu XT, Yuan D, Udall J, Xie W, Wing RA, Zhang Q, Poland J, Zhang J, Chen LL (2021). Two gap-free reference genomes and global view of the centromere architecture in rice. Molecular Plant 14(10):1757-1767.

Sønsteby A & Heide OM (2008). Temperature responses, flowering and fruit yield of the June-bearing strawberry cultivars Florence, Frida and Korona. Scientia Horticulturae 119(1): 49-54.

Soubeyrand E, Colombié S, Beauvoit B, Dai Z, Cluzet S, Hilbert G, Renaud C, Maneta-Peyret L, Dieuaide-Noubhani M, Mérillon JM, Gibon Y, Delrot S, Gomès E (2018). Constraint-based modeling highlights cell energy, redox status and α-ketoglutarate availability as metabolic drivers for anthocyanin accumulation in grape cells under nitrogen limitation. Frontiers in Plant Science 9: 421.

Stewart PJ & Folta KM (2010). A review of photoperiodic flowering research in strawberry (Fragaria spp.). Critical Reviews in Plant Sciences 29(1): 1-13.

Suguiyama VF, Silva EA, Meirelles ST, Centeno DC, Braga MR (2014). Leaf metabolite profile of the Brazilian resurrection plant Barbacenia purpurea Hook. (Velloziaceae) shows two time-dependent responses during desiccation and recovering. Frontiers in Plant Science 5:96.

Sun C, Gao X, Zhou J, Wu X (2015). Metabolic response of maize (Zea mays L.) plants to combined drought and salt stress. Plant and Soil 388: 99-117.

Sun R, Li S, Chang L, Dong J, Zhong C, Zhang H, Wei L, Gao Y, Wang G, Zhang Y, Sun J (2022). Chromosome-level genome assembly of Fragaria pentaphylla using PacBio and Hi-C technologies. Frontiers and Genetics 13.

Sun S (2019). Accuracy, robustness and scalability of dimensionality reduction methods for single-cell RNA-seq analysis. Genome Biology 20, 269.

Sun X, Zhan Y, Li S, Liu Y, Fu Q, Quan X, Xiong J, Gang H, Zhang L, Qi H, Wang A, Huo J, Qin D, Zhu C (2023). Complete chloroplast genome assembly and phylogenetic analysis of blackcurrant (Ribes nigrum), red and white currant (Ribes rubrum), and gooseberry (Ribes uva-crispa) provide new insights into the phylogeny of Grossulariaceae. PeerJ 11:e16272.

Sung J, Lee S, Lee Y, Ha S, Song B, Kim T, Waters BM, Krishnan HB (2015). Metabolomic profiling from leaves and roots of tomato (Solanum lycopersicum L.) plants grown under nitrogen, phosphorus or potassium-deficient conditions. Plant Science 241: 55-64.

Szabados L and Savouré A (2010). Proline: a multifunctional amino acid. Trends in Plant Science 15(2): 89-97.

Székely G, Abrahám E, Cséplo A, Rigó G, Zsigmond L, Csiszar J, Ayaydin F, Strizhov N, Jásik J, Schmelzer E, Koncz C, Szabados L (2008). Duplicated P5CS genes of Arabidopsis play distinct roles in stress regulation and developmental control of proline biosynthesis. Plant J 53(1):11–28.

Taji T, Ohsumi C, Iuchi S, Seki M, Kasuga M, Kobayashi M, Yamaguchi-Shinozaki K, Shinozaki K (2002). Important roles of drought- and cold-inducible genes for galactinol synthase in stress tolerance in Arabidopsis thaliana. Plant Journal 29: 417–426.

Takasaki H, Maruyama K, Kidokoro S, Ito Y, Fujita Y, Shinozaki K, Yamaguchi-Shinozaki K, Nakashima K (2010). The abiotic stress-responsive NAC-type transcription factor OsNAC5 regulates stress-inducible genes and stress tolerance in rice. Mol Genet Genomics 284:173–183.

Tan KT, Slevin MK, Meyerson M, Li H (2022). Identifying and correcting repeat-calling errors in nanopore sequencing of telomeres. BioRxiv 475254.

Taylor DR, Atkey PT, Wickenden MF, Crips CM (1997). A morphological study of flower initiation and development in strawberry (*Fragaria ananassa*) using cryo-scanning electron microscopy. Annual Applied Biology 130: 141-152.

Tello Ruiz MK, Jaiswal P, Ware D (2022). Gramene: A Resource for Comparative Analysis of Plants Genomes and Pathways. Methods Mol Biol. 2443:101-131.

Tenreira T, Lange MJP, Lange T, Bres C, Labadie M, Monfort A, Hernould M, Rothan C, Denoyes B (2017). A specific gibberellin 20-oxidase dictates the flowering-runnering decision in diploid strawberry. The Plant Cell 29(9): 2168-2182.

The Arabidopsis Information Resource (TAIR), Carnegie Institution, Stanford, CA and National Center for Genome Resources, Santa Fe, NM [http://arabidopsis.org, (12, 2024)].

The UniProt Consortium (2019). UniProt: a worldwide hub of protein knowledge. Nucleic Acids Research 47, D506–D515.

The UniProt Consortium (2025). UniProt: the Universal Protein Knowledgebase in 2025. Nucleic Acids Research 53: D0-D0.

Thole V, Bassard JE, Ramírez-González R, Trick M, Afshar BG, Breitel D, Hill L, Foito A, Shepherd L, Freitag S, Nunes dos Santos C, Menezes R, Bañados Naesby M, Wang L, Sorokin A, Tikhonova O, Shelanga T, Stewart D, Vain P, Martin C (2019). RNA-seq, de novo transcriptome assembly and flavonoid gene analysis in 13 wild and cultivated berry fruit species with high content of phenolics. BMC Genetics 20: 995.

Thomas TD, Ebert D, Muruganujan A, Mushayahama T, Albou LP, Mi H (2021). PANTHER: Making genome-scale phylogenetics accessible to all. Protein Science 31(1).

Toyota M, Spencer D, Sawai-Toyota S, Jiaqi W, Zhang T, Koo AJ, Howe GA, Gilroy S (2018). Glutamate triggers long-distance, calcium-based plant defense signaling. Science 361(6407): 1112-1115.

Tran LS, Nakashima K, Sakuma Y, Simpson SD, Fujita Y, Maruyama K, Fujita M, Seki M, Shinozaki K, Yamaguchi-Shinozaki K (2004). Isolation and functional analysis of Arabidopsis stress-inducible NAC transcription factors that bind to a drought-responsive cis-element in the early response to dehydration stress 1 promoter. Plant Cell 16:2481–2498.

Trych U, Buniowska M, Skapska S, Kapusta I, Marszalek K (2022). Bioaccessibility of Antioxidants in Blackcurrant Juice After Treatment Using Supercritical Carbon Dioxide. Molecules 27(3), 3.

Ulahannan N, Pendleton M, Deshpande A, Schwenk S, Behr JM, Dai X, Tyer C, Rughani P, Adney E, Tian H, Wilkes D, Mosquera JM, Stoddart D, Turner DJ, Juul S, Harrington E, Imielinski M (2019). Nanopore sequencing of DNA concatemers reveals higher-order features of chromatin structure. bioRxiv preprint.

Ullah N, Yüce M, Gökçe ZNÖ, Budak H (2017). Comparative metabolite profiling of drought stress in roots and leaves of seven Triticeae species. BMC Genomics 18: 969.

Valdivia ER, Chevalier D, Sampedro J, Taylor I, Niederhuth CE, Walker JC (2012). DVL genes play a role in the coordination of socket cell recruitment and differentiation. Journal of Experimental Botany 63(3): 1405-1412.

Vallarino JG, de Abreu e Lima F, Soria C, Tong H, Pott DM, Willmitzer L, Fernie AR, Nikoloski Z, Osorio S (2018). Genetic diversity of strawberry germplams using metabolomic biomarkers. Scientific reports 14386.

Valliyodan B, Nguyen HT (2006). Understanding regulatory networks and engineering for enhanced drought tolerance in plants. Plant Biology 9(2):189–195.

Van Dijk EL, Jaszczyszyn Y, Naquin D, Thermes C (2018). The third revolution on sequencing technologies. Trends in Genetics 34 (9): 666-681.

van Rengs WMJ, Schmidt MH-W, Effgen S, Le DB, Wang Y, Zaidan MWAM, Huettel B, Schouten HJ, Usadel B, Underwood CJ (2022). A chromosome scale tomato genome built from complementary PacBio and Nanopore sequences alone reveals extensive linkage drag during breeding. Plant Journal 110:572–588.

van Schie CCN, Haring MA, Schuurink RC (2006). Regulation of terpenoid and benzoid production in flowers. Current Opinion in Plant Biology 9(2): 203-208.

Vaser R, Sović I, Nagarajan N, Šikić M (2017). Fast and accurate de novo genome assembly from long uncorrected reads. Genome Research 27(5):737-746.

Venturini L, Caim S, Kaithakottil G, Mapleson DL, Swarbreck D (2018). Leveraging multiple transcriptome assembly methods for improved gene structure annotation. GigaScience 7(8).

Verheul MJ, Sønsteby A, Grimstad SO (2006). Interactions of photoperiod, temperature, duration of short-day treatment and plant age on day treatment and plant age on flowering of Fragaria x ananassa Duch. cv. Korona. Scientia Horticulturae 107(2): 164-170.

Verheul MJ, Sønsteby A, Grimstad SO (2007). Influences of day and night temperatures on flowering of Fragaria x ananassa Duch., cvs. Korona and Elsanta, at different photoperiods. Scientia Horticulturae 112(2): 200-206.

Vince-Prue D, Guttridge CG (1973). Floral initiation in strawberry: Spectral evidence for the regulation of flowering by long-day inhibition. Planta 110: 165-172.

Waese J and Provart NJ (2016). The Bio-analytic resource: Data visualization and analytic tools for multiple levels of plant biology. Current Plant Biology 7-8: 2-5.

Wahl V, Punnu J, Schlereth A, Arrivault S, Langenecker T, Franke A, Feil R, Lunn JE, Stitt M, Schmid M (2013). Regulation of Flowering by Trehalose-6-Phosphate Signaling in Arabidopsis thaliana. Science 339(6120): 704-707.

Walker BJ, Abeel T, Shea T, Priest M, Abouelliel A, Sakthikumar A, Cuomo CA, Zeng Q, Wortman J, Young SK, Earl AM (2014) Pilon: An Integrated Tool for Comprehensive Microbial Variant Detection and Genome Assembly Improvement. PLoS ONE 9(11): e112963.

Wan T, Feng Y, Liang C, Pan L, He L, Cai Y (2021). Metabolomics and transcriptomics analysis of two contrasting cherry rootstocks in response to drought stress. Biology (Basel) 10(3): 201.

Wang B, Yang X, Jia Y, Dang N, Wang S, Wang S, Xu T, Zhao X, Gao S, Dong Q, Ye K (2021). High-quality Arabidopsis thaliana genome assembly with nanopore and hifi long reads. Genomics, Proteomics and Bioinformatics 20(1): 4-13.

Wang C, Yang A, Yin H, Zhang J (2008). Influence of water stress on endogenous hormone contents and cell damage of maize seedlings. Journal of International Plant Biology 50:427-434.

Wang J, Hu M, Wang J, Qi J, Han Z, Wang G, Qi Y, Wang HW, Zhou JM, Chai J (2019a). Reconstitution and structure of a plant NLR resistosome conferring immunity. Science 364:eaav5870.

Wang J, Wang J, Hu M, Wu S, Qi J, Wang G, Han Z, Qi Y, Gao N, Wang HW, Zhou JM, Chai J (2019b). Ligand-triggered allosteric ADP release primes a plant NLR complex. Science 364:eaav5868.

Wang JP, Matthews ML, Williams CM, Shi R, Yang C, Tunlaya-Anukit S, Chen HS, Li Q, L CY, Naik P, Sun YH, Loziuk PL, Yeh TF, Kim H, Gjersing E, Shollenberger T et al. (2018). Improving wood properties for wood utilization through multi-omics integration in lignin biosynthesis. Nature Communication 9(1): 1579.

Wang K, Ding Y, Cai C, Chen Z, Zhu C (2018). The role of C2H2 zinc finger proteins in plant response to abiotic stresses. Physiologia Plantarum 165(4): 690-700.

Wang L, Nägele T, Doerfler H, Fragner L, Chaturvedi P, Nukarinen E, Bellaire A, HUber W, WEiszmann J, Engelmeier D, Ramsak Z, Gruden K, WEckwerth W (2016). System level analysis of cacao seed ripening reveals a sequential interplay of primary and secondary metabolism leading to polyphenol accumulation and preparation of stress resistance. Plant Journal 87 (3): 318–332.

Wang W, Sijacic P, Xu P, Lian H, Liu Z (2018). Arabidopsis TSO1 and MYB3R1 from regulatory module to coordinate cell proliferation with differentiation in shoot and root. PNAS 115(13): E3045-E3054.

Weberling F (1989). Morphology of flowers and inflorescences. 1st Edition Cambridge, UK Cambridge University Press.

Wei K, Wang Y, Zhong X, Pan S (2014). Protein kinase structure, expression and regulation in maize drought signaling. Molecular Breeding 34: 583-602.

Wei N, Cronn R, Liston A, Ashman TL (2019). Functional trait divergence and trait plasticity confer polyploid advantage in heterogeneous environments. New Phytologist 221(4):2286-2297

Weighill D, Tschaplinski TJ, Tuskan GA, Jacobson D (2019). Data integration in poplar: 'Omics layers and integration strategies.frontiers in Genetics 10.

Weil HL, Schneider K, Tschöpe M, Bauer J, Maus O, Frey K, Brilhaus D, Martins Rodrigues C, Doniparthi G, Wetzels F, Lukasczyk J, Kranz A, Grüning B, Zimmer D, Deßloch S, von Suchodoletz D, Usadel B, Garth C, Mühlhaus T (2023). PLANTdataHUB: a collaborative platform for continuous FAIR data sharing in plant research. Plant J. 116:974-988. doi: 10.1111/tpj.16474.

Weis JH, Tan SS, Martin BK, Wittwer CT (1992). Detection of rare mRNAs via quantitative RT-PCR. Trends in Genetics 8:263–264

Wellmer F, Riechmann JL (2010). Gene networks controlling the initiation of flower development. Review Trends in Genetics 26(12): 519-527.

Wen J, Lease KA, Walker JC (2004). DVL, a novel class of small polypeptides: overexpression alters Arabidopsis development. The Plant Journal. 37(5): 668-677.

Whitelaw CA, Barbazuk WB, Pertea G et al. (2003) Enrichment of gene-coding sequences in maize by genome filtration. Science 302, 2118– 2120.

Wick RR, Judd LM, Gorrie CI, Holt KE (2017). Completing bacterial genome assemblies with multiplex MinION sequencing. Microbial Genomics 3(10):e000132.

Wick RR, Judd LM, Holt KE (2019). Performance of neural network basecalling tools for Oxford Nanopore sequencing. Genome Biology 20 (129).

Wickham H (2022). _stringr: Simple, Consistent Wrappers for Common String Operations_. R package version 1.5.0, <https://CRAN.R-project.org/package=stringr>.

Wickham H, François R, Henry L, Müller K, Vaughan D (2023). _dplyr: A Grammar of Data Manipulation_. R package version 1.1.2, <https://CRAN.R-project.org/package=dplyr>.

Wickland DP, Hanzawa Y (2015). The FLOWERING LOCUS TERMINAL FLOWER 1 Gene Family: Functional evolution and molecular mechanisms. Molecular Plant 8; 983-997.

Wickland DP, Hanzawa Y (2015). The FLOWERING LOCUS TERMINAL FLOWER 1 Gene Family: Functional evolution and molecular mechanisms. Molecular Plant 8; 983-997.

Wolff J, Rabbani L, Gilsbach R, Richard G, Manke T, Backofen R, Grüning BA (2020). Galaxy HiCExplorer 3: a web server for reproducible Hi-C, capture Hi-C and single-cell Hi-C data analysis, quality control and visualization. Nucleic Acids Research 48(W1): W177-W184.

Woodger FJ, Millar A, Murray F, Jacobson JV, Gubler F (2003). The role of GAMYB transcription factors in GA-regulated gene expression. Journal of Plant Growth Regulation. 22: 176-184.

Wurtele ES, Li J, Diao L, Zhang H, Foster CM, Fatland B, Dickerson J, Brown A, Cox Z, Cook D, Lee EK, Hofmann H (2003). MetNet: Software to build and model the biogenetic lattice of Arabidopsis. Comparative and Functional Genomics 4(2): 239-245.

Wyatt R (1982). Inflorescence architecture: how flower number, arrangement, and phenology affect pollination and fruit-set. American Journal of Botany 69: 585-594.

Xia EH, Wu Q, Wei S, Zhao J, Zhang ZZ, Wei CL, Wan XC (2020). Tea plant genomics: achievements, challenges and perspectives. Horticulture Research 7.

Xia Y, Xue B, Shi M, Zhan F, Wu D, Jing D, Wang S, Guo Q, Liang G, He Q (2020). Comparative transcriptome analysis of flower bud transition and functional characterization of EjAGL17 involved in regulating floral initiation in loquat. PLoS One 15(10): e0239382.

Yang L, Yang Y, Huang L, Cui X, Liu Y (2023). From single-to multi-omics: future research trends in medicinal plants. Brief Bioinformatics 24(1): bbac485.

Yang R, Guo Q, Gu Z (2013). GABA shunt and polyamine degradation pathway on γ-aminobutyric acid accumulation in germinating fava bean (Vicia faba L.) under hypoxia. Food Chemistry 2013, 136, 152–159.

Yang T, Wang L, Li C, Liu Y, Zhu S, Qi Y, Liu X, Lin Q, Luan S, Yu F (2015). Receptor protein kinase FERONIA controls leaf starch accumulation by interacting with glyceraldehyde-3-phosphate dehydrogenase. Biochemical and Biophysical Research Communications 465(1): 77-82.

Yang X, Lu M, Wang Y, Wang Y, Liu Z, Chen S (2021). Response mechanism of plants to drought stress. Horticulturae 7: 50.

Yang Y, Saand MA, Huang L, Abdelaal WB, Zhang J,Wu Y, Li J, Siroh MG, Wang F (2021). Applications of Multi-Omics Technologies for Crop Improvement. Frontiers in Plant Science. 12

Yapo BM (2011). Rhamnogalacturonan-I: A structurally puzzling and functionally versatile polysaccharide from plant cell walls and mucilages. Polymer Reviews 51(4): 391-413.

Yardımcı GG, Ozadam H, Sauria MEG, Yan KK; Yang T, Chakraborty A, Kaul A, Lajoie BR, Zhan Y, Ay F, Gerstein M, Kundaje A, Li Q, Taylor J, Yue F, Dekker J, Noble WS (2019). Measuring the reproducibility and quality of Hi-C data. Genome Biology 20:57.

Ye X, Wang H, Chen P, Fu B, Zhang M, Li J, Zheng X, Feng J (2017). Combination of iTRAQ proteomics and RNA-seq transcriptomics reveals multiple levels of regulation in phytoplasma-infected Ziziphus jujuba mill. Horticulture Research 4:17080.

You J, Zhang Y, Liu A, Li D, Wang X, Dossa K, Zhou R, Yu J, Zhang Y, Wang L, Zhang X (2019). Transcriptomic and metabolomic profiling of drought-tolerant and susceptible sesame genotypes in response to drought stress. BMC Plant Biology 19.

Yu H, Ito Y, Zhao Y, Peng J, Kumar P, Meyerowitz E (2004). Floral homeotic genes are targets of gibberellin signaling in flower development. Biological Sciences 101(20): 7827-7832.

Yu J, Hu SN, Wang J, Wong GKS, Li SG, Liu B, Deng Y, Dai L, Zhou Y, Zhang X, Cao M, Liu J, Sun J, Tang J, Chen Y, Huang X, Lin W, Ye C, Tong W, Cong L, Geng J, Han Y, Li L, Li W (2002). A draft sequence of the rice genome (Oryza sativa L. ssp indica). Science 296:. 79-92.

Yu J, hulse-Kemp AM, Babiker E, Staton M (2021). High-quality reference genome and annotation aids understanding of berry development for evergreen blueberry (Vaccinium darrowii). Horticulturae Research 8(228).

Yuan J, Jiang S, Liu M, Yue Z, Xu J, Li J, Xu C, Lin L, Jing Y, Zhang X, Chen H, Zhang L, Fu T, Yu S, Wu Z, Zhang Y, Wang C, Zhang X, Huang L, Wang H, Hong D, Chen XY, Hu Y (2022). Genomic basis of the giga-chromosomes and giga-genome of tree peony Paeonia ostii. Nature Communications 13: 7328.

Zhang D, Ren L, Yue JH, Wang I, Zhuo LH, Shen XH (2013). A comprehensive analysis of flowering transition in Agapanthus praecox ssp. orientalis (Leighton) Leighton by using transcriptomic and proteomic techniques. Journal of Proteomics 80: 1-125.

Zhang JS, Zhang XT, Tang HB, Zhang Q, Hua XT, Ma XK, Zhu F, Jones T, Zhu X, Bowers J, Wai CM, Zheng C, Shi Y, Chen S, Xu X, Yue J,Nelson DR, Huang L, Li Z (2018). Allele-defined genome of the autopolyploid sugarcane Saccharum spontaneum L. Nature Genetics 50: 1565-1573.

Zhang T, Zhou J, Gao W, Jia Y, Wei Y, Wang G (2022). Complex genome assembly based on long-read sequencing. Briefings in Bioninformatics 23(5): bbac305.

Zhang Y, Dong Q, Wang Z, Liu Q, Yu H, Sun W, Cheema J, You Q, Ding L, Cao X, He C, Ding Y, Zhang H (2024). A fine-scale Arabidopsis chromatin landscape reveals chromatin conformation-associated transcriptional dynamics. Nature Communications 15(3253).

Zhang Y, Seeram NP, Lee R, Feng L, Heber D (2008). Isolation and identification of strawberry phenolics with antioxidant and human cancer cell antiproliferative properties. Journal of Agricultural Food Chemistry 56(3): 670-675.

Zhang Y, Shewry PR, Jones H, Barcelo P, Lazzeri PA, Halford NG (2001). Expression of antisense SnRK1 protein kinase sequence causes abnormal pollen development and male sterility in transgenic barley. Plant Journal 28(4): 431-441.

Zhao S, Fernald RD (2005). Comprehensive algorithm for quantitative real-time polymerase chain reaction. Journal of Computational Biology 12(8): 1047-1064.

Zhao SW, Gup JF, Kong L, Nie S,Yan XM, Shi TL, Tian XC, Ma HY, Bao YB, Li ZC, CHen ZY, Zhang RG, Ma YP, EL-Kassaby YA, Porth I, Zhao W, Mao JF (2023). Haplotype-resolved genome assembly of Coriaria nepalensis a non-legume nitrogen-fixing shrub. Scientific data 10: 259.

Zheng S, Lyu Z, Narisetti SR, Xu D, Joshi T (2018). Knowledge base commons (KBCommons) v1.0: A multi OMICS' web based data integration framework for biological discoveries. 2018 IEEE International Conference on Bioinformatics and Biomedicine (BIBM) 589-594.

Zhou C, McCarthy SA, Durbin R (2022). YaHS: yet another Hi-C scaffolding tool. BMC Bioinformatics 39(1): btac808.

Zhou G, Ewald J, Xia J (2021). OmicsAnalyst: a comprehensive web-based platform for visual analytics of multi-omics data. Nature Communications 12:2279.

Zhu L, Zhou Y, Li X, Zhao J, Guo N, Xing H (2018). Metabolomics analysis of soybean hypocotyls in response to Phytophthora sojae infection. Frontiers in Plant Science 9: 1530.

Zhu S, Chen J, Zhao J, Comes HP, Li P, Fu C, Xie X, Lu R, Xu W, Feng Y, Ye W, Sakaguchi S, Isagi Y, Li L, Lascoux M, Qiu Y (2020). Genomic insights on the contribution of balancing selection and local adaptation to the long-term survival of a widespread living fossil tree, Cercidiphyllum japonicum. New Phytologist 228(5): 1674-1689.

Ziegler MR, Gaston A, Guy K, Devers M, Krüger E, Brauksiepe B, Eimert K, Osorio S, Denoyes B, Usadel B (2025). Molecular mechanisms underlying the early steps of floral initiation in seasonal flowering genotypes of cultivated strawberry. bioRxiv 633581.

Ziegler FMR, Rosenthal V, Vallarino JG, Genzel F, Spettmann S, Seliga L, Keller S, Munnes L, Sønsteby A, Osorio S, Usadel B (2024). A full genome assembly reveals drought stress effects on gene expression and metabolite profiles in blackcurrant (*Ribes nigrum* L.). Horticulture Research 12(2).

Zielinski QB (1953). Chromosome numbers and meiotic studies. Botanical Gazette 114(3): 265-274

Zu Y, Klasfeld S, Jeong CW, Jin R, Goto K, Yamaguchi N, Wagner D (2020). Terminal flower 1-FD complex target genes and competition with FLOWERING LOCUS T. Nature communications 11: 5118.

10 Supplemental Material

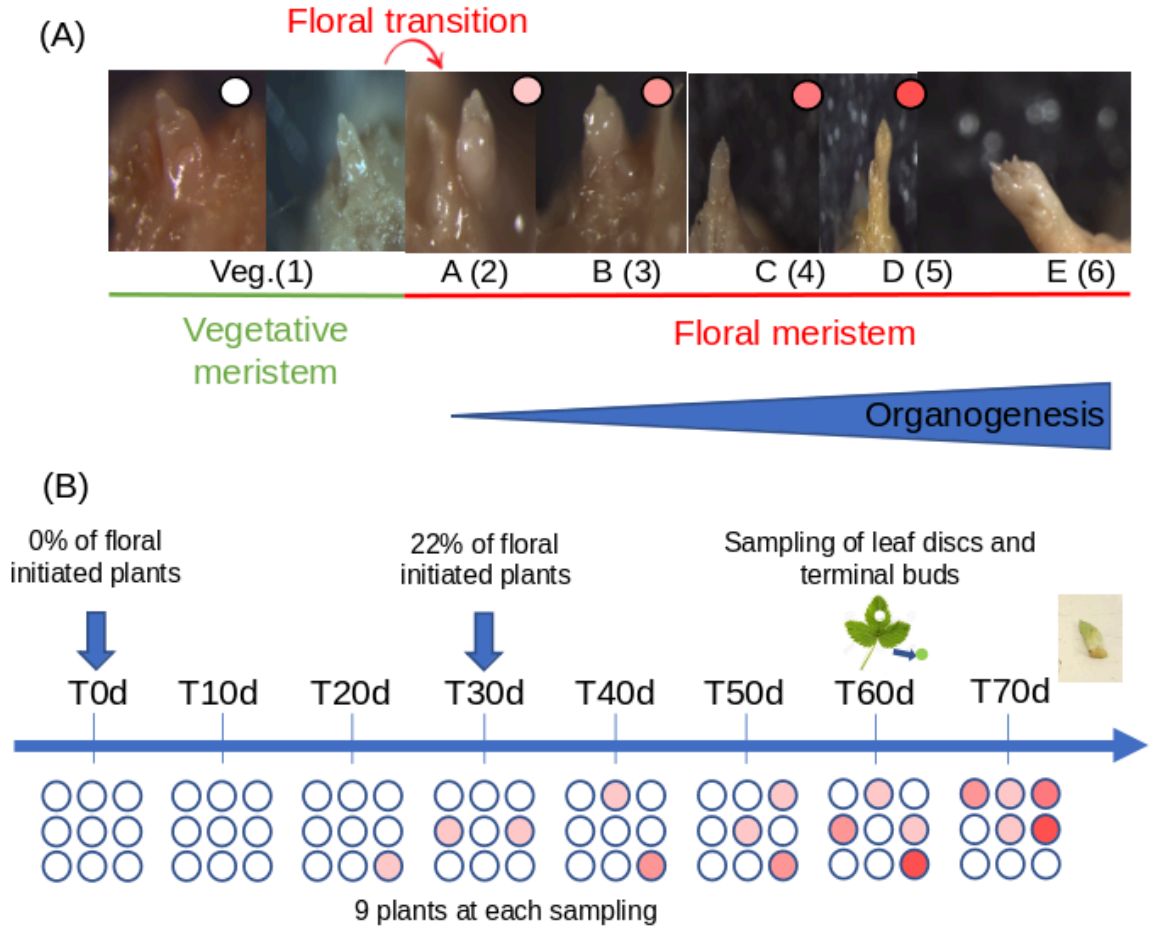

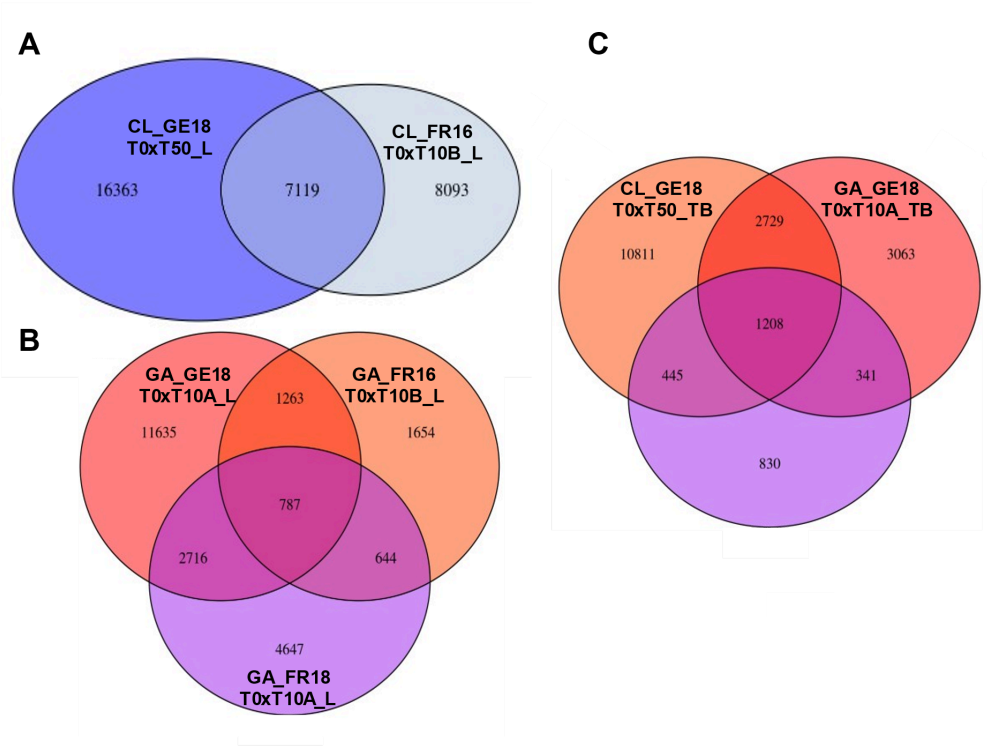
A
CL_GE18
T0xT50_L
16363
7119
CL_FR16
T0xT10B_L
8093
B
GA_GE18
T0xT10A_L
11635
1263
GA_FR16
T0xT10B_L
1654
787
2716
644
4647
GA_FR18
T0xT10A_L
C
CL_GE18
T0xT50_TB
10811
2729
GA_GE18
T0xT10A_TB
3063
1208
445
341
830

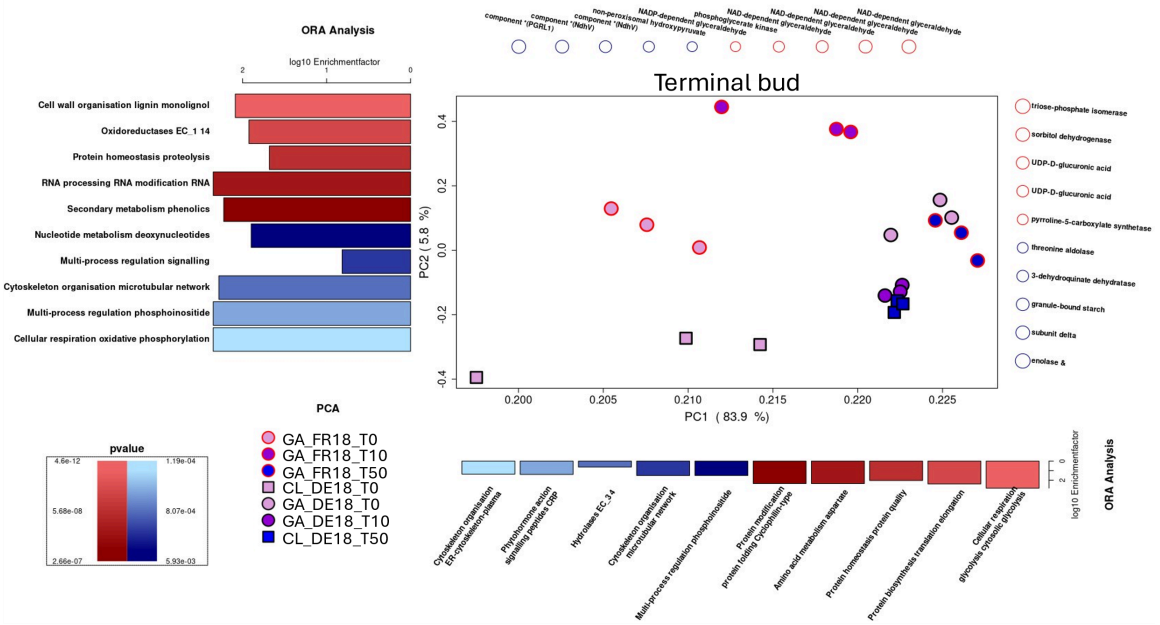
ORA Analysis
log10 Enrichmentfactor
Cell wall organisation lignin monolignol
Oxidoreductases EC_1 14
Protein homeostasis proteolysis
RNA processing RNA modification RNA
Secondary metabolism phenolics
Nucleotide metabolism deoxynucleotides
Multi-process regulation signalling
Cytoskeleton organisation microtubular network
Multi-process regulation phosphoinositide
Cellular respiration oxidative phosphorylation
component 1 (PGRL1)
component 1 (NdhV)
component 1 (NdhV)
non-peroxisomal hydroxypyruvate
NADP-dependent glyceraldehyde
phosphoglycerate kinase
NAD-dependent glyceraldehyde
NAD-dependent glyceraldehyde
NAD-dependent glyceraldehyde
NAD-dependent glyceraldehyde
Terminal bud
PC2 (5.8 %)
PC1 (83.9 %)
triose-phosphate isomerase
sorbitol dehydrogenase
UDP-D-glucuronic acid
UDP-D-glucuronic acid
pyrroline-5-carboxylate synthetase
threonine aldolase
3-dehydroquinate dehydratase
granule-bound starch
subunit delta
enolase &
PCA
GA_FR18_T0
GA_FR18_T10
GA_FR18_T50
CL_DE18_T0
GA_DE18_T0
GA_DE18_T10
CL_DE18_T50
pvalue
4.6e-12
1.19e-04
5.68e-08
8.07e-04
2.66e-07
5.93e-03
Cytoskeleton organisation ER-cytoskeleton-plasma
Phytohormone action signalling peptides CRP
Hydrolase EC_3 4
Cytoskeleton organisation microtubular network
Multi-process regulation phosphoinositide
Protein modification protein folding Cyclophilin type
Amino acid metabolism aspartate
Protein homeostasis protein quality
Protein biosynthesis translation elongation
Cellular respiration glycolysis cytosolic glycolysis
log10 Enrichmentfactor
ORA Analysis

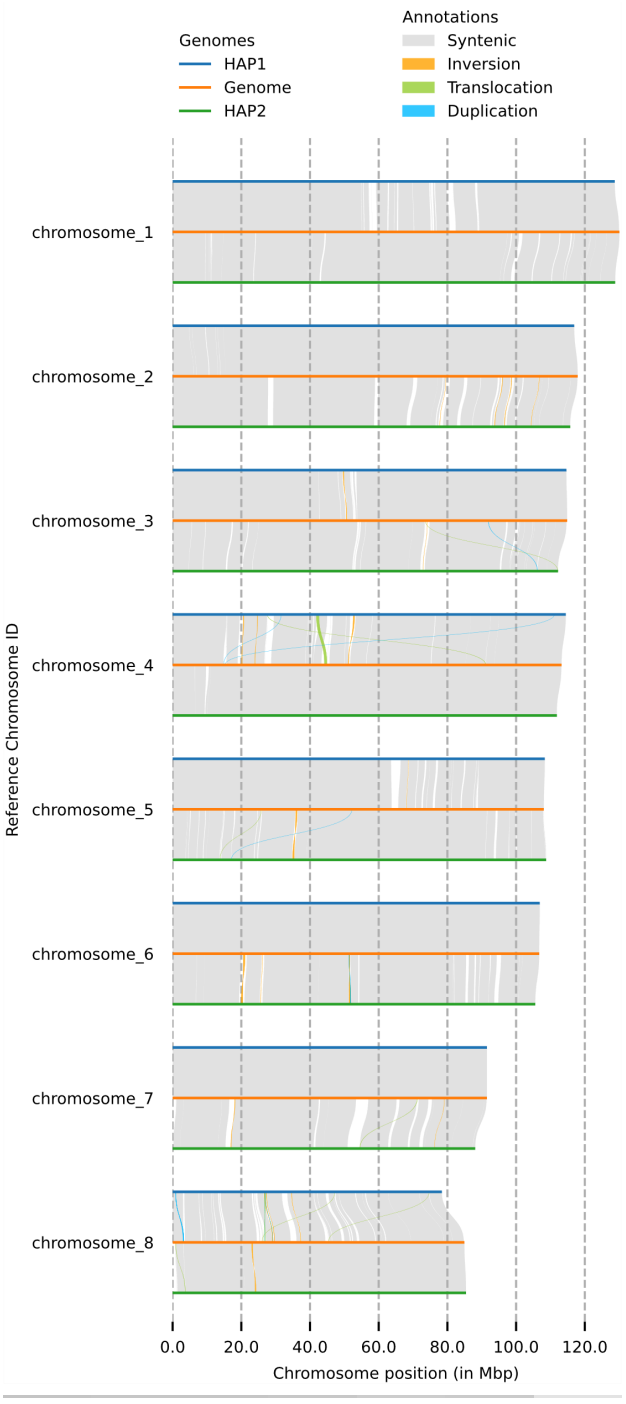
Annotations
Syntenic
Inversion
Translocation
Duplication
Genomes
HAP1
Genome
HAP2
chromosome_1
chromosome_2
chromosome_3
chromosome_4
chromosome_5
chromosome_6
chromosome_7
chromosome_8
Reference Chromosome ID
0.0
20.0
40.0
60.0
80.0
100.0
120.0
Chromosome position (in Mbp)

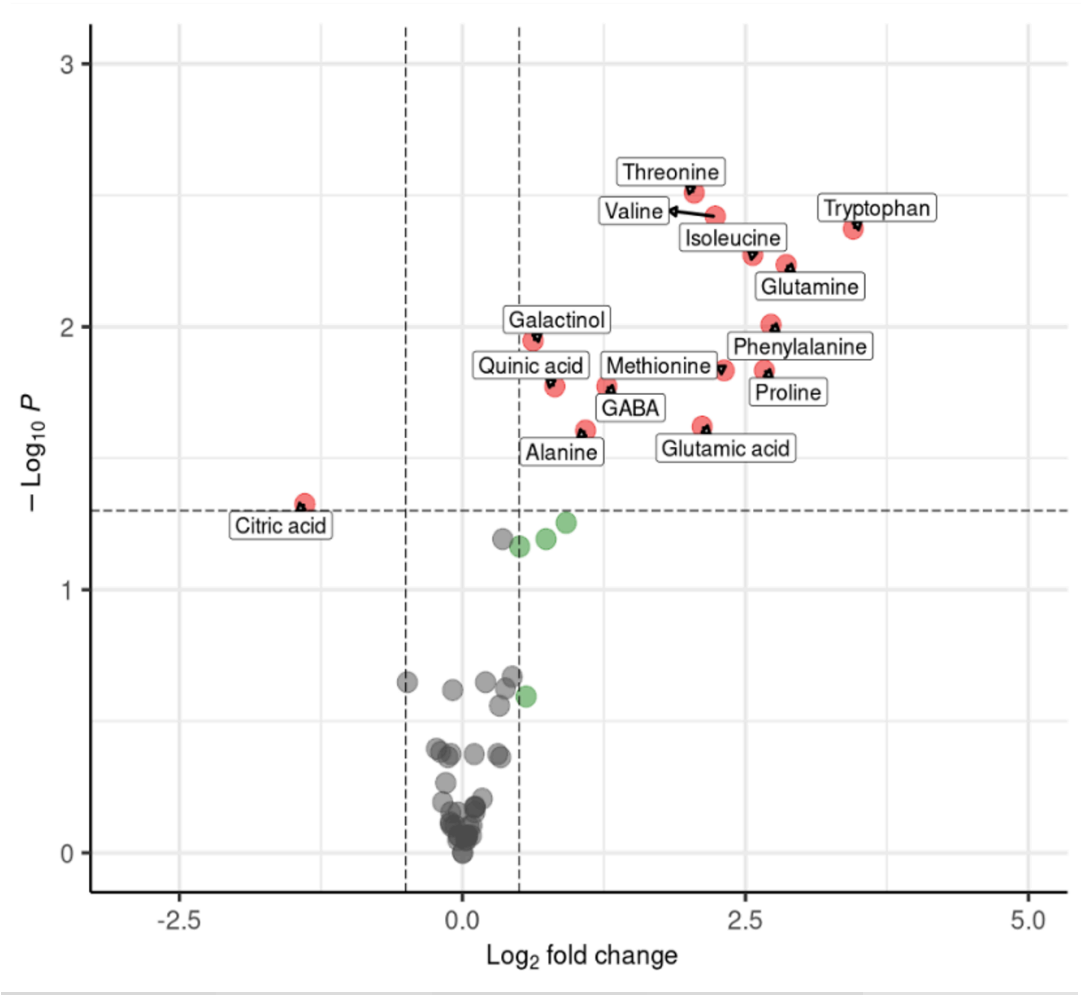
Threonine
Valine
Tryptophan
Isoleucine
Glutamine
Galactinol
Phenylalanine
Quinic acid
Methionine
Proline
GABA
Alanine
Glutamic acid
Citric acid
3
2
1
0
-2.5
0.0
2.5
5.0
− Log10 P
Log2 fold change

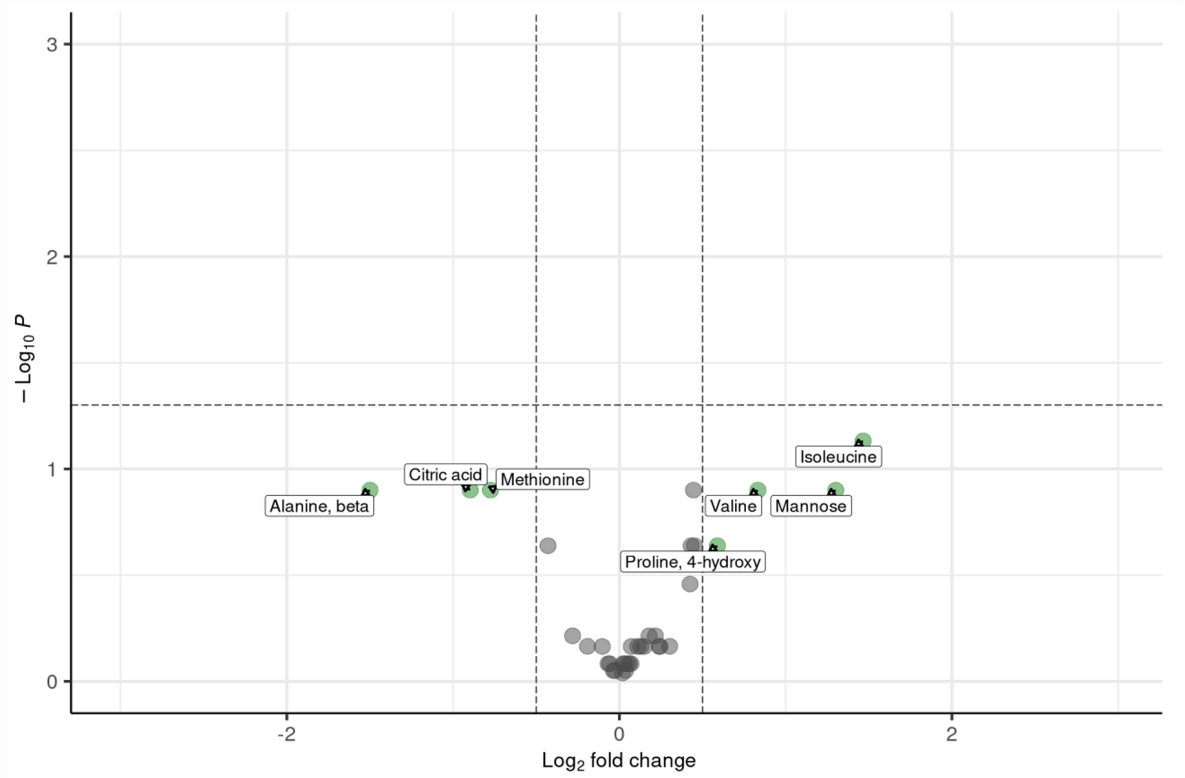
3
2
1
0
$-\text{Log}_{10}\ P$
-2
0
2
Log_2 fold change
Isoleucine
Citric acid
Methionine
Alanine, beta
Valine
Mannose
Proline, 4-hydroxy

Supplemental Table S1: Pore-C metrics for seven single samples of *S. tuberosum* leaf tissue after alignment and deduplication. Cis and trans contacts denote the chromatin interactions occurring within the same chromosome (cis) compared to those occurring between different chromosomes (trans).

Pore-C metrics	Sample 1	Sample 2	Sample 3	Sample 4	Sample 5	Sample 6	Sample 7
Measuring date	2023/03/30	2023/04/07	2023/04/08	2023/08/18	2023/08/18	2023/08/23	2023/08/23
Total reads	2,566,838	33,472,890	37,401,385	4,433,937	16,023,499	21,417,910	23,055,400
Total unmapped reads	1,246,661	15,384,605	17,119,292	1,998,609	7,316,022	9,983,880	10,749,738
Total mapped reads	580,409	8,028,726	9,040,662	505,062	1,879,015	2,202,542	2,352,632
Duplicated reads	52,663	1,884,382	2,127,156	1,179	7,537	13,038	14,006
Cis contacts	468,214	5,190,803	5,787,446	238,478	799,514	1,031,774	1,079,748
Trans contacts	59,532	953,541	1,126,060	265,405	1,071,964	1,157,730	1,258,878
cis:trans ratio	7.86	5.44	5.14	0.89	0.75	0.89	0.85

Supplemental Table S2: Genome assembly statistics for the scaffolded blackcurrant genome and its haplotypes 1 and 2.

Genome features	*R. nigrum* genome assembly	Haplotype 1	Haplotype 2
Total length [bp]	871,555,738	901,851,302	885,535,873
Number of scaffolds	29	441	216
GC content [%]	36.97	37.18	37.11
N50 [bp]	113,235,913	61,129,474	51,685,379
N75 [bp]	106,733,054	54,530,870	37,891,422
N90 [bp]	84,956,319	18,472,649	20,831,317

Supplemental Table S3: Number of telomeric repeat sequences (AAACCTT) at the chromosome start and end within a 20-kbp window for the blackcurrant genome at the pseudo-chromosomal level. Fewer than 10 telomeric sequences were assigned to the designation 'NA'.

Chromosome	Chromosome Start [No. telomeric sequences]	Chromosome End [No. telomeric sequences]
Chr 1	*NA*	*NA*
Chr 2	1600	*NA*
Chr 3	*NA*	1329
Chr 4	1508	*NA*
Chr 5	*NA*	714
Chr 6	*NA*	1553
Chr 7	*NA*	581
Chr 8	1114	1624

Supplemental Table S4: Comparative analysis of 73 markers from the *R. nigrum* SCRI 9328 and MP7 genetic linkage map (Russell *et al.,* 2011) and the physical map of the *R. nigrum* reference genome, positioned on eight pseudo-chromosomes (Chr 1–8).

Marker Linkage Map	Linkage Map Chromosome	SCRI 9328 [cM]	MP7 [cM]	Genome Chromosome	Start [bp]	End [bp]
CL609Contig2-2658	LG1	7.3	0	Chr 4	638708	638828
CL2096Contig1-429	LG1	14.3	2.4	Chr 4	1114243	1114123
CL1830Contig1-456	LG1	21.4	16.6	Chr 4	2139595	2139699
CL1323Contig1-649	LG1	26.7	22.3	Chr 4	2577468	2577588
CL222Contig2-432	LG1	29.9	28.1	Chr 4	2931420	2931540
CL1Contig17-1834	LG1	44	38.4	Chr 4	82725526	82725406
CL105Contig1-1202	LG1	45.5	39.1	Chr 4	21083182	21083302
CL1199Contig1-699	LG1	51	45.9	Chr 4	97016057	97015958
CL1092Contig1-971	LG1	76	55.7	Chr 4	108542558	108542676
CL177Contig2-445	LG1	76.8	59.1	Chr 4	109094719	109094839
CL1060Contig1-488	LG1	81.3	65.9	Chr 4	110308523	110308643
CL139Contig3-846	LG1	93.3	79.2	Chr 4	111647131	111647011
CL2142Contig1-425	LG5	9.2	0	Chr 2	109059399	109059519
CL1Contig385-914	LG5	25.4	19.3	Chr 2	94163591	94163711
CL1Contig968-64	LG5	26.5	21.6	Chr 2	80198611	80198492
CL351Contig1-633	LG5	30	21.6	Chr 2	31466291	31466171
CL17Contig1-545	LG5	47.3	38	Chr 2	7569443	7569323
CL754Contig1-758	LG5	58.3	33.7	Chr 2	8821332	8821212
CL1Contig38-1121	LG2	0	1.4	Chr 5	191071	191191
CL895Contig1-1185	LG2	3.1	0	Chr 5	308098	307978
CL163Contig3-1046	LG2	7.7	12.7	Chr 5	1899532	1899652
CL1Contig694-1457	LG2	29.8	26.2	Chr 5	4515495	4515615
CL151Contig8-1373	LG2	33.9	24.3	Chr 5	4567401	4567521
CL1191Contig1-435	LG2	41.1	31.8	Chr 5	6298630	6298750
CL7Contig12-122	LG2	49.5	42.8	Chr 5	14864056	14863936
CL122Contig7-1607	LG2	49.8	42.9	Chr 5	18910750	18910650
CL1Contig264-1457	LG2	49.9	42.3	Chr 5	73078768	73078648
CL1Contig460-66	LG2	49.9	42.8	Chr 5	28177879	28177997
CL1Contig971-186	LG2	52.8	46.3	Chr 5	93946827	93946707
CL1Contig53-1007	LG2	53.1	43.6	Chr 5	98974380	98974500
CL13Contig2-733	LG2	53.1	43.6	Chr 5	99321955	99322075
CL1111Contig1-166	LG2	54.6	44.7	Chr 5	105885506	105885624
CL59Contig6-588	LG2	56.1	45.8	Chr 5	107134002	107133882
CL1Contig889-534	LG3	23.4	5.4	Chr 1	126325232	126325112
CL176Contig1-230	LG3	39.5	23.5	Chr 1	121027220	121027340
CL951Contig1-190	LG3	44.1	29	Chr 1	118888486	118888606
CL61Contig1-2372	LG3	46.6	34.4	Chr 1	113252662	113252542

CL2001Contig1-304	LG3	48.1	30.1	Chr 1	114489899	114489779
CL1057Contig1-870	LG3	49.3	33.2	Chr 1	114408733	114408630
CL836Contig1-1017	LG3	50	36.6	Chr 1	22581652	22581772
CL1Contig931-1929	LG3	50.9	37.6	Chr 1	46624585	46624465
CL1488Contig1-196	LG3	62.3	49.2	Chr 1	4787255	4787341
CL1Contig973-658	LG3	102.7	69.5	Chr 1	280879	280994
CL1Contig291-268	LG3	104.9	71.9	Chr 1	79062	79182
CL1Contig693-482	LG4	41	17.3	Chr 6	2688407	2688285
CL1Contig648-852	LG4	42.9	0	Chr 6	3411774	3411656
CL119Contig1-1274	LG4	50.9	5.1	Chr 6	5763824	5763704
CL1Contig1024-757	LG4	53.9	5.1	Chr 6	9398156	9398276
CL1Contig861-213	LG4	54	6.6	Chr 6	10620135	10620015
CL1071Contig1-950	LG4	54.2	5.1	Chr 6	52912735	52912855
CL134Contig1-762	LG4	56	5.1	Chr 6	97011570	97011450
CL1192Contig1-848	LG4	70.6	23.6	Chr 6	102808854	102808734
CL1Contig255-477	LG4	72.3	27.6	Chr 6	102784967	102784847
CL1Contig138-1240	LG4	85.1	38.8	Chr 6	104382117	104382237
CL1Contig337-459	LG4	88.1	37.1	Chr 6	104596052	104596172
CL225Contig2-220	LG4	102.9	52.9	Chr 6	106168032	106168152
CL2Contig70-1576	LG6	3.3	0	Chr 8	61240259	61240139
CL285Contig1-1074	LG6	6.7	1.7	Chr 8	4897359	4897270
CL198Contig1-761	LG6	14.1	8.8	Chr 8	75728979	75729099
CL258Contig2-288	LG7	0	0.6	Chr 7	91022131	91022038
CL1218Contig1-144	LG7	10.1	9.1	Chr 7	90610612	90610732
CL88Contig2-932	LG7	12.1	11.2	Chr 7	90433737	90433617
CL18Contig2-1072	LG7	16.1	12.6	Chr 7	90119706	90119586
CL600Contig1-730	LG7	23.5	14.8	Chr 7	89541594	89541474
CL113Contig1-641	LG7	41	23.9	Chr 7	88129148	88129028
CL1Contig245-186	LG8	0	0	Chr 3	110019132	110019252
CL1Contig96-259	LG8	4.2	5.4	Chr 3	108916220	108916340
CL148Contig3-1357	LG8	9.8	14.4	Chr 3	69132505	69132586
CL1Contig735-1426	LG8	9.8	14.5	Chr 3	79303246	79303126
CL1Contig494-651	LG8	10.4	11.1	Chr 3	103630457	103630577
CL9Contig1-194	LG8	10.8	10.6	Chr 3	104861613	104861493
CL152Contig5-1081	LG8	12.4	15.8	Chr 3	13574896	13574777
CL1Contig969-1027	LG8	20.9	20.3	Chr 3	7247140	7247020

Supplemental Table S5: Number of genes and additional information for the *R. nigrum* genome assembly.

Stat	Total	Average	Mode	Min	1%	5%	10%	Median	75%	95%	99%	Max
Number of genes	46.544	NA	NA	NA	NA	NA	NA	NA	NA	NA	NA	NA
Number of genes (coding)	44.071	NA	NA	NA	NA	NA	NA	NA	NA	NA	NA	NA
Number of monoexonic genes	7.215	NA	NA	NA	NA	NA	NA	NA	NA	NA	NA	NA
Transcripts per gene	50.767	01.09	1.0	1	1	1	1	1	1	2	3	6
Coding transcripts per gene	47.83	01.03	1.0	0	0	0	1	1	1	2	2	6
CDNA lengths	77,725,931	1,531.03	439.0	200	242	344	448	1.265	2.015	3.606	5.309	19.49
CDNA lengths (mRNAs)	75,347,928	1,575.33	439.0	200	240	345	461	1.324	2.071	3.656	5.399	19.49
CDS lengths	53,304,437	1,049.98	0.0	0	0	0	216	801	1.434	2.847	4.227	16.27
CDS lengths (mRNAs)	NA	1,114.46	459.0	67	147	219	276	864	1.479	2.88	4.287	16.27
CDS/cDNA ratio	NA	69.63	100.0	7	22	34	42	71	84	98	100	100
Monoexonic transcripts	7.241	1,277.26	324.0	233	268	346	421	974	1.678	3.15	4.696	11.06
MonoCDS transcripts	10.916	901.74	276.0	67	126	198	243	621	1.218	2.562	3.456	6.879
Exons per transcript	272720	5.37	2.0	1	1	1	1	4	7	15	24	86
Exons per transcript (mRNAs)	3543	5.54	2.0	1	1	1	1	4	7	15	24	86
Exon lengths	NA	285.00	1.0	1	1	2	28	141	328	1.013	2.136	11.06
Exon lengths (mRNAs)	NA	284.31	1.0	1	1	2	25	138	326	1.018	2.146	11.06
Intron lengths	NA	539.57	85.0	20	55	77	84	205	561	1.766	5.845	20
Intron lengths (mRNAs)	NA	517.50	85.0	20	55	76	84	199	541	1.675	5.536	20
CDS exons per transcript	2.642	4.72	1.0	0	0	0	1	3	7	14	23	86
CDS exons per transcript (mRNAs)	2.642	05.01	1.0	1	1	1	1	3	7	14	23	86
CDS exon lengths	53,304,437	222.36	1.0	1	1	3	29	119	225	813	1.836	7.986
CDS Intron lengths	94,359,779	491.73	87.0	20	56	76	83	187	510	1.574	5.349	19.99
5'UTR exon number	47.83	1.27	1.0	0	0	1	1	1	1	2	4	14
3'UTR exon number	47.83	1.19	1.0	0	0	1	1	1	1	2	4	22
5'UTR length	8,331,188	174.18	1.0	0	0	1	3	119	240	531	1.039	10.09
3'UTR length	13,712,303	286.69	1.0	0	0	1	7	245	376	736	1.436	6.969
Stop distance from junction	NA	22.61	0.0	0	0	0	0	0	0	119	511	6.387
Intergenic distances	NA	15,008.75	2.0	53.90	1.992	2	216	4.674	15.90	65.4	138.51	922.80
Intergenic distances (coding)	NA	16,026.13	2.0	53.90	1.245	2	211	4.722	16.71	70.7	150.54	922.88

Supplemental Table S6: Enrichment analysis of MapMan annotated Single nucelotide polymorphisms (SNPs) with either stop gained or stop lost function on the *R. nigrum* genome.

MapMan annotation	ERF	pvalue
Photosynthesis	0.16	**0.00**
Cellular respiration	0.82	0.74
Carbohydrate metabolism	0.46	0.08
Amino acid metabolism	0.96	1.00
Lipid metabolism	0.67	0.14
Nucleotide metabolism	0.38	0.18
Coenzyme metabolism	0.54	0.12
Polyamine metabolism	0.85	1.00
Secondary metabolism	1.69	**0.05**
Redox homeostasis	0.64	0.46
Phytohormone action	0.24	**0.00**
Chromatin organisation	0.88	0.72
Cell division	0.72	0.14
DNA damage response	0.72	0.66
RNA biosynthesis	0.73	**0.02**
RNA processing	1.03	0.80
Protein biosynthesis	0.63	**0.04**
Protein modification	0.85	0.30
Protein homeostasis	0.70	**0.02**
Cytoskeleton organisation	0.95	1.00
Cell wall organisation	0.64	0.11
Vesicle trafficking	0.72	0.20
Protein translocation	0.94	1.00
Solute transport	0.60	**0.00**
Nutrient uptake	1.24	0.46
External stimuli response	1.14	0.52
Multi-process regulation	0.43	**0.00**
Plant reproduction	0.51	0.29
Plant organogenesis	0.30	0.07
Clade-specific metabolism	0.00	1.00
Enzyme classification	1.02	0.77

Supplemental Table S7: Differentially expressed transcripts under drought stress in *R. nigrum* leaf and root tissue and their MapMan annotations. Upregulation (red) and downregulation (blue) according to

log_2FC. Significance level of adjusted p values (FDR) shown in bold (FDR < 0.1), and marked *FDR < 0.05, **FDR < 0.01 and ***FDR < 0.001. Genes that are not differentially expressed are marked N.e.

		Adult plants				Young plants	
Gene ID	Mercator annotation	Leaf [log_2FC]	Leaf [FDR]	Root [log_2FC]	Root [FDR]	Leaf [log_2FC]	Leaf [FDR]
RN6G007260.1	abscisic aldehyde oxidase *(AAO)	-0.53	0.40	-0.39	0.35	NA	NA
RN6G007260.2	abscisic aldehyde oxidase *(AAO)	-0.53	0.40	-0.39	0.35	-0.03	0.91
RN6G007270.1	abscisic aldehyde oxidase *(AAO)	-0.67	0.27	-0.38	0.39	-0.03	0.94
RN6G007290.1	abscisic aldehyde oxidase *(AAO)	-0.60	0.36	-0.36	0.41	0.07	0.72
RN6G007230.1	abscisic aldehyde oxidase *(AAO)	-0.46	0.50	-0.44	0.33	0.44	0.00
RN1G022930.1	beta-1,3-galactosyltransferase	0.04	0.96	0.46	0.15	0.27	0.09
RN7G021400.1	beta-1,3-galactosyltransferase	0.21	0.74	-0.48	***0.04****	-0.01	0.95
RN6G009060.1	beta-1,6-galactosyltransferase *(GALT29)	-1.17	0.36	-2.49	***0.002****	-1.37	0.00
RN6G029710.1	hydroxyproline-O-galactosyltransferase *(GALT)	0.44	0.85	-2.71	***0.004****	-0.82	0.03
RN2G017560.1	hydroxyproline-O-galactosyltransferase *(GALT)	-0.58	0.56	-1.13	***0.02****	NA	NA
RN7G023180.1	hydroxyproline-O-galactosyltransferase *(GALT)	0.18	0.77	-0.61	0.12	-0.21	0.24
RN8G017280.1	hydroxyproline-O-galactosyltransferase *(GALT)	0.00	1.00	0.09	0.66	0.44	0.01
RN7G033750.1	LRR-domain extensin	0.13	0.80	-2.25	0.00	-0.68	0.03
RN2G011230.1	LRR-I protein kinase	-1.49	0.39	-0.96	0.11	0.81	0.28
RN2G011230.2	LRR-I protein kinase	-1.72	0.32	-0.96	0.11	NA	NA
RN8G030870.1	LRR-I protein kinase	0.30	0.73	-0.53	0.29	-0.80	0.01
RN1G016380.1	LRR-I protein kinase	-0.54	0.43	-0.55	***0.03****	NA	NA
RN5G014400.1	LRR-I protein kinase	-1.41	0.18	-1.23	***0.02****	-0.47	0.24
RN3G020030.1	LRR-I protein kinase	-3.69	0.10	-1.50	***0.02****	0.11	0.55
RN3G048180.1	LRR-I protein kinase	-3.08	0.15	-0.16	0.73	0.09	0.41
RN6G053890.1	LRR-I protein kinase	-0.34	0.81	-1.64	***0.001****	NA	NA
RN6G054120.1	LRR-I protein kinase	-0.72	0.42	-1.60	***0.002****	-0.52	0.00
RN6G054140.1	LRR-I protein kinase	-0.87	0.52	-1.03	***0.01****	NA	NA
RN1G062740.1	LRR-II protein kinase	0.43	0.25	0.05	0.88	0.21	0.07
RN1G062750.1	LRR-II protein kinase	-0.39	0.70	0.54	0.40	1.18	0.00
RN2G020690.1	LRR-II protein kinase	-0.05	0.98	-0.91	0.26	-1.02	0.02
RN5G005760.1	LRR-II protein kinase	0.42	0.22	0.10	0.60	-0.01	0.95
RN5G005760.2	LRR-II protein kinase	0.42	0.22	0.10	0.60	NA	NA
RN5G004050.1	LRR-II protein kinase	-0.26	0.60	0.56	0.08	0.88	0.33
RN1G015740.1	LRR-II protein kinase	1.54	0.10	-1.15	***0.008****	NA	NA
RN7G016370.1	LRR-II protein kinase	-2.22	0.16	-1.75	***0.02****	-0.45	0.02
RN7G026250.1	LRR-II protein kinase	-0.10	0.87	-0.73	***0.03****	-0.28	0.01
RN1G062720.1	LRR-II protein kinase	0.25	0.61	0.05	0.90	-0.10	0.88
RN5G026220.1	LRR-III protein kinase	-0.89	0.54	-2.82	***0.002****	-0.93	0.00
RN3G044010.1	LRR-III protein kinase	-1.39	0.33	-2.62	***0.0005*****	-0.79	0.00
RN4G030430.1	LRR-III protein kinase	-1.25	0.60	-3.22	***0.005****	-4.18	0.00
RN3G031170.1	LRR-III protein kinase	0.00	1.00	-4.05	***0.0003*****	-3.61	0.00

RN8G021040.1	LRR-III protein kinase	-0.29	0.48	-0.26	0.43	-0.31	0.28
RN7G002750.1	LRR-III protein kinase	-1.14	0.37	-0.58	0.07	-0.66	0.00
RN7G028120.1	LRR-III protein kinase	-2.71	0.10	0.56	0.42	0.58	0.47
RN1G062760.1	LRR-III protein kinase	-0.17	0.85	-0.33	0.54	0.72	0.10
RN7G033190.1	LRR-III protein kinase	-1.09	0.26	-1.97	***0.002****	-0.72	0.00
RN4G014450.1	LRR-III protein kinase	1.43	0.20	-1.07	***0.006****	-0.31	0.08
RN6G025550.1	LRR-III protein kinase	0.26	0.90	-1.44	***0.009****	-0.97	0.00
RN3G033690.1	LRR-III protein kinase	-0.83	0.66	-1.08	0.08	-0.65	0.00
RN6G000160.1	LRR-III protein kinase	-1.71	0.36	-2.40	***0.0004****	-1.10	0.00
RN4G057830.1	LRR-III protein kinase	0.56	0.39	-2.05	***0.004****	-0.76	0.00
RN5G010820.1	LRR-III protein kinase	-1.73	0.39	-1.30	***0.03****	-0.36	0.04
RN7G008510.1	LRR-III protein kinase	0.52	0.60	-1.35	***0.007****	-0.85	0.00
RN5G011100.1	LRR-III protein kinase	-4.50	0.10	-1.84	***0.001****	0.04	0.78
RN4G024710.1	LRR-III protein kinase	-0.40	0.48	-0.56	0.10	-0.37	0.21
RN5G030960.1	LRR-III protein kinase	-0.68	0.68	-1.96	***0.003****	NA	NA
RN6G053520.1	LRR-III protein kinase	1.55	0.08	0.37	0.16	-1.07	0.00
RN1G061510.1	LRR-III protein kinase	-2.90	0.24	-2.99	***0.008****	-0.44	0.21
RN3G002470.1	LRR-III protein kinase	-1.78	0.17	-0.95	0.11	-1.06	0.00
RN3G038050.1	LRR-III protein kinase	1.28	0.13	-1.53	***0.003****	-1.47	0.00
RN7G010530.1	LRR-III protein kinase	1.35	0.12	-1.00	***0.01****	-0.27	0.28
RN4G021860.1	LRR-IV protein kinase	-0.31	0.73	-0.52	0.26	-1.10	0.02
RN6G015500.1	LRR-IV protein kinase	-3.27	0.13	-3.00	***0.001****	-0.90	0.00
RN1G017130.1	LRR-IX protein kinase	0.16	0.85	-0.82	***0.03****	-0.63	0.00
RN7G015060.1	LRR-IX protein kinase	0.06	0.93	-0.61	0.05	-0.27	0.12
RN6G007620.1	LRR-IX protein kinase	0.26	0.63	-0.70	***0.03****	-0.14	0.56
RN2G013530.1	LRR-V protein kinase	-0.21	0.79	1.19	***0.007****	NA	NA
RN1G067330.1	LRR-V protein kinase	-0.48	0.48	-1.35	***0.004****	-0.51	0.00
RN2G013530.2	LRR-V protein kinase	-0.21	0.79	1.19	***0.007****	0.87	0.07
RN3G005320.1	LRR-V protein kinase	-0.12	0.95	-1.14	0.21	-0.36	0.20
RN7G029140.1	LRR-V protein kinase	-1.38	0.12	-0.85	0.02	-0.29	0.08
RN2G008760.1	LRR-V protein kinase	-2.33	0.13	-2.82	***0.0004****	-0.44	0.08
RN2G059350.1	LRR-VI-1 protein kinase	-3.45	0.22	-0.49	0.40	NA	NA
RN3G056400.1	LRR-VI-1 protein kinase	-5.76	0.09	-1.14	0.05	0.15	0.34
RN8G022740.1	LRR-VI-1 protein kinase	-1.54	0.41	-2.27	***0.04****	-1.39	0.06
RN8G022740.2	LRR-VI-1 protein kinase	-1.58	0.29	-2.19	***0.02****	-1.65	0.00
RN7G022410.1	LRR-VI-1 protein kinase	0.16	0.72	-1.53	***0.001****	0.71	0.00
RN6G028830.1	LRR-VI-2 protein kinase	-0.32	0.65	-0.30	0.30	-0.08	0.63
RN2G021450.1	LRR-VI-2 protein kinase	0.86	0.23	0.59	0.10	-0.29	0.02
RN2G021450.2	LRR-VI-2 protein kinase	0.86	0.23	0.59	0.10	NA	NA
RN3G033380.1	LRR-VII protein kinase	-3.37	0.44	-2.76	***0.02****	-1.11	0.01
RN2G041770.1	LRR-VII protein kinase	-1.14	0.54	-2.83	***0.004****	-0.47	0.03
RN2G021230.1	LRR-VII protein kinase	1.14	0.18	-0.28	0.34	0.55	0.01
RN5G020590.1	LRR-VII protein kinase	-1.09	0.26	-2.12	***0.02****	-1.56	0.00
RN4G003290.1	LRR-VII protein kinase	0.99	0.20	-1.52	***0.003****	-0.72	0.00

RN4G046010.1	LRR-VII protein kinase	-0.64	0.80	-1.89	0.09	-2.32	0.00
RN4G034920.1	LRR-VII protein kinase	-0.52	0.62	-2.58	***0.001****	-0.84	0.00
RN8G036840.1	LRR-VIII-2 protein kinase	-0.19	0.81	-0.05	0.92	-0.18	0.35
RN8G036850.1	LRR-VIII-2 protein kinase	-0.95	0.18	-0.46	0.27	-0.91	0.00
RN8G036870.1	LRR-VIII-2 protein kinase	-1.13	0.13	-0.48	0.11	-0.50	0.00
RN8G036890.1	LRR-VIII-2 protein kinase	-0.02	1.00	-1.36	0.02	0.61	0.01
RN8G036920.1	LRR-VIII-2 protein kinase	0.32	0.65	-0.97	0.05	-0.66	0.05
RN8G037110.1	LRR-VIII-2 protein kinase	-0.68	0.43	-1.33	***0.03****	-2.22	0.00
RN8G037150.1	LRR-VIII-2 protein kinase	0.27	0.74	-1.15	***0.03****	-1.02	0.00
RN8G037220.1	LRR-VIII-2 protein kinase	0.71	0.21	-0.13	0.62	0.18	0.11
RN8G037250.1	LRR-VIII-2 protein kinase	-0.24	0.70	-0.81	***0.009****	-0.03	0.90
RN8G037290.1	LRR-VIII-2 protein kinase	-0.40	0.57	-0.88	***0.007****	-0.38	0.12
RN8G037330.1	LRR-VIII-2 protein kinase	-0.09	0.91	-0.83	***0.009****	-0.25	0.18
RN8G037370.1	LRR-VIII-2 protein kinase	-0.59	0.52	-0.67	0.24	0.28	0.05
RN1G072830.1	LRR-VIII-2 protein kinase	-1.65	0.26	0.85	0.27	-0.05	0.85
RN1G072840.1	LRR-VIII-2 protein kinase	-1.55	0.29	0.92	0.27	-0.08	0.88
RN8G037490.1	LRR-VIII-2 protein kinase	-0.15	0.86	0.40	0.54	-0.47	0.00
RN8G037500.1	LRR-VIII-2 protein kinase	-0.85	0.28	-0.31	0.61	-0.62	0.02
RN8G037460.1	LRR-VIII-2 protein kinase	0.21	0.80	0.45	0.42	-0.80	0.02
RN2G020290.1	LRR-VIII-2 protein kinase	0.41	0.59	1.07	0.05	0.75	0.01
RN2G020310.1	LRR-VIII-2 protein kinase	0.46	0.53	0.97	***0.04****	0.50	0.01
RN8G037040.1	LRR-VIII-2 protein kinase	-1.33	0.19	-0.87	0.11	-0.89	0.00
RN8G037240.1	LRR-VIII-2 protein kinase	-1.43	0.15	-0.74	0.10	NA	NA
RN8G037240.2	LRR-VIII-2 protein kinase	-1.38	0.15	-0.88	0.05	-0.27	0.17
RN8G037400.1	LRR-VIII-2 protein kinase	-0.14	0.85	0.30	0.60	-0.47	0.04
RN8G037420.1	LRR-VIII-2 protein kinase	-0.32	0.64	0.10	0.88	NA	NA
RN8G037420.2	LRR-VIII-2 protein kinase	-0.32	0.64	0.08	0.90	-0.37	0.02
RN8G037430.1	LRR-VIII-2 protein kinase	0.00	1.00	0.47	0.48	-1.42	0.00
RN2G020280.1	LRR-VIII-2 protein kinase	-0.27	0.87	-0.04	0.89	0.02	0.93
RN2G020280.2	LRR-VIII-2 protein kinase	-0.06	0.99	-0.11	0.72	0.44	0.09
RN8G036950.1	LRR-VIII-2 protein kinase	-2.17	0.24	-2.14	0.06	-0.67	0.00
RN2G001530.1	LRR-VIII-2 protein kinase	-1.01	0.18	-1.07	0.05	-1.11	0.00
RN8G036440.1	LRR-VIII-2 protein kinase	0.45	0.69	-0.98	0.05	0.25	0.34
RN8G036880.1	LRR-VIII-2 protein kinase	-0.11	0.91	-1.54	***0.03****	-1.92	0.00
RN8G037050.1	LRR-VIII-2 protein kinase	0.70	0.55	-1.24	0.14	NA	NA
RN8G037120.1	LRR-VIII-2 protein kinase	-0.60	0.71	-1.44	0.11	NA	NA
RN8G037230.1	LRR-VIII-2 protein kinase	0.40	0.65	-0.94	0.07	NA	NA
RN8G037320.1	LRR-VIII-2 protein kinase	0.17	0.70	-0.17	0.46	-0.17	0.14
RN8G037340.1	LRR-VIII-2 protein kinase	0.26	0.72	-1.17	***0.03****	0.21	0.20
RN8G037350.1	LRR-VIII-2 protein kinase	0.40	0.55	-0.81	0.10	-0.18	0.18
RN8G037380.1	LRR-VIII-2 protein kinase	0.10	0.81	-0.14	0.51	-1.09	0.01
RN1G008470.1	LRR-VIII-2 protein kinase	-0.54	0.43	0.22	0.69	-0.69	0.03
RN2G001400.1	LRR-VIII-2 protein kinase	-0.67	0.33	-0.81	0.12	-0.60	0.00
RN2G001410.1	LRR-VIII-2 protein kinase	-0.49	0.38	0.07	0.90	-0.13	0.35

RN2G001420.1	LRR-VIII-2 protein kinase	-0.73	0.20	-0.49	0.18	0.17	0.27
RN2G001470.1	LRR-VIII-2 protein kinase	-0.59	0.26	-0.14	0.72	-0.48	0.00
RN2G001480.1	LRR-VIII-2 protein kinase	-0.42	0.44	-0.22	0.66	-0.69	0.00
RN2G001510.1	LRR-VIII-2 protein kinase	-1.13	0.16	-0.66	0.21	-1.12	0.00
RN2G001560.1	LRR-VIII-2 protein kinase	-0.89	0.15	0.13	0.74	-0.59	0.00
RN2G001610.1	LRR-VIII-2 protein kinase	-0.84	0.17	-0.52	0.19	-0.47	0.00
RN2G001630.1	LRR-VIII-2 protein kinase	-0.68	0.32	-0.89	0.11	-0.38	0.05
RN2G001650.1	LRR-VIII-2 protein kinase	-0.65	0.23	-0.37	0.33	-0.71	0.00
RN2G001670.1	LRR-VIII-2 protein kinase	-0.51	0.33	-0.58	0.15	-0.29	0.01
RN2G001690.1	LRR-VIII-2 protein kinase	-0.44	0.45	-0.78	0.06	-0.20	0.06
RN2G001390.1	LRR-VIII-2 protein kinase	-0.14	0.93	0.04	0.96	-0.13	0.59
RN2G001430.1	LRR-VIII-2 protein kinase	0.49	0.23	0.89	***0.003*** **	-0.15	0.19
RN2G001460.1	LRR-VIII-2 protein kinase	-0.61	0.37	-0.26	0.65	-0.20	0.35
RN2G001510.2	LRR-VIII-2 protein kinase	-1.06	0.21	-0.73	0.19	-0.81	0.00
RN2G001590.1	LRR-VIII-2 protein kinase	0.67	0.68	-0.73	0.16	-0.48	0.01
RN2G020300.1	LRR-VIII-2 protein kinase	-1.86	0.11	-0.08	0.77	-0.71	0.00
RN2G020320.1	LRR-VIII-2 protein kinase	-0.86	0.27	-0.07	0.79	0.02	0.91
RN8G036960.1	LRR-VIII-2 protein kinase	-2.29	0.09	-0.92	***0.02*** *	-0.57	0.02
RN5G034870.1	LRR-Xa protein kinase	0.64	0.16	0.48	***0.04*** *	0.38	0.00
RN1G020920.1	LRR-Xa protein kinase	0.52	0.24	0.02	0.94	0.15	0.16
RN7G014160.1	LRR-Xb protein kinase	0.57	0.74	-1.43	***0.004*** **	-1.44	0.00
RN4G061740.1	LRR-Xb protein kinase	0.07	0.90	-0.76	***0.01*** *	-0.05	0.89
RN7G013130.1	LRR-Xb protein kinase	0.40	0.37	0.62	***0.01*** *	0.10	0.50
RN8G034340.1	LRR-Xb protein kinase	1.34	0.12	0.38	0.37	0.29	0.06
RN8G012700.1	LRR-Xb protein kinase	0.53	0.77	0.31	0.65	0.58	0.19
RN14G000070.1	LRR-Xb protein kinase	0.77	0.19	0.13	0.73	0.30	0.01
RN3G039560.1	LRR-Xc protein kinase	-2.80	0.36	-1.86	***0.002*** **	-0.06	0.97
RN4G053430.1	LRR-Xc protein kinase	0.23	0.64	0.16	0.45	0.34	0.02
RN4G023740.1	LRR-XI protein kinase	-1.60	0.21	-0.92	0.04	-1.04	0.00
RN7G030700.1	LRR-XI protein kinase	-0.39	0.70	-0.64	0.24	0.15	0.17
RN5G013920.1	LRR-XI protein kinase	-3.81	0.14	-2.63	***0.02*** *	-0.37	0.04
RN6G034060.1	LRR-XI protein kinase	-1.13	0.60	-1.58	0.11	-0.79	0.04
RN2G034040.1	LRR-XI protein kinase	0.62	0.26	0.47	0.08	0.16	0.09
RN3G038360.1	LRR-XI protein kinase	-5.07	0.12	-3.09	***0.001*** **	-0.47	0.07
RN4G044770.1	LRR-XI protein kinase	-0.62	0.42	-1.09	0.08	-0.80	0.00
RN4G055720.1	LRR-XI protein kinase	-1.08	0.25	0.13	0.80	-0.30	0.08
RN4G063600.1	LRR-XI protein kinase	-0.01	1.00	1.37	***0.01*** *	0.27	0.01
RN3G006620.1	LRR-XI protein kinase	0.79	0.68	-1.18	0.05	0.37	0.06
RN1G039170.1	LRR-XI protein kinase	0.31	0.87	0.49	0.52	0.51	0.17
RN4G055710.1	LRR-XI protein kinase	1.31	0.11	0.26	0.43	0.94	0.00
RN1G069740.1	LRR-XI protein kinase	-1.18	0.13	-1.53	***0.004*** **	0.35	0.05
RN2G023110.1	LRR-XI protein kinase	-0.81	0.31	0.11	0.83	0.12	0.15
RN1G055620.1	LRR-XI protein kinase	-1.18	0.19	-0.31	0.34	-0.78	0.00
RN6G034270.1	LRR-XI protein kinase	-0.01	1.00	-1.87	***0.003*** **	-0.59	0.03

RN8G019760.1	LRR-XI protein kinase	-1.03	0.39	-1.47	***0.005***	-1.16		0.00
RN8G041910.1	LRR-XI protein kinase	-1.49	0.28	-1.01	***0.025***	-1.39		0.00
RN3G028370.1	LRR-XI protein kinase	-0.04	1.00	-2.08	***0.007***	0.59		0.12
RN6G053450.1	LRR-XI protein kinase	-1.00	0.16	-0.82	0.07	NA	NA	
RN4G054600.1	LRR-XI protein kinase	-0.70	0.82	-2.46	***0.02***	-0.54		0.30
RN5G013810.1	LRR-XI protein kinase	-0.33	0.63	-0.83	***0.02***	NA	NA	
RN3G011250.1	LRR-XII protein kinase	0.35	0.58	-0.65	0.08	0.23		0.73
RN5G047880.1	LRR-XII protein kinase	0.38	0.61	-1.17	0.08	NA	NA	
RN7G000290.1	LRR-XII protein kinase	0.56	0.42	-0.96	0.13	-0.99		0.12
RN1G071870.1	LRR-XII protein kinase	-2.54	0.13	0.45	0.59	0.57		0.27
RN2G020630.1	LRR-XII protein kinase	-0.69	0.37	0.12	0.84	-2.23		0.00
RN5G013680.1	LRR-XII protein kinase	0.44	0.61	-1.49	***0.04***	NA	NA	
RN7G000280.1	LRR-XII protein kinase	0.47	0.52	-0.99	0.14	-0.35		0.61
RN1G072030.1	LRR-XII protein kinase	-2.60	0.17	0.65	0.45	0.93		0.05
RN2G021100.1	LRR-XII protein kinase	-1.30	0.18	-0.37	0.27	-0.14		0.21
RN2G054130.1	LRR-XII protein kinase	-1.23	0.24	-0.34	0.25	-0.82		0.02
RN2G055040.1	LRR-XII protein kinase	-1.85	0.18	0.15	0.69	-0.07		0.67
RN5G033250.1	LRR-XII protein kinase	-1.13	0.22	-0.65	0.34	0.60		0.03
RN5G049080.1	LRR-XII protein kinase	-0.98	0.29	0.55	0.24	0.71		0.24
RN1G003040.1	LRR-XII protein kinase	-2.09	0.18	-1.11	0.20	NA	NA	
RN1G003170.1	LRR-XII protein kinase	-1.93	0.15	-0.72	0.37	NA	NA	
RN1G003180.1	LRR-XII protein kinase	-2.09	0.17	-1.23	0.14	NA	NA	
RN3G048540.1	LRR-XII protein kinase	0.71	0.37	0.22	0.70	0.10		0.61
RN3G048550.1	LRR-XII protein kinase	1.40	0.25	0.54	0.49	NA	NA	
RN1G044120.1	LRR-XII protein kinase	-2.62	0.14	0.87	0.33	-0.41		0.67
RN2G021070.1	LRR-XII protein kinase	-1.06	0.41	-0.51	0.54	0.23		0.25
RN6G003880.1	LRR-XII protein kinase	0.06	0.98	-1.39	***0.03***	-0.02		0.97
RN1G001000.1	LRR-XII protein kinase	-2.01	0.09	-0.99	***0.01***	0.40		0.07
RN1G001030.1	LRR-XII protein kinase	-2.05	0.09	-1.02	***0.01***	NA	NA	
RN4G059690.1	LRR-XII protein kinase	-2.05	0.09	-0.83	***0.02***	0.31		0.21
RN4G059700.1	LRR-XII protein kinase	-2.16	0.09	-0.90	***0.01***	-0.32		0.32
RN4G059730.1	LRR-XII protein kinase	-0.57	0.33	-0.55	0.08	0.48		0.32
RN4G062230.1	LRR-XII protein kinase	-2.16	0.09	-0.79	0.03	-0.20		0.70
RN1G003070.1	LRR-XII protein kinase	-1.59	0.30	-0.77	0.49	NA	NA	
RN1G003020.1	LRR-XII protein kinase	-1.86	0.11	-0.65	0.33	NA	NA	
RN1G003060.1	LRR-XII protein kinase	-1.70	0.13	-0.73	0.24	NA	NA	
RN1G003150.1	LRR-XII protein kinase	-0.61	0.44	-0.58	0.40	NA	NA	
RN1G003210.1	LRR-XII protein kinase	-3.15	0.11	-1.04	0.29	-0.50		0.65
RN1G022120.1	LRR-XII protein kinase	-0.12	0.92	0.67	0.16	0.54		0.68
RN1G022120.2	LRR-XII protein kinase	-0.21	0.85	0.66	0.16	0.31		0.26
RN3G055290.1	LRR-XII protein kinase	0.91	0.38	-0.15	0.72	1.51		0.07
RN4G059670.1	LRR-XII protein kinase	-0.39	0.83	-0.59	0.27	-0.34		0.67
RN4G059710.1	LRR-XII protein kinase	-1.96	0.09	-0.86	0.02	0.05		0.90
RN4G059740.1	LRR-XII protein kinase	-2.05	0.09	-0.86	***0.01***	0.36		0.35

RN4G059750.1	LRR-XII protein kinase	-2.07	0.09	-0.63	0.05	0.24		0.27
RN6G051840.1	LRR-XII protein kinase	-0.96	0.48	-0.78	0.34	NA	NA	
RN6G051850.1	LRR-XII protein kinase	-0.94	0.59	-0.78	0.33	NA	NA	
RN6G051860.1	LRR-XII protein kinase	-2.84	0.32	-0.69	0.43	NA	NA	
RN2G055020.1	LRR-XII protein kinase	-1.91	0.16	-0.79	***0.03****	-1.11		0.00
RN2G055130.1	LRR-XII protein kinase	-0.96	0.27	-0.21	0.51	-0.45		0.01
RN2G054170.1	LRR-XII protein kinase	-0.48	0.46	-0.47	0.11	0.94		0.00
RN2G054690.1	LRR-XII protein kinase	-0.37	0.61	-0.62	0.07	NA	NA	
RN2G006380.1	LRR-XII protein kinase	-1.72	0.19	-0.40	0.29	0.02		0.96
RN2G020570.1	LRR-XII protein kinase	0.78	0.20	0.60	0.16	-0.34		0.28
RN3G007170.1	LRR-XII protein kinase	-0.96	0.52	-2.69	***0.006****	0.18		0.79
RN3G007180.1	LRR-XII protein kinase	-1.49	0.37	-2.68	***0.004****	-0.50		0.06
RN4G004390.1	LRR-XII protein kinase	0.68	0.80	0.95	0.24	NA	NA	
RN2G051050.1	LRR-XII protein kinase	-0.63	0.49	0.58	0.23	0.76		0.01
RN2G051680.1	LRR-XII protein kinase	-1.16	0.16	0.28	0.47	-0.09		0.87
RN2G054120.1	LRR-XII protein kinase	-0.87	0.31	0.54	0.14	-0.20		0.39
RN2G054150.1	LRR-XII protein kinase	-1.50	0.19	-0.69	***0.04****	0.07		0.86
RN2G054510.1	LRR-XII protein kinase	-1.09	0.34	-0.02	0.98	0.64		0.17
RN2G054580.1	LRR-XII protein kinase	-1.13	0.26	-0.52	0.09	1.05		0.00
RN2G054600.1	LRR-XII protein kinase	-1.08	0.19	-0.45	0.08	-0.64		0.02
RN2G054620.1	LRR-XII protein kinase	-2.22	0.13	-0.84	***0.04****	-1.09		0.00
RN2G054630.1	LRR-XII protein kinase	-0.88	0.23	-0.37	0.18	-0.52		0.04
RN2G054760.1	LRR-XII protein kinase	-1.21	0.23	-0.51	0.10	NA	NA	
RN2G054780.1	LRR-XII protein kinase	-1.15	0.26	-0.54	0.12	0.49		0.26
RN2G054940.1	LRR-XII protein kinase	-1.12	0.29	0.00	1.00	-0.34		0.46
RN2G054970.1	LRR-XII protein kinase	-1.44	0.19	-0.66	***0.04****	-0.55		0.01
RN2G054990.1	LRR-XII protein kinase	-1.23	0.18	0.06	0.86	-0.39		0.03
RN2G055090.1	LRR-XII protein kinase	-0.23	0.84	-0.41	0.33	-0.47		0.11
RN2G055150.1	LRR-XII protein kinase	-2.29	0.12	-0.80	0.06	-1.13		0.02
RN2G055160.1	LRR-XII protein kinase	-1.51	0.19	-0.54	0.15	NA	NA	
RN2G055180.1	LRR-XII protein kinase	-2.09	0.12	-0.75	0.05	-0.80		0.02
RN2G055190.1	LRR-XII protein kinase	-0.84	0.28	-0.34	0.24	NA	NA	
RN3G002530.1	LRR-XII protein kinase	-1.75	0.35	0.02	0.98	0.45		0.21
RN8G038110.1	LRR-XIIIa protein kinase	1.13	0.46	4.91	0.01	NA	NA	
RN2G050050.1	LRR-XIIIa protein kinase	0.42	0.43	-0.10	0.72	-0.37		0.01
RN8G015590.1	LRR-XIIIa protein kinase	0.00	1.00	-2.10	***0.01****	-1.75		0.00
RN1G045950.1	LRR-XIV protein kinase	0.37	0.60	-0.90	0.04	-0.11		0.60
RN4G047430.1	LRR-XIV protein kinase	0.92	0.19	0.41	0.14	0.62		0.00
RN7G035580.1	LRR-XV protein kinase	0.78	0.43	0.25	0.69	1.04		0.04
RN7G035590.1	LRR-XV protein kinase	0.80	0.41	0.04	0.95	1.05		0.00
RN1G013090.1	LRR-XV protein kinase	0.02	0.99	-0.16	0.63	-0.16		0.22
RN7G018890.1	LRR-XV protein kinase	-0.60	0.44	-0.73	0.14	0.32		0.22
RN3G015760.1	PERK protein kinase	-1.44	0.13	0.88	***0.008****	0.47		0.00
RN7G034400.1	PERK protein kinase	-0.68	0.46	-1.64	***0.003****	-0.47		0.01

RN7G025360.1	PERK protein kinase	-0.28	0.89	-2.97	***0.003***	-0.78	0.00	
RN7G016120.1	PERK protein kinase	-1.02	0.11	0.23	0.37	0.39	0.01	
RN3G012730.1	PERK protein kinase	-1.63	0.22	-0.46	0.24	-0.21	0.11	
RN4G048640.1	PERK protein kinase	-0.98	0.70	-2.93	***0.01***	-0.15	0.63	
RN4G001560.1	RLCK-IXb receptor-like protein kinase	0.02	1.00	2.69	***0.01***	NA	NA	
RN1G045860.1	RLCK-V receptor-like protein kinase	-5.96	0.08	-1.75	***0.004***	-0.70	0.00	
RN1G073400.1	RLCK-V receptor-like protein kinase	0.35	0.85	-1.73	***0.004***	-1.16	0.00	
RN2G040080.1	RLCK-V receptor-like protein kinase	-0.24	0.65	-0.91	***0.005***	-0.01	0.96	
RN5G052120.1	RLCK-V receptor-like protein kinase	0.62	0.41	-0.77	0.12	-0.61	0.00	
RN4G050720.1	RLCK-V receptor-like protein kinase	-0.61	0.37	-0.96	***0.006***	-1.52	0.00	
RN5G010110.1	RLCK-V receptor-like protein kinase	-2.95	0.13	-1.67	***0.007***	-0.43	0.16	
RN6G020790.1	RLCK-V receptor-like protein kinase	-0.77	0.34	-1.04	***0.03***	-0.66	0.02	
RN4G051950.1	RLCK-VI receptor-like protein kinase	0.09	0.93	-2.08	***0.002***	-0.52	0.35	
RN4G002670.1	RLCK-VI receptor-like protein kinase	-1.97	0.17	0.50	0.29	-0.19	0.64	
RN4G008750.1	RLCK-VI receptor-like protein kinase	-1.21	0.67	-1.46	0.16	-0.68	0.12	
RN1G011660.1	RLCK-VI receptor-like protein kinase	-3.07	0.10	-2.45	***0.001***	-0.13	0.63	
RN1G053710.1	RLCK-VI receptor-like protein kinase	-3.57	0.15	-2.48	***0.01***	-0.92	0.01	
RN4G044590.1	RLCK-VI receptor-like protein kinase	0.30	0.78	0.48	0.62	0.92	0.01	
RN5G045590.1	RLCK-VI receptor-like protein kinase	-1.76	0.46	-1.48	0.28	NA	NA	
RN6G046780.1	RLCK-VI receptor-like protein kinase	0.07	0.99	-1.33	0.08	0.24	0.64	
RN5G003740.1	RLCK-VI receptor-like protein kinase	0.94	0.20	0.01	0.99	-0.92	0.00	
RN5G015660.1	RLCK-VI receptor-like protein kinase	1.45	0.16	-0.13	0.70	0.21	0.34	
RN6G003430.1	RLCK-VIIa receptor-like protein kinase	0.04	0.97	0.75	***0.02***	0.41	0.01	
RN2G045970.1	RLCK-VIIa receptor-like protein kinase	0.83	0.75	-0.22	0.80	NA	NA	
RN1G028210.1	RLCK-VIIa receptor-like protein kinase	-2.00	0.13	-0.78	0.22	0.14	0.54	
RN3G024170.1	RLCK-VIIa receptor-like protein kinase	-0.71	0.56	-1.80	***0.005***	-0.34	0.04	
RN2G050640.1	RLCK-VIIa receptor-like protein kinase	0.45	0.60	1.09	***0.006***	0.36	0.02	
RN2G053870.1	RLCK-VIIa receptor-like protein kinase	0.38	0.48	0.89	***0.03***	0.49	0.03	
RN4G041650.1	RLCK-VIIa receptor-like protein kinase	-0.31	0.58	-0.93	***0.02***	-0.38	0.05	
RN7G022190.1	RLCK-VIIa receptor-like protein kinase	0.11	0.84	0.40	0.08	0.52	0.00	
RN6G005350.1	RLCK-VIIa receptor-like protein kinase	0.73	0.22	1.50	***0.007***	0.40	0.09	
RN3G048390.1	RLCK-VIIa receptor-like protein kinase	0.43	0.24	0.60	***0.02***	0.43	0.00	
RN3G034380.1	RLCK-VIIa receptor-like protein kinase	-1.13	0.17	-0.69	***0.01***	NA	NA	
RN3G050020.1	RLCK-VIIa receptor-like protein kinase	0.44	0.37	0.46	0.06	0.21	0.10	
RN4G038460.1	RLCK-VIIa receptor-like protein kinase	0.02	0.97	0.13	0.57	-0.70	0.52	
RN4G038460.2	RLCK-VIIa receptor-like protein kinase	0.02	0.97	0.13	0.55	-0.57	0.00	
RN1G051820.1	RLCK-VIIa receptor-like protein kinase	0.03	0.99	0.11	0.87	1.21	0.17	
RN1G051820.2	RLCK-VIIa receptor-like protein kinase	0.03	0.99	0.11	0.87	NA	NA	
RN4G041660.1	RLCK-VIIa receptor-like protein kinase	0.32	0.77	0.62	0.14	1.11	0.00	
RN5G024270.1	RLCK-VIIa receptor-like protein kinase	0.28	0.42	0.46	0.07	0.10	0.47	
RN2G032230.1	RLCK-VIIa receptor-like protein kinase	0.84	0.10	0.40	0.08	0.28	0.06	
RN4G035650.1	RLCK-VIIa receptor-like protein kinase	0.15	0.76	-0.35	0.27	0.14	0.38	
RN1G022130.1	RLCK-VIIa receptor-like protein kinase	-0.32	0.52	-1.17	0.00	NA	NA	
RN1G022130.2	RLCK-VIIa receptor-like protein kinase	-0.32	0.52	-1.18	***0.004***	NA	NA	

RN7G022650.1	RLCK-VIIa receptor-like protein kinase	0.70	0.15	0.14	0.52	-0.13	0.38
RN7G031910.1	RLCK-VIIa receptor-like protein kinase	-0.76	0.34	0.27	0.47	0.11	0.76
RN3G001280.1	RLCK-VIIa receptor-like protein kinase	0.47	0.21	0.21	0.23	0.16	0.20
RN3G046880.1	RLCK-VIIa receptor-like protein kinase	0.26	0.51	0.47	0.05	NA	NA
RN4G027570.1	RLCK-VIIa receptor-like protein kinase	0.14	0.69	-0.32	0.17	NA	NA
RN4G027570.2	RLCK-VIIa receptor-like protein kinase	0.14	0.69	-0.32	0.17	0.44	0.30
RN6G003420.1	RLCK-VIIa receptor-like protein kinase	0.64	0.44	-0.19	0.67	NA	NA
RN7G038050.1	RLCK-VIIa receptor-like protein kinase	0.90	0.52	0.11	0.86	1.44	0.18
RN7G024330.1	RLCK-VIIb receptor-like protein kinase	-0.72	0.55	-1.81	***0.005*** **	-0.29	0.54
RN3G036680.1	RLCK-VIII receptor-like protein kinase	-0.71	0.63	-0.47	0.69	-0.15	0.81
RN6G031350.1	RLCK-VIII receptor-like protein kinase	0.50	0.29	-0.02	0.95	-0.15	0.20
RN6G031350.2	RLCK-VIII receptor-like protein kinase	0.51	0.29	-0.01	0.96	NA	NA
RN2G027670.1	RLCK-VIII receptor-like protein kinase	0.11	0.85	0.16	0.40	-0.15	0.23
RN2G040090.1	RLCK-VIII receptor-like protein kinase	0.30	0.46	-0.08	0.65	-0.05	0.73
RN2G040090.2	RLCK-VIII receptor-like protein kinase	0.30	0.46	-0.08	0.65	NA	NA
RN2G056060.1	RLCK-VIII-sis receptor-like protein kinase	0.73	0.26	-1.20	***0.01*** *	-0.49	0.00
RN1G032180.1	RLCK-X receptor-like protein kinase	-1.27	0.38	-1.76	***0.004*** **	-1.31	0.00
RN3G008490.1	RLCK-X receptor-like protein kinase	-1.67	0.23	-2.46	***0.001*** **	-0.47	0.08
RN3G007740.1	RLCK-XI receptor-like protein kinase	0.12	0.97	-1.80	***0.01*** *	-1.32	0.00
RN4G020510.1	RLCK-XI receptor-like protein kinase	0.69	0.22	0.63	***0.02*** *	0.21	0.19
RN6G016710.1	RLCK-XI receptor-like protein kinase	-1.74	0.28	-0.72	0.19	-0.03	0.88
RN4G042940.1	RLCK-XII receptor-like protein kinase	0.33	0.41	0.42	***0.04*** *	-0.30	0.01
RN6G012230.1	RLCK-XII receptor-like protein kinase	0.14	0.72	0.35	0.12	0.35	0.03
RN6G019400.1	RLCK-XII receptor-like protein kinase	0.45	0.29	0.43	0.13	-0.03	0.84
RN3G051940.1	RLCK-XII receptor-like protein kinase	-2.86	0.13	-3.03	***0.001*** **	-0.15	0.71
RN3G051940.2	RLCK-XII receptor-like protein kinase	-3.15	0.18	-3.03	***0.001*** **	-0.63	0.01
RN6G002460.1	RLCK-XII receptor-like protein kinase	0.17	0.89	-0.26	0.48	-0.36	0.27
RN6G028340.1	RLCK-XII receptor-like protein kinase	-0.42	0.54	-0.78	***0.02*** *	-0.04	0.82
RN3G011210.1	RLCK-XV receptor-like protein kinase	0.03	0.98	0.05	0.91	0.02	0.93
RN4G008740.1	RLCK-XV receptor-like protein kinase	0.00	1.00	-5.00	***0.005*** **	NA	NA
RN4G020460.1	RLCK-XV receptor-like protein kinase	-2.68	0.42	-1.14	0.23	NA	NA
RN6G046810.1	RKF3 protein kinase	0.48	0.48	0.29	0.26	0.07	0.87
RN1G056630.1	RKF3 protein kinase	0.37	0.42	0.41	0.21	0.52	0.01
RN8G017870.1	U-Box-group-II E3 ubiquitin ligase	0.71	0.34	0.67	0.03	-0.14	0.33
RN1G020140.1	U-Box-group-II E3 ubiquitin ligase	-0.56	0.61	-0.24	0.47	0.43	0.04
RN2G053850.1	bZIP class-A transcription factor	0.37	0.49	0.49	0.08	0.10	0.71
RN3G023210.1	bZIP class-A transcription factor	0.18	0.73	-0.13	0.68	0.27	0.14
RN3G055830.1	bZIP class-A transcription factor	-0.65	0.21	-0.97	***0.01*** *	-0.64	0.00
RN1G042680.1	bZIP class-A transcription factor	-0.35	0.61	-1.08	0.08	-0.78	0.01
RN4G050400.1	bZIP class-A transcription factor	0.66	0.21	1.51	***0.003*** **	1.68	0.00
RN4G050400.2	bZIP class-A transcription factor	0.66	0.21	1.51	***0.003*** **	NA	NA
RN1G042680.2	bZIP class-A transcription factor	-0.34	0.61	-1.09	0.08	-0.41	0.02
RN1G057350.1	bZIP class-A transcription factor	0.43	0.42	0.51	0.12	0.69	0.00
RN4G063250.1	bZIP class-A transcription factor	0.99	0.27	0.77	***0.01*** *	0.30	0.11

RN3G001770.1	bZIP class-A transcription factor	-2.54	0.12	-3.10	***0.02****	NA		NA	
RN4G044370.1	bZIP class-A transcription factor	-1.46	0.14	-0.53	0.13	0.31			0.32
RN5G022090.1	bZIP class-A transcription factor	-3.39	0.33	0.43	0.36	NA		NA	
RN5G033930.1	bZIP class-C transcription factor	-0.36	0.42	0.06	0.82	NA		NA	
RN5G033930.2	bZIP class-C transcription factor	-0.36	0.42	0.06	0.81	0.36			0.11
RN5G042710.1	bZIP class-C transcription factor	1.45	0.16	0.38	0.34	-1.50			0.18
RN6G049490.1	bZIP class-C transcription factor	0.73	0.27	0.54	***0.04****	NA		NA	
RN2G048900.1	bZIP class-G transcription factor	0.53	0.21	0.47	***0.03****	-0.03			0.83
RN1G005870.1	bZIP class-G transcription factor	0.79	0.23	1.47	***0.001****	0.51			0.00
RN4G048040.1	bZIP class-G transcription factor	-0.05	0.90	0.74	***0.007****	NA		NA	
RN5G016410.1	bZIP class-G transcription factor	0.41	0.43	2.32	***0.001****	0.03			0.87
RN6G025430.2	bZIP class-G transcription factor	0.28	0.62	0.58	0.14	NA		NA	
RN6G025430.3	bZIP class-G transcription factor	0.26	0.63	0.54	0.15	-0.42			0.33
RN1G001960.1	bZIP class-G transcription factor	0.57	0.59	0.85	0.19	NA		NA	
RN4G035010.1	bZIP class-I transcription factor	0.56	0.35	-1.00	***0.005****	-0.61			0.00
RN1G048070.1	bZIP class-I transcription factor	-0.30	0.41	-0.43	0.09	0.15			0.13
RN4G045860.1	bZIP class-I transcription factor	-0.01	0.99	-0.03	0.91	0.28			0.07
RN6G036800.1	bZIP class-I transcription factor	0.33	0.54	-0.11	0.65	0.23			0.14
RN6G000310.1	bZIP class-I transcription factor	0.00	1.00	-2.92	***0.001****	-0.84			0.01
RN4G062950.1	bZIP class-I transcription factor	0.37	0.48	0.97	***0.004****	0.69			0.00
RN1G056310.1	bZIP class-L transcription factor	0.44	0.46	0.09	0.69	-0.25			0.17
RN1G016010.1	bZIP class-S/SE transcription factor	0.00	1.00	-2.05	***0.01****	NA		NA	
RN7G017050.1	bZIP class-S/SE transcription factor	0.00	1.00	0.77	0.16	NA		NA	
RN2G030010.1	bZIP class-S/SE transcription factor	0.29	0.59	0.45	***0.03****	0.41			0.17
RN2G038420.1	bZIP class-S/SE transcription factor	1.13	0.50	2.18	***0.001****	0.27			0.22
RN5G016370.1	HD-ZIP I/II-type transcription factor	0.26	0.90	1.06	***0.005****	NA		NA	
RN5G016380.1	HD-ZIP I/II-type transcription factor	-0.77	0.80	1.21	***0.008****	NA		NA	
RN1G019330.1	HD-ZIP I/II-type transcription factor	0.33	0.57	-0.92	0.06	0.08			0.56
RN8G035700.1	HD-ZIP I/II-type transcription factor	-0.61	0.68	-1.23	0.18	NA		NA	
RN7G022150.1	HD-ZIP I/II-type transcription factor	-2.91	0.14	-2.64	***0.001****	0.13			0.49
RN3G036870.1	HD-ZIP I/II-type transcription factor	-1.96	0.38	-1.18	0.05	0.00			0.99
RN4G055920.1	HD-ZIP I/II-type transcription factor	-2.75	0.59	-1.31	0.22	NA		NA	
RN5G013560.1	HD-ZIP I/II-type transcription factor	0.62	0.28	0.11	0.65	-0.02			0.94
RN6G013540.1	HD-ZIP I/II-type transcription factor	-0.85	0.27	0.37	0.48	0.29			0.21
RN1G007550.1	HD-ZIP I/II-type transcription factor	0.18	0.86	1.72	***0.03****	0.31			0.16
RN3G054100.1	HD-ZIP I/II-type transcription factor	0.02	1.00	0.38	0.24	-0.27			0.24
RN8G004410.1	HD-ZIP IV-type transcription factor	-0.87	0.42	0.05	0.91	-0.33			0.15
RN4G018660.1	HD-ZIP IV-type transcription factor	-2.54	0.34	-1.86	***0.04****	NA		NA	
RN6G017980.1	HD-ZIP IV-type transcription factor	-0.22	0.86	-2.28	0.05	0.07			0.44
RN3G015540.1	HD-ZIP IV-type transcription factor	0.25	0.47	0.84	***0.008****	0.25			0.07
RN8G014480.1	MYB class-R2R3 subgroup-1 transcription factor	0.53	0.50	2.05	***0.04****	0.72			0.00
RN2G012460.1	MYB class-R2R3 subgroup-11 transcription factor	0.49	0.62	-0.16	0.73	1.29			0.00
RN1G066330.1	MYB class-R2R3 subgroup-11 transcription factor	0.06	1.00	0.43	0.63	NA		NA	
RN8G031950.1	MYB class-R2R3 subgroup-11 transcription factor	-0.27	0.93	0.56	0.60	2.23			0.07

RN8G007780.1	MYB class-R2R3 subgroup-19/20 transcription factor	0.89	0.64	0.61	0.48	1.61	0.01
RN2G028720.1	MYB class-R2R3 subgroup-19/20 transcription factor	-0.75	0.60	2.06	***0.004****	NA	NA
RN6G030450.1	MYB class-R2R3 subgroup-19/20 transcription factor	0.62	0.68	0.44	0.34	1.53	0.01
RN5G040330.1	MYB class-R2R3 subgroup-2 transcription factor	-0.60	0.77	-1.32	***0.02****	NA	NA
RN6G050930.1	MYB class-R2R3 subgroup-2 transcription factor	0.69	0.37	0.06	0.93	NA	NA
RN6G050890.1	MYB class-R2R3 subgroup-2 transcription factor	0.41	0.82	-0.30	0.46	NA	NA
RN3G052030.1	MYB class-R2R3 subgroup-22/23 transcription factor	0.72	0.21	0.40	0.10	0.07	0.76
RN4G050010.1	MYB class-R2R3 subgroup-22/23 transcription factor	0.72	0.75	-3.53	***0.002****	-1.38	0.00
RN1G061460.1	MYB class-R2R3 subgroup-22/23 transcription factor	1.94	0.26	2.78	***0.002****	1.63	0.04
RN5G011130.1	MYB class-R2R3 subgroup-22/23 transcription factor	0.31	0.57	0.29	0.29	1.22	0.00
RN4G033590.1	MYB class-R2R3 subgroup-22/23 transcription factor	0.32	0.41	0.81	***0.007****	0.40	0.07
RN3G050010.1	MYB class-R2R3 transcription factor *(AS1)	0.42	0.45	0.29	0.50	-0.17	0.09
RN7G022170.1	MYB class-R2R3 transcription factor *(FLP/MYB88)	-0.84	0.39	-1.21	***0.02****	0.12	0.52
RN1G016490.1	MYB class-R2R3 transcription factor *(MYB20/42/43/85)	0.92	0.35	1.00	***0.009****	0.18	0.68
RN1G006190.1	MYB class-R2R3 transcription factor *(MYB20/42/43/85)	0.27	0.89	1.62	***0.001****	-1.07	0.02
RN1G025340.1	MYB class-R2R3 transcription factor *(MYB46/83)	0.00	1.00	-2.00	***0.01****	NA	NA
RN3G029000.1	MYB class-R2R3 transcription factor *(MYB46/83)	1.86	0.32	-0.40	0.59	-1.02	0.16
RN1G027240.1	MYB class-R2R3 transcription factor *(MYB5)	0.18	0.77	0.60	***0.02****	0.38	0.03
RN7G031950.1	MYB class-R2R3 transcription factor *(MYB82)	0.82	0.40	-3.33	***0.003****	NA	NA
RN6G039270.1	R0R1R2R3-MYB transcription factor	0.60	0.27	-0.05	0.91	-0.15	0.82
RN6G039270.2	R0R1R2R3-MYB transcription factor	0.72	0.22	-0.06	0.88	0.49	0.24
RN5G029040.1	R1R2R3-MYB transcription factor	0.01	1.00	-1.49	***0.005****	-1.32	0.00
RN6G029240.1	R1R2R3-MYB transcription factor	0.56	0.53	1.06	0.17	0.08	0.91
RN5G006450.1	SnRK2 SNF1-related protein kinase	-1.18	0.18	-0.29	0.70	1.00	0.00
RN5G008330.1	SnRK2 SNF1-related protein kinase	0.23	0.54	0.05	0.86	0.01	0.95
RN4G060490.1	SnRK2 SNF1-related protein kinase	0.29	0.54	0.95	***0.01****	0.21	0.12
RN1G009320.1	SnRK2 SNF1-related protein kinase	-1.55	0.09	-0.58	0.10	-0.20	0.53
RN1G043780.1	SnRK2 SNF1-related protein kinase	0.33	0.44	-0.31	0.28	0.05	0.63
RN4G059370.1	regulatory protein *(FLZ) of SnRK1 complex	-2.15	0.13	-1.39	***0.008****	-0.56	0.02
RN5G004920.1	regulatory protein *(FLZ) of SnRK1 complex	-1.26	0.13	-1.99	***0.002****	-0.08	0.81
RN6G041530.1	regulatory protein *(FLZ) of SnRK1 complex	0.08	0.91	-0.91	***0.02****	0.35	0.16
RN1G049510.1	regulatory protein *(FLZ) of SnRK1 complex	0.33	0.93	-0.22	0.94	NA	NA
RN4G001540.1	regulatory protein *(FLZ) of SnRK1 complex	0.46	0.43	0.69	***0.01****	1.17	0.00
RN6G048620.1	regulatory protein *(FLZ) of SnRK1 complex	-0.18	0.91	0.77	0.34	0.22	0.65
RN6G024420.1	subgroup ERF-I transcription factor	0.11	0.93	0.38	0.58	0.25	0.29
RN4G059470.1	subgroup ERF-I transcription factor	0.03	1.00	0.35	0.14	0.22	0.11
RN5G005020.1	subgroup ERF-I transcription factor	0.65	0.36	1.27	***0.001****	-0.25	0.16
RN1G067630.1	subgroup ERF-I transcription factor	0.05	1.00	0.73	0.10	0.67	0.15
RN2G025820.1	subgroup ERF-I transcription factor	1.25	0.47	-1.06	0.20	NA	NA
RN5G010760.1	subgroup ERF-II-DEAR transcription factor	1.05	0.28	-0.83	***0.009****	-0.07	0.81
RN3G031160.1	subgroup ERF-IV/DREB2 transcription factor	1.10	0.47	1.34	0.16	0.81	0.31
RN4G030260.1	subgroup ERF-IV/DREB2 transcription factor	0.15	0.95	1.42	***0.02****	2.71	0.12
RN5G040070.1	subgroup ERF-IX transcription factor	-1.69	0.52	-1.73	0.06	NA	NA
RN6G050810.1	subgroup ERF-IX transcription factor	1.04	0.39	0.46	0.56	NA	NA

RN1G008250.1	subgroup ERF-IX transcription factor	-0.93	0.38	0.62	0.05	-0.78	0.00
RN6G031930.1	subgroup ERF-IX transcription factor	-0.91	0.58	-1.48	0.04*	NA	NA
RN6G013790.1	subgroup ERF-IX transcription factor	0.61	0.20	1.23	***0.001****	NA	NA
RN1G008190.1	subgroup ERF-IX transcription factor	0.27	0.73	1.43	***0.04****	0.63	0.07
RN1G008210.1	subgroup ERF-IX transcription factor	0.32	0.67	1.46	***0.04****	0.27	0.41
RN1G008240.1	subgroup ERF-IX transcription factor	0.03	1.00	1.86	***0.03****	0.05	0.91
RN4G025010.1	subgroup ERF-IX transcription factor	-1.26	0.26	1.03	0.16	0.39	0.49
RN4G025020.1	subgroup ERF-IX transcription factor	0.08	0.97	1.57	***0.01****	0.97	0.06
RN6G031860.1	subgroup ERF-IX transcription factor	-3.41	0.50	-0.81	0.58	NA	NA
RN6G050780.1	subgroup ERF-IX transcription factor	0.00	1.00	-2.30	0.28	NA	NA
RN6G050800.1	subgroup ERF-IX transcription factor	0.00	1.00	-1.63	0.29	NA	NA
RN6G031840.1	subgroup ERF-IX transcription factor	0.06	1.00	-4.13	***0.03****	NA	NA
RN2G022680.1	subgroup ERF-IX transcription factor	0.16	0.96	2.21	***0.008****	1.37	0.02
RN4G024960.1	subgroup ERF-IX transcription factor	-0.47	0.47	-0.12	0.77	-0.95	0.00
RN4G014400.1	subgroup ERF-VI transcription factor	-0.85	0.70	-1.76	***0.02****	-1.27	0.10
RN6G025340.1	subgroup ERF-VI transcription factor	0.39	0.43	0.24	0.44	-0.36	0.30
RN1G005820.1	subgroup ERF-VI transcription factor	0.73	0.20	0.57	0.11	0.25	0.71
RN7G008170.1	subgroup ERF-VI transcription factor	-0.41	0.58	0.60	***0.03****	0.12	0.49
RN8G008340.1	subgroup ERF-VI transcription factor	-0.60	0.46	1.22	***0.003****	0.63	0.05
RN6G000190.1	subgroup ERF-VI transcription factor	0.19	0.58	1.10	***0.004****	0.33	0.26
RN7G028790.1	subgroup ERF-VII transcription factor	0.72	0.28	0.37	0.11	0.44	0.00
RN7G028790.2	subgroup ERF-VII transcription factor	0.72	0.28	0.37	0.11	NA	NA
RN2G037730.1	subgroup ERF-VII transcription factor	-0.54	0.30	-0.65	***0.04****	0.33	0.01
RN2G015340.1	subgroup ERF-VIII transcription factor	0.02	0.99	-0.33	0.34	-0.58	0.02
RN6G049920.1	subgroup ERF-VIII transcription factor	0.07	0.97	0.08	0.92	0.94	0.05
RN1G063510.1	subgroup ERF-VIII transcription factor	0.62	0.38	0.89	***0.006****	0.27	0.01
RN8G027720.1	subgroup ERF-VIII transcription factor	0.39	0.36	0.97	***0.005****	0.30	0.05
RN2G015350.1	subgroup ERF-VIII transcription factor	0.78	0.43	0.88	***0.007****	-0.60	0.00
RN8G034570.1	subgroup ERF-VIII transcription factor	0.00	1.00	0.75	0.12	0.52	0.03
RN1G042490.1	subgroup ERF-X transcription factor	0.34	0.91	2.22	***0.04****	0.08	0.92
RN1G042500.1	subgroup ERF-X transcription factor	0.34	0.91	2.22	***0.04****	NA	NA
RN5G009510.1	subgroup ERF-X transcription factor	-1.10	0.20	-0.90	0.10	NA	NA
RN5G009520.1	subgroup ERF-X transcription factor	-1.69	0.10	-1.39	***0.03****	NA	NA
RN5G009540.1	subgroup ERF-X transcription factor	-1.53	0.13	-1.17	0.12	NA	NA
RN5G009560.1	subgroup ERF-X transcription factor	-0.74	0.59	0.25	0.76	NA	NA
RN3G000430.1	subgroup ERF-X transcription factor	1.08	0.27	1.47	***0.01****	1.78	0.00
RN8G024660.1	subgroup ERF-X transcription factor	0.78	0.47	-0.18	0.87	NA	NA
RN4G061880.1	subgroup ERF-X transcription factor	0.50	0.83	1.92	0.04	2.21	0.01
RN4G022780.1	regulatory co-chaperone *(BAG7) of S1P/S2P-bZIP17/28 pathway	1.31	0.29	-0.34	0.16	NA	NA
RN4G022780.2	regulatory co-chaperone *(BAG7) of S1P/S2P-bZIP17/28 pathway	1.31	0.29	-0.34	0.16	-0.84	0.00
RN2G032820.1	regulatory E3 ubiquitin ligase *(PIR) of IRE1-bZIP60 pathway	0.77	0.20	0.51	0.05	0.26	0.06
RN6G046940.1	regulatory E3 ubiquitin ligase *(PIR) of IRE1-bZIP60 pathway	-1.75	0.22	0.25	0.71	0.24	0.45
RN6G022390.1	regulatory mediator of IRE1-bZIP60 UPR pathway	0.20	0.85	-0.59	0.08	0.39	0.40
RN1G071010.1	regulatory mediator of IRE1-bZIP60 UPR pathway	0.00	1.00	-5.52	***0.02****	NA	NA

RN2G021690.1	regulatory mediator of IRE1-bZIP60 UPR pathway	-1.91	0.75	-5.13	***0.02****	NA	NA	
RN5G051810.1	regulatory mediator of IRE1-bZIP60 UPR pathway	0.41	0.63	-0.41	0.65	0.29		0.05
RN2G018430.1	regulatory mediator of IRE1-bZIP60 UPR pathway	0.34	0.72	0.49	0.12	0.22		0.63
RN7G029220.1	PSY peptide receptor *(PSY-R)	-0.26	0.85	-1.33	0.06	-0.47		0.23
RN3G055010.1	transcription factor *(bZIP17/28)	0.48	0.28	0.51	0.02	0.32		0.04
RN2G040460.1	transcription factor *(CBF/DREB1)	0.21	0.94	0.29	0.81	NA	NA	
RN2G040500.1	transcription factor *(CBF/DREB1)	-0.21	0.91	0.63	0.30	0.48		0.46
RN4G019420.1	transcription factor *(CBF/DREB1)	-0.10	0.98	2.03	0.05	NA	NA	
RN2G040520.1	transcription factor *(CBF/DREB1)	-0.52	0.83	-0.06	0.94	NA	NA	
RN4G014400.1	transcription factor *(CRF)	-0.85	0.70	-1.76	***0.02****	-1.27		0.10
RN6G025340.1	transcription factor *(CRF)	0.39	0.43	0.24	0.44	-0.36		0.30
RN1G005820.1	transcription factor *(CRF)	0.73	0.20	0.57	0.11	0.25		0.71
RN7G008170.1	transcription factor *(CRF)	-0.41	0.58	0.60	***0.03****	0.12		0.49
RN8G008340.1	transcription factor *(CRF)	-0.60	0.46	1.22	***0.003****	0.63		0.05
RN1G062740.1	brassinosteroid co-receptor protein kinase *(BAK/SERK)	0.43	0.25	0.05	0.88	0.21		0.07
RN1G062720.1	brassinosteroid co-receptor protein kinase *(BAK/SERK)	0.25	0.61	0.05	0.90	-0.10		0.88
RN1G041860.1	pythosulfokine peptide receptor *(PSKR)	0.35	0.68	-0.49	0.45	NA	NA	
RN7G013130.1	pythosulfokine peptide receptor *(PSKR)	0.40	0.37	0.62	***0.01****	0.10		0.50
RN8G034340.1	pythosulfokine peptide receptor *(PSKR)	1.34	0.12	0.38	0.370	0.29		0.06
RN4G023740.1	TDIF-peptide receptor *(PXY)	-1.60	0.21	-0.92	***0.04****	-1.04		0.00
RN3G007350.1	MAP2K protein kinase	0.70	0.27	0.23	0.256	0.02		0.89
RN5G010030.1	MAP3K-MEKK protein kinase	-2.08	0.08	-0.14	0.803	0.13		0.70
RN5G048220.1	MAPK-kinase protein kinase *(NPK/ANP)	1.15	0.38	-1.22	***0.02****	-1.08		0.27
RN6G042750.1	MAPK-kinase protein kinase *(NPK/ANP)	0.82	0.65	-2.79	***0.001****	NA	NA	
RN4G017130.1	MAPKK-kinase protein kinase *(YDA)	-0.10	0.89	0.67	0.08	0.13		0.27
RN2G016520.1	MAPKK-kinase protein kinase *(YDA)	-0.43	0.43	-0.44	0.16	NA	NA	
RN8G015700.1	MAPKK-kinase protein kinase *(YDA)	-0.12	0.85	-0.35	0.26	0.48		0.49
RN1G018720.1	MAPKKK-kinase protein kinase *(TOT3)	0.22	0.62	0.28	0.24	0.12		0.31
RN7G025300.1	MAPKKK-kinase protein kinase *(TOT3)	0.08	0.89	0.40	0.05	0.31		0.04
RN8G010100.1	transcriptional regulator *(AP1/CAL/FUL) of floral meristem identity	0.29	0.59	0.44	0.25	-0.13		0.29
RN1G012270.1	transcriptional regulator *(AP1/CAL/FUL) of floral meristem identity	-0.46	0.52	-0.75	0.08	-0.03		0.94
RN3G024010.1	CDPK protein kinase	0.19	0.59	-0.14	0.53	-0.28		0.01
RN3G024010.2	CDPK protein kinase	0.19	0.59	-0.14	0.53	NA	NA	
RN3G024010.3	CDPK protein kinase	0.20	0.58	-0.14	0.53	NA	NA	
RN3G057250.1	CDPK protein kinase	-0.67	0.41	0.18	0.75	0.19		0.43
RN6G026020.1	CDPK protein kinase	-0.02	0.99	-0.28	0.22	-0.28		0.02
RN8G028510.1	CDPK protein kinase	0.89	0.27	0.24	0.34	0.12		0.26
RN3G057110.1	CDPK protein kinase	0.53	0.38	-0.56	0.15	-0.40		0.01
RN2G009670.1	CDPK protein kinase	0.46	0.35	0.63	0.04	0.10		0.65
RN5G020920.1	CDPK protein kinase	0.51	0.19	-0.42	0.08	0.31		0.01
RN4G043980.1	CDPK protein kinase	-0.01	1.00	-0.46	0.20	-0.23		0.34
RN3G039080.1	CDPK protein kinase	0.46	0.66	0.60	0.05	0.15		0.29
RN4G053220.1	CDPK protein kinase	0.11	0.85	-0.35	0.16	NA	NA	
RN1G051580.1	CDPK protein kinase	0.39	0.27	0.09	0.61	0.02		0.83

RN1G025100.1	CDPK protein kinase	0.61	0.22	0.64	***0.008***	0.05		0.70
RN3G055230.1	CDPK protein kinase	-0.68	0.32	-0.54	0.06	0.27		0.04
RN1G043640.1	CDPK protein kinase	-0.59	0.31	-1.26	***0.002***	NA		NA
RN5G008650.1	CDPK protein kinase	-0.02	0.98	-0.66	***0.03***	-0.13		0.17
RN2G008920.1	DUF26 protein kinase	0.52	0.70	-0.78	0.54	-2.02		0.00
RN2G010680.1	DUF26 protein kinase	0.39	0.67	-0.17	0.74	NA		NA
RN2G010730.1	DUF26 protein kinase	-0.24	0.64	-0.40	0.29	NA		NA
RN2G010740.1	DUF26 protein kinase	0.30	0.69	-0.26	0.48	NA		NA
RN2G010750.1	DUF26 protein kinase	-0.36	0.45	-0.94	***0.02***	0.21		0.76
RN2G010800.1	DUF26 protein kinase	-0.33	0.56	-0.78	0.10	0.39		0.50
RN2G010820.1	DUF26 protein kinase	-1.42	0.16	0.72	0.15	0.40		0.24
RN2G010890.1	DUF26 protein kinase	-0.45	0.78	2.09	***0.04***	0.06		0.91
RN2G010910.1	DUF26 protein kinase	-0.56	0.59	-0.41	0.57	-0.61		0.27
RN2G011000.1	DUF26 protein kinase	-1.56	0.39	-1.37	0.10	-0.82		0.12
RN2G011020.1	DUF26 protein kinase	-0.64	0.49	0.14	0.80	NA		NA
RN2G011050.1	DUF26 protein kinase	-0.23	0.85	-0.03	0.96	-0.22		0.48
RN2G011060.2	DUF26 protein kinase	-0.25	0.86	-0.17	0.81	-0.13		0.53
RN2G011070.1	DUF26 protein kinase	-0.12	0.94	-0.08	0.90	-0.09		0.56
RN2G011080.1	DUF26 protein kinase	-1.12	0.23	-0.97	0.11	-0.66		0.35
RN2G011100.1	DUF26 protein kinase	-1.82	0.36	-0.82	0.28	NA		NA
RN2G011140.1	DUF26 protein kinase	-0.48	0.59	-0.36	0.51	-0.60		0.27
RN3G012070.1	DUF26 protein kinase	-1.31	0.13	-0.23	0.40	0.71		0.00
RN3G058390.1	DUF26 protein kinase	-1.00	0.11	-0.21	0.49	0.17		0.15
RN2G038490.1	DUF26 protein kinase	1.12	0.19	0.30	0.25	0.25		0.06
RN8G019550.2	DUF26 protein kinase	0.57	0.42	0.26	0.62	1.73		0.28
RN8G019570.1	DUF26 protein kinase	0.58	0.24	0.52	0.14	1.22		0.00
RN2G008970.1	DUF26 protein kinase	-0.23	0.73	-0.53	0.11	NA		NA
RN2G010710.1	DUF26 protein kinase	-0.04	0.95	-0.49	0.12	0.83		0.02
RN2G010720.1	DUF26 protein kinase	-0.32	0.49	-0.83	***0.03***	-0.14		0.87
RN2G010760.1	DUF26 protein kinase	-0.78	0.20	-0.43	0.28	0.08		0.87
RN2G010790.1	DUF26 protein kinase	-0.57	0.28	-0.94	***0.03***	-0.09		0.70
RN3G058400.1	DUF26 protein kinase	-2.77	0.11	-1.28	***0.006***	NA		NA
RN5G047110.1	bHLH class-Ia transcription factor	-1.91	0.50	-2.61	***0.002***	NA		NA
RN4G060720.1	bHLH class-Ia transcription factor	-2.11	0.29	-1.89	***0.003***	-2.07		0.00
RN6G019670.1	bHLH class-IIIf transcription factor	-0.75	0.22	-0.95	***0.03***	-0.32		0.03
RN6G028220.1	bHLH class-IIIf transcription factor	-1.15	0.24	-1.22	***0.01***	0.18		0.09
RN1G039420.1	bHLH class-IVa transcription factor	0.19	0.83	0.06	0.94	0.52		0.66
RN1G039420.2	bHLH class-IVa transcription factor	0.21	0.81	0.12	0.88	2.21		0.14
RN5G014000.1	bHLH class-IVa transcription factor	1.08	0.53	-2.14	***0.005***	NA		NA
RN1G022490.1	bHLH class-IVb transcription factor	0.46	0.51	0.74	***0.02***	-0.25		0.05
RN8G014800.1	bHLH class-IVb transcription factor	0.52	0.42	0.64	***0.04***	1.50		0.01
RN8G014800.2	bHLH class-IVb transcription factor	0.61	0.39	0.71	***0.02***	0.05		0.84
RN5G040060.1	bHLH class-IVc transcription factor	-0.25	0.72	-1.29	***0.006***	-0.76		0.00
RN6G031740.1	bHLH class-IVc transcription factor	0.44	0.62	-0.08	0.81	-0.18		0.73

RN1G065390.1	bHLH class-IVc transcription factor	-2.13	0.10	-1.48	***0.002***	-0.51		0.15
RN2G011150.1	bHLH class-IVc transcription factor	-0.44	0.32	-0.39	0.06	NA		NA
RN2G031040.1	bHLH class-IVc transcription factor	-0.15	0.89	-0.01	0.98	NA		NA
RN4G025910.1	bHLH class-IVc transcription factor	0.17	0.84	0.11	0.82	NA		NA
RN8G030760.1	bHLH class-IVc transcription factor	0.44	0.28	0.00	0.99	0.00		0.99
RN5G040050.1	bHLH class-IVc transcription factor	0.75	0.40	-1.17	***0.04***	NA		NA
RN8G009630.1	bHLH class-Va transcription factor	0.83	0.16	0.69	***0.02***	-0.72		0.00
RN2G021870.1	bHLH class-Vb transcription factor	0.21	0.61	-1.05	***0.007***	0.14		0.54
RN4G046750.1	bHLH class-X transcription factor	1.30	0.08	-1.64	***0.001***	NA		NA
RN8G030180.1	bHLH class-X transcription factor	0.82	0.43	-0.58	0.44	NA		NA
RN8G030180.2	bHLH class-X transcription factor	0.82	0.43	-0.58	0.44	0.59		0.31
RN8G030180.3	bHLH class-X transcription factor	0.82	0.43	-0.58	0.44	NA		NA
RN4G003070.1	bHLH class-XI/LRL transcription factor	-0.68	0.22	0.75	***0.01***	-0.03		0.88
RN7G038630.1	bHLH class-XI/LRL transcription factor	0.92	0.12	-0.69	***0.02***	0.44		0.58
RN7G038630.2	bHLH class-XI/LRL transcription factor	1.04	0.11	-0.69	***0.02***	-0.35		0.89
RN5G042640.1	bHLH class-XI/LRL transcription factor	-0.03	0.98	-1.02	***0.009***	NA		NA
RN6G039890.1	bHLH class-XI/LRL transcription factor	-0.14	0.82	0.24	0.49	NA		NA
RN6G039890.2	bHLH class-XI/LRL transcription factor	-0.15	0.82	0.24	0.48	0.44		0.02
RN6G049530.1	bHLH class-XI/LRL transcription factor	-0.11	0.90	0.60	0.10	0.39		0.01
RN2G024240.1	bHLH class-XII transcription factor	-0.01	1.00	-1.13	***0.02***	0.00		1.00
RN4G056130.1	bHLH class-XII transcription factor	0.03	0.99	-0.89	***0.01***	-0.40		0.07
RN4G061140.1	bHLH class-XIV/SACL transcription factor	0.82	0.11	-0.58	***0.04***	0.08		0.60
RN7G022120.1	bHLH class-XV/PRE transcription factor	-5.62	0.13	-3.43	***0.007***	-0.85		0.07
RN1G005500.1	transcription factor *(WRKY)	1.20	0.37	-0.07	0.88	-0.27		0.43
RN3G033490.1	transcription factor *(WRKY)	-2.46	0.08	-0.02	0.97	-0.92		0.34
RN5G036700.1	transcription factor *(WRKY)	0.31	0.53	0.80	***0.03***	0.12		0.39
RN8G043210.1	transcription factor *(WRKY)	0.18	0.67	0.25	0.27	0.60		0.00
RN8G043210.2	transcription factor *(WRKY)	0.17	0.67	0.25	0.27	NA		NA
RN7G020370.1	transcription factor *(WRKY)	0.40	0.32	0.81	***0.009***	0.94		0.00
RN1G014450.1	transcription factor *(WRKY)	0.92	0.23	1.18	***0.006***	0.32		0.01
RN2G027180.1	transcription factor *(WRKY)	0.54	0.61	0.84	***0.03***	0.85		0.00
RN2G029220.1	transcription factor *(WRKY)	-0.22	0.66	0.29	0.24	1.10		0.02
RN3G048380.1	transcription factor *(WRKY)	-0.26	0.60	-0.84	***0.01***	0.89		0.02
RN6G000650.1	transcription factor *(WRKY)	0.25	0.84	1.13	***0.02***	0.62		0.00
RN4G045650.1	NAC transcription factor	0.55	0.25	0.43	0.05	0.00		0.99
RN4G045660.1	NAC transcription factor	-0.16	0.90	-0.05	0.90	0.46		0.71
RN4G045660.2	NAC transcription factor	-0.16	0.90	-0.05	0.90	NA		NA
RN1G062860.1	NAC transcription factor	1.29	0.56	-2.34	***0.02***	NA		NA
RN5G002330.1	NAC transcription factor	0.83	0.53	3.00	***0.005***	NA		NA
RN4G054270.1	NAC transcription factor	0.72	0.28	0.58	***0.01***	NA		NA
RN4G051370.1	NAC transcription factor	0.92	0.42	1.80	***0.004***	0.58		0.01
RN5G002980.1	NAC transcription factor	-0.87	0.50	0.76	0.30	0.28		0.31
RN7G021080.1	NAC transcription factor	1.39	0.26	1.98	***0.002***	3.56		0.00
RN1G003970.1	NAC transcription factor	0.00	1.00	-0.69	0.40	NA		NA

RN1G003970.2	NAC transcription factor	1.89	0.50	-0.69	0.40	-1.30	0.17
RN8G004520.1	NAC transcription factor	0.94	0.49	-0.87	0.08	-0.04	0.96
RN8G040780.1	NAC transcription factor	2.02	0.48	-1.50	0.04	NA	NA
RN2G048420.1	NAC transcription factor	-3.11	0.11	-1.40	***0.02****	-0.07	0.92
RN2G023050.1	NAC transcription factor	0.05	0.89	-0.36	0.11	NA	NA
RN8G001700.1	NAC transcription factor	-0.04	0.96	-0.94	***0.008****	-1.25	0.45
RN1G000050.1	NAC transcription factor	0.44	0.50	1.08	***0.005****	1.11	0.04
RN1G000050.2	NAC transcription factor	0.33	0.61	1.14	***0.008****	0.91	0.18
RN3G001230.1	NAC transcription factor	0.96	0.43	0.41	0.38	-0.09	0.68
RN8G023880.1	NAC transcription factor	0.00	1.00	-0.87	0.16	-1.83	0.05
RN4G026160.1	NAC transcription factor	0.85	0.26	1.21	***0.03****	NA	NA
RN8G033090.1	NAC transcription factor	0.77	0.68	1.86	***0.03****	2.08	0.00
RN2G013620.1	NAC transcription factor	0.01	1.00	-0.12	0.78	NA	NA
RN2G023020.1	NAC transcription factor	-0.26	0.89	-0.69	0.34	0.59	0.23
RN6G006360.1	NAC transcription factor	-1.13	0.60	-0.89	0.14	NA	NA
RN8G033080.1	NAC transcription factor	0.40	0.57	1.71	***0.004****	1.11	0.12
RN4G063830.1	NAC transcription factor	-4.18	0.34	-4.13	***0.008****	NA	NA
RN2G043430.1	NAC transcription factor	0.20	0.65	0.64	***0.02****	0.37	0.00
RN7G004110.1	NAC transcription factor	0.16	0.74	-0.30	0.31	NA	NA
RN7G004890.1	NAC transcription factor	-0.08	0.92	-0.25	0.56	NA	NA
RN1G004350.1	NAC transcription factor	-6.05	0.08	-1.73	***0.002****	-1.64	0.17
RN1G004350.3	NAC transcription factor	-4.05	0.08	-1.72	***0.002****	NA	NA
RN7G005630.1	NAC transcription factor	0.20	0.52	0.64	***0.01****	-0.03	0.93
RN1G015140.1	NAC transcription factor	0.49	0.67	2.28	***0.001****	1.37	0.00
RN8G008070.1	NAC transcription factor	1.19	0.52	0.13	0.77	NA	NA
RN8G013610.1	NAC transcription factor	0.30	0.72	1.37	***0.02****	2.31	0.00
RN4G050760.1	NAC transcription factor	0.82	0.31	0.67	***0.01****	0.80	0.00
RN3G034560.1	NAC transcription factor	0.38	0.84	1.17	***0.03****	1.06	0.02
RN4G048170.1	NAC transcription factor	-0.27	0.61	0.70	***0.02****	0.05	0.75
RN5G051000.1	C2H2 class-Di19 transcription factor	0.56	0.31	1.14	***0.001****	0.50	0.00
RN2G015440.1	C2H2 class-Di19 transcription factor	0.67	0.26	0.93	***0.01****	0.09	0.50
RN2G037370.1	C2H2 class-Di19 transcription factor	0.47	0.45	1.04	***0.004****	NA	NA
RN6G043390.1	C2H2 class-Di19 transcription factor	0.12	0.87	0.20	0.49	NA	NA
RN6G043390.2	C2H2 class-Di19 transcription factor	0.12	0.87	0.20	0.48	0.09	0.50
RN3G000170.1	C2H2 class-IDD/IDZ transcription factor	1.32	0.55	-1.50	0.05	NA	NA
RN5G016470.1	C2H2 class-IDD/IDZ transcription factor	0.78	0.21	0.68	***0.02****	0.48	0.01
RN6G045540.1	C2H2 class-IDD/IDZ transcription factor	0.20	0.84	0.01	0.98	NA	NA
RN1G069780.1	C2H2 class-IDD/IDZ transcription factor	0.36	0.73	-1.02	***0.03****	-0.80	0.03
RN5G005470.1	C2H2 class-STOP transcription factor	0.29	0.48	0.59	***0.02****	-0.26	0.21
RN3G031060.1	receptor component *(PYL/RCAR) of cytoplasm-localized abscisic acid receptor complex	-0.61	0.49	-3.00	***0.003****	-3.67	0.00
RN4G030230.1	receptor component *(PYL/RCAR) of cytoplasm-localized abscisic acid receptor complex	0.00	1.00	-4.81	***0.004****	NA	NA
RN4G030240.1	receptor component *(PYL/RCAR) of cytoplasm-localized abscisic acid receptor complex	1.91	0.64	-4.94	***0.01****	NA	NA
RN4G014070.1	receptor component *(PYL/RCAR) of cytoplasm-localized abscisic acid receptor complex	-0.56	0.27	-0.87	***0.004****	0.02	0.95
RN6G024490.1	receptor component *(PYL/RCAR) of cytoplasm-localized abscisic acid receptor complex	0.49	0.26	0.35	0.18	-0.33	0.01

RN1G005390.1	receptor component *(PYL/RCAR) of cytoplasm-localized abscisic acid receptor complex	-0.65	0.35	-0.48	0.12	-0.02	0.94
RN8G015080.1	hydrogen peroxide receptor kinase *(GHR1)	0.00	1.00	-1.60	***0.04****	NA	NA
RN3G034510.1	hydrogen peroxide receptor kinase *(HPCA)	-0.83	0.12	-0.39	0.12	-0.14	0.41
RN1G049800.1	hydrogen peroxide receptor kinase *(HPCA)	-1.40	0.38	-0.42	0.42	1.76	0.44

Supplemental Table S8: Differentially expressed transcripts with metabolic functions under drought stress in *R. nigrum* leaf and root tissue and their MapMan annotations. Genes with enzymatic functions are sorted by their role (TCA cycle; GABA; cysteine and methionine metabolism; alanine, aspartate and glutamate metabolism; valine, leucine and isoleucine metabolism; ABA metabolism). Upregulation (red) and downregulation (blue) according to log_2FC. Significance level of adjusted p values (FDR) shown in bold and marked *FDR < 0.05, **FDR < 0.01 and ***FDR < 0.001. Genes that are not differentially expressed are marked N.e.

			Adult plants				Young plants	
Gene ID	**Mercator annotation**	**Enzyme Name**	**Leaf [log_2FC]**	**Leaf [FDR]**	**Root [log_2FC]**	**Root [FDR]**	**Leaf [log_2FC]**	**Leaf [FDR]**
		Citrate cycle						
RN7G026170.1	ATP citrate (pro-S)-ligase	ACLY	-0.53	0.20	-1.72	***0.0004***	-0.43	***0.004****
RN2G040370.1	ATP citrate (pro-S)-ligase	ACLY	0.02	0.97	-0.02	0.93	0.20	0.07
RN1G064920.1	Aconitase	ACO	1.08	0.22	-0.05	0.91	0.37	***0.01****
RN5G022620.1	Aconitase	ACO	0.49	0.23	-0.03	0.93	-0.14	0.35
RN3G047050.1	Isocitrate dehydrogenase heterodimer subunit 1	IDH3	0.63	0.47	0.48	***0.04****	0.15	0.12
RN1G052020.1	Isocitrate dehydrogenase heterodimer subunit 2	IDH3	0.70	0.56	-0.24	0.68	0.22	0.52
RN5G023840.1	Isocitrate dehydrogenase heterodimer subunit 3	IDH3	0.58	0.35	0.38	0.14	NA	NA
RN5G023840.2	Isocitrate dehydrogenase heterodimer subunit 4	IDH3	0.58	0.35	0.38	0.14	0.06	0.65
RN5G023840.3	Isocitrate dehydrogenase heterodimer subunit 5	IDH3	0.58	0.35	0.38	0.14	0.02	0.95
		GABA						
RN1G036920.1	bifunctional gamma-hydroxybutyrate dehydrogenase and glyoxylate reductase	4HbD	-0.65	0.2258	-1.47	***0.002****	-0.26	***0.04****
RN3G011970.1	bifunctional gamma-hydroxybutyrate dehydrogenase and glyoxylate reductase	4HbD	-0.67	0.2372	-0.04	0.9036	-0.39	***0.002****
RN1G050800.1	GABA pyruvate transaminase	GABAPT	0.62	0.1800	1.15	***0.002****	0.74	***0.00002*****
RN3G004700.1	GABA transporter *(GAT)	GAT	0.79	0.3791	0.84	***0.049****	1.82	***0.002****
RN6G009840.1	GABA transporter *(GAT)	GAT	0.73	0.4061	1.09	***0.02****	1.32	***0.0002*****
RN6G049890.1	GABA transporter *(GAT)	GAT	0.76	0.2773	0.61	0.1954	1.12	0.12
RN6G024940.1	GABA transporter *(GAT)	GAT	0.93	0.4244	-0.64	0.1189	0.04	0.85
RN8G004280.1	glutamate decarboxylase *(GAD)	GAD	-0.06	0.9349	1.73	***0.001****	1.51	***0.00001*****
RN6G036970.1	glutamate decarboxylase *(GAD)	GAD	0.18	0.8026	-1.69	***0.002****	-0.69	***0.005****
RN8G040690.1	Succinate-semialdehyde dehydrogenase (NAD+)	SSADH	-0.85	0.1180	1.40	***0.001****	NA	NA
		Cysteine and methionine metabolism						
RN1G015090.1	cystathionine gamma-synthase	CGS	-0.46	0.2781	-0.43	0.0536	-0.81	***0.0002*****
RN6G048670.1	homocysteine S-methyltransferase	BHMT2	0.44	0.4773	0.94	0.0446	-0.60	***0.007****
RN6G041070.1	homocysteine S-methyltransferase	BHMT2	0.26	0.9142	-0.23	0.5917	-0.24	0.42
RN3G056530.1	5-methyltetrahydropteroyltriglutamate homocysteine methyltransferase	metE	0.48	0.3589	-1.40	***0.002****	-0.83	***0.0006*****
RN6G007400.1	5-methyltetrahydropteroyltriglutamate homocysteine methyltransferase	metE	-0.38	0.4791	-0.12	0.5934	NA	NA

Alanine, aspartate, glutamate metabolism								
RN1G032210.1	Aspartate transaminase	ASAT	0.33	0.5376	0.55	0.0982	0.35	***0.008****
RN5G029070.1	Aspartate transaminase	ASAT	1.20	0.4476	2.07	***0.001****	2.43	***0.00006*****
RN5G029070.2	Aspartate transaminase	ASAT	1.42	0.3776	1.92	***0.001****	1.54	***0.002****
RN7G034560.1	Aspartate transaminase	ASAT	0.30	0.5678	-0.19	0.4119	-0.03	0.87
RN1G072430.1	Aspartate transaminase	ASAT	0.64	0.6529	0.69	***0.04****	NA	NA
RN1G072460.1	Aspartate transaminase	ASAT	0.67	0.6900	1.03	***0.02****	-0.31	0.08
RN7G018010.1	Aspartate transaminase	ASAT	-0.35	0.6447	0.33	0.4343	0.02	0.94
RN1G048120.1	Amidophosphoribosyltransferase	ASE	-1.55	0.1447	0.49	***0.04****	-0.66	***0.0003*****
RN3G000600.1	Aspartate kinase	AK	-0.16	0.7830	-0.20	0.5430	-0.60	0.08
RN3G000600.2	Aspartate kinase	AK	-0.16	0.7830	-0.20	0.5430	-0.08	0.49
RN7G006630.1	aspartate-semialdehyde dehydrogenase	ASD	0.03	0.9695	-0.88	***0.006****	NA	NA
RN7G006630.2	aspartate-semialdehyde dehydrogenase	ASD	0.04	0.9636	-0.88	***0.006****	-1.02	***0.00003*****
RN6G054830.1	aspartate-semialdehyde dehydrogenase	ASD	-1.09	0.1344	-0.37	0.3165	NA	NA
RN6G054850.1	aspartate-semialdehyde dehydrogenase	ASD	-1.20	0.1279	-0.26	0.4218	0.21	0.56
RN4G064160.1	homoserine dehydrogenase	HSD	-0.04	0.9467	-0.30	0.2894	-0.11	0.65
RN1G016670.1	cytosolic glutamine synthetase	GLN1	-0.50	0.3443	-1.10	***0.005****	-0.40	***0.01****
RN1G056170.1	cytosolic glutamine synthetase	GLN1	1.60	0.2184	-3.28	***0.006****	NA	NA
RN1G056200.1	cytosolic glutamine synthetase	GLN1	1.11	0.3466	-2.83	***0.009****	NA	NA
RN2G031700.1	plastidial glutamine synthetase	GLN2	-0.57	0.6926	-2.71	***0.09****	-0.76	***0.00007*****
RN7G026750.1	Glycine transaminase	GGAT	-0.17	0.7874	-1.34	***0.001****	-0.30	***0.02****
RN1G051620.1	Homoserine kinase	HSK	-1.48	0.0903	-0.50	***0.02****	0.40	***0.003****
RN5G001410.1	small subunit *(CarA) of carbamoyl phosphate synthetase heterodimer	small subunit *(CarA) of CPS	-0.39	0.4655	0.11	0.6518	0.01	0.97
RN4G039170.1	large subunit of carbamoyl phosphate synthetase heterodimer	CPS	-0.87	0.1472	-0.46	0.1138	0.30	***0.02****
RN4G039170.2	large subunit of carbamoyl phosphate synthetase heterodimer	CPS	-0.87	0.1451	-0.46	0.1106	NA	NA
RN6G005850.1	large subunit of carbamoyl phosphate synthetase heterodimer	CPS	0.87	0.2024	0.01	0.9698	0.27	***0.03****
RN4G012930.1	NADH-dependent glutamate synthase	NADH-GOGAT	1.27	0.2198	-0.18	0.6010	-0.18	0.22
RN3G032140.1	Alanine aminotransferase	PYD4	-0.12	0.8632	0.01	0.9674	0.35	0.25
RN2G048560.1	serine hydroxymethyltransferase	SHMT	-0.30	0.5633	0.35	***0.09****	0.20	***0.04****
RN2G024860.1	serine hydroxymethyltransferase	SHMT	-0.08	0.8829	-0.86	***0.01****	-0.77	***0.0004*****
RN1G056560.1	serine hydroxymethyltransferase	SHMT	0.60	0.1590	0.04	0.8937	NA	NA
RN4G058830.1	serine hydroxymethyltransferase	SHMT	-0.11	0.8270	0.70	0.0841	0.78	***0.00009*****
RN4G055380.1	serine hydroxymethyltransferase	SHMT	-1.03	0.1224	-0.65	***0.02****	-0.41	***0.006****
RN5G014480.1	serine hydroxymethyltransferase	SHMT	-0.39	0.6461	-1.47	***0.008****	-0.21	0.11
RN6G049510.1	subunit alpha of tryptophan synthase complex	trpA	-1.65	0.0903	-0.81	0.0096	-0.69	***0.0002*****
RN8G029350.1	subunit beta of tryptophan synthase complex	trpB	-0.25	0.4709	0.00	0.9970	-0.28	***0.008****
RN5G040660.1	threonine aldolase	TA	-1.50	0.1076	-1.70	***0.009****	-0.43	***0.02****
RN7G037350.1	threonine synthase	TS	0.29	0.5725	0.87	0.0245	0.34	0.17
RN3G011430.1	threonine synthase	TS	0.20	0.6397	-0.30	0.2117	0.03	0.87
Valine, leucine, isoleucine metabolism								
RN2G016250.1	Acetolactate synthase	ACS	0.31	0.9002	-1.11	***0.09****	0.13	0.70
RN8G023300.1	Acetolactate synthase	ACS	0.27	0.5270	0.60	***0.02****	-0.25	***0.02****
RN5G013510.1	branched-chain-amino-acid transaminase	BCAT	-0.27	0.4894	0.07	0.7688	-0.45	***0.005****

RN4G055960.1	branched-chain-amino-acid transaminase	BCAT	2.30	0.2042	-0.50	0.6475	-1.19	***0.009***
RN4G055970.1	branched-chain-amino-acid transaminase	BCAT	0.60	0.5404	0.30	0.2204	1.66	***0.0002***
RN2G048380.1	branched-chain-amino-acid transaminase	BCAT	0.94	0.1096	-0.14	0.5525	-0.09	0.57
RN1G070810.1	ketol-acid reductoisomerase	KARI	0.03	0.9695	0.70	***0.008***	-0.16	0.28
RN2G026490.1	dihydroxy-acid dehydratase	DAD	-0.10	0.9266	0.23	0.4542	-0.40	***0.01****
RN2G003670.1	threonine dehydratase	TD	0.56	0.4799	-0.32	0.2656	NA	NA
RN2G030520.1	threonine dehydratase	TD	0.73	0.3509	-0.35	0.2094	NA	NA
RN3G041150.1	threonine dehydratase	TD	0.41	0.7224	0.39	0.2947	NA	NA
RN4G019660.1	threonine dehydratase	TD	0.68	0.3983	-0.32	0.2496	-0.37	0.36
RN8G015240.1	threonine dehydratase	TD	0.24	0.8110	-0.19	0.5397	-0.30	0.85
RN3G044350.1	threonine dehydratase	TD	0.51	0.4264	-0.10	0.6987	-0.29	***0.02****
RN6G010130.1	threonine dehydratase	TD	0.00	1.0000	-3.29	***0.0009*****	-0.21	0.50
RN6G010130.2	threonine dehydratase	TD	0.00	1.0000	-3.29	***0.0009*****	-0.30	0.11

Supplemental Table S9: Metabolites in blackcurrant leaf and root tissue for adult and young plants that change in abundance in response to drought stress. Upregulation (red) and downregulation (blue) is shown according to the log2FC of the genes. Significance levels of adjusted p values (FDR) are shown in bold.

	Leaf				Root			
	Adult plants		Young plants		Adult plants		Young plants	
Metabolite	**Log_2FC**	**FDR**	**Log_2FC**	**FDR**	**Log_2FC**	**FDR**	**Log_2FC**	**FDR**
Amino acids								
Alanine	1.09	0.025*	-0.74	0.174	0.18	0.61	1.57	0.04*
Valine	2.23	0.004**	0.66	0.03*	0.83	0.13	1.73	0.04*
Isoleucine	2.57	0.005**	0.75	0.043	1.47	0.07	1.84	0.04*
Proline	2.67	0.015*	0.64	0.03*	0.59	0.23	1.20	0.04*
Serine	0.92	0.056	-0.86	0.199	-0.10	0.23	0.83	0.17
Threonine	2.05	0.003**	0.43	0.049	0.15	0.68	NA	NA
GABA	1.28	0.017*	0.78	0.041*	-0.28	0.61	0.87	0.16
Methionine	2.31	0.015*	-0.01	0.454	-0.78	0.13	0.98	0.16
Glutamic acid	2.12	0.024*	-0.66	0.03*	0.43	0.23	NA	NA
Phenylalanine	2.72	0.009**	1.23	0.021*	0.45	0.13	1.11	0.10
Glutamine	2.86	0.006**	-0.11	0.070	0.05	0.83	1.33	0.16
Tryptophan	3.45	0.004**	-0.06	0.380	NA	NA	NA	NA
Organic acids								
Quinic acid	0.82	0.017*	-0.16	0.199	NA	NA	NA	NA
Citric acid	-1.39	0.047*	-0.10	0.203	-0.90	0.13	0.04	0.24
Sugars & derivatives								
Galactinol	0.62	0.011*	-0.56	0.037*	NA	NA	NA	NA

Supplemental Table S10: Genes were quantified using qRT-PCR, including their functional annotation, corresponding RNA sequences, and primer sequences utilized for amplification.

Gene ID	Enzyme name	Gene Annotation	Primer sequence forward	Primer sequence reverse
RN4G046750	bHLH110	bHLH-X-class transcriptional regulator *(bHLH110)	CATTTGGCCATCCTCCGACT	CGGGAGAGTTGAGGGTCCTA
RN1G036920	4HbD	bifunctional gamma-hydroxybutyrate dehydrogenase	TGTAATCCTTGCTGCTGGGG	TGCTCCATTCCCAACTTCCC
RN4G059370	FLZ	regulatory protein *(FLZ) of SnRK1 complex	CCGTCGGATCCACATCAGAA	GGTGATGAGACCGTCGTAGC
RN6G009060	GALT29	beta-1,6-galactosyltransferase	GGGTCGGTACAGGACGTTTT	GTGCAAAACTCGCCGGAAAT
RN5G011100	LRR-III	LRR-III protein kinase	GCTCTGTTCTCAACGACCCA	TTATGCCGTGCCAGGAACAT
RN1G061460	MYB R2R3	MYB class-R2R3 subgroup-22/23 transcription factor	TCCAGGGAGATCGGGAAAGT	ACGATCGGTGTTCAACCTCC
RN5G002330	NAC	NAC transcription factor	ATGTCAAGCTTCCTCCTGGT	GCGAAGATCGAGATCGGGAAT
RN2G017990	OAT	ornithine aminotransferase	AGGACAGGAAGAATGCTGGC	CTTTGCAAAACGGATGCCGA
RN4G032560	P5CS	pyrroline-5-carboxylate synthetase	AAGAGGAAGTGGGCAAGTGG	CCCGCCTCTTTCGTCATCAT
RN3G051940	RLCK-XII	RLCK-XII receptor-like protein kinase	GATTTTGCTGCGAAGGGGAC	CCCTCAACCTCATTGCCCAT
RN5G004920	FLZ SnRK1	regulatory protein *(FLZ) of SnRK1 complex	GCACCAGAGCCGTCTGATT	GTCACGACCAGGTGACAAAC
RN1G009320	SnRK2	SnRK2 SNF1-related protein kinase	GCAGCACCACGCCTTAAAAT	AAAGGACCTCTGGGGCAATG
RN7G020370	WRKY	WRKY transcription factor	TCGTCGTCATCGTCATCACC	GTCCCACCTGTGAACATCGT

Supplemental Table S11: Sequencing Statistics of used data. The N50 is the length of the shortest contig or scaffold at which 50% of the total genome assembly is represented by contigs or scaffolds of that length or longer. The Quality Value (QV) measures the accuracy of a genome assembly, with higher QV scores indicating fewer sequencing errors and greater assembly precision.

Genome features	Gbases	Read Number	N50	QV
PacBio	83.96	4,906,139	17,584	23
NanoPore	40.63	581,583	67,949	16
Illumina Short Reads	73.67	525,844,005	149	25
Illumina RNA-Seq	48.29	345,694,690	140	28
ONT RNA-Seq	371.82	502,447,299	1041	15
Pore-C	83.49	150,060,697	657	15

11 Acknowledgement

This work would not have been possible without the support and guidance of many individuals, to whom I would like to express my sincere gratitude.

I am grateful to my supervisor, Prof. Dr. Björn Usadel, for his invaluable insights, critical feedback, and continuous support throughout the entire research process.

Furthermore, I would like to thank my colleagues at Forschungszentrum Jülich and Heinrich Heine University Düsseldorf, especially Dr. Elisa Senger, Volkan Cevic, Zahra Zangishei, and Vivien Rosenthal, for the stimulating discussions, inspiring collaboration, friendly atmosphere, and unwavering support.

My deepest and most heartfelt thanks go to my family and friends, who accompanied me through this challenging time with patience, encouragement, and motivation. Without their support, this work would not have been possible in its present form.

12 Contributions

The study on floral initiation in strawberry was funded by the European Union's Horizon 2020 program under grant agreement number 679303. Freya M. R. Ziegler conducted data analysis and written the manuscript. We acknowledge Dr. Richard M. Twyman for manuscript proofreading and express our gratitude to Béatrice Denoyes, Amèlia Gaston, and Björn Usadel for their support and supervision. Additionally, we thank Béatrice Denoyes, Amèlia Gaston, Marie Devers, Karine Guy, Sonia Osorio, Erika Krüger, and Bastienne Brauksipe for generating and providing RNA-Seq data.

In the study on the full genome assembly of blackcurrant and the effects of drought stress on gene expression and metabolite profiles, Freya M. R. Ziegler performed ONT sequencing, data analysis, and manuscript writing, with support and supervision from Björn Usadel. Metabolite measurements were conducted by Sonia Osorio and Juan Gabriel Vallarino, while Vivien Rosenthal assisted with ONT PoreC sequencing. Lucas Munnes provided RNA-Seq data from the drought stress experiment, and Fransziska Genzel and Sarah Spettmann carried out qPCR analysis of selected candidate genes. Furthermore, Anita Sønsteby, Łukasz Seliga, and Sylwia Keller-Przybyłkowicz contributed RNA-Seq data for genome annotation. We acknowledge Dr. Richard M. Twyman and Dr. Elisa Senger for manuscript proofreading.

For this work, the AI tool ChatGPT was utilized for spelling, style, and grammatical corrections. However, the final review and full responsibility for the content remained with the author.

13 Publications

Ziegler FMR, Gaston A, Guy K, Devers M, Krüger E, Brauksiepe B, Eimert K, Osorio S, Denoyes B, Usadel B (2025). Molecular mechanisms underlying the early steps of floral initiation in seasonal flowering genotypes of cultivated strawberry. bioRxiv 633581. doi: 10.1101/2025.01.20.633581

Ziegler FMR, Rosenthal V, Vallarino JG, Genzel F, Spettmann S, Seliga L, Keller S, Munnes L, Sønsteby A, Osorio S, Usadel B (2024). A full genome assembly reveals drought stress effects on gene expression and metabolite profiles in blackcurrant (*Ribes nigrum* L.). Horticulture Research 12(2). doi: 10.1093/hr/uhae313

Mari RS, Schrinner S, Finkers R, Ziegler FMR, Arens P, Schmidt MHW, Usadel B, Klau GW, Marschall T (2024). Haplotype-resolved assembly of a tetraploid potato genome using long reads and low-depth offspring data. Genome Biology 25(1). doi: 10.1186/s13059-023-03160-z

Muñoz P, Castillejo C, Gómez JA, Enamorado LM, Lesemann S, Olbricht K, Petit A, Chartier P, Haugeneder A, Trinkl J, Mazzoni L, Masny A, Zurawicz E, Ziegler FMR, Usadel B, Schwab W, Denoyes B, Mezzeti B, Osorio S, Sevilla JSF, Amaya I (2023). QTL analysis for ascorbic acid content in strawberry fruit reveals a complex genetic architecture and association with GDP-L-galactose phosphorylase. Horticulture Research 10(3). doi: 10.1093/hr/uhad006

14 Eidesstattliche Erklärung

Hiermit versichere ich, dass ich die vorliegende Arbeit zur Erlangung des Grades „Doctor rerum naturalium“ eigenständig, ohne fremde Hilfe und nur unter Verwendung der angegebenen Hilfsmittel angefertigt habe. Ich versichere, dass ich keine anderen, als die angegebenen Quellen benutzt und alle wörtlich oder sinngemäß aus anderen Werken übernommenen Aussagen oder Abbildungen, in jedem einzelnen Fall unter Angabe der Quelle als Entlehnung kenntlich gemacht habe.
Ich versichere an Eides Statt, dass die Dissertation von mir selbständig und ohne unzulässige fremde Hilfe unter Beachtung der „Grundsätze zur Sicherung guter wissenschaftlicher Praxis an der Heinrich-Heine-Universität Düsseldorf“ erstellt worden ist.

Düsseldorf, den 06.03.2025

Freya Ziegler